COMPLEX DEFORMATION HISTORY OF THE SILICA NAPPE, AGGTELEK MTS:

Inherited Triassic salt structures and their role during the Alpine deformation

MASTER THESIS

WRITTEN BY:

ÉVA ORAVECZ

MASTER STUDENT IN GEOLOGY

SUPERVISORS:

GÁBOR HÉJA

MTA-ELTE GEOLOGICAL, GEOPHYSICAL AND SPACE SCIENCES RESEARCH GROUP

LÁSZLÓ FODOR DSC

MTA-ELTE GEOLOGICAL, GEOPHYSICAL AND SPACE SCIENCES RESEARCH GROUP,

MTA-ELTE VOLCANOLOGICAL RESEARCH GROUP

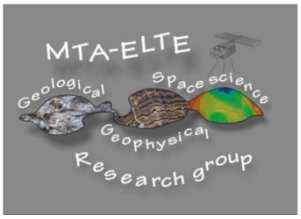

Emberi Erőforrások Minisztériuma

BOLYAI Kollégium 1992

EÖTVÖS LORÁND UNIVERSITY OF BUDAPEST

INSTITUTE OF GEOGRAPHY AND EARTH SCIENCES

MTA-ELTE GEOLOGICAL, GEOPHYSICAL AND SPACE SCIENCES RESEARCH GROUP

Budapest, 2019

TABLE OF CONTENTS

I. INTRODUCTION

In the last decades understanding salt deformation has became a subject of growing interest in many salt-bearing fold-and-thrust belts. More and more studies report the significance and controlling role of inherited normal faults and connected salt structures in predetermining the kinematics and geometry of the orogens (e.g. GRANADO ET AL. (2018) in the Northern Calcareous Alps; GRAHAM ET AL. (2012) in the Western Alps; TARI & JABOUR (2013) in offshore Morocco and MORAGAS ET AL. (2018), MARTÍN-MARTÍN ET AL. (2017) in the High Atlas; JAHANI ET AL. (2017) and HASSANPOUR ET AL. (2018) in the Zagros; and KERGARAVAT ET AL. (2017) in Central Anatolia). By recognizing early salt tectonics many unusual structural features like onlap surfaces, growth strata and thickness variations in pre-orogenic sedimentary successions, and also young-on-older thrust contacts could be explained. Separating salt structures like salt domes, salt anticlines and minibasins from regular shortening-related anticlines and synclines is, however, still a challenging task, especially in poor outcrop conditions. That is why salt tectonic features still go unnoticed even until today in so many fold-and-thrust belts.

In the Aggtelek Mts. the presence of Permian to Lowermost Triassic evaporites has been long known but the role of salt deformation has not been studied in details. The Perkupa Evaporite Formation presently forms the tectonic base of the Silica Nappe which is the uppermost tectonic unit of the Aggtelek Mts. The primary aim of my master thesis was to analysis the Cretaceous deformation in the Silica Nappe, emphasizing on determining the original nappe transport direction. It became quickly clear, however, that the extent of salt deformation has been vastly underestimated in the Aggtelek Mts. Results of the field work and structural mapping revealed significant Triassic structural elements with major control on sedimentation. As more and more salt structure were recognized, it became obvious that understanding the Cretaceous shortening is only possible by understanding the much older pre-orogen deformation geometry. Consequently, the aim of my thesis work was modified to studying the effects of salt tectonics in the Aggtelek Mts.

II. GEOLOGICAL BACKGROUND

II.1. Large-scale tectonic position of the Aggtelek Mts.

The Mesozoic basement of the Pannonian Basin consists of structural units with different origin and deformation history which were juxtaposed during the Late Oligocene — Early Miocene tectonic processes (***Fig.1***, BALLA 1988, CSONTOS ET AL. 1992, HAAS ET AL. 2000, KÁZMÉR & KOVÁCS 1985, TARI 1994). The northwestern part of the Pannonian Basin is built up by the ALCAPA Mega Unit which shows close relation to the Adriatic units (CSONTOS AND VÖRÖS 2004, HAAS ET AL. 2014, SCHMID ET AL. 2008). SCHMID ET AL. (2008) defined the units of the ALCAPA Unit as the tectonic units originally positioned S of the Piemont-Liguria Ocean. The presence of a second oceanic realm (Neotethys Ocean) is a complicating but a definitive factor: the different units of the ALCAPA were positioned N, W and S of the Neotethys Ocean (SCHMID ET AL. 2008). The tectonic elements forming part of the ALCAPA Unit are called Austroalpine nappes in the Alps and in the Central- and Inner Western Carpathians (SCHMID ET AL. 2004, PLAŠIENKA ET AL. 1997). The Austroalpine nappes were originally defined in the Eastern Alps (e.g. TOLLMANN 1977), however, their continuation can be further traced in the Western Carpathians, thus the different nappes of the Eastern Alps and the Western Carpathians can be correlated (FROTZHEIM ET AL. 2008, SCHMID ET AL. 2004). The Aggtelek Mts. forms part of the Western Carpathians, therefore only this orogenic system will be introduced in details.

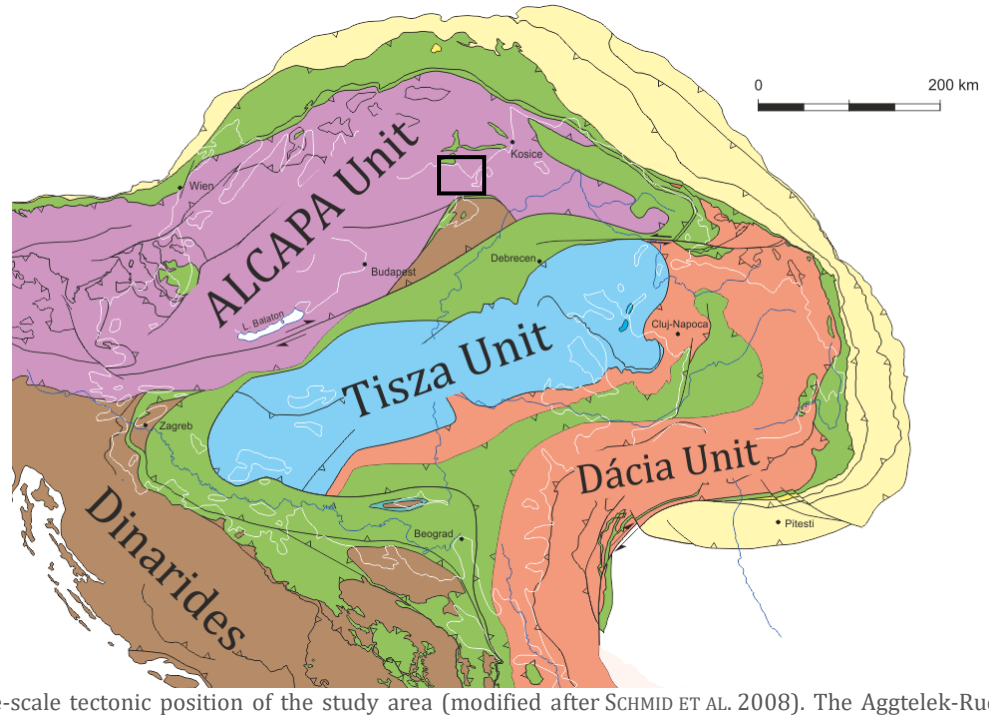

Fig.1. Large-scale tectonic position of the study area (modified after SCHMID ET AL. 2008). The Aggtelek-Rudabánya Mts. located in the northeastern part of the Pannonian Basin (marked with a black frame) form part of the Inner Western Carpathians, therefore the ALCAPA Mega Unit.

The nappe system of the Western Carpathians is currently divided into three parts: External Western Carpathians (EWC) in the N, Central Western Carpathians (CWC) in the middle and Inner Western Carpathians (IWC) in the S (***Fig.2***, FROITZHEIM ET AL. 2008, PLAŠIENKA 2018). The sedimentological and structural evolution of the Central- and Inner Western Carpathians was

controlled by the opening and closure of two different oceans: the older Neotethys Ocean in the south and the younger Alpine Tethys in the north (PLAŠIENKA 2018, SCHMID ET AL. 2008). The EWC can be considered as a Late Cretaceous — Cenozoic accretionary prism detached from the European plate and/or the basement of the Alpine Tethys (PLAŠIENKA 2018). The nappes of the CWC were situated between the Alpine Tethys and the Neotethys Oceans, and they represent the northern part of the Adriatic plate. The IWC were located on the southern margin of the Neotethys (southern part of the Adriatic plate), consequently the suture of the Neotethys Ocean can be traced along the boundary of the CWC and IWC.

Regarding the Alpine evolution of the Western Carpathians the following milestones should be mentioned: Permian rifting (FINGER ET AL. 2003, MILLER & THÖNI 1997, SCHUSTER ET AL. 2001, SCHUSTER & STÜWE 2008) was followed by the Late Anisian continental break-up and initiation of spreading of the Neotethys Ocean (GAWLICK ET AL. 2012, GAWLICK & MISSONI 2015, KOZUR 1991, SUDAR ET AL. 2013). The continental rifting of the southern branch of the Alpine Tethys (Piemont-Ligurian or Vahic Ocean) started during Late Triassic — Early Jurassic times. The Middle Jurassic oceanic spreading of the Alpine Tethys was connected to the initial closure of the Neotethys Ocean. This progress was manifested in a S- or SE-ward dipping intra-oceanic subduction zone in the later Western Carpathian realm (PLAŠIENKA 2018, SCHMID ET AL. 2008). The Jurassic intra-oceanic subduction was followed by the Late Jurassic to Early Cretaceous collision and nappe stacking (DALLMEYER ET AL. 2008, FARYAD & HENJES-KUNST 1997, GAWLICK ET AL. 1999, LEXA ET AL. 2003). During this process the nappes of the CWC represented the lower plate, whereas the nappes of the IWC represented the upper plate. During this collisional phase the formation of the Central- and Inner Western Carpathians involved both thick-skinned and thin-skinned nappe stacking (PLAŠIENKA 2003, PLAŠIENKA ET AL. 1997). The locus of compressional deformation gradually migrated northward in the CWC and more external units became part of the orogenic wedge (PLAŠIENKA 2018). This northward migrating orogenic front is evidenced by syn-tectonic deposits of thick-skinned (Tatric) and thin-skinned (Fatric, Hronic) nappes, and by the age of metamorphism of the basement nappes (Gemer, Vepor, ***Fig.2***, PLAŠIENKA 2018, PLAŠIENKA ET AL. 1997). The far-travelled thin-skinned nappes (Fatric, Hronic) of the Western Carpathians represented the detached sedimentary cover of the thick-skinned nappes in the CWC (PLAŠIENKA 2018).

The Silica Nappe occupies a somewhat problematic position in the Western Carpathians. The Silica Unit is a thin-skinned nappe which represents the uppermost tectonic unit both in the CWC and IWC (LESS 2000, LESS ET AL. 2006, PLAŠIENKA 2018, PLAŠIENKA ET AL. 1997). However, the direction and age of nappe-emplacement is unknown due to the lack of syn-orogenic sediments and controversial tectonic data and concepts (DEÁK-KÖVÉR 2012, GRILL ET AL. 1984). The original basement of the Silica Nappe is also unknown, moreover, its position relative to the Neotethys is controversial (see details in *Chapter II.4*).

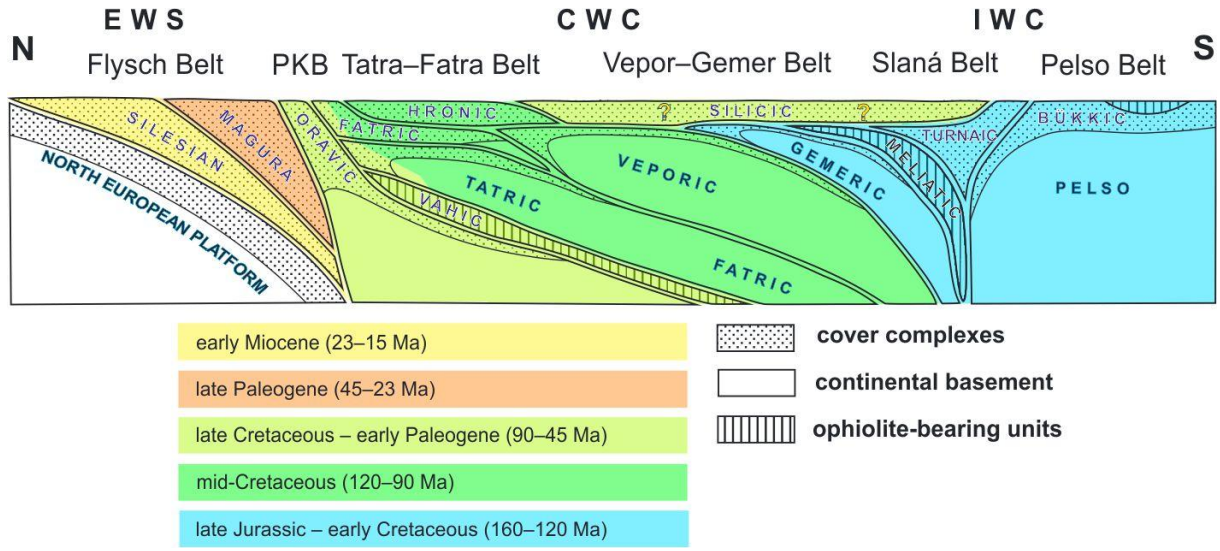

Fig.2. Schematic cross-section of PLAŠIENKA (2018) on the tectonic relationship of the major structural units of the Western Carpathians. These units are divided into three parts: Inner Western Carpathians in the S, Central Western Carpathians in the middle and External Western Carpathians in the N. The colors indicate the major deformation ages of the different units. The Silica Unit is in the uppermost thin-skinned nappe unit of the Inner and Central Western Carpathians.

When the exhumation of the Central Western Carpathians started in the Late Cretaceous the Inner Western Carpathians became the rear area of the continuously growing orogenic wedge (JEŘÁBEK ET AL. 2012, KRÁLIKOVÁ ET AL. 2014, PLAŠIENKA ET AL. 2007). Meanwhile the subduction of the Alpine Tethys also started during the Cretaceous. According to most recent studies the subduction of the Neotethys and the Alpine Tethys occurred along one single slab (STÜWE & SCHUSTER 2010, PLAŠIENKA 2018): the subduction front retreated from the Neotethys to the Alpine Tethys by decoupling of the mantle lithosphere under the CWC. The subduction of the Alpine Tethys and finally the European distal lithosphere continued up until the Miocene (Alpine orogeny) during which the accretionary prism of Cretaceous to Miocene flysch units formed (OSZCZYPKO 2006, ROURE ET AL. 1993). These units now constitute the nappes of the External Western Carpathians (FROITZHEIM ET AL. 2008, PLAŠIENKA 2018). Miocene retreat of this slab is responsible for the formation of the Miocene Pannonian back-arc basin (HORVÁTH 1993, ROYDEN ET AL. 1982, TARI ET AL. 1999).

The Aggtelek Mts. located in NE Hungary form one of the southernmost exposures of the Inner Western Carpathians (LESS 2000, PLAŠIENKA ET AL. 1997). They are morphologically the continuation of the Slovak Karst and geologically they are closely related to the Rudabánya Mts. The neighboring Aggtelek and Rudabánya Mts. are divided by an Oligo-Miocene sinistral strike-slip that runs along the Szőlősardó-Perkupa-Bódvarákó-Hídvégardó-Žarnov villages (***Fig.3,*** LESS 2000, SZENTPÉTERY 1997). This sinistral strike-slip is part of the major Darnó Deformation Zone (FODOR ET AL. 2005, LESS ET AL. 2006).

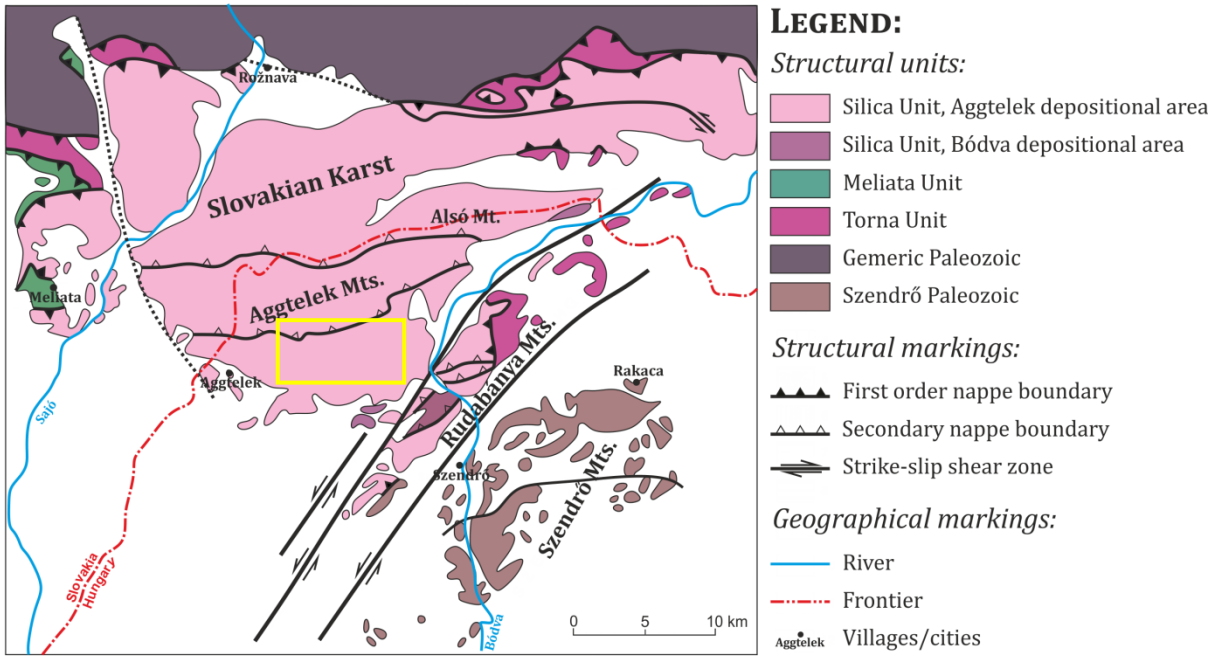

Fig.3. Regional structural map of the Aggtelek-Rudabánya Mts. and their surroundings (modified after KOVÁCS 1989). The nappe boundaries around the Silica Nappe meet in triple points, indicating that the Silica Nappe has structural contact with every other nappe. The yellow box marks the study area.

II.2. Structural division of the Aggtelek Mts.

The nappes of the Aggtelek-Rudabánya Mts. originally formed part of the passive margin of the Neotethys Ocean. These nappes were assigned into three larger structural units (Torna, Meliata and Silica Nappes) based on their formations, structural positions and metamorphic grades (***Fig.3,*** ÁRKAI & KOVÁCS 1986, KOVÁCS ET AL. 1989, KÖVÉR ET AL. 2009, LESS 2000, LESS ET AL. 2006).

The lowermost Torna Unit consists of sediments originally deposited on thinned continental crust (KOVÁCS ET AL. 1989, LESS 2000, LESS ET AL. 2006) which was affected by anchizonal and epizonal metamorphism during nappe stacking (ÁRKAI & KOVÁCS 1986). The subsequent Meliata Unit is built up by formations related to thinned continental crust as well as to the oceanic crust which include sedimentary rocks, mafic magmatic rocks and their serpentinized versions (LESS 2000, MELLO ET AL. 1983). In the Aggtelek Mts. the occurrences of the formations of the Meliata Unit *(=Bódvavölgy Ofiolitic Complex)* are only known from the evaporitic mélange that forms the tectonic base of the Silica Nappe (ÁRVA-SÓS ET AL. 1987, DOSZTÁLY & JÓZSA 1992, HORVÁTH 1997, KOVÁCS ET AL. 1989). IN the Slovakian part of the more widespread Meliata Unit these rocks bear the signs of multiphase Alpine metamorphosis: the peak metamorphosis with its calculated 7 kbar pressure and maximum 350°C temperature was followed by a retrograde greenschist facies metamorphic event which is probably the result of successive burial due to nappestacking (ÁRKAI ET AL. 2003, HORVÁTH AND ÁRKAI 1998, FARYAD AND HENJES-KUNST 1995).

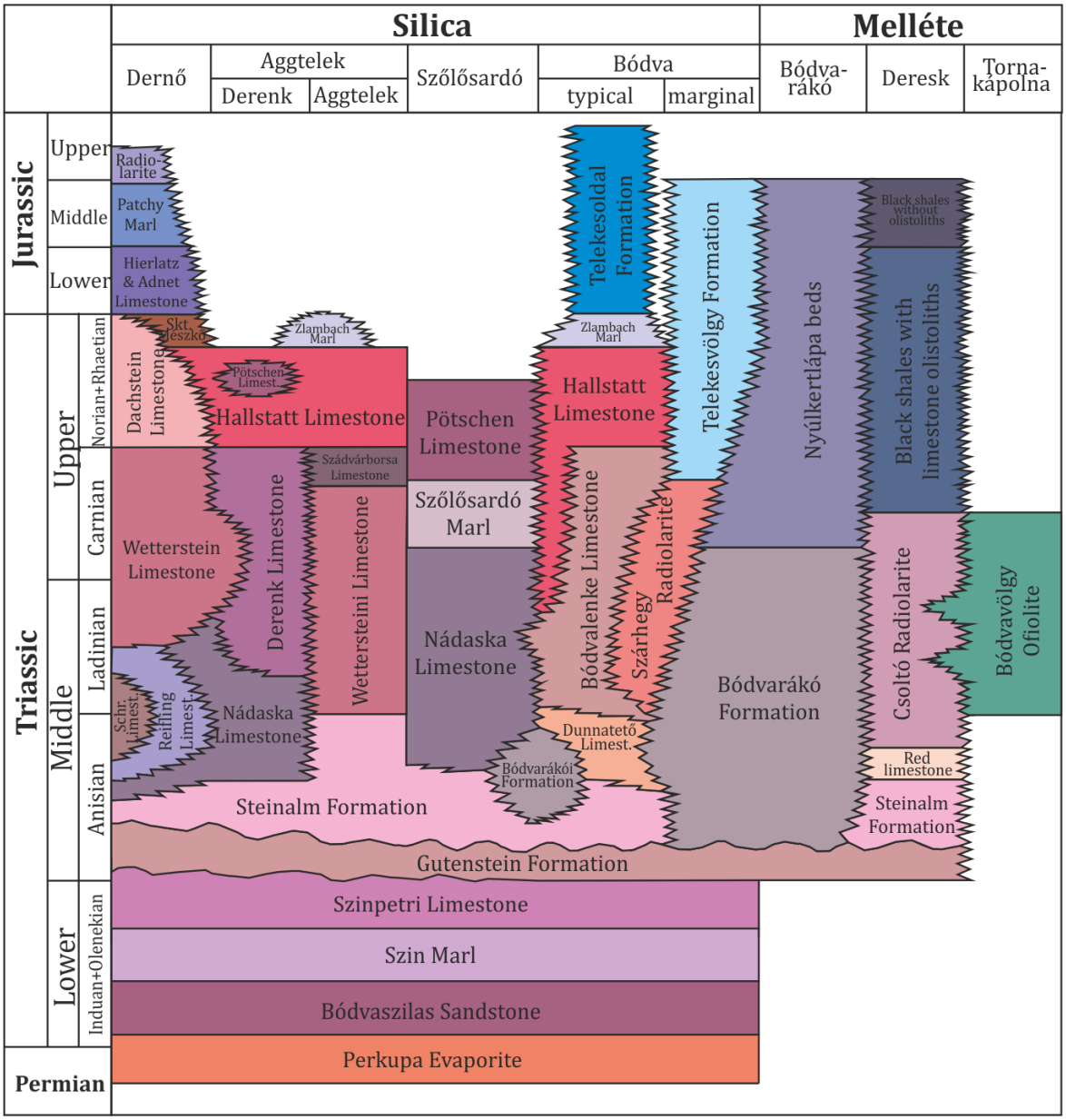

Fig.4. Stratigraphic subdivision of the Permo-Mesozoic formations of the Aggtelek-Rudabánya Mts (after LESS ET AL. 2006). Used abbreviations: Schr.=Schreyalm Limestone; Stk.=Szörnyűkút Limestone.

The Silica Nappe found in the uppermost tectonic position consists of detached sedimentary successions deposited on thinned continental crust (ANDRUSOV 1956, KOVÁCS ET AL. 1989, KOZUR AND MOCK 1973A, 1973B, LESS 2000). In the Aggtelek Mts. its sedimentary sequence starts with the Permian to Lower Triassic **Perkupa Evaporite** formed in sabkha environment. While the original base of these evaporates are unknown, the subsequent **Bódvaszilas Sandstone** is interpreted as the original sedimentary cover of the Perkupa Evaporite (***Fig.4***, GRILL & SZENTPÉTERY 1988). The Bódvaszilas Sandstone is the first element of the Lower Triassic transgressive and can be interpreted as the local equivalent of the Alpine Seis Beds. As the siliciclastic input decreased and the carbonatic content increased, the Bódvaszilas Sandstone was followed first by the **Szin Marl** (Campil Beds), then the **Szinpetri Limestone** (Wurstlkalk) (HIPS 1995, 1996A, KOVÁCS 1989).

Significant changes in the depositional relief are observed from the Anisisian when different depositional areas were formed due to the break-up of the previously flat and ramp environment (***Fig.5***, KOVÁCS 1984, KOVÁCS ET AL. 1989, VELLEDITS ET AL. 2011). This change in the paleomorphology

is interpreted as the consequence of final continental break-up, shoulder uplift and onset of spreading in the Neotethyan realm (GAWLICK ET AL. 2012, GAWLICK & MISSONI 2015, KOZUR 1991, SUDAR ET AL. 2013). The morphological changes were consequently accompanied by changes in depositional environment: carbonatic platforms were formed on the basement highs **(Aggtelek depositional area)**, whereas in the deeper basinal areas the dominant pelagic carbonate deposition (red, grey, black cherty limestones and rarely radiolarites) was interrupted only by thin Carbian shale and marl intercalations **(Bódva depositional area).** In the transitional areas between the platforms and intraplatform basins slope deposits with typical resediment characteristics and slump structures accumulated **(Szőlősardó depositional area).** The Aggtelek succession appears mostly in the Aggtelek Mts. while the Bódva succession is outcropping dominantly in the Rudabánya Mts. Following several Late Triassic drowning event the shallow water sedimentation disappeared for good from the Silica area. The youngest Mesozoic formations of the Silica Unit are thin Jurassic carbonates and Oxfordian radiolarites and olistostroms in Slovakia (OŽVOLDOVÁ 1998, SÝKORA & OŽVOLDOVÁ 1996).

Since the Silica Unit occupied the uppermost tectonic position during nappe stacking it was not affected by metamorphosis, it only reached the middle and deep burial diagenetic domains (ÁRKAI AND KOVÁCS 1986). GRILL ET AL. (1984) and GRILL (1989) separated four smaller nappes within the Hungarian parts of the Silica Unit:

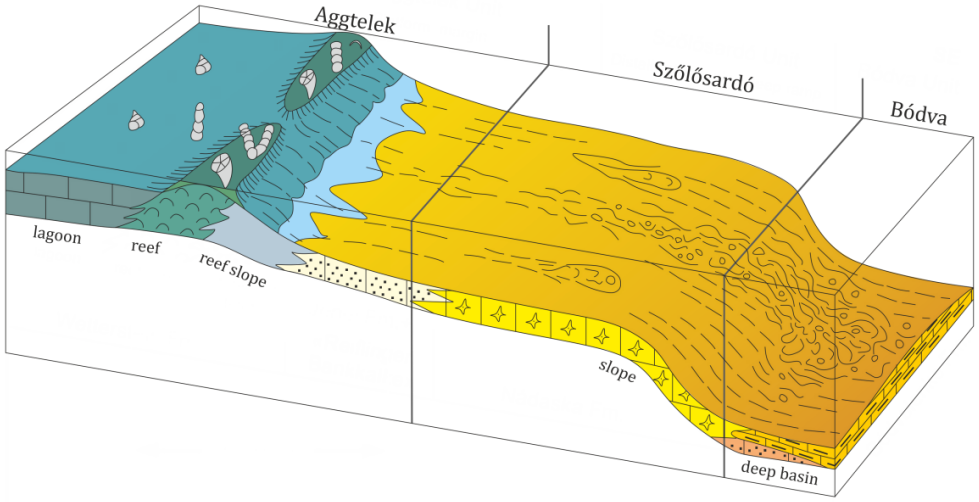

Fig.5. Differentiation of the Silica area during the Anisian (modified after VELLEDITS ET AL. 2011). On the topographic highs carbonate platforms evolved **(Aggtelek depositional area)** while in the deeper basins shallow water sedimentation was changed to pelagic sedimentation **(Bódva depositional area).** On the transitional area between the highs and basins resedimentation and typical slope deposits appeared **(Szőlősardó depositional area).**

- **Silica Nappe:** covers most of the Aggtelek Mts. The formations of the Silica Nappe were originally deposited in the Aggtelek depositional area.
- **Szőlősardó Nappe:** outcropped only around the village of Szőlősardó in the southern part of the Aggtelek Mts. Its formations show typical signs of slope deposits (Szőlősardó depositional area).
- **Bódva Nappe:** covers the Rudabánya Mts. Its formations are related to the Bódva depositional area.

- **Komjáti Nappe:** the lowermost nappe of the Silica Unit in Hungary. The Komját Nappe is in fact the evaporitic mélange found at the base of the Silica Unit which contains numerous sedimentary and magmatic blocks tectonically sheared from deeper structural units (Meliata Unit, GRILL & SZENTPÉTERY 1988).

The existence of the Komját Nappe as a separate nappe unit was based on the fact that the boundary between the Perkupa Evaporite and the Bódvaszilas Sandstone was originally thought to be a tectonic boundary (GRILL ET AL. 1984). The recent sedimentary studies proved, however, that the boundaries of the siliciclastic bodies within the evaporites are not exclusively tectonic but often sedimentary. This means that these siliciclastic rocks are present in the evaporitic succession as, sedimentary intercalations (HIPS 1995). Based on this the contact of the Perkupa Evaporite and the covering Bódvaszilas Sandstone should at least in some places be sedimentary, their transition in turn should be continuous. In this case the evaporite cannot be separated from the Silica Nappe. During nappe stacking the lubricated evaporitic sole incorporated several bodies of different origin (including Meliata sediments and oceanic lithospheric remnants).

II.3. Introduction to the mapped formations

Stratigraphical subdivision of the formations of the Aggtelek—Rudabánya Mts. was carried out during the geological mapping projects of the 1980's (GRILL 1989, GRILL ET AL. 1984, GRILL & SZENTPÉTERY 1988, LESS ET AL. 1988, LESS ET AL. 2006) and was later refined by HIPS (1995). In the lights of the new sedimentological, paleontological and tectonic results the original stratigraphical table was slightly modified later ***(Fig.4).*** In the following chapters only those formations are introduced in details which were mapped and studied.

Perkupa Evaporite Formation: $^{p}P\text{-}T_1$

The oldest known formation of the Silica and Bódva successions is the Perkupa Anhydrite Formation (or Perkupa Evaporite) the deposition of which is connected to hypersaline lagoons (HIPS 1995). Its original base is unknown. The age of the evaporite was determined by ILAVSKÁ (1965) as Late Permian but HIPS (1996B) showed that its deposition continued until the Early Triassic (Early Induan).

The salt rocks themselves cannot be studied on the surface in the Aggtelek Mts. but several wells (e.g. *Jő-2, Jő-3, Szn-1*) and a closed underground evaporite mine in the village of Perkupa proved that the Perkupa Evaporite is present in shallow depths or right under the Quaternary cover. On the other hand, there are siliciclastic intercalations within the evaporitic succession. According to LESS ET AL. (2006) grey and black shales and siltstones are also present in these sedimentary intercalations based on which the Perkupa Evaporite – or rather its remains – can be identified ***(Fig.6)***. The most remarkable outcrops of the Perkupa Evaporite was found N of Tornakápolna (*Szn-019)* and in the surroundings of Jő-2 well (*Jsv-095,* see detailed descriptions of my observations in *Chapter IV*).

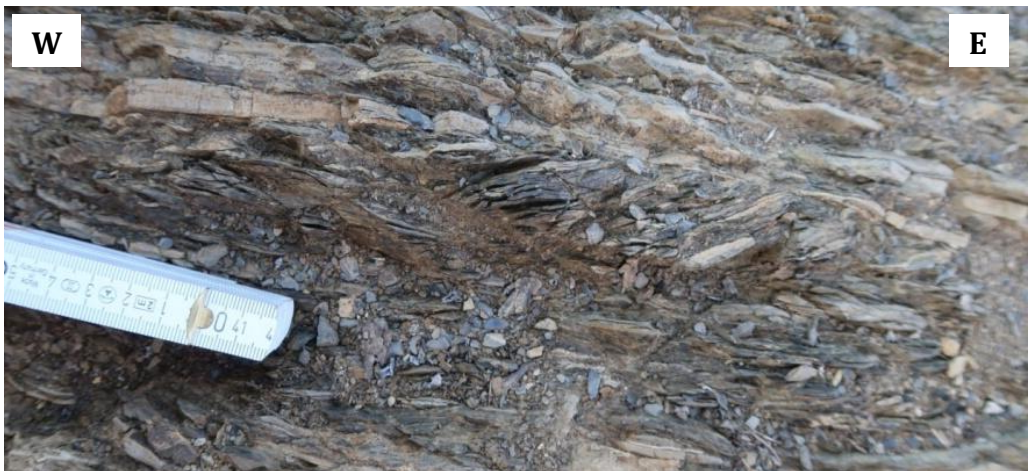

Fig.6. Black and dark gray shale with carbonate (dolomite) intercalations at *Szn-019*. These in-situ rocks were interpreted as sedimentary siliciclastic intercalations of the Perkupa Evaporite succession.

Bódvaszilas Sandstone Formation: $^{b}T_1$

The Bódvaszilas Sandstone is a shallow marine sandstone the deposition of which is connected to the intertidal and subtidal zones (lagoons and tidal flats) (HIPS 1995, 1996A, KOVÁCS ET AL. 1989). HIPS (1995,1996A) determined the age of the Bódvaszilas Sanstone as Griesbachian and Smithian (Induan to Early Olenekian).

This is mainly very fine- and fine-grained, red and grayish purple colored sandstone mainly with siltstone and shale intercalations ***(Fig.7)***. Rarely its color may change to riffle-green (e.g. in my *Per-089* point). The sandstone beds are usually full of with mica grains, and soft sedimentary deformation structures like dewatering structures occur very often. Besides all this, characteristic wrinkle marks suggesting blowing wind induced waving in very shallow water appear as sole marks (HIPS 2001). The fossils found in the Bódvaszilas Sandstone were common snails with maximum of 0.5 cm size.

On the field it is usually very difficult to make a difference between the Bódvaszilas Sanstone and certain parts of the younger Szin Mar. Clear distinction is only possible in large in-situ outcrops or by recognizing the stratigraphical continuity. Two of the most important outcrops of the Bódvaszilas Sandstone within the studied area are N of Perkupa, around the entrance of the former underground salt mine at *Per-089* and in the Szerelem Valley at *Per-063*. The lower boundary towards the Perkupa Evaporite was considered to be tectonic everywhere by GRILL (1989) and GRILL ET AL. (1984). Later, however, HIPS (1995) showed that the boundary of the Perkupa Evaporite and the Bódvaszilas Sandstone should be sedimentary at least at some places.

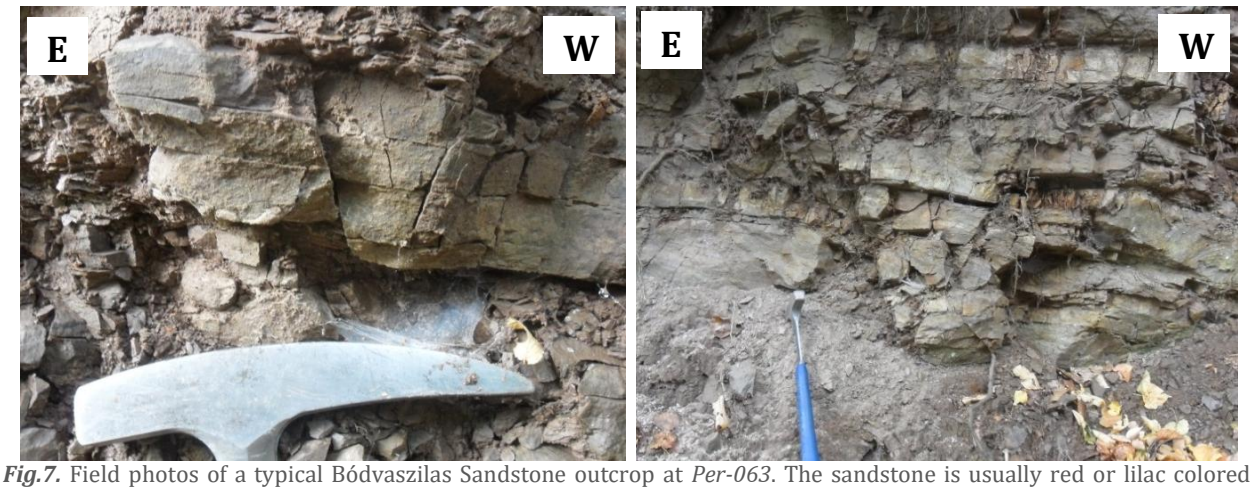

Fig.7. Field photos of a typical Bódvaszilas Sandstone outcrop at *Per-063*. The sandstone is usually red or lilac colored fine-grained sandstone with high mica content.

Szin Marl Formation: $^{sm}T_1$

The Szin Marl is a remarkably variable and relatively thick formation deposited on the Early Triassic sedimentary ramp. The detailed subdivision of this formation was carried out in HIPS KINGA's PhD dissertation in 1995 who separated 6 different members within the Szin Marl based on lithology and fossil content. During field work I followed her subdivision.

The lowermost A member of the Szin Marl mainly consists of thin bedded grey limestones and marls but shale and siltstone intercalations do occur between the carbonatic beds ***(Fig.8/a-b)***. The limestones are mostly fine grained, sometimes consist of middle sized carbonate crystals. One of the main characteristics of this member is that in general, it contains a lot of ooids and crinoidea fragments, sometimes even Ostracodes and Ammonites (HIPS 1995). The other characteristics of the A member are the marks and traces of intensive bioturbation. The more or less continuous sections at *Per-082—083* and at *Per-109—110* W of Perkupa suggest that the thickness of the lowermost A member is probably only a few meters (~8-10 m). The above mentioned section at *Per-082—083* and the former mine N of Perkupa at *Per-089* are the most important outcrops of this member, the latter of which also proves the sedimentary nature of the formation boundary between the lower Bódvaszilas Sandstone and the Szin Marl.

The B member contains the most siliciclastic particles within the Szin Marl which marks the deepest water depth that occurred in the history of the Early Triassic sedimentary ramp of the Aggtelek-Rudabánya area (HIPS 1995). On one hand, this also means that the B member contains the most varied and mixed lithology ***(Fig.8/c)***. On the other, the consistency of this member is far worse than of the A member and it also contains much more shales, clay marls, siltstones and mica-rich sandtones. Its color is usually gray, riffle-green or green if the glauconite content locally increases (HIPS 1995), and towards the upper and more sandy part of the B member its color may change to red. Common small snail and shell fossils are very frequent but the Ammonites are very rare in this B member. The wrinkle marks observed in the Bódvaszilas Sandstone are also present here (HIPS 1995). Further mechanical sole marks (gutter marks) and (sometimes more than 10-15 cm sized) dewatering structures were found as well ***(Fig.8/d)***. The B member has several significant in-situ outcrops in the surroundings of Perkupa, e.g. in the valley of Vízvölgy Creek at

Per-019, Per-083 and Per-088, in the Vég Valley N of Perkupa at *Per-001 and Per-009—011*, or E of Szin at *Per-025 and Per-027*. The detailed description of these outcrops will be discussed in *Chapter IV*.

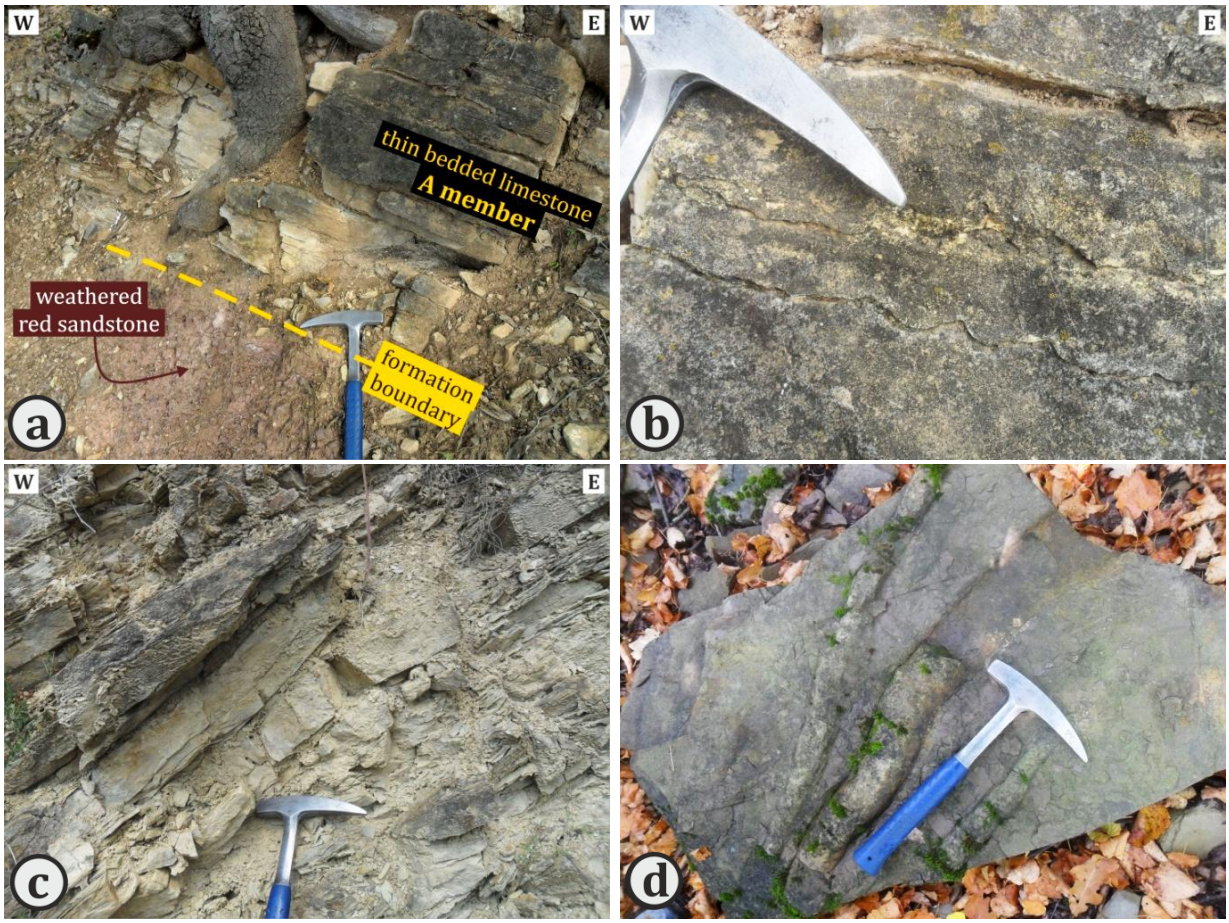

Fig.8. Field photos of the lower A-B-C members of the Szin Marl. **A.)** Formation boundary of the Bódvaszilas Sandstone and the lowermost A member of the Szin Marl directly exposed at *Per-089*. This A member is built up by thin bedded fine-grained limestones with ooids and crinoidal fragments. **B.)** Dewatering structures in the limestone beds of the A member at *Per-089*. **C.)** Field photo of a typical outcrop of the B member with varied lithology (limestone, marl, shale and sandstone beds) at *Per-081*. **D)** Gutter marks observed on the bedding soles of the B member at *Per-102*.

The thick bedded C member of the Szin Marl is an easily followable marker horizon which is only 2-3 m thick. Its lilac color, grainstone pattern and its black colored shell fossils (lumashellas) make it impossible to mistake the limestone beds of this member for any other part of the Lower Triassic (HIPS 1995). The best outcrops of the C member may be found along the road between Perkupa and Varbóc at *Per-087—088* and in the Vég Valley N of Perkupa at *Per-092—094* (*Chapter IV*).

The D member shows very similar features to the uppermost part of the B member: it is mainly built up by thin bedded gray and red marls and sandstones with occasional limestone intercalations. The siliciclastic beds are full of with mica grains. In the absence of field exposure of the C or E marker members, the only guidance for knowing our way around the B, D and F members is to pay attention for the ratio of siliciclastics versus limestone beds because the B and F members contain much more carbonates than the D member (it hardly contains carbonatic beds). The best field exposures of the D members were found in the upper part of the Gelleház Valley at *Per-013—014 and Per-115* and along the road towards Varbóc at *Per-087* (see details in *Chapter IV*).

Just like the C member, the E member is also a marker horizon within the Szin Marl. Even though it is only a few meters thick, its greyish purple, lilac or light gray color and its varicolored clasts are easily recognizable. These limestone beds have grainestone patterns with moderately coarse or coarse crystals and very frequent ooids and crinoidal fragments. In a few cases shell fossils were also observed but unlike in the C member, their color is not black. The greatest field exposures of this E member that I have encountered with are located in the Gelleház Valley at *Per-114* and in the Szövetény Valley at *Szn-055*.

The uppermost F member of the Szin Marl is practically the same as the B member only with much more carbonates: it mainly consists of alternating thin bedded featureless limestones, sandstones, marls and siltstones. Snails and shell fossils are very frequent bioclasts but the ribbed shells are considered index fossils for this member. During my mapping work I have found the F member in-situ exposed in the Gelleház Valley at *Per-015—017*, SE of Szin at *Per-028—029 and Per-050—052*, in the Szövetény Valley at *Szn-056—061*, and along the road between Szinpetri and Jósvafő at *Jsv-020—025*.

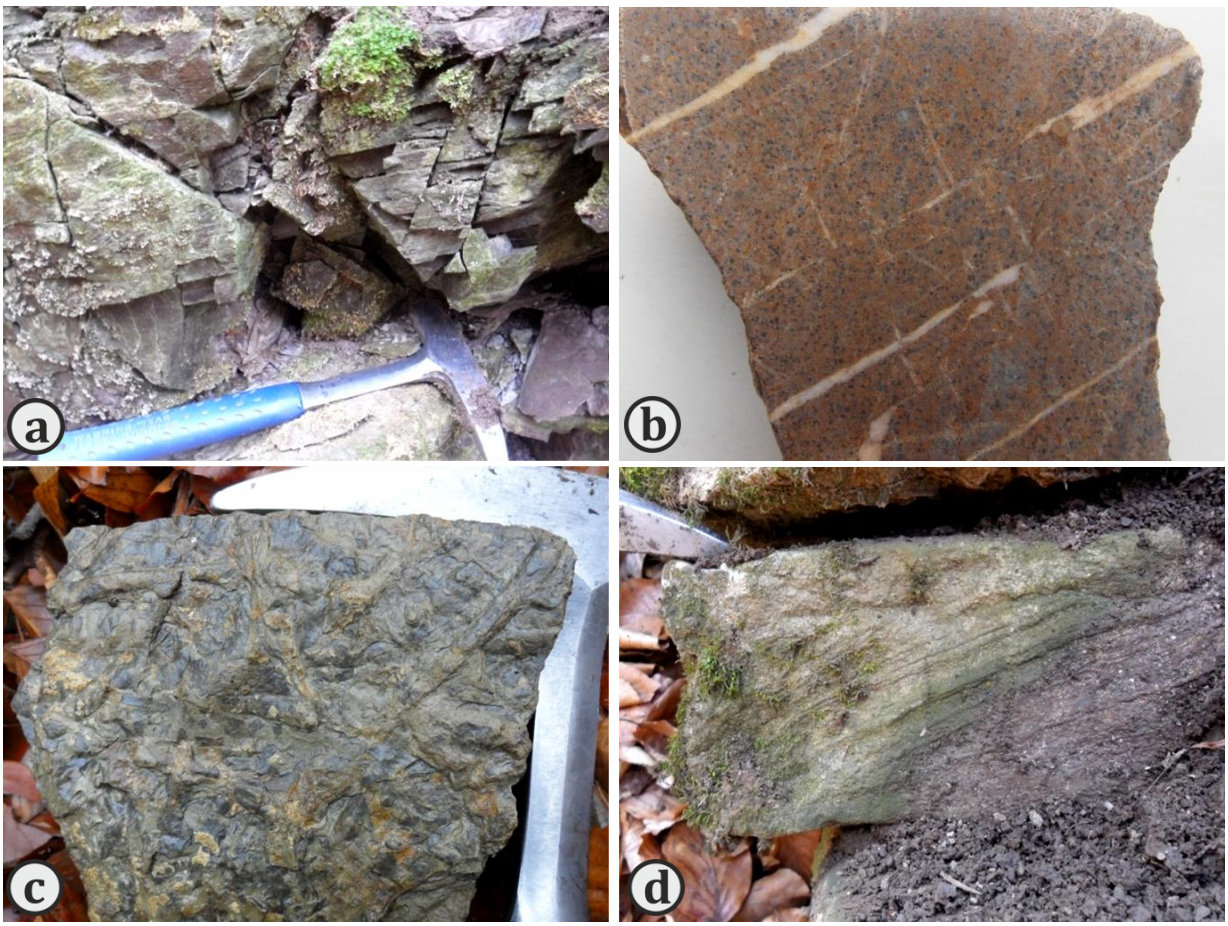

Fig.9. Field photos of the upper D-E-F members of the Szin Marl. **A.)** A typical in-situ outcrop of the lilac colored D member *(Per-063).* **B.)** Cropped surface of a hand-sized sample of the E member from *Szn-055*. The longer side of the photo is about 10 cm. **C.)** Trace fossils on the sole of a thicker layer of the F member *(Szn-057)*. **D.)** Sedimentary cross lamination observed in the F member at *Szn-104*.

All in all, the Szin Marl consists of the alternation of marls, limestones and sandstones, less frequently shales and siltstones, and at bad outcrop conditions it is utterly difficult to separate certain members of the Szin Marl from each other or from other formations like the Bódvaszilas

Sandstone and the Szinpetri Limestone. The red and lilac mica-rich sandstones may be from the upper part of the B member, from the lower half of the D member, from the Bódvaszilas or even from some parts of the F member. Moreover, the carbonatic and marly part of the B and D members are very similar, and the F member of the Szin Marl has a gradual transition into the Szinpetri Limestone thus they are very hard to separate as well.

Szinpetri Limestone Formation: $^{sp/jl}T_1$

The Szinpetri Formation was deposited in deeper sublitoral environment, under the storm base during the Spathian (Late Olenekian) (HIPS 1995, LESS ET AL. 2006). As its siliciclatic content gradually decreases upward, the formation was later separated into two members.

The upper Szinpetri Limestone Member is very similar to the F member of the Szin Marl in its appearance: it is a thin bedded, characteristically vermicular and lenticular gray limestone with thin yellow or gray marl films and intercalations ***(Fig.10)***. Its lower boundary toward the F member of the Szin Marl is gradual. Even though the bedding is easily observable in the Szinpetri Limestone, making measurements on the bedding surfaces is very hard due to its lenticular and uneven appearance. Moreover, soft-sedimentary deformation structures are very frequent as well, which are usually small-scale (maximum of 4-5 cm) slump folds and dewatering structures. The Szinpetri Limestone is exposed in a large area, mostly between Szin and Szinpetri, between the Szövetény and the Kecskekút Valley, as well as in the surroundings of Tornakápolna. Its best outcrops were found along the road between Szinpetri and Jósvafő at *Jsv-017—019 and Jsv-027—030*, along the road to Szelcepuszta at *Szn-001*, and in the Kecskekút Valley at *Szn-038—045.*

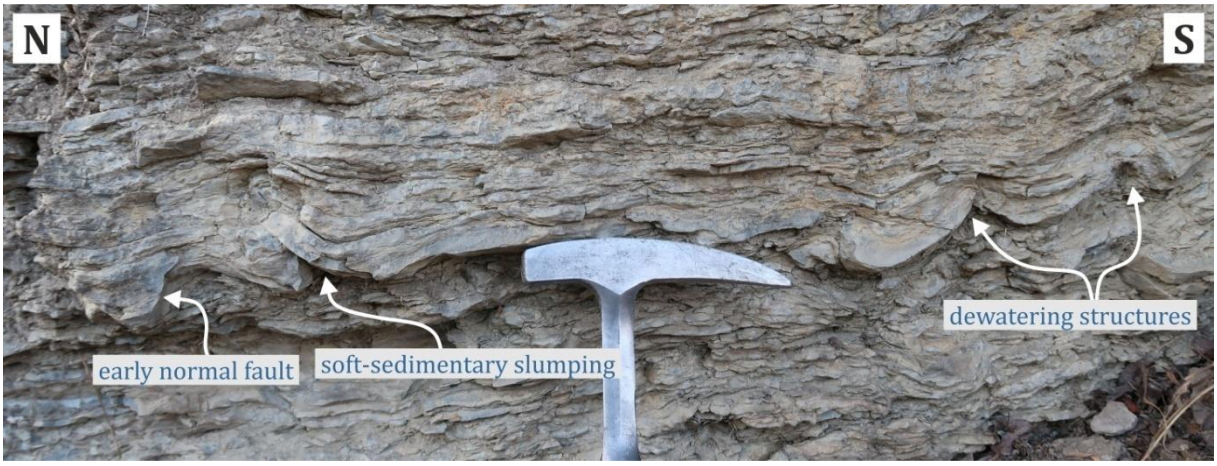

Fig.10. Characteristic vermicular and lenticular thin bedded Szinpetri Limestone Member at *Jsv-029*. This outcrop also exposes several small-scale sedimentary deformation structures (slump folds and dewatering structures).

Opposite to that, the upper Jósvafő Limestone Member is a well bedded and easily followable, mostly thin bedded, but occasionally thick-bedded dark gray fine-grained limestone ***(Fig.11)***. It contains only a few marl intercalations. It was mapped in the wider surroundings of Jósvafő.

Fig.11. Steeply dipping thin bedded Jósvafő Limestone Member at *Jsv-010*. It contains marl intercalations only locally.

Gutenstein Limestone Formation: $^{g}T_2$

The dark gray or black colored, often bitumenous thin bedded Gutenstein Limestone looks very similar to the Jósvafő Member of the Szinpetri Formation – they are hardly ever distinguishable for sure on the field. That is why their separation during geological mapping and cross-section constructing was only based on the geological maps of HIPS (2001) and LESS ET AL. (1988). The only guidance for the separation of the Gutenstein and Jósvafő Limestones was that in general the Gutenstein Limestone is often densely dissected by characteristic white calcite veins. Moreover, the Gutenstein Limestone is completely lack of inbenthos fauna elements that are present in the Szinpetri Formation, still this is also very hard to observe on the field (LESS ET AL. 2006).

The Lowermost Anisian deposition of the Gutenstein Limestone happened in deeper ramp environment (KOVÁCS ET AL. 1989). According to KOVÁCS (1984) the Gutenstein Limestone represents the earliest phase of the Neotethyan rifting. Within the study area this formation was mapped along the tourists' road N of Jósvafő at *Jsv-064—065 and Jsv-069—072* (see detailed description in *Chapter IV*). Here according to my observations, the boundary between the Jósvafő and the overlying Gutenstin Limestones at *Jsv-062—063* is tectonic.

Middle Triassic platform carbonates: T_2

According to Kovács (1984) intensive shallow water carbonate production started on the basement highs during the Anisian which resulted in the deposition of a very thick Middle Triassic platform carbonate sequence. Its thickness certainly reached at least a few hundred meters but certain well data *(Szi-1)* may even suggest more than 1000 m thickness. As the detailed categorization and mapping of the different platform carbonates were not part of this thesis, they were only delineated from other Lower Triassic formations and their boundary was studied in details, but all these rocks were mapped only as "Middle Triassic platform carbonates". These platform carbonates occurred in the northern parts of the study area, along the tourists' road N of Jósvafő at *Jsv-066—069*, in the surroundings of the Kuriszlán Spring at *Jsv-042—043, Jsv-045 and Jsv-047*, and along the road to Szelcepuszta at *Szn-003 and Szn-012—014*.

Rauhwackes: RW

Rauhwackes are basically breccias that consist of mainly carbonate clasts, matrix and cement (GYENGE 2017, SCHAAD 1995). Due to the different physical and chemical processes rauhwackes are often so altered that the original host rock cannot be identified any longer ***(Fig.12)***. Sometimes the litoclasts sitting in the matrix may be recognized and used for host rock identification. Just like a normal fault rock rauhwackes may contain litoclasts from every formations that they have been in contact with. The high porosity and typical "pitty" appearance of the rauhwackes are also attributed to chemical processes during which the easily dissolvable clasts and evaporites are dissolved. The formation of rauhwackes is still debated: some say rauhwackes are fully the results of sedimentary processes (KRAUTER 1971) whereas others believe they are partly or fully by tectonic processes (MILOVSKY ET AL. 1999). Furthermore, the appearance of rauhwackes is often connected to the presence of evaporites (e.g. in the Northern Calcareous Alps, LEITNER & SPÖTL 2017, SPÖTL 1989, WARREN 2016).

In the Aggtelek Mts. rauhwackes were already discovered during the geological mapping projects of the 1980's. Rauhwackes have never been subdivided into a separate formation but have always been categorized as part of other (surrounding) formations like Jósvafő or Gutenstein Limestones. Similarly to normal tectonic rocks, however, the genetics of the rauhwackes makes it necessary to separate them from other formations so during the field work rauhwackes were mapped separately. The most remarkable rauhwacke outcrops were found E of Jósvafő, along the main road *(Jsv-004, Jsv-031, Jsv-076, **Fig.12/a**)* and in the surroundings of the road to Szelcepuszta *(Szn-007, **Fig.12/b**)*.

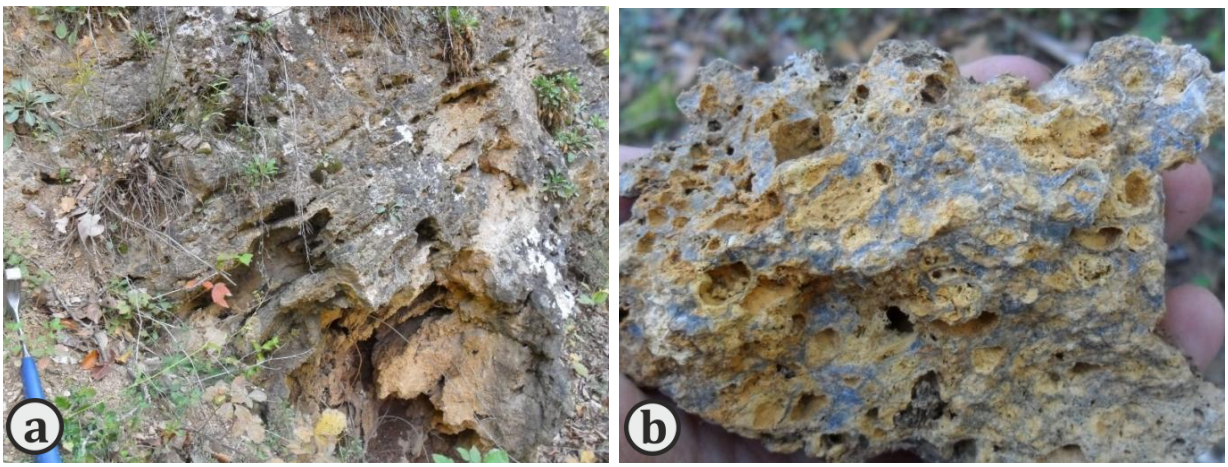

Fig.12. Field photos of rauhwackes. **A.)** In-situ rauhwacke E of Jósvafő at *Jsv-031*. **B.)** Rauhwacke sample collected at *Szn-007* in the wider surroundings of the road from Szin to Szelcepuszta.

II.4. Structural problems related to the Silica Unit

Understanding the origin and deformation history of the Silica Unit is still an enigmatic point in the tectonic development of the Alpine-Carpathian region. DUSAN PLAŠIENKA (2018) has just wrote in his latest monography on the evolution of the entire Western Carpathians that *"…the original paleogeographic position and emplacement time of the Silica nappes are the most ambiguous issues of the entire story presented in this article".* Different authors have different opinions about the

tectonic transport direction of the Silica Unit the question of which leads back to another even more essential question: where was the Silica Unit originally located during the first part of the Mesozoic? Does it come from the northern passive margin of the Neotethys Ocean or it originates from the southern margin?

Therefore, the principal question regarding the Silica Unit is to determine the direction (and age) of tectonic transport. Everybody agrees on the fact that the Silica Unit occupies the uppermost structural position in the nappe system of the Inner Western Carpathians (PLAŠIENKA ET AL. 1997). In addition to that the nappe boundaries meeting in triples junctions unequivocally imply that the Silica Unit has tectonic contacts with every other nappe, i.e. the Meliata, Torna and Gemer Nappes ***(Fig.3)***. In addition to being a major structural boundary, the base of the Silica Unit also represent a significant change in metamorphic grade with respect to the underlying units (ÁRKAI & KOVÁCS 1986, FARYAD & HENJES-KUNST 1997, KORIKOVSKY ET AL. 1997, PLAŠIENKA ET AL. 1999). Two solutions exist for this structural geometry: according to the first the lower boundary of the Silica Unit is a low-angle normal fault while the other solution suggests out-of-sequence thrusting ***(Fig.13)***.

Fig.13. Schematic models explaining the possible structural positions of the Silica Unit (modified after Deák-KÖVÉR 2012). **A.)** The contact between the Silica Unit and the other units is a post-nappe stacking low-angle normal fault. **B.)** The SIlica Nappe is in contact with every other structural unit by an out-of-sequence thrust.

Furthermore, the Silica Nappe is a so-called cover nappe or thin-skinned nappe whose Permian to Mesozoic formations were sheared off of their original Paleozoic basement which then travelled far from their original position and formed a thin but widespread allochtonous body. This makes the correlations even more difficult as the original basement of the Silica Cover Nappe is unknown.

One part of the geological society believes that the blue schist formations of the Meliata Unit mark the suture of the subducted Meliata Ocean (Rožnava Suture, MELLO ET AL. 1996, PLAŠIENKA ET AL. 1997). This would rightly imply that the Silica Unit must have come from the southern passive margin of the Neotethys Ocean (CSONTOS & VÖRÖS 2004, DALLMEYER ET AL. 2008, HÓK ET AL. 1995). This idea corresponds with the non-metamorfic character of the Silica Unit.

Most authors, however, put the Silica on the northern passive margin of the Neotethys Ocean due to its resemblances to facies types and deformation history of other northern units, particularly the Northern Calcareous Alps (HAAS ET AL. 1995, KOVÁCS 1984, KOVÁCS ET AL. 1989, KOZUR 1991, KOZUR & MOCK 1973, LESS 2000, SCHMID ET AL. 2008). Since during the closure of the Meliata Ocean it was the northern margin that subducted below the southern one, every northern unit should have been in lower plate position with respect to the suture zone of the Meliata Ocean. In a normal subductional geometry the lower plate position is inconsistent with the non-metamorphic state of the Silica nappes. SCHMID ET AL (2008) solved the contradiction with complex model: they imagined that while the primary in-sequence nappe stacking was north-vergent, a south-vergent back-trust placed the Silica Unit on the top of the obducted Meliata Unit and formed a triangle zone ***(Fig.14).*** If the back-

thrusting happened contemporaneously with the obduction, a triangle zone would explain how the Silica Unit escaped metamorphosis in spite of its original lower plate position.

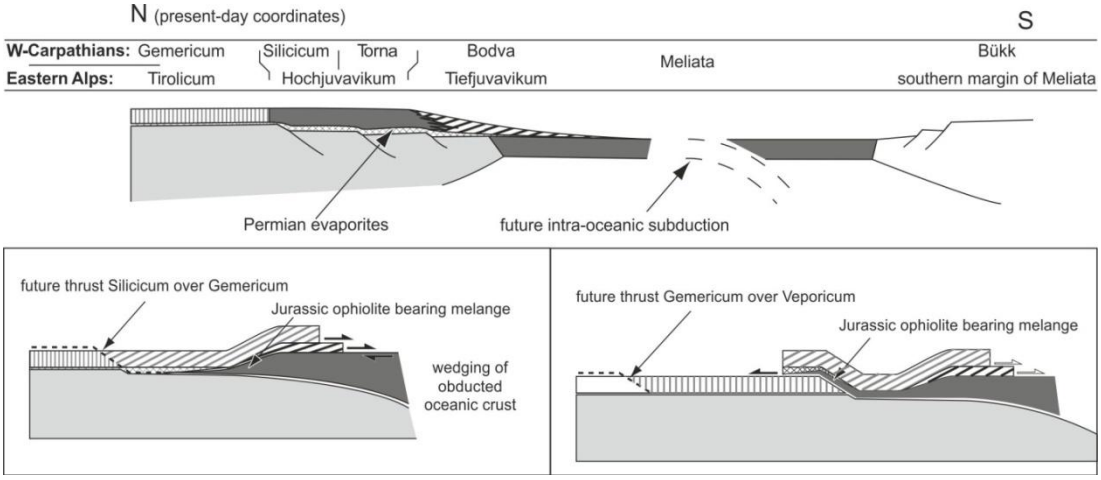

Fig.14. Triangle zone model of SCHMID ET AL. (2008). According to this model the Silica Unit was originally part of the subducting northern margin but a S-vergent back-thrust put the Silica Nappe over the obducting Meliata Unit in a triangle zone. This model may also explain why the Silica Unit is non-metamorphic.

DEÁK-KÖVÉR (2012) and KÖVÉR ET AL. (2018a) suggested another solution to the same contradiction: they took on the idea of the Late Jurassic to Early Cretaceous E-W transfer strike-slip fault zones of e.g. SCHMID ET AL. (2008) and STÜWE & SCHUSTER (2010) which presumably had an important role in shaping the paleogeographic arrangement of the different tectonic units within the western region of the Neotethys Ocean. The lateral (most probably sinistral) movements resulted in the re-positioning of the Silica Unit south of the Meliata Unit ***(Fig.15).*** During subsequent thrusting the Silica Unit would get into upper plate position.

The problem regarding the contradictional theories on the Mesozoic paleoposition and original tectonic transport direction of the Silica Unit roots in poorly understanding the field observations. In the Hungarian part of the Silica Nappe GRILL ET AL. (1984) and GRILL (1989) were ones of firsts to publish a specifically structural work on the deformation history of the Aggtelek-Rudabánya Mts. In their opinion the first NW-SE compressional deformation phase was followed by N-S compression. They did not state the tectonic transport direction of the Silica Nappe, only that they believed that the first phase was cotemporaneous with the formation of the Western Carpathian nappe system, and that the age of the N-S compression was Oligocene to Middle Miocene.

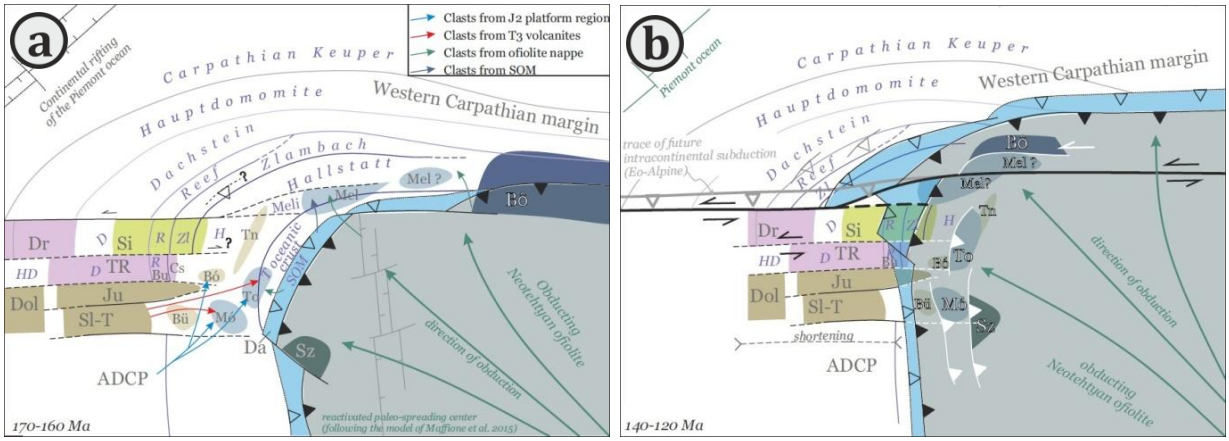

Fig.15. Palinspatic and tectonic reconstruction of KÖVÉR ET AL. (2018a) for the Neotethyan embayment in the **A.)** Middle to Late Jurassic and **B.)** in the Early Cretaceous. The Silica Unit (marked by Si on the map) got in the southern position relative to the Meliata Ocean (Mel) by moving along a sinistral strike-slip transfer fault prior to or contemporaneously with the Late Jurassic to Early Cretaceous nappe stacking. Consequently, during subduction the Silica Unit was in upper plate position which explains why it remained non-metamorphic even though it shows close relations to other units of the former northern margins.

Similarly to that, LESS (2000) suggested that the formation of the primary nappe structure is related to the N-ward subduction of the Meliata Ocean, thus he considered the original nappe transport direction was to the S. Similarly to Grill (1989) he dated the subsequent NW-SE compressional deformation phase as Miocene. In agreement with LESS (2000) HIPS (2001) considered the N-S compression as the first main shortening phase which was followed by NW-SE compression and perpendicular extension that resulted in NE-SW trending map-scale folds and thrust faults, young-on-older thrusts and E-W striking dextral strike-slip faults. HIPS (2001) separated a third folding event with NE-SW shortening direction. On the other hand, the results of KÖVÉR ET AL. (2009) and DEÁK-KÖVÉR (2012) from the Rudabánya Mts. showed that the primary nappe stacking was related to SE-vergent thrusting and that neither the NW-SE, nor the N-S directed shortening cannot be older than Late Cretaceous (based on their K/Ar data). SE of the study area of this MSc thesis, in the surroundings of Szőlősardó the observations of HORVÁTH ET AL. (2012) showed a first-order SE-vergent nappe stacking, a second N-S directed compressional event that resulted in young-on-older thrusts and a third NW-SE directed compressional event that reactivated the previous structures. They correlated this third reactivational event to the early Miocene (prior to Late Ottnangian) transpressional deformation of the nearby Darnó Deformation Belt.

II.5. Evaporites in the Aggtelek Mts.

The presence of evaporites, specifically the Perkupa Evaporite has always been known among mapping geologists but the deformation history of these evaporites and their role during the Cretaceous deformation has not been studied in details. The largest known outcrop of the evaporitic sequence is in the wide Bódva Valley where numerous wells was drilled during the active underground salt mining and exploration period during the second half of the 20th century. The deepest well here was the *Szn-1* well with its 1600 m depth which still did not drilled out of the Perkupa Evaporite ***(Fig.24)***. Still, it is widely accepted that this evaporitic succession lubricated the tectonic base of the Silica Nappe and worked as the main detachment level during the Cretaceous deformation (GRILL 1989, GRILL ET AL. 1984, GRILL & SZENTPÉTERY 1988, LESS 2000, LESS ET AL. 2006).

Moreover, several previous studies suggested that there may be isolated salt diapirs in other parts of the Aggtelek Mts., rooting in the Perkupa Evaporite (GRILL 1989, GRILL ET AL. 1988, HIPS 2001, LESS 2000, LESS ET AL. 2006, ZELENKA ET AL. 2005). They placed the supposed salt diapirs at the isolated occurrences of the lowermost Triassic surrounded completely by younger Lower or Middle Triassic formations (e.g. at the Bódvaszilas Sandstone occurrence in the Jósva Valley or at the Szin Marl occurrence in the Almás Valley). Some of these isolated "lenses" were targeted by cored drillings which ultimately confirmed the presence of the Perkupa Evaporite in shallow depths (i.e. Jő-2, Jő-3, Tk-3 wells, ***Fig.24***). According to the interpretation of LESS (2000) and HIPS (2001) these salt "injections" are located at push-up structures between NE-SW striking thrust faults and E-W trending lateral segments.

In their later work LESS ET AL. (2006) connected the formation of these salt diapirs to N-S directed compression and S-vergent folding during which the salt penetrated the cores of the anticlines. They believed that in the final stage of this folding process parts of the map-scale folds' limbs or even whole synclinal cores slid gravitationally into the cores of the anticline filled with evaporites ***(Fig.16)***. This idea was the latest interpretation for the occurrence of the Bódvaszilas Sandstone within the Jósvafő Formation and also for the whole Derenk Zone located W of Bódvaszilas and N of the main Middle Triassic platform area.

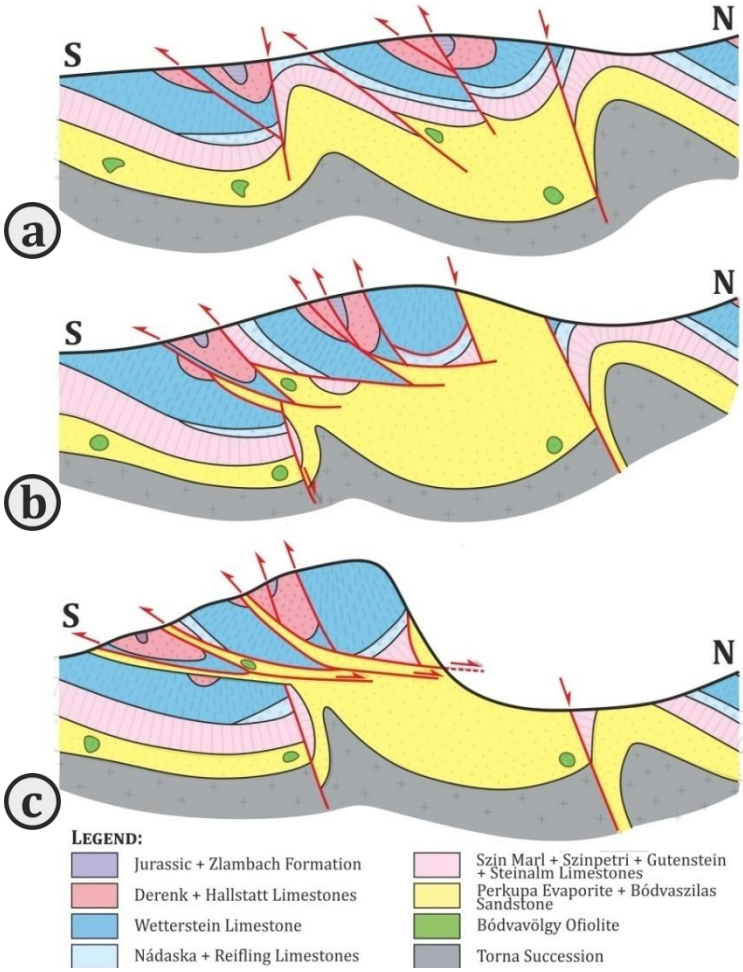

Fig.16. Schematic cross sections explaining the formation of the 'secondary nappes" in the model of LESS ET AL. (2006). **A.)** Initial evaporite mobilization contemporaneously with the S-vergent thrusting and folding. **B.)** Mature stage of the salt mobilization – the evaporites reach the surface. **C.)** Gravitational sliding of the klippes into the depression formed by the erosion of the Perkupa Evaporite (=secondary nappe formation).

II.6. Salt tectonics and related structures

Evaporites are typically not or had not always been in mechanical equilibrium with their surrounding rocks. This means that mechanically even completely dry salt rocks are weaker than any other sedimentary rock, except for completely extremely weak unconsolidated shales with less than 100 meters burial depths. The so-called wet salt rocks may, however, be even 100 times weaker than dry salt rocks, thus they are able to behave like a near Newton-type fluids (JACKSON & VENDEVILLE 1994, URAI ET AL. 1987). Moreover, while other rocks have their porosity gradually decreased and their density and mechanical strength increased during burial, the density of evaporites stagnates at a constant 2.2 g/cm3 after reaching 100-200m burial depth and they become nearly uncompressible until 6-8km depth (LEWIS & HOLNESS 1996). Considering all this, everywhere where salt rocks are present in the sedimentary record we have to count on them getting mobilized, and the deformation rate related to moving salt bodies may be very high even in geological time scale. This kind of deformation that is the result of the mobilized evaporites is called salt tectonics (or *halokinesis*).

The most dominant salt structures are probably the salt diapirs. Salt diapirs are by definition structures formed by flowing salt rocks whose geometry clearly reflects the weak mechanical properties of the evaporites, and which have discordant boundaries towards its surrounding rocks (WARREN 2016). The presence of the sedimentary cover thick enough is one of the basic conditions for the formation of salt diapirs. It is essential on one hand for putting enough (differential) loading on the primary salt body which is in fact a driving force to mobilize evaporites, but on the other hand, too thick sedimentary cover may hamper the salt from piercing through the cover and moving upward. In case of sufficiently big sedimentary loading diapirs may form even without regional extension, but extension makes the initiation of salt flowing substantially easier.

In extensional stress regime active and reactive diapirs may be distinguish based on the relationship of the diapir formation and regional extension (HUDEC & JACKSON 2007, VENDEVILLE & JACKSON 1992, ***Fig.17***). Active diapirs actively uplift and pierce their sedimentary covers while moving upward. The basic requirement for the formation of an active diapir is that the sedimentary cover should be thin enough for the salt pressure to be able to defeat the brittle strength of the cover. This means that active diapirs may initiate even when there are no faults present. Opposite to that, reactive diapirs initiate only at pre-existing normal faults which have already extended, thinned and weakened the sedimentary cover. In this case the evaporites do not pierce actively their cover but they only fill up the "holes" and weakened zones formed due to the regional extension. There is a third group of diapirs: passive diapirs form when a diapir reached the surface where it can flow out freely. Complying the boundary conditions a single diapir may change its type several times during its lifetime (e.g. from reactive diapir to active diapir and finally to passive diapir).

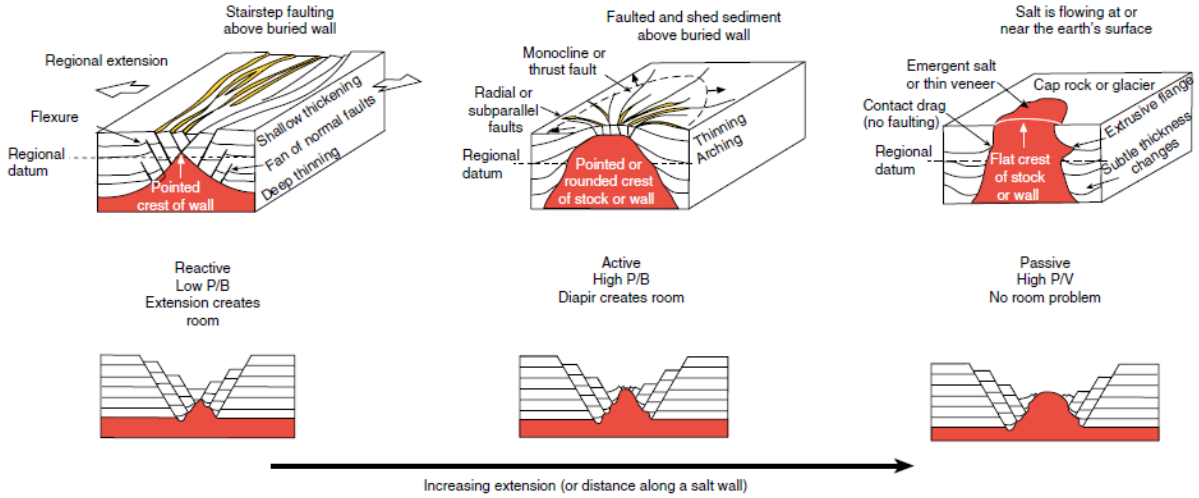

Fig.17. Types of diapir formation in extensional stress regimes (WARREN 2016). The formation of reactive diapirs is closely related to extensional faults while active dipairs may form independently of the pre-existing faults by actively uplifting and piercing their sedimentary cover. When a dipair reaches the surface it evolves into a passive dipair that may flow freely.

Even though flowing salt rocks are able to pierce their thin or thinned and weakened cover, active piercement and lateral displacement of the cover is not a diagnostic factor for defining salt diapirs. We may distinguish autochtonous and allochtonous salt structures. Autochtonous salts still have connection to the primary salt body situated in its original stratigraphical position while allochtonous salt structures are separated from the primary salt body and are usually migrated into stratigraphically younger structural positions (e.g. *teardrop structures, detached salt stocks and salt sheets,* ***Fig.18***). Based on their geometry salt diapirs may appear on the surface as isolated bodies *(salt stocks or salt plugs)*, concentric forms (e.g. mushroom shaped diapirs), linear zones *(salt walls, salt anticlines, salt rollers)* or in completely irregular shapes *(salt sheets, salt canopies)*.

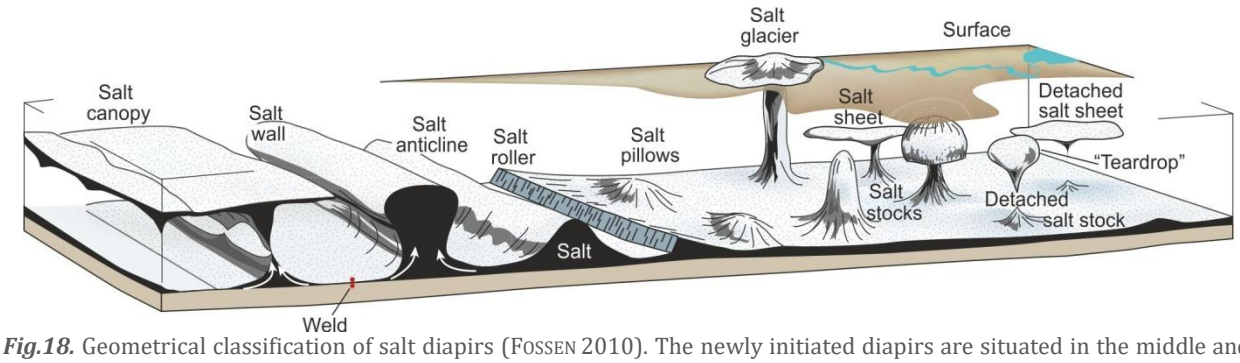

Fig.18. Geometrical classification of salt diapirs (FOSSEN 2010). The newly initiated diapirs are situated in the middle and the diapirs get more and more mature towards the edges. Linear type of diapirs are to the left, isolated column-like diapirs are to the right.

Let's take the simplest case of a single salt stock or salt plug into consideration. When the upward moving salt stock pierces through its sedimentary cover, the country rocks are dragged concentrically around the stock. Due to this drag folding the measurable dips face concentrically outward and the dip angles also decreases outward. Somewhat away from the salt stock the effect of the drag folding is negligible, what is more, the cover start to sink as more and more evaporite is getting sucked out of the primary salt body, from under the surrounding sedimentary cover in order to maintain the upward growth of the salt stock ***(Fig.19)***. The sinking related to this effect lasts until the whole evaporitic body is moved into the growing salt stock and the primary salt body

runs out. When this happens, the base and top of the primary salt body touches along a surface which is called *primary salt weld* (WAGNER III & JACKSON 2016). The small-scale asymmetric basin forming around the salt diapir is called a *rim syncline*. In special cases *minibasins* may form which are basins surrounded on every side by evaporites (CALLOT ET AL. 2016, JACKSON & TALBOT 1991, HUDEC ET AL. 2009, LEHNER 1969, TRUSHEIM 1960, WORREL & SNELSON 1989, ***Fig.19***).

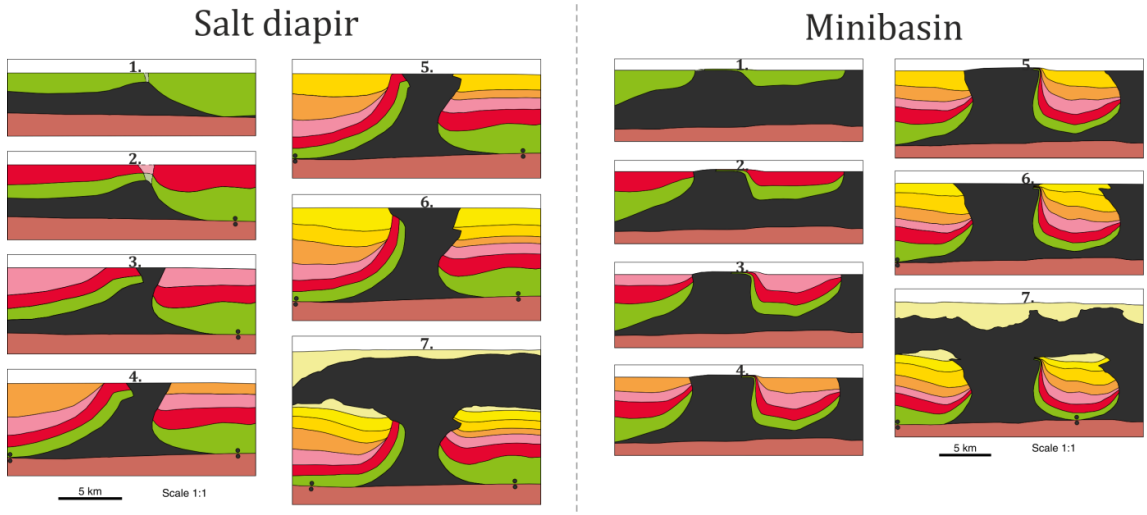

Fig.19. Schematic sections showing the syn-sedimentary growth of a salt diapir and a minibasin (ROWAN ET AL. 2016). The thickening strata and unconformities are clear signs of the syn-sedimentary salt tectonics. The two black circles on the two sides of the surfaces mark the places of primary salt welds.

Besides drag folding unconformities and extreme thickness variations in the syn-halokinetic successions are also characteristic features of minibasins. Be it any type of stress regime the country rocks may steepen even until sub-vertical or overturned positions within a relative narrow zone around the upward moving salt bodies. Depending on the scale of drag folding *halokinetic sequences* or *composite halokinetic sequences* may be identified within a basin (GILES & LAWTON 2002, ROWAN ET AL. 2003, ***Fig.20***). These sedimentary sequences thicken towards the middle of the basins and thin towards the salt stocks, and they often contains unconformities. When the country rocks are dragged in such an extreme manner that they become sub-vertical or overturned and the scale of the dragging reaches around 1 km, the folded strata is called a *megaflap* (ROWAN ET AL. 2016, ***Fig.20***).

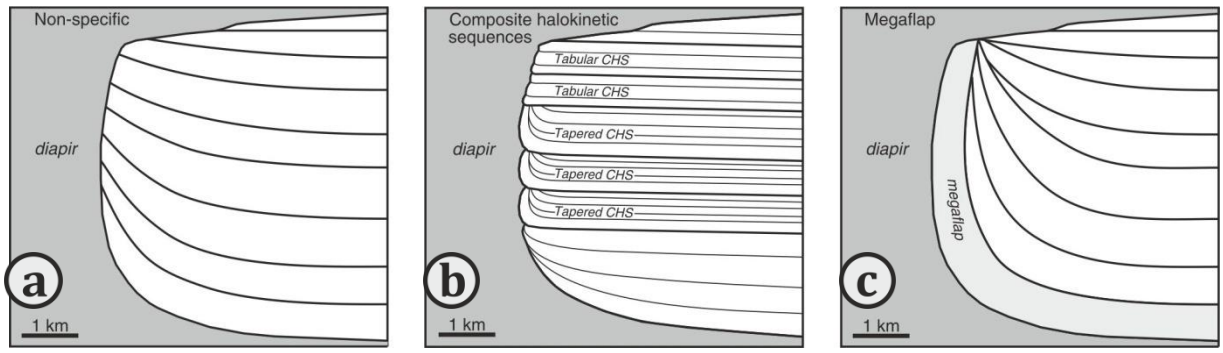

Fig.20. Types of drag folding around salt diapirs (ROWAN ET AL. 2016). **A.)** Simple drag folding. **B.)** Composite halokinetic sequence with multiple unconformity surfaces and near-vertical dragged strata within the narrow zone surrounding the diapir. **C.)** Km-scale extreme drag folding with sub-vertical or even overturned strata (megaflaps).

In extensional regimes the exact nature and deformation geometry of the salt tectonics depends on the timing of salt deposition and salt tectonics with respect to the the temporal and areal evolution

of the rift basin. Following the work of PÉRON-PINVIDIC ET AL. (2013) on rift margins' structural evolution ROWAN (2014) separated pre-rift, syn-stretching, syn-thinning and syn-exhumation salt-bearing rift basins in passive margin environments. **Pre-rift salts** are deposited prior to the initiation of rifting so they are fully affected by the subsequent stretching. In pre-rift salt basins this means that while the base of the salt is offset by normal faults (thick-skinned extension), the sedimentary cover sequence above the evaporite is only dragged and forms drape folds above basement-involved faults (JACKSON & VENDEVILLE 1994, ROWAN 2014). In **syn-stretching salt basins** the salt is deposited syn-kinematically with the active normal faults and the half-graben formation (thick-skinned extension), consequently its thickness varies from place to place (ROWAN 2014). The difference between pre-rift and syn-stretching salt is that in syn-stretching basins the evaporites get mobilized almost immediately after the deposition and if a thin sedimentary cover begins to seal the evaporites, it will also be stretched, the salt quickly pierces through it and reactive diapirism initiate (HUDEC & JACKSON 2007, VENDEVILLE & JACKSON 1992). As the diapirs continue to grow, the minibasins slowly sink into the evaporites until no evaporite remains below the basin (primary salt weld, JACKSON ET AL. 2014, WAGNER III & JACKSON 2016). In the **thinning and hyperextension phase** of PÉRON-PÉNVIDIC ET AL. (2013) the syn-kinematic salt becomes an extremely important detachment media that decouples the deformation of the basement from the mainly gravity driven extension of the sedimentary cover above (thin-skinned extension, ***Fig.21***, ROWAN 2014, JAMMES ET AL. 2010). The most common structural features in this gravity-driven salt-deformation system are the (low-angle) normal faults and extension-related salt structures in the updip areas, and folding and contractional salt deformation (e.g. weld formation, salt-cored anticlines) in the downdip areas (BRUN & FORT 2011, MARTON ET AL. 2000, WARREN 2016). Similar gravity-driven systems appear in **syn-exhumation salt basins** as well where the evaporites may have direct sedimentary contacts with the exhumed (and serpentinized) mantle rocks (Rowan 2014).

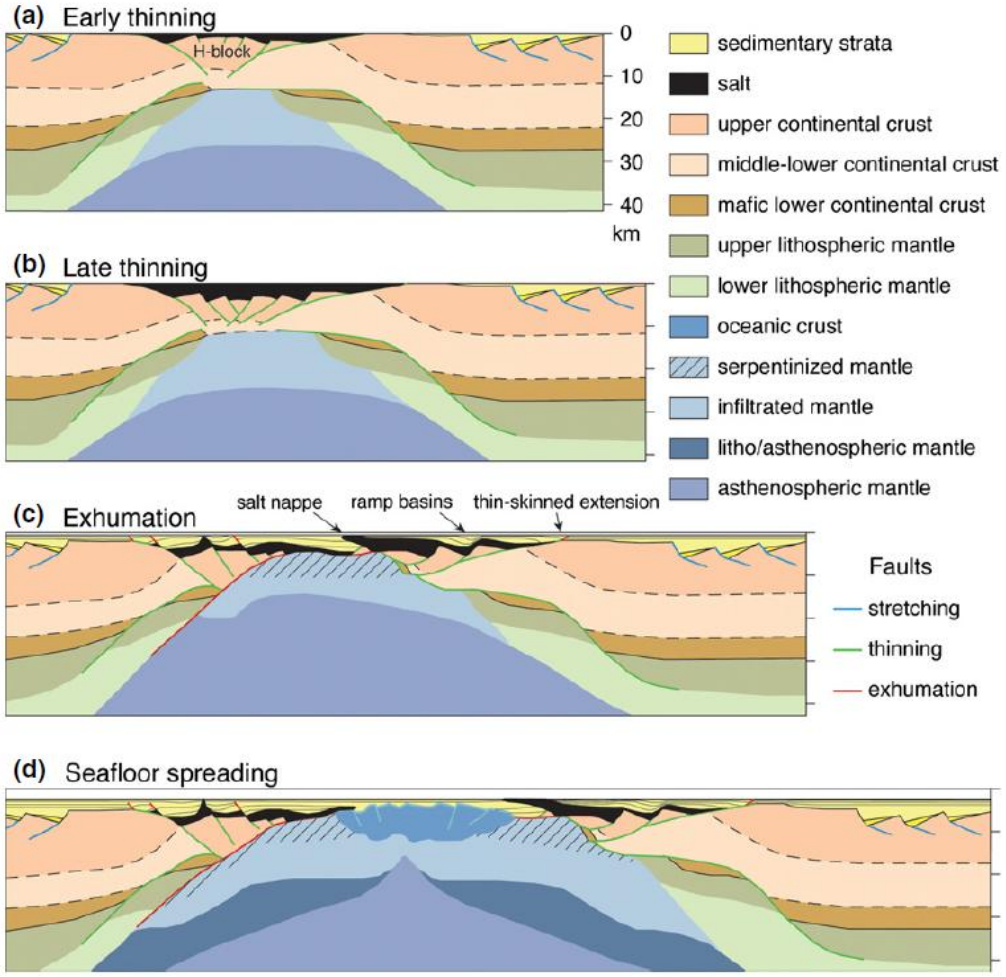

Fig.21. Schematic model of a syn-thinning salt basin (ROWAN 2014, modified after PÉRON-PINVIDIC ET AL. 2013). **A.)** Early stage of thinning with syn-tectonic salt deposition. **B.)** Formation of large thinning faults in the later stage of the thinning phase. **C.)** Exhumation phase with the initiation of thin-skinned gravity-driven salt tectonics (salt diapirism, salt nappe formation). The evaporites may get in direct tectonic contact with serpentinized mantle rocks. **D.)** Initiation of the oceanic spreading with continuous thin-skinned deformation and salt diapirism.

In a compressional stress regime the salt gets mobilized (again). During this mobilization the salt moves towards the smallest resistance so it often uses and reactivates pre-existing weakness zones, i.e. faults and fractures. As more and more salt leaves, the opposite sides of the salt structure get closer and closer until they get in direct contact (squeezed diapir). This surface along which the opposite sides of the salt structure touch is called a *secondary salt weld* (WAGNER III & JACKSON 2016, ***Fig.22***). Along this weld we may often (but not necessarily) experience structural discordance. Another characteristic feature of the welds is that the rocks are very altered in the narrow zone within which breccias, rauhwackes and non-dissolvable clay residuals mark the place of the late salt rocks that have already been squeezed out.

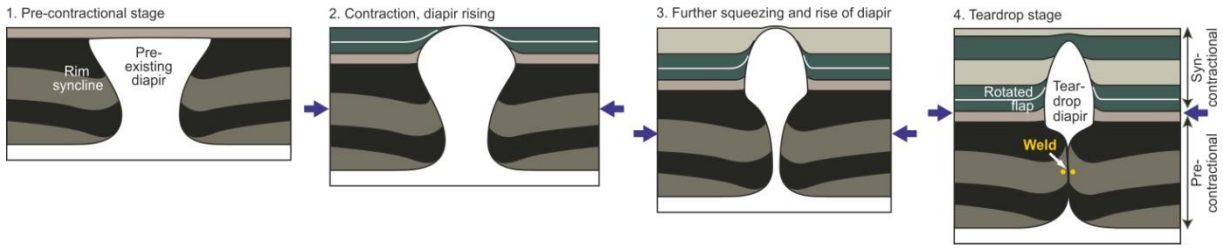

Fig.22. Flow diagram showing the formation of a secondary salt weld (modified by HUDEC & JACKSON 2007 after FOSSEN 2010). Due to compression the salt diapir starts to grow in vertical direction and as the salt gets squeezed out, the two opposite sides of the structures get in touch along the surface of the secondary salt weld.

III. APPLIED METHODS

III.1. Delineation of the study area

I began my thesis work with the analysis of the previous geological maps of the Aggtelek Mts. – e.g. the geological and structural maps of LESS ET AL. (1988), the geological map of the Lower Triassic formations by HIPS (2001) and the carbonatic reef map of PÉRÓ ET AL. (2015). Based on these maps several structurally interesting smaller areas were selected in the eastern part of the Aggtelek Mts. for detailed mapping ***(Fig.23)***. In this area the stratigraphy of the Lower Triassic formations is very well known (Hips 1995) and these formations are usually well bedded and easy to measure, the Middle Triassic formations are thick bedded platform carbonates in which it is normally very hard to do any structural observations, even carrying out dip measurements. The primary targets for studying salt structures were the isolated lens-like outcrops of the lowermost Lower Triassic formations surrounded by higher stratigraphic units (e.g. the Bódvaszilas Sandstone in the area around the Jő-2 well or the Szin Marl at the head of the Almás Valley and around the Jő-3 well).

III.2. Field observations and measurements

Detailed structural mapping of the selected study areas was carried out between the summer of 2018 and the spring of 2019. Mapping was coupled by lithological observations and sample collection with oriented sampling where relevant for later optical microscopic observations and paleontological dating. Every observation locality was assigned a unique identity code, GPS coordinates in EOV system (Hungarian National Grid) and the measured data. The coordinates of the observed outcrops are presented in *Appendix 1*. In significant and complex outcrops structural observations were recorded as field drawings in a field textbook as well. Dip and structural data (e.g. fold axis and faults with or without striae) were measured by a Freiberg-type geological compass. Nineteen observation maps were prepared (see them in *Chapter IV*).

III.3. Fault-slip analysis and fold axis estimations

Digitalization and evaluation of the measured field data was carried out in the program package of Professor Angelier (ANGELIER 1984). The measured data of the different localities were first imported into the MEASURE program separately and the “raw” data were displayed on stereoplots by using the DIAGRA and TRADUC programs.

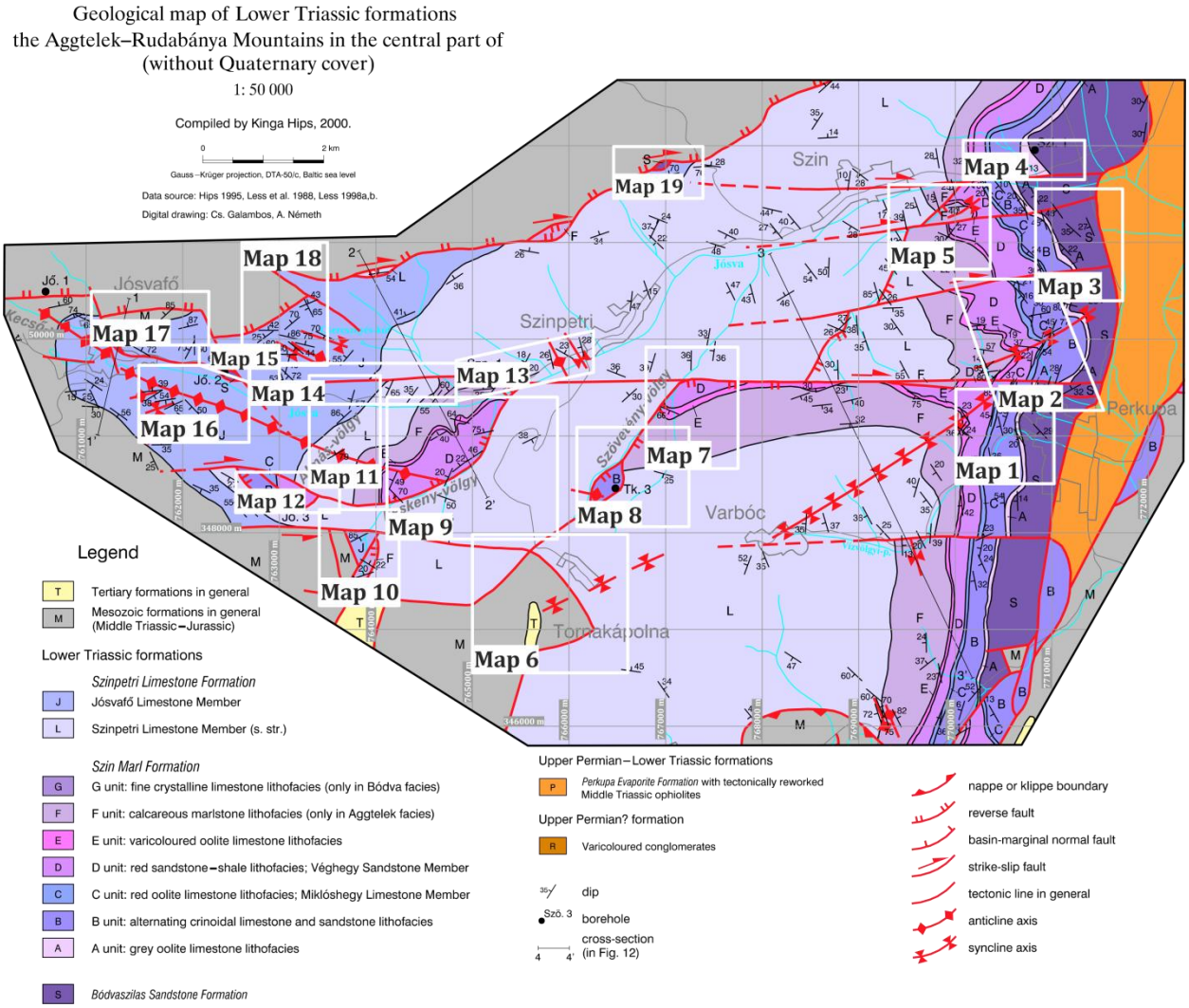

Fig.23. Geological map of the Lower Triassic formations in the eastern part of the Aggtelek Mts (HIPS 2001). White squares border the mapped areas during my thesis work. The observation maps of these areas are presented in *Chapter IV.*

Data evaluation was carried out in two steps: the data were first evaluated separately for every outcrop, then the results of the individual outcrops were merged and interpreted together. As a final step deformation phases were separated and their possible relative chronological order was set. Where the structural geometry suggested pre-tilt origin tilt-tests were done in the ROTILT program. In case of positive outputs (proved pre-tilt nature) the back-tilted data were used for the rest of the evaluation process. Separation of the deformation phases was done either manually by graphically separating the stereoplots in Corel Draw or automatically by the PHASES program. Automatic separation was only possible if at least four faults with striae were measured from the same phase. Similarly, if at least four faults with striae got grouped together after merging the data from the different localities but from the same deformation phases, automatic tensor calculations became possible by using the TENSOR program. For the lack of four faults with striae only manually estimated stress field could be given for the given deformation phase. The separated field data and their stereoplots are shown in *Appendix 3* with legend in *Appendix 2*.

III.4. Digital database, geological map and cross-section construction

In order to build a digital geological database the previously published geological maps (e.g. LESS ET AL. 1988, HIPS 2001) were first georeferenced, i.e. the maps stored as raster files were given the proper coordinates in EOV coordinate system. Then all available data and stratigraphical column of every relevant well located within the study area were collected from the well database of the MBFSZ[1] and were compiled into a single Excel table ***(Fig.24)***.

Two geological databases were built in two different sofwares in order to exploit the advantages of both programs. The database built in Global Mapper contains the previously published geological maps, observation localities, dip data, as well as information for the mapped formations. The greatest advantage of the Global Mapper is that both the observation maps and the Pre-Cenozoic geological map could be easily constructed in it and the result is a relatively easily exportable vectorgraphic file. The constructred observation maps that contain only my observations and data are presented in *Chapter IV*, while the interpreted geological-structural map is shown in *Appendix 4*. For the final geological map I took over some observations of LESS AT AL. (1988) and Hips (2001) in the areas where my own data was not enough or completely absent.

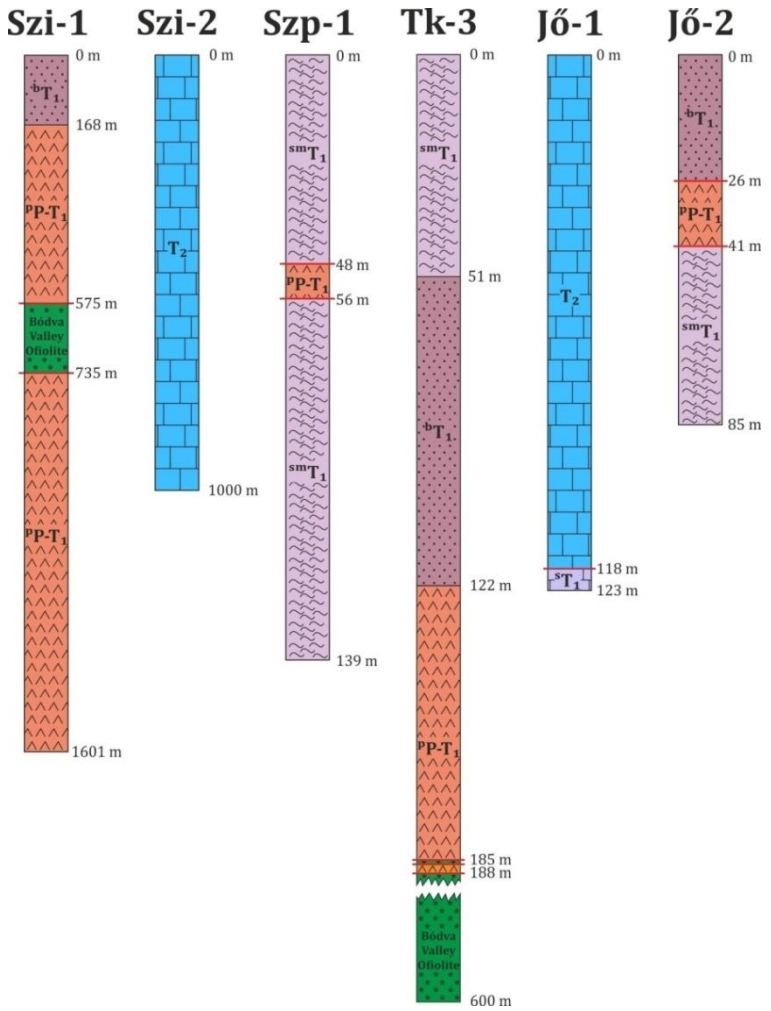

Fig.24. Stratigraphical columns of the most important wells in the study area. The exact location of the wells are shown in *Appendix 4*. The vertical scale of the first two columns is 1:10 000, whereas for the other four columns it is 1:1 000.

[1] Hungarian State Geological, Geophysical and Mining Databank

On the contrary, the advantage of the MOVE software developed by Midland Valley is that it is able to work with 3D data and modeling so both the structural interpretation and the cross-section construction were carried out in MOVE. After importing the geological maps, my own field data and the compiled well data, I also manually digitalized the dip data shown on the geological map of LESS ET AL. (1988) and HIPS (2001) in order to improve the amount of available data. The dips and well data were projected into cross-sections that run more or less perpendicular to the strike of the main structures and parallel to the general dip direction. The applied projection was usually "Normal to Section" but in the few cases where the sections were oblique to the strike of the structures, the plunge azimuth was set manually. In the end four geological cross-sections were constructed that are presented in the text as ***Section 1, Section 2*** and ***Section 3***.

IV. FIELD OBSERVATIONS

Field observations are discussed in several sections. The division of these sections was based on the areal location of the discussed outcrops (see the coordinates of the observation points in *Appendix 1*). Enlarged observation maps were constructed for each sub-chapter in order to make the text more understandable and the structural context more evident.

IV.1. Perkupa and the valley of the Vízvölgy Creek

A continuous sedimentary succession starting with the Bódvaszilas Sandstone and ending in the F member of the Szin Marl is outcropped W and SW of Perkupa, along the road towards Varbóc, in the valley of Vízvölgy Creek *(**Map 1,** Per-018, Per-019—024, Per-080—088, Per-102—109).* Up until the top of the C member of the Szin Marl seemingly undisturbed, shallow and moderate (~20-40°) dips are towards W or rarely SW. While there are no map-scale structures, only monoclinal dips, small centimeter or decimeter-scale folds do appear locally in the relatively thick B member of the Szin Marl (***Fig.25*** in *Per-019,* ***Fig.26*** in *Per-088*). After the C member of the Szin Marl the only well outcropped continuous section was found at *Per-087* where the 2-30 cm thick shale, marl and sandstone layers are heavily folded ***(Fig.28)***. At the contact between the C and D members the measured dips became steeper and steeper, until they reached 55-60°. Most of the outcrops are in a really poor condition, therefore only the most important outcrops of the valley of the Vízvölgy Creek will be introduced in details here.

Important outcrops in the valley of the Vízvölgy Creek:

Per-019: $^{sm/B}T_1$

At *Per-019* slightly asymmetric overturned folds with top-to-S vergency appear in thin marl beds ***(Fig.25/a).*** The folding detaches on the top of a thick undeformed limestone bed (detachment fold) while the top of the folds are truncated by the next un-deformed thin marl beds. Based on their interlimb angles the folds are tight folds. Within the hinge zone some deformed beds thicken (similar fold) while the upper part of the fold is overturned.

Beside the folds, brittle structures are also present in this outcrop: even though they don't have easily measureable discrete fault planes – it is like their fault planes have been sealed – shallow thrust faults with WNW-ESE strike cross-cut each other in the thicker carbonate beds ***(Fig.25/b)***.

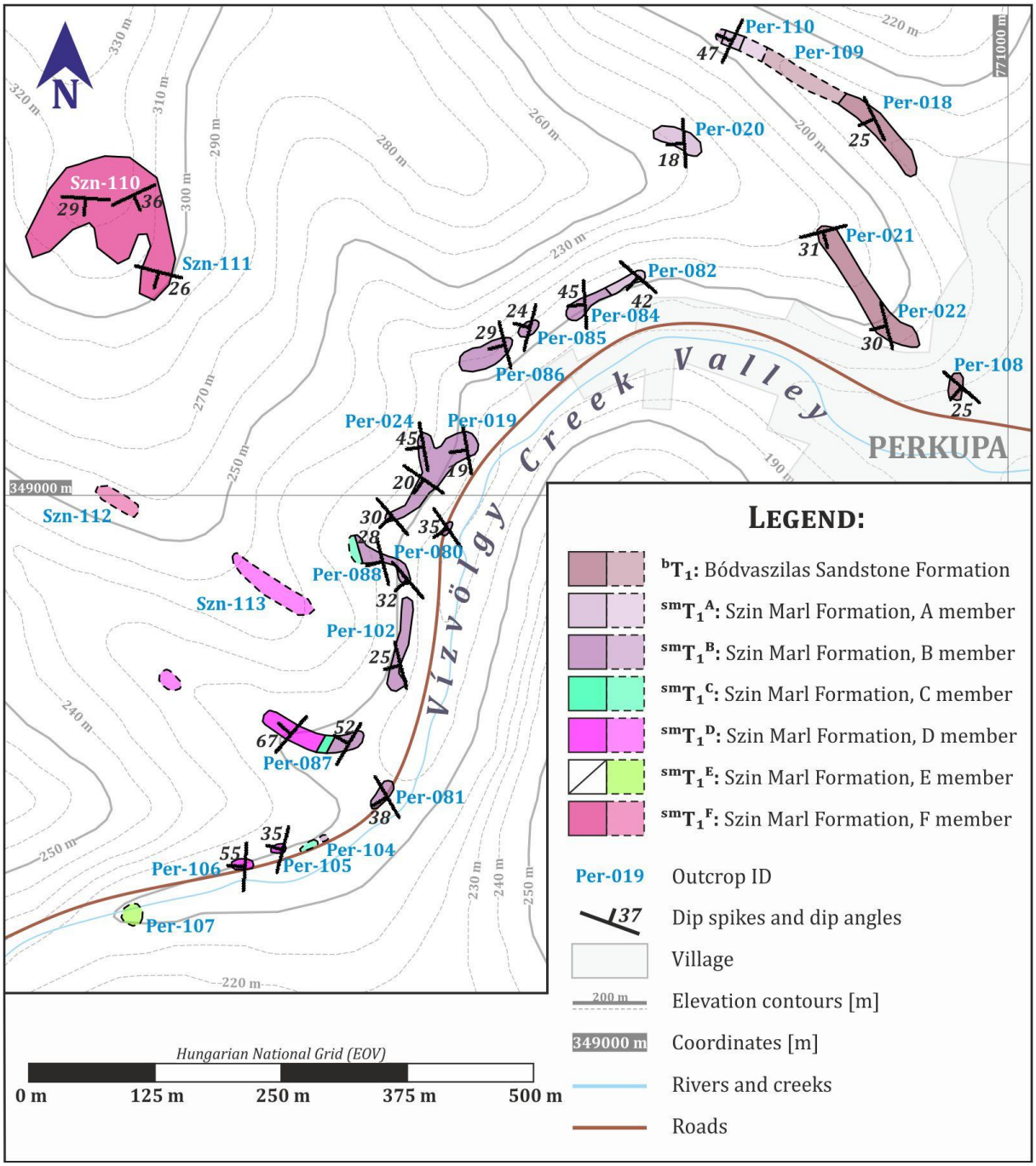

Map 1. Observation map of Perkupa and the valley of the Vízvölgy Creek. This area outcrops a continuous sedimentary succession between the Bódvaszilas Sandstone and the uppermost F member of the Szin Marl.

There are thrusts dipping toward both S and N, but since most thrust faults dip towards N and it's the N-ward dipping thrusts that cut the other thrusts, the overall vergency of the brittle thrust faults is top-to-S while the S-ward dipping thrusts are considered to be back-thrusts. These thrust faults are also sealed by the next thin marl beds so they never continue in the subsequent thick limestone beds. If the imaginary symmetry axis of the opposite dipping thrust faults would be drawn, it would be perpendicular to the undisturbed bedding (~20° towards WSW-SW, ***Fig.25/b***). The tilt-test carried out on the measured detachment fold data gave a positive result as well (the fold axis became completely horizontal after the tilt-test). Additional WSW-ENE trending normal faults and calcite veins were also found that discreetly cross-cut the marl and limestone beds, suggesting NNW-SSE extension *(Appendix 3)*.

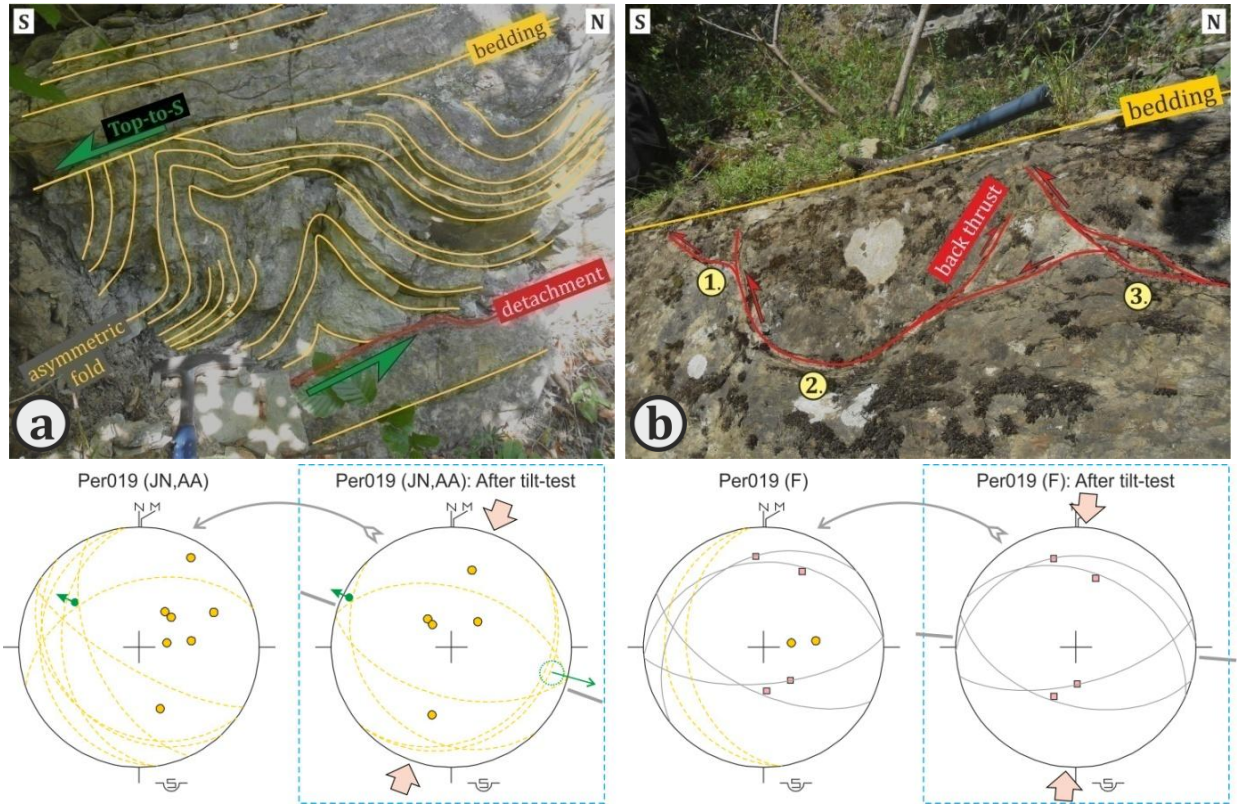

Fig.25. Detachment fold and small-scale thrust faults in the Szin Marl at *Per-019*. **A.)** Asymmetric detachment fold (slump fold) with thickness variations and top-to-S vergency. The fold is truncated by the subsequent undeformed beds. **B.)** Small-scale cross-cutting (early) thrust faults in the upper part of a thick limestone bed. Just like the detachment fold, the thrusts show top-to-S vergency and they are sealed by the subsequent undeformed beds. **Stereoplots** show the measured data (to the left) and the back-tilted data (to the right). The general legend of the stereoplots can be found in the *Appendix 2*.

Per-088: $^{sm/B}T_1$

Another outcrop-scale fold was found at *Per-088* where WSW-ward directed shallow (~30°) dips turn into SSE-directed moderate (~50°) dips. The geometry of this asymmetric open fold suggests top-to-SE vergency ***(Fig.26)***. Additional oblique thrust faults were found as well which were formed in a NW-SE compressional stress-field.

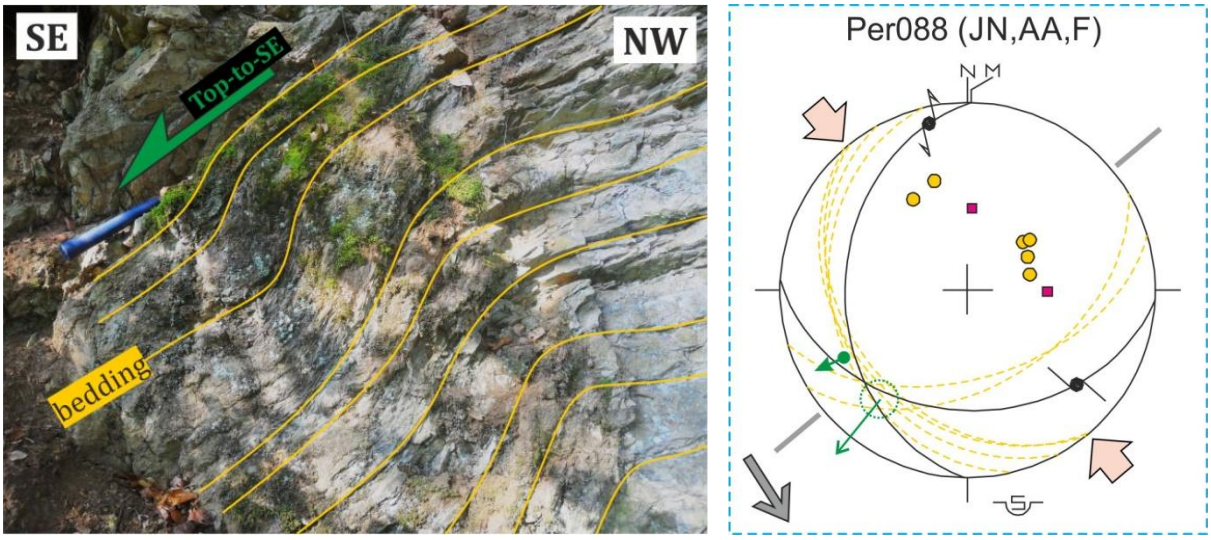

Fig.26. Asymmetric open fold and oblique thrust faults found at *Per-088*, indicating top-to-SE vergency.

Per-087: $^{sm/B\text{-}C\text{-}D}T_1$

In the heavily folded section of *Per-087* the observed folds are usually tight Chevron-type similar folds with angular hinge zones and layer parallel shearing along the limbs ***(Fig.27, Fig.28/a)***. Unfortunately the sense of shearing could not be determined. The wavelength of these folds is approximately 20-30m. Folds with rounded hinge zones also occur but due to space problems intense deformation is present in their hinge zones: while the incompetent marls and siltstones deform relatively easily, the more competent layers deform in a more brittle way and form imbricates within the core of the folds ***(Fig.28/b)***. There are also some decimeter-scale S- and Z-folds: the Z-folds were observed on the western limbs and most S-folds on the steeper eastern limbs, but a few special cases S-folds occurred on the western limbs as well.

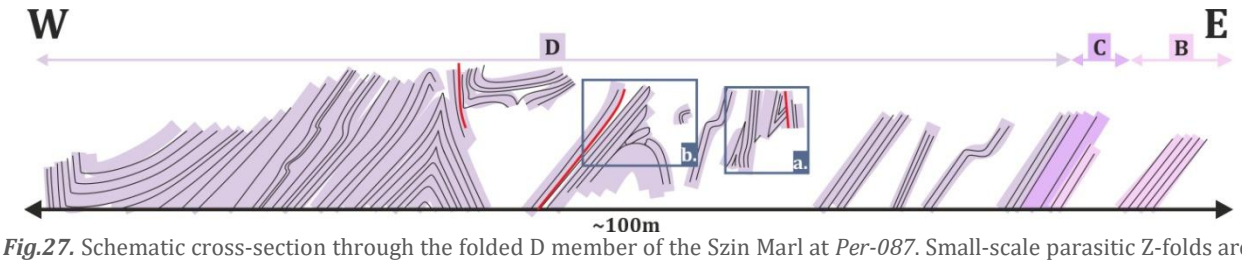

Fig.27. Schematic cross-section through the folded D member of the Szin Marl at *Per-087*. Small-scale parasitic Z-folds are positioned on the western limbs, whereas the S-folds were observed on the steeper eastern limbs. The blue frames mark the place for the detailed field photos presented in ***Fig.28***.

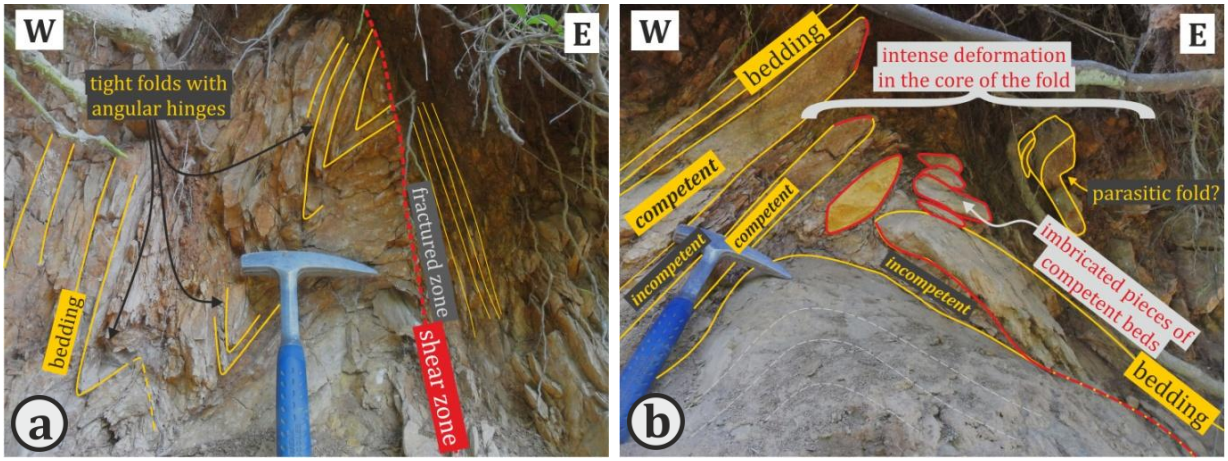

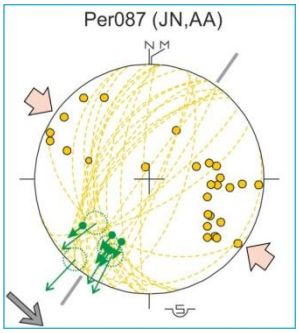

Fig.28. Field photos of the folded D member of the Szin Marl at *Per-087*. **A.)** Interpreted field photo of Chevron-type fight folds. **B.)** Detailed photo of a deformed hinge zone of an angular open fold. While the incompetent marl and shale layers deformed relatively easily, the more competent limestone deformed in a brittle way and formed imbricates within the hinge zone. **Stereoplot** of the measured and estimated fold axis suggests SE vergency.

IV.2. The area N of Perkupa, the Vég and Gelleház Valleys

The old underground anhydrite mine of Perkupa was located in the northern end of the village, right at the entrance of the Vég Valley. On the hillside above the closed pit there is an abandoned

quarry which was opened in the late '80s specifically for producing rocks for plugging the underground mine. This quarry outcrops the sedimentary contact of the Bódvaszilas Sandstone and the A member of the Szin Marl *(Per-089)*. Both dip shallowly (~30°) towards N ***(Map 2)***. After the A member in-situ outcrops of the B member followed in the Vég Valley. At *Per-001* the grey and riffle-green colored shale-rich formation with the occasional relatively thick bedded limestone intercalations was identified as the typical lowermost part of the B member, while more and more carbonates appeared towards the upper parts at *Per-003*. The general dip of the B member is 40° towards W at *Per-001* and 25° towards SW between *Per-002—003*. This means that even though a continuous sedimentary transition is assumable between the A and lowermost B members, a sharp change in dip direction was observed between the *Per-089* and *Per-001* outcrops. Adding to the supposed continuous sedimentary transition, the apparent dextral offset of the formation boundaries in the Vég Valley and everything else W and SW of Perkupa (*Per-018, Per-020* and *Per-109—110* on ***Map 2***) implies that there must be a structural element running approximately in E-W direction.

After *Per-003* another sharp change in dip direction was observed: at *Per-092* the C member of the Szin Marl dips moderately (~45°) towards NNW ***(Map 2)***. From this point on a very complex structural situation follows and sometimes even identifying the outcropped formation itself proved to be a difficult task. The C member being a marker member of the Szin Marl is easily identifiable, e.g. at *Per-092 and Per-094*, but the division of the thin bedded limestones, siltstones and sandstones was questionable. ***Fig.29*** shows the schematic cross-section drawn in the middle part of the Vég Valley: while in the lowermost and uppermost parts of the valley at *Per-001—003 and Per-010—012* the same, seemingly undisturbed SW-ward shallow dips were observed, in the middle the measured dips steepened until sub-vertical or even overturned positions while the dip direction changes to N-ward or S-ward. Based on the measurements ~E-W trending open synclines and tight to isoclinal anticlines may be reconstructed. The synclines and anticlines do not form a continuously folded succession, however, but there is always a clear displacement within the cores of the anticlines, meaning that the fold limbs are offset relative to each other along approximately the axial planes of the anticlines.

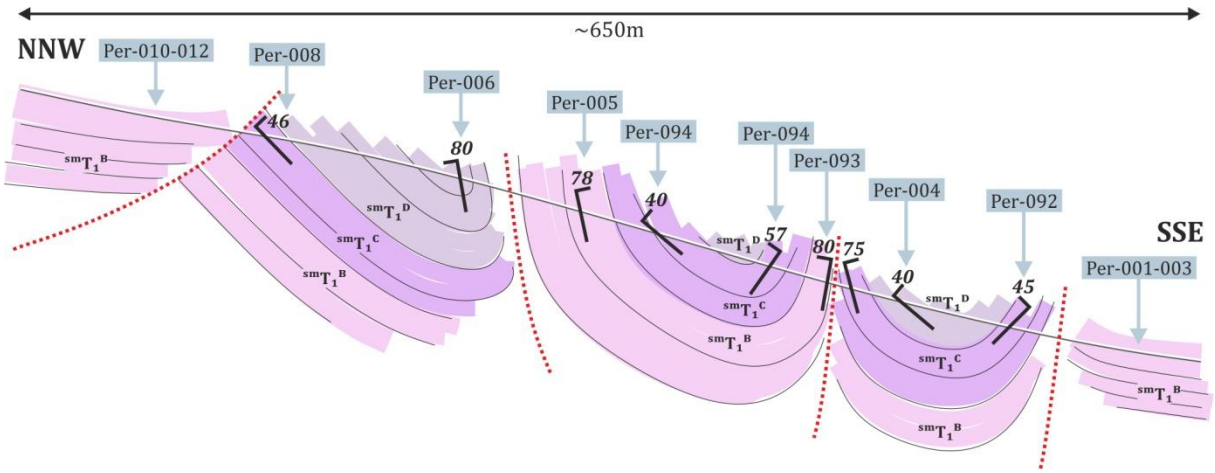

Fig.29. Schematic cross-section through the middle part of the Vég Valley. The measured dips indicate that the Szin Marl is folded into open synclines and tight to isoclinal anticlines, and that the limbs of the anticlines are offset relative to each other along approximately the axial planes of the anticlines. See the position of the section in ***Map 2***.

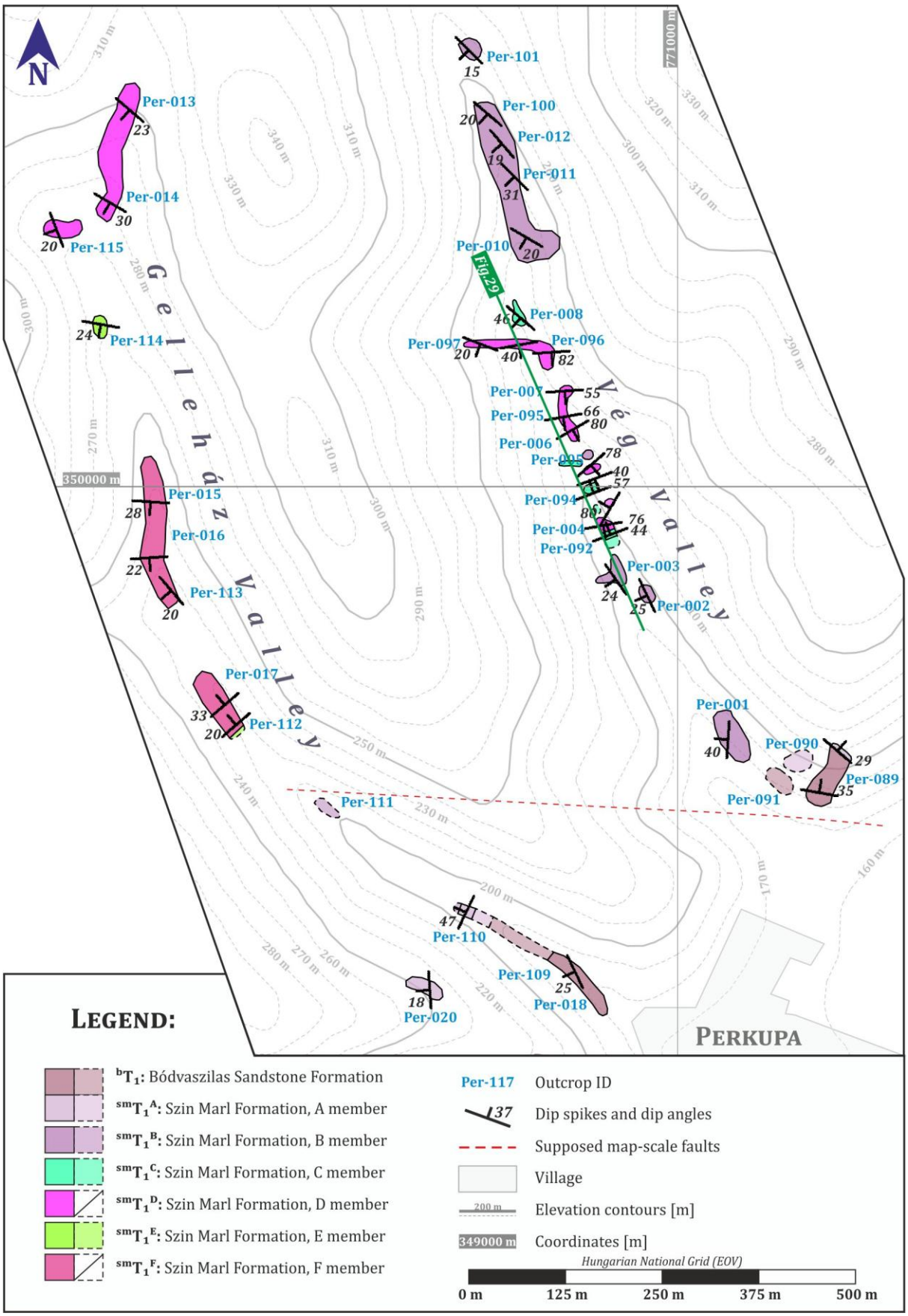

Map 2. Observation map of the northern part of Perkupa, the Vég and Gelleház Valleys. The green line is the cross-section trajectory for ***Fig.29***.

In the upper part of the Gelleház Valley – that is parallel to the Vég Valley – the D member of the Szin Marl has in-situ outcrops *(Per-013—014, Per-115)*. The measured dips are shallow (20-30°)

SW-ward or WSW-ward dips which are consistent with the dip data of the B member measured in the Vég Valley at *Per-010—012*, thus they form a continuous succession. At *Per-114* a few light grey, almost white limestone beds were discovered and interpreted as the E marker member of the Szin Marl. Here there is a change in dip direction: the E member dip shallowly (~25°) towards S. This S-ward dip may be followed to *Per-015—016* where the F member is outcropped. At *Per-113* the F member suddenly takes a turn towards SW, then at *Per-017 and Per-112* towards NW. These sharp changes in dip directions reflect folding of the Szin Marl. As in the next outcrop at *Per-111* already the B member appears, the C-D-E members are missing. This discordance is probably the same as the one observed between the northern parts of Perkupa and the abandoned quarry at the underground salt mine at *Per-089*. Finally in the lower part of the Gelleház Valley *Per-109* outcrops a continuous section of the A-B members of the Szin Marl and the Bódvaszilas Sandstone. The measured dips are shallow to moderate (20-45°) toward W and SW.

Relatively spectacular outcrops were found only in the Vég Valley, therefore in the following section I am describing these most important outcrops in the next section.

Important outcrops in the Vég Valley:

Per-001: $^{sm/B}T_1$

In the southwestern side of the *Per-001* the fine-grained siliciclastic beds are folded into asymmetric overturned folds ***(Fig.30)***. The interesting thing about the folds is that while the fold axes of the folds are similar, completely opposite vergencies are present in the outcrop: there are 3-5 cm scale folds with top-to-SE vergency in the marls in the western part of the section which detach on thicker and more competent underformed limestone beds ***(Fig.30/a)***, whereas the larger, 50-60 cm scale folding in the middle of the section shows WNW vergency ***(Fig.30/b)***. The latter folds seem to be detachment folds as well and there are onlap surfaces within the fold limbs ***(Fig.31/a)***.

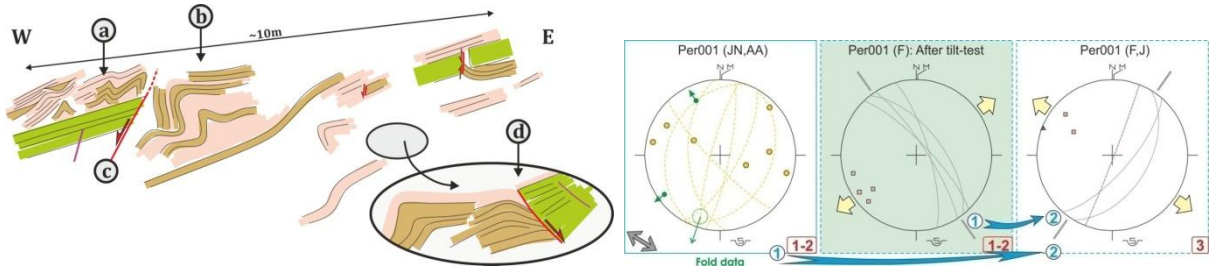

Fig.30. Schematic field drawing of *Per-001* showing detachment folding of the incompetent layers and small-scale normal faulting. There are onlap surfaces within the folded strata as well as sealed (syn-sedimentary) normal faults. **Stereoplots** show the separated field data.

The folds are overprinted by a high-angle discrete NNE-SSW trending fault (probably a normal fault, ***Fig.30/c***). Beside this fault and parallel fractures, perpendicular NW-SE striking small-scale discrete faults were measured as well, these faults are, however, sealed and their tilt-tests gave positive results ***(Fig.30/d)***. There are also normal drag folds along the faults ***(Fig.31/b)***. All in all, stereoplots of the measured data suggest approximately WNW-ESE directed folding, a pre-tilt NE-SW extension and NW-SE post-tilt extension ***(Fig.30)***.

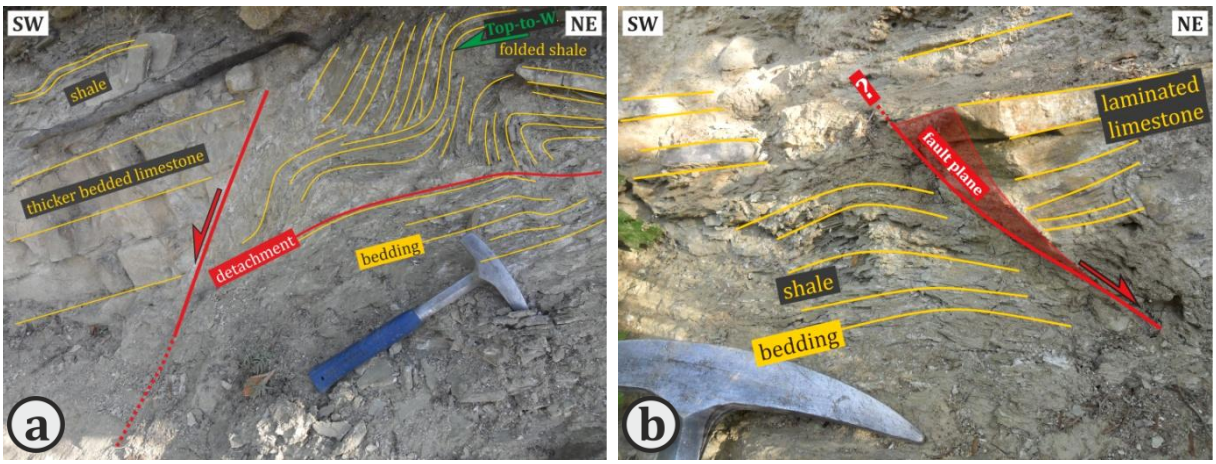

Fig.31. Field photos from *Per-001*. **A.)** Zoomed-in photo of the folded shales which contain onlap surfaces. The folds are overprinted by fault movement along a NW-ward dipping high-angle discrete fault (**a-b-c** parts of ***Fig.30***). **B.)** Field photo of a sealed small-scale (syn-sedimentary) normal fault with normal drag folds (**d** part of ***Fig.30***).

Per-003: $^{sm/B}T_1$

At *Per-003* the thick bedded limestones and thin-bedded marls are reversely offset along N-ward dipping shallow discrete faults ***(Fig.32)***. Upon reaching the layer boundaries the faults usually flatten into the bedding plane or at least it runs along the bedding plane for some time before cross-cutting again the subsequent layer. The fractures all together form a flat-ramp-flat geometry within a S-vergent compressional duplex system (***Fig.32/a*** stereoplot). Along some of the faults reverse drag folds were found with E-W trending fold axis while further fold-like features were interpreted as dewatering structures. Interestingly, the strike of the axis of the sedimentary structures is also E-W (***Fig.32/b*** stereoplot).

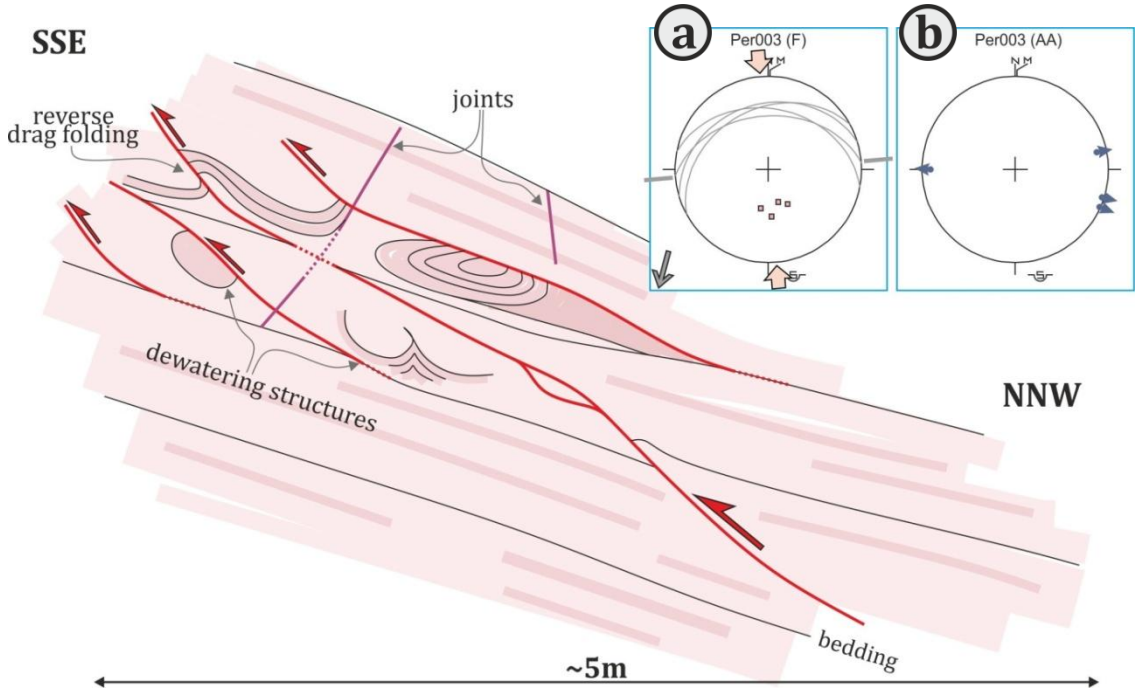

Fig.32. Field section and stereoplots of the measured fault data at *Per-003*. The N-ward dipping thrust faults usually flatten into the bedding planes, forming flat-ramp-flat geometry. Altogether the faults form a compressional duplex system.

Per-010—011: $^{sm/B}T_1$

At *Per-010—011* oppositely dipping normal faults were found in the B member of the Szin Marl. The faults cross-cut the bedding at approximately 60°, meaning that their symmetry axes are perpendicular to the bedding ***(Fig.33)***. At *Per-011* the faults cannot be followed upward at some point so they seem to be sealed by the subsequent limestone beds. The tilt-test carried out on the faults gave positive results, the back-tilted data thus suggest pre-tilt N-S extension.

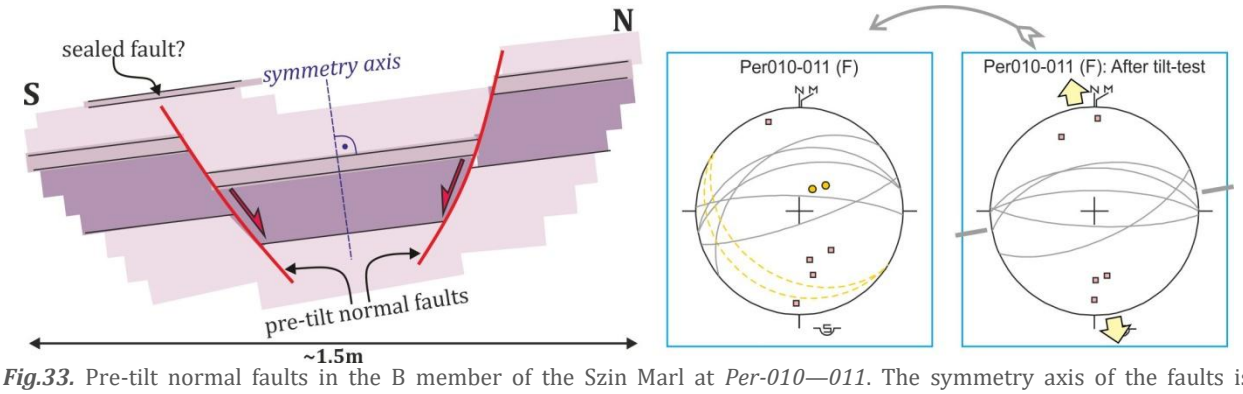

Fig.33. Pre-tilt normal faults in the B member of the Szin Marl at *Per-010—011*. The symmetry axis of the faults is perpendicular to the bedding. **Stereoplot** of the back-tilted data shows N-S extension.

IV.3. Outcrops around the Jósvafő-Aggtelek train station

In the Szerelem Valley which is located S of the Jósvafő-Aggtelek train station typical red sandstones of the Bódvaszilas Sandstone Formation with high mica content are outcropped along a foresters' roadcut *(**Map 3**, Per-062—065).* Here shallow to moderate (15-35°) dips were measured with S, SW or W dip directions. At *Per-066* detritus of thin bedded grey colored, fine grained limestones were found which may as well be the remnants of the A member of the Szin Marl. The same continuous sedimentary succession was observed W of the train station ***(Map 3)***. Here both the Bódvaszilas Sandstone and the B member of the Szin Marl dip monotonously towards SW-SSW with various dip angles ranging between 10 and 50° *(Per-031—036, Per-38—040, Per-067—068)*. The A and C members appear only in detritus.

In this area *Per-063* (in the Szerelem Valley) was the only outcrop in reasonably good condition so in the next section this outcrop will be introduced in details.

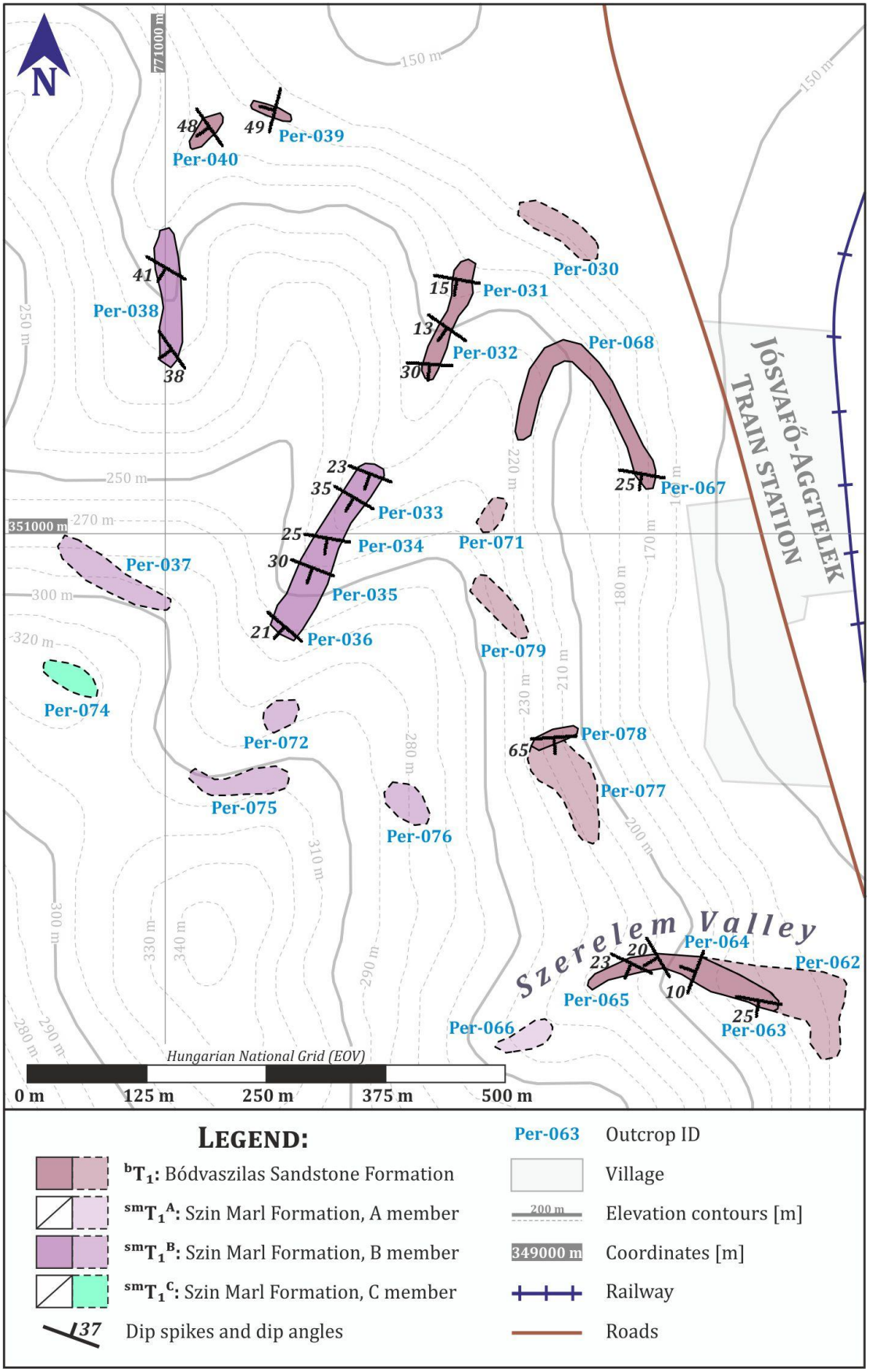

Map 3. Observation map of the area around the Jósvafő-Aggtelek train station. This area outcrops the lowermost part of the Lower Triassic – the Bódvaszilas Sandstone and the Szin Marl.

Most important outcrop of the Szerelem Valley:

Per-063: $^{b}T_1$

In the outcrop of *Per-063* normal faults and joints cut through 3-20 cm thick red sandstone layers ***(Fig.34)***. One of the main characteristics of these fractures is that after a point they cannot be followed upward so they are sealed by the subsequent undeformed beds ***(Fig. 34/a)***. The offset along the faults is a few centimeters. Although the general dip of the sandstone is relatively shallow here (20° towards S), the symmetry axis of the normal fault and joint conjugate pairs seems to be parallel to the normal vector of the bedding. Normal drag folds formed along some of the faults but in a single case, inverse drag folds appear as well next to the normal drag folds, suggesting compressional reactivation of the extensional faults ***(Fig. 34/b)***. This also sets a relative chronological order between the two different deformational phases: approximately E-W extension was followed by (oblique?) compression along pre-existing high angle fractures. Thickening of beds towards the faults are also evident at some places and in one case onlaping of sandstone layers on the surfaces of the normal drag folds can also be observed.

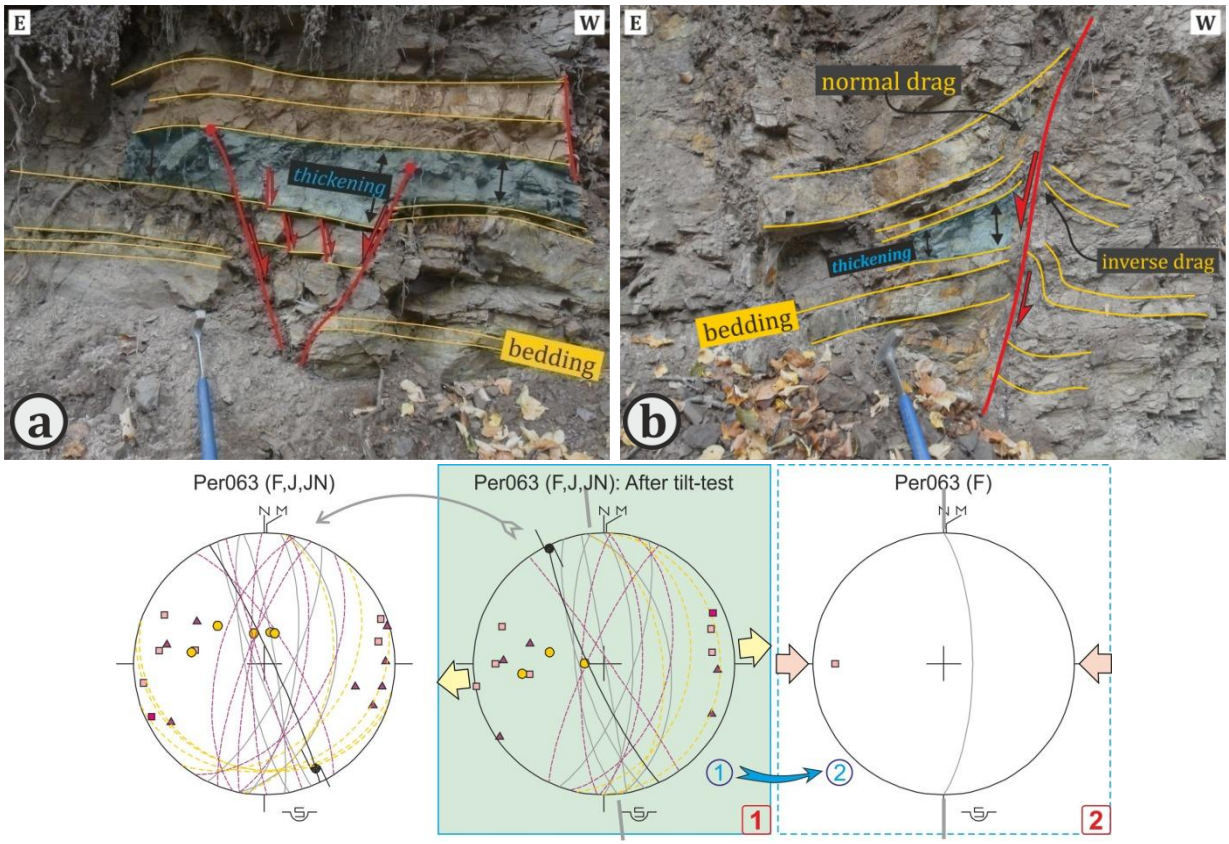

Fig.34. Normal faults in the Bódvaszilas Sandstone at *Per-063*. **A.)** Symmetric normal fault conjugate pairs sealed by subsequent undeformed beds. Thickening of the sandstone beds towards the faults was observed (syn-sedimentary deformation). **B.)** Normal drag folds and inverse dragging observed at the same high-angle fault, indicating compressional reactivation of the pre-existing normal faults. **Stereoplots** show the measured and back-tilted data.

IV.4. The Szn-1 well and its closer surroundings

In the junction of the 27th main street towards Szin a continuous sedimentary succession was observed starting with the Bódvaszilas Sandstone and ending with the B member of the Szin Marl

(Map 4). The measured shallow to moderate (15-35°) dips show a general W-ward younging direction *(Per-025—027 and Per-116—120)*. The *Szi-1* well drilled very close to the road junction went through first 168 m of Bódvaszilas Sandstone, then drilled Perkupa Evaporite down until 1601 m ***(Fig.24)***. In the following very nice outcrops and quarries will be described in details along the road, from E to W.

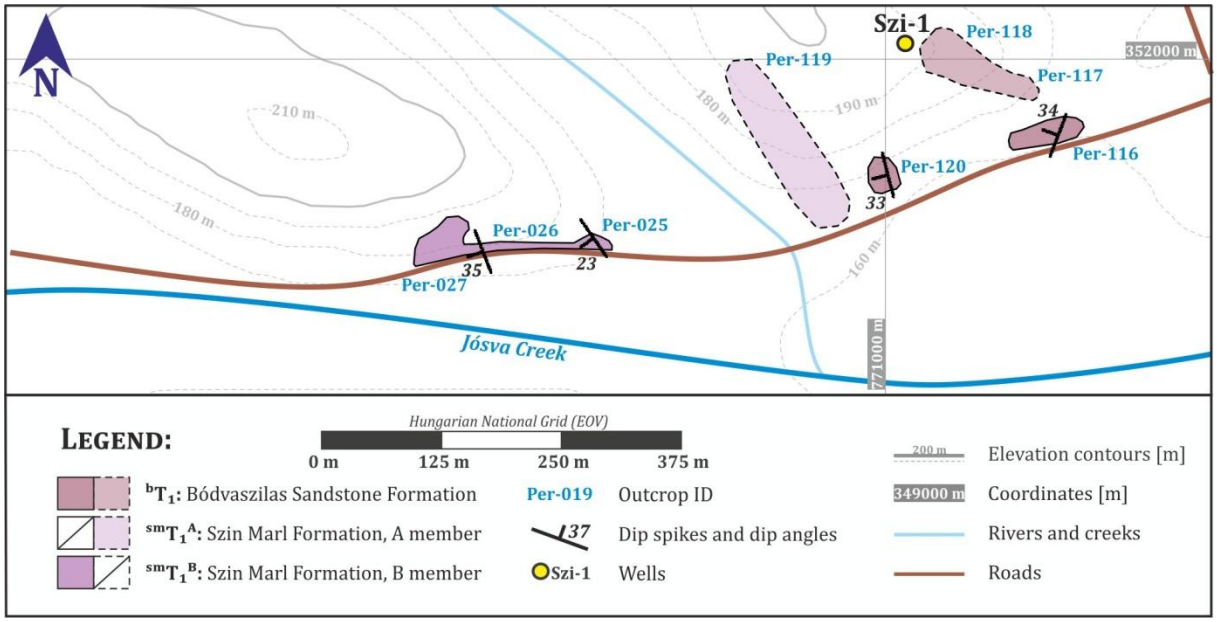

Map 4. Observation map of the area E of Szin which outcrops a continuous sedimentary succession between the Bódvaszilas Sandstone and the B member of the Szin Marl.

Important outcrops E of Szin:

Per-116: $^{b}T_1$

In the Bódvaszilas Sandstone small-scale folding was observed within two layers. The folded beds show lateral thickness variations. They are also covered by the subsequent undeformed layers while the folds detach on the underlying layers ***(Fig.35)***. Elsewhere in the *Per-116* outcrop small-scale NW-SE trending normal faults and joints were found with very small (mm to cm scale) offsets, intermediate or steep (53-75°) dip angles and NE or SW dip directions. The symmetry axis of the oppositely dipping fractures is perpendicular to the bedding. The deformation along these fractures is confined to only one layer in every case.

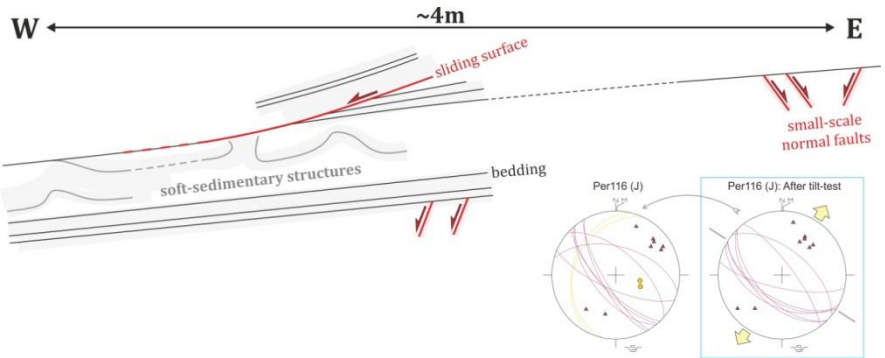

Fig.35. Normal faults and sedimentary deformation (dewatering) structures observed in the Bódvaszilas Sandstone at *Per-116*. The stereoplots show the measured and back-tilted data – the latter clearly became more symmetric after tilt-correction.

Per-025: $^{sm/b}T_1$

While the A member of the Szin Marl is only found in detritus at *Per-119*, the B member has two important outcrops here. In the *Per-025* section two major oppositely dipping high-angle faults and several small-scale normal faults were observed ***(Fig.36)***. Based on the normal drag folds along the fault planes the two major faults are probably normal faults, calcite syn-kinematic minerals or striations proving the normal kinematics of the faults, however, were not found at all. The offset along one of the faults is unknown, at least 2 meters but probably more, whereas the other has around 60 cm offset. The smaller normal faults observed in the footwall of one of the major faults usually deforms only two or three layers before getting sealed by the subsequent underformed layers. Discrete fault planes only appear in more competent limestone layers while in incompetent marls and shales the faults can only be followed with difficulty or they quickly flatten into the bedding. Moreover, in the upper part of the section the marl layers onlap on the surface of the normal drag folds in the hanging wall of the major normal faults. As the strike of the tilted normal faults is NNW-SSE an approximately ENE-WSW extension can be estimated.

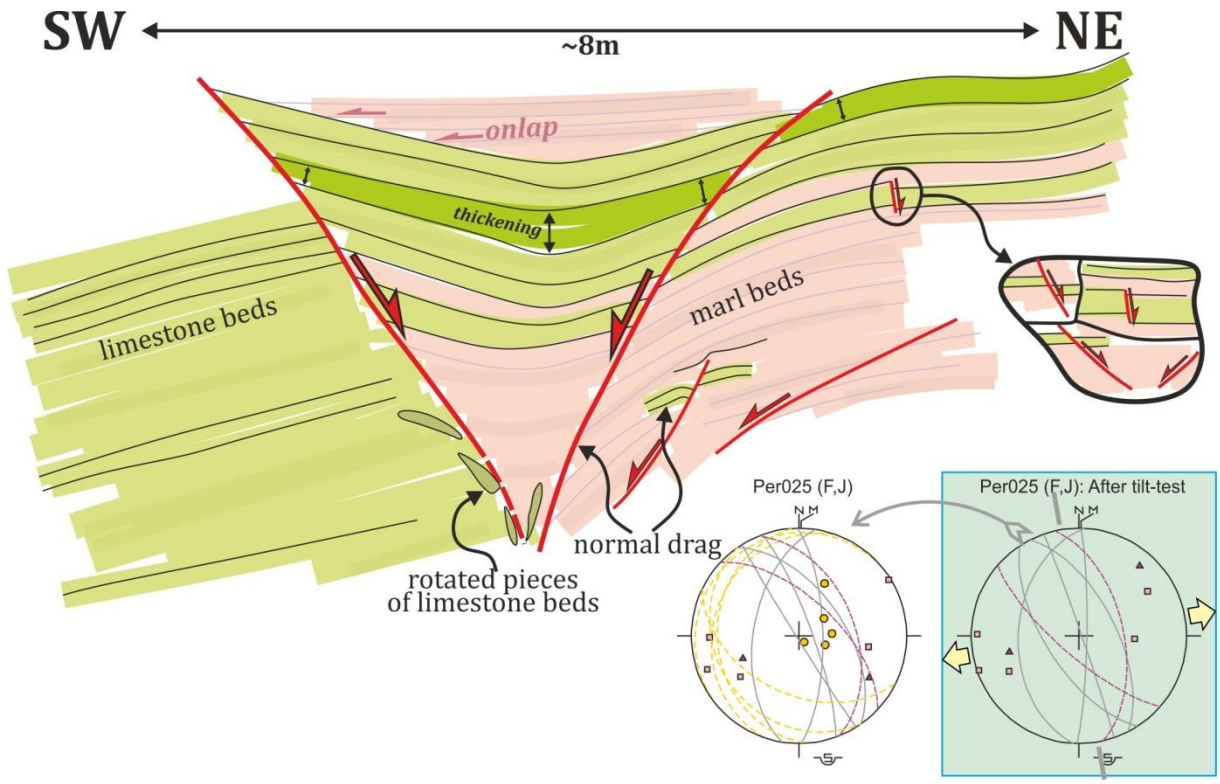

Fig.36. Normal faults in the Szin Marl at *Per-025*. Normal drag folds indicate normal fault kinematics along the two major faults of the outcrops. Thickness variations, onlap surfaces and sealed small-scale normal faults were also observed suggesting syn-sedimentary deformation. The **stereoplots** show the positive results of the tilt-test carried out on the measured normal fault data.

Per-027: $^{sm/b}T_1$

Normal faults with similar geometrical characteristics were observed in the quarry located at the *Per-027* point as well. The difference is that beside normal drag folds reverse drag folds are also present along the faults, implying that the faults were reactivated at least once ***(Fig.37).***

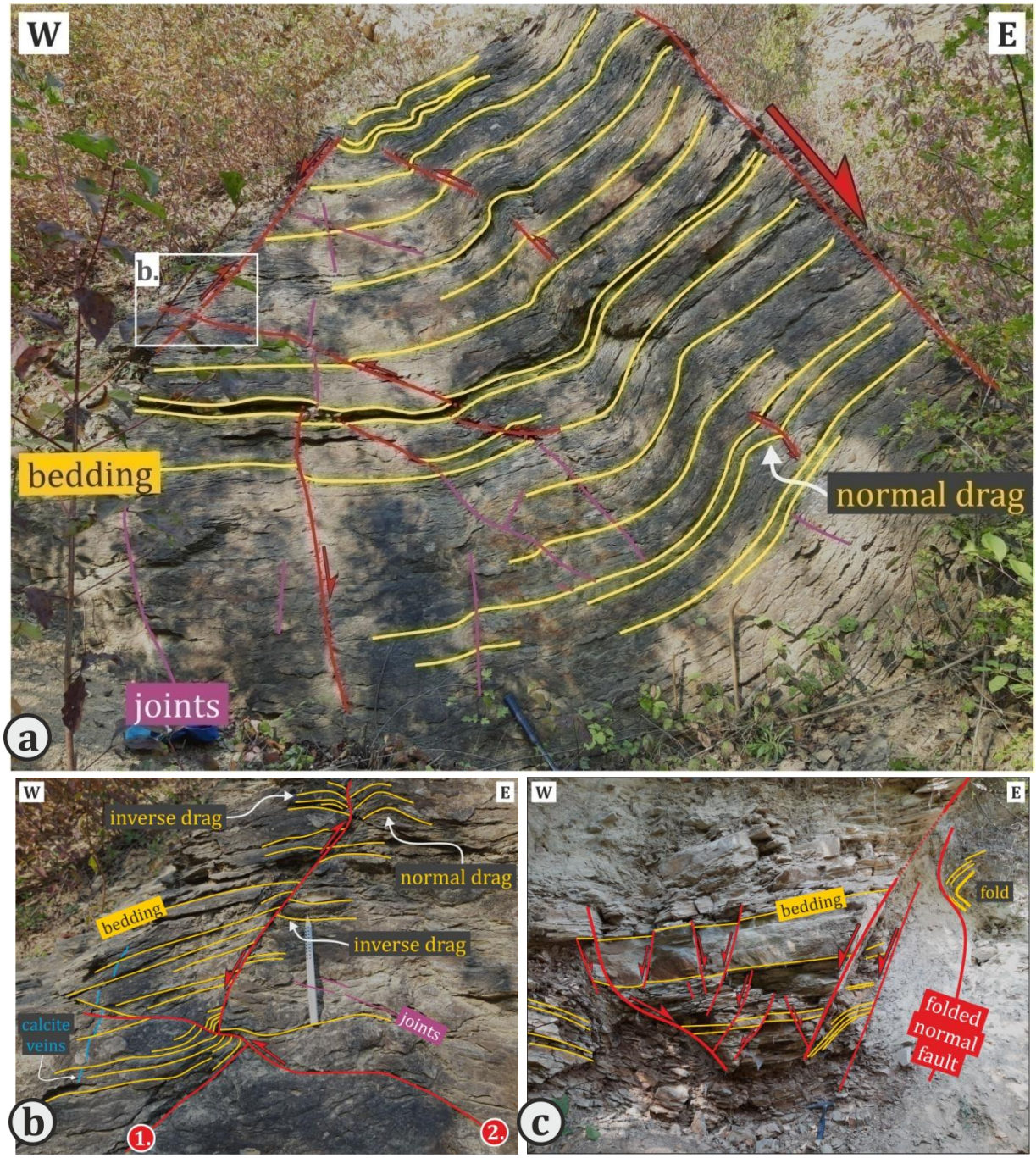

Fig.37. Field photos of the extensional structures at *Per-027* that were later obliquely reactivated by a compressional event. **A.)** High-angle normal faults, low-angle thrust faults and asymmetric W-vergent folds in the marl beds. The white frame marks the location of the following detailed field photo. **B.)** Interpreted field photo of cross-cutting normal and thrust faults. Normal drag folds as well as inverse drag folds present along the high-angle fault suggest reactivation of pre-existing normal faults. Apparent offset of the calcite veins indicate that they were formed early, prior to deeper burial and pressure solution. **C.)** Symmetric normal fault conjugate pairs. One of the faults seems to be folded.

To determine the relative chronological order of the normal and inverse movements along the same faults the following observations may be taken into consideration: (1) the reactivated faults are steep fractures with respect to the bedding ***(Fig.37/a and c)***; (2) there are calcite veins parallel to the normal faults which show step-like geometry due to pressure solution along the sedimentary laminae ***(Fig.37/b)***; (3) there are also shallow dipping thrust faults with similar but slightly oblique strike directions, some of which seem to offset the reactivated normal faults ***(Fig.37/b)***, and (4) one of the normal faults seems to be folded ***(Fig.37/c)***. All these observations confirm that the NNW-SSE striking early pre-tilt normal faults were reactivated as reverse faults during a second

compressional event ***(Fig.38)***. Asymmetric folds with approximately top-to-W vergency and horizontal N-S axis were also formed related to this compressional event. These folds usually nucleated above or are somehow connected to the normal faults. Finally, additional normal faults and oblique strike-slip striae were measured which suggest a NNE-SSW extension which certainly post-dates both the normal faults and the folds ***(Fig.38)***.

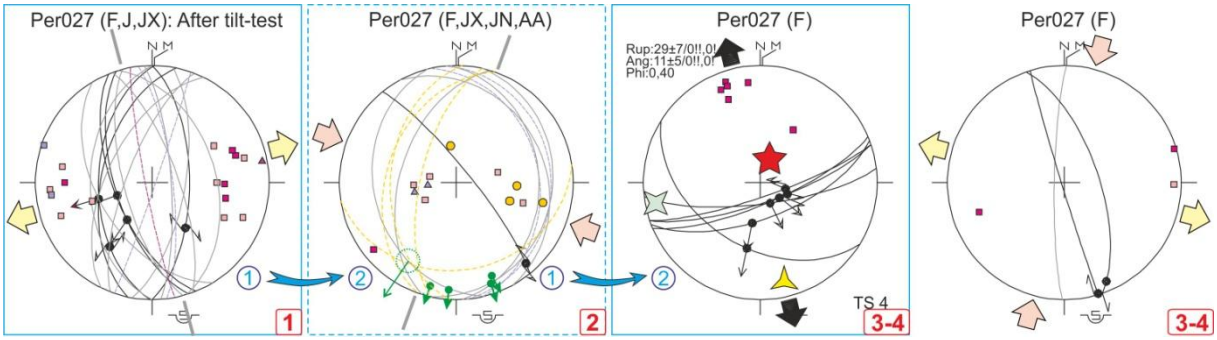

Fig.38. Stereoplots of the measured and back-tilted data at *Per-027*. The results suggest at least four deformation events: a pre-tilt ENE-WSW extension (1), a WNW-ESE directed oblique compressional reactivation of the faults (2), and two post-tilt deformation events (3-4).

IV.5. The area SE of Szin

In the Párózsa Valley and on the Bükk Slope the D and F members of the Szin Marl and the Szinpetri Limestone were mapped, mostly in detritus and very small outcrops ***(Map 5)***. The measured dips are moderate (20-45°) and point towards SW and WSW. In agreement with the measured dips a general younging towards WSW-SW was observed. Due to poor outcrop conditions structural observations were done only at *Per-028*.

Most important outcrop of the area SE of Szin:

Per-028: $^{sm/f}T_1$

In the very small outcrop of the F member of the Szin Marl at *Per-028* small-scale normal fault Mohr pairs with NW-SE strike were found ***(Fig.39)***. Where these faults have discrete fault planes the thin bedded marl beds thicken towards the normal faults and contain onlap surfaces, whereas in other parts of the faults the discrete features disappear and only the monoclonal normal drag folds indicate the continuation of the faults.

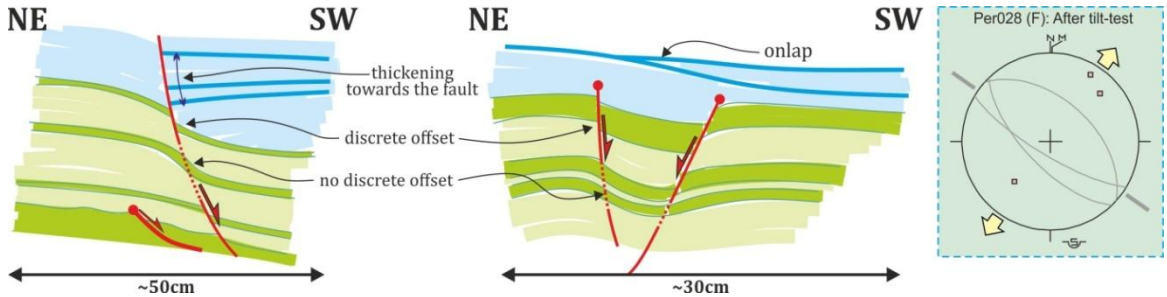

Fig.39. Small-scale (syn-sedimentary) normal faults at *Per-028*. The faults are sealed, the marl beds thicken toward the fault plane and there are onlap surfaces as well. **Stereoplot** of the measured faults suggests NE-SW extension.

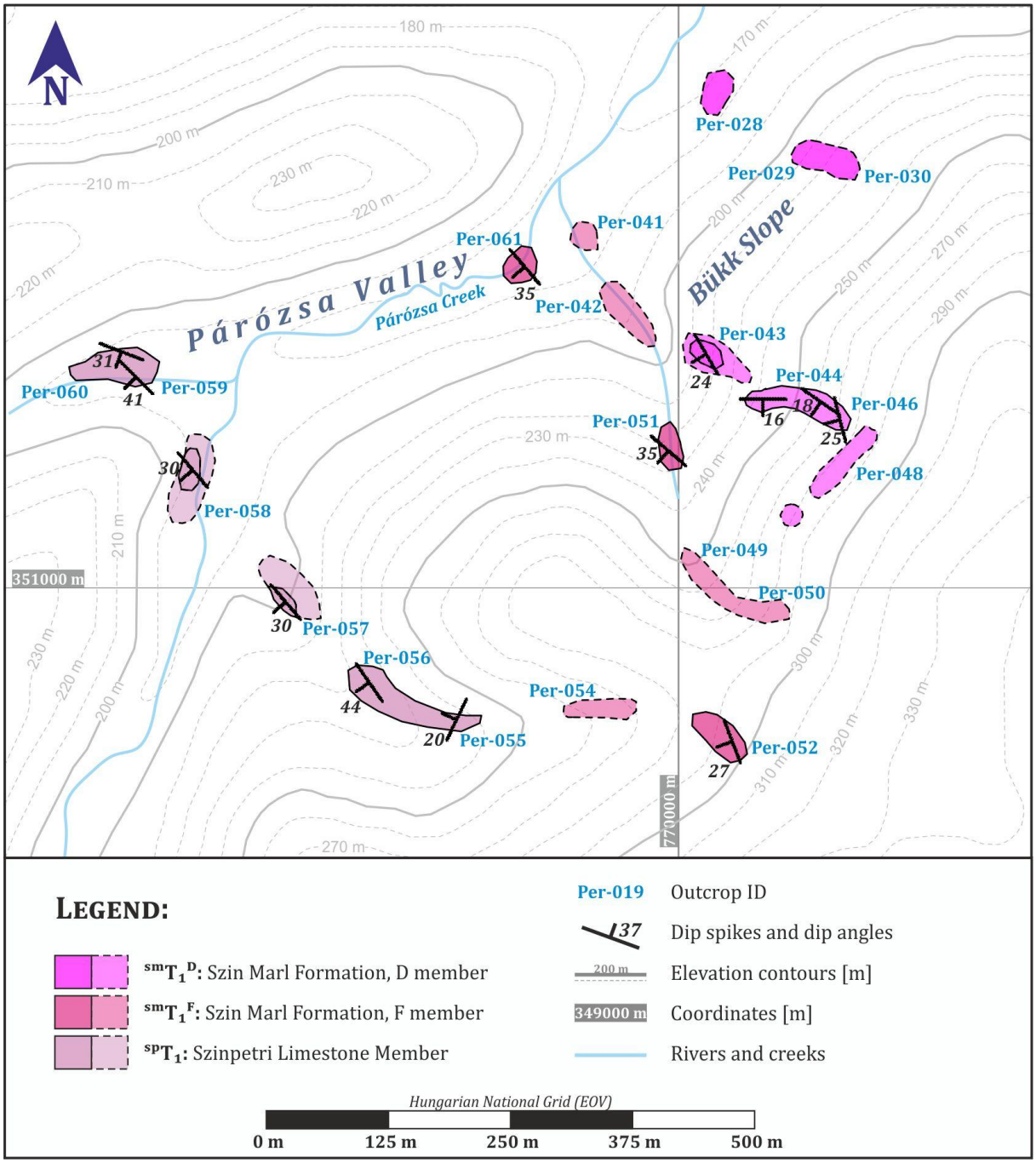

Map 5. Observation map of the area SE of Szin. The area is dominated by the uppermost part of the Szin Marl and the lowermost part of the Szinpetri Limestone. The transition from the Szin Marl to the Szinpetri Limestone is gradual. The general younging direction is towards SW.

IV.6. Tornakápolna and the Teresztenye Plateau

In the northwestern end of Tornakápolna a small but deep valley outcrops the steeply (~60°) S-ward dipping Szinpetri Limestone *(**Map 6**, Szn-079)*. Following it in strike direction, however, the lithology changes: a new drainage ditch getting built in October 2018 along an old foresters' road running in E-W direction revealed black, dark grey and riffle-green shales with siltstone and carbonatic (dolomite?) intercalations and occasional rauhwackes at *Szn-019.* These formations were interpreted as sedimentary siliciclastic intercalations of the Perkupa Evaporite. Their presence means that there is sedimentary or structural unconformity between *Szn-019 and Szn-079*.

While the black shales are still present at *Szn-020*, they completely disappear and are substituted by the thin bedded black and dark grey vermicular limestones of the Szinpetri Limestone by *Szn-080—081*. Here the measured dips are first parallel to the NE-SW trending dips of the Perkupa Evaporite at *Szn-020* but has shallower dip angles (25-30°), then they turn into shallow (25°) S-ward directed dips. Detritus of the Szinpetri Limestone continues to be present along the rest of the foresters' road but it was found in in-situ position only at *Szn-082*.

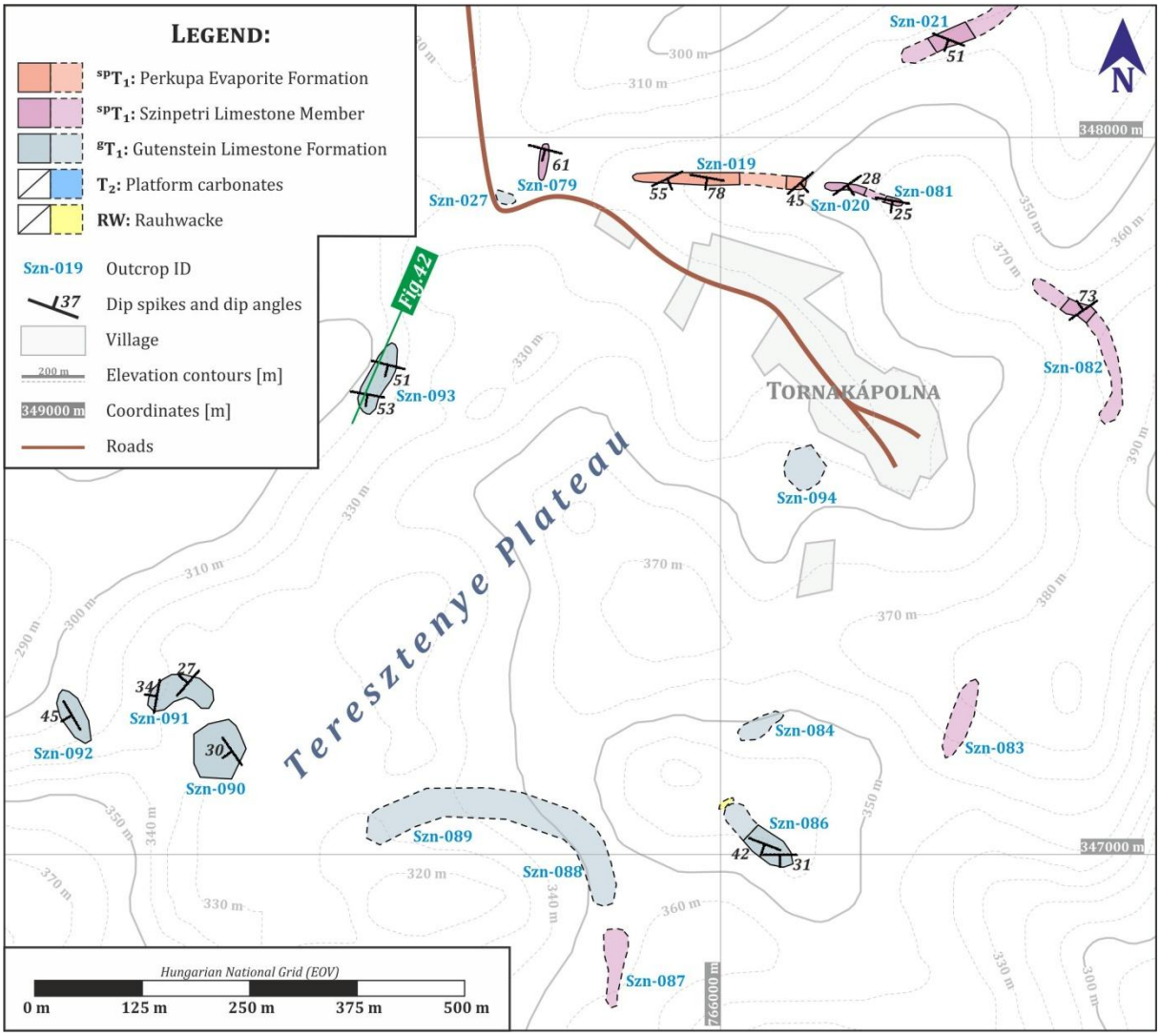

Map 6. Observation map of the area around Tornakápolna and the Teresztenye Plateau. The Teresztenye Plateau is covered by the Gutenstein Limestone which is surrounded by the Szinpetri Limestone in almost every direction, except for the in-situ outcrop of the Perkupa Evaporite N of Tornakápolna.

On the Teresztenye Plateau a thick bedded black limestone was mapped which – following the interpretation of Less et al. 1988 – was interpreted as the Gutenstein Limestone at *Szn-084*, *Szn-086, Szn-088—094* ***(Map 6)***. The Gutenstein Limestone outcrops of the Teresztenye Plateau are almost completely surrounded by the Szinpetri Limestone. Their boundary is approximately E-W in the S and N at *Szn-083 and Szn-087*, probably NE-SW or NNE-SSW trending in the SE, but there is no other information on the strike of their contact zone. At *Szn-086* an altered, red colored variation of the Gutenstein Limestone was found. Dip measurements in the Gutenstein Limestone showed moderate (30-45°) S-ward dips in the S *(Szn-086)* and moderate (30-45°) WSW-ward and W-ward dips in the W *(Szn-090—092)*.

Important outcrops of the area around Tornakápolna:

Szn-019: ^{p}P-T_1

In the western end of *Szn-019* the measured dips are very chaotic: they alternate between shallow to moderate (20-45°) E-ward and W-ward dips and moderate to steep (35-75°) or even sub-vertical S-ward and occasional N-ward dips. Unfortunately the gradual (or sudden) changes in dip directions can hardly be followed due to the unfortunate view from above so it is very hard to interpret the actual geometry of the folds. Eastward the measured bedding dips are dominantly steep (60-80°) S-ward dips but occasional SE-ward dips do appeared and became the dominant ones at *Szn-020*.

A few small-scale folds were found as well on the bottom of the drainage ditch. Firstly, ***Fig.40/a and c*** show open to tight folds with WNW-ESE trending sub-horizontal axis. In ***Fig.40/d*** an asymmetric fold is displayed with S-ward dipping longer limbs and steeply plunging (near vertical) fold axis. ***Fig.40/b*** presents a strike-slip duplex system observed in the steeply dipping shales and carbonatic layers.

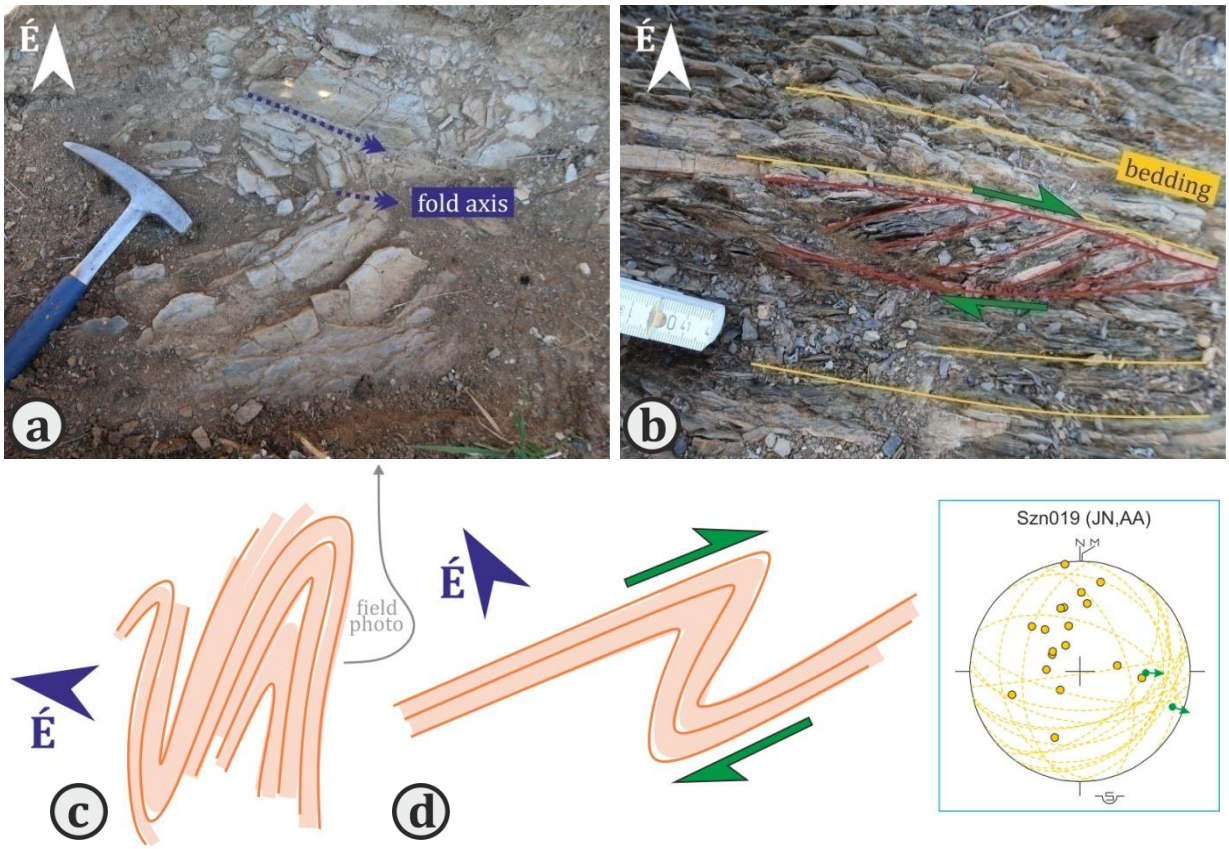

Fig.40. Field photos and field drawings of the structures observed at *Szn-019*. **A.)** Field photo of open to tight folds with E-W trending axis. **B.)** Field photo of a strike-slip duplex system, indicating dextral shearing. **C.)** Simplified field drawing of the folds in figure A. **D.)** Asymmetric shear fold with steeply plunging axis. **Stereoplot** shows all the measured dips and fold axis at *Jsv-019*.

Szn-093: $^{g}T_2$

In the northern part of the Teresztenye Plateau the Gutenstein Limestone was intensively folded at *Szn-093*: the measured dip directions were mainly towards S or SSW but with various dip angles (20-75°). Occasionally N-ward steep and sub-vertical dips were measured as well, suggesting a general top-to-N vergency ***(Fig.41)***. Numerous small-scale S- and Z-folds were observed on the fold limb as well with E-W or WNW-ESE trending axis. The Z-folds were positioned on the southern shallower limbs of the folds, whereas the S-folds were observed on the steeper northern limbs ***(Fig.42)***. Moreover, indications for rauhwacke occurrences were found as well but only in detritus.

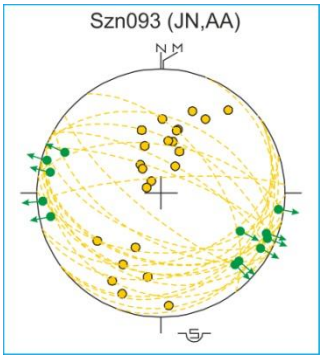

Fig.41. Stereoplot of the measured dip and fold axis data at *Szn-093*.

The measured dips and the Gutenstein Limestone occurrences suggest that the contact of the Gutenstein and Szinpetri Limestones is approximately E-W trending in the N (between *Szn-079 and Szn-093*) and in the S (between *Szn-086—087*). Towards E their boundary is uncertain (between *Szn-083—084, Szn-082 and Szn-082*).

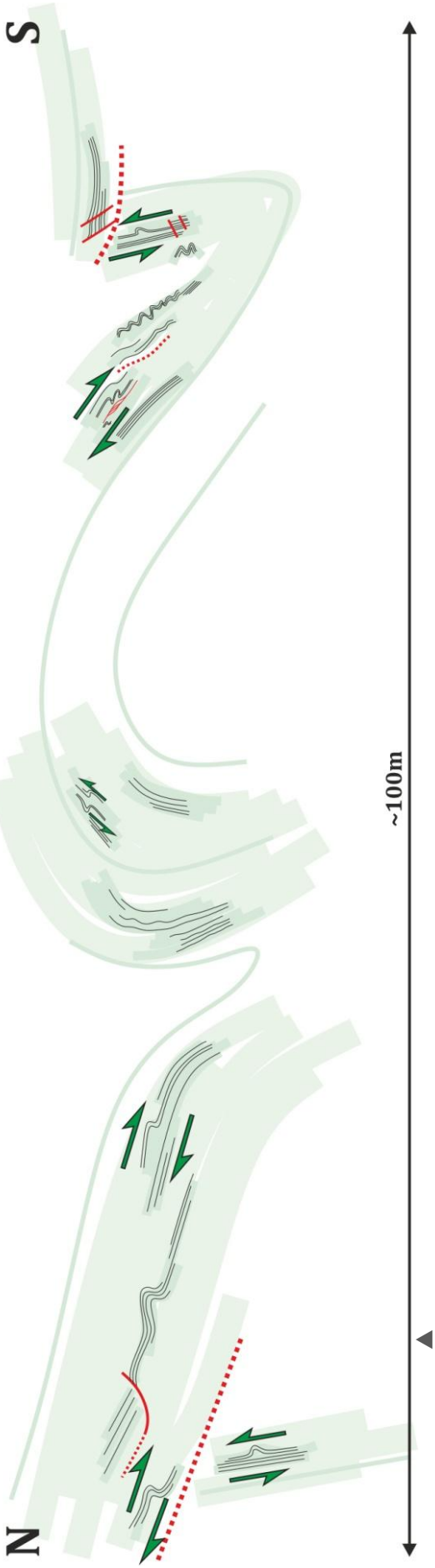

Fig.42. Folded Gutenstein Limestone layers at *Szn-093*. Small-scale asymmetric S- and Z-folds were observed on the larger scale folds' limbs: the Z-folds were positioned on the shallower southern limbs, whereas the S-folds were found on the steeper northern limbs.

IV.7. The Bükk and Szövetény Valleys

Going towards N from Tornakápolna in-situ outcrops of the Szinpetri Limestone were found at *Szn-021—022* ***(Map 7)***. Here the measured dips (moderate (35-50°) dip angles towards SSW) are similar to the general dips of *Szn-019*. The missing Lower Triassic sequences from between the Perkupa Evaporite and the Szinpetri Limestone, however, indicate discordance or displacement between the two outcrops.

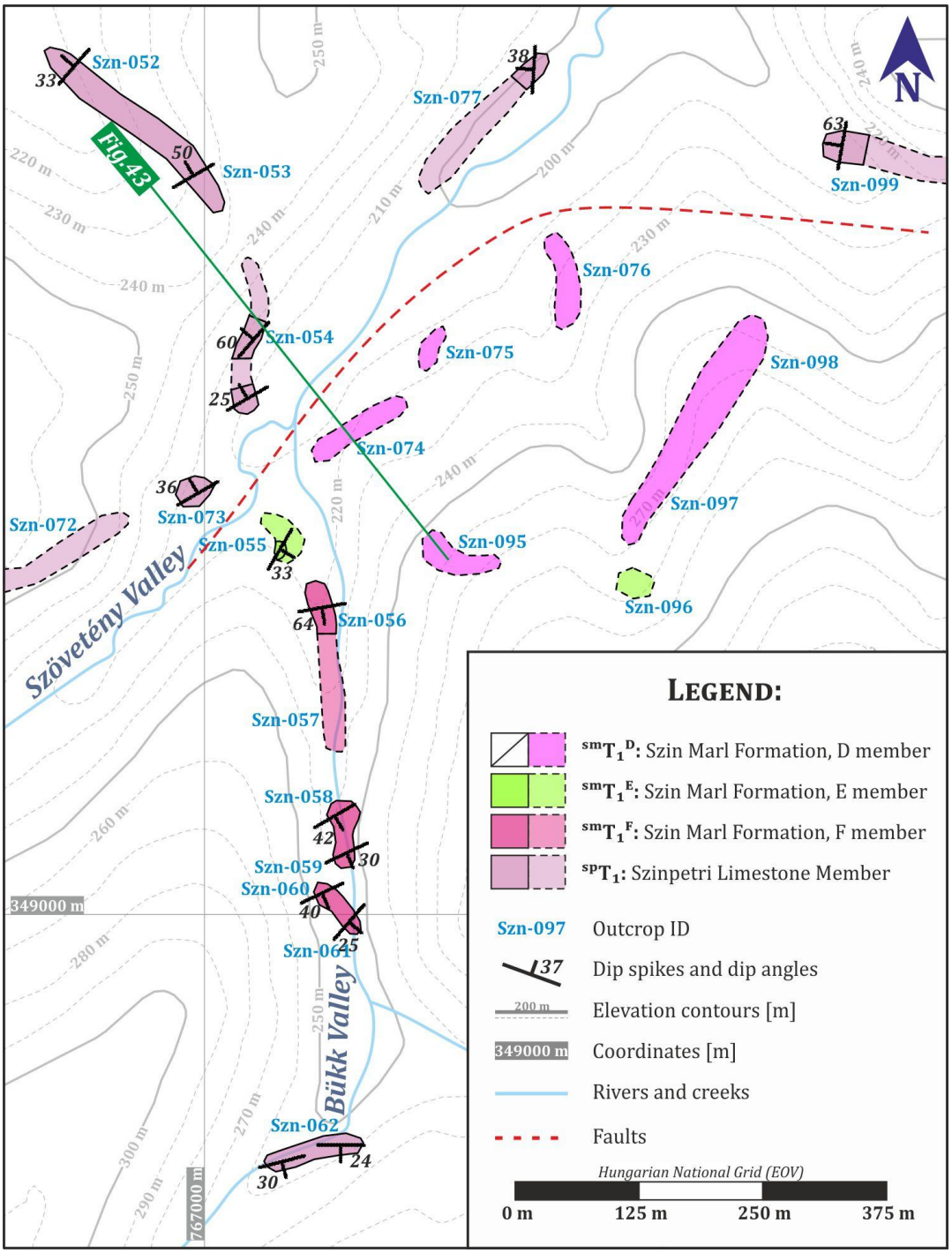

Map 7. Observation map of the Bükk Valley and the northern part of the Szövetény Valley. The Bükk Valley outcrops a continuous sedimentary succession between the D-E-F members of the Szin Marl and the Szinpetri Limestone. The Szinpetri Limestone was again returned in the Szövetény Valley and its presence here indicates a structural boundary.

Continuing from *Szn-021—022* the Szinpetri Limestone can be followed up until the *Szn-062* point in the Bükk Valley where shallow (25-30°) S-ward or SSE-ward dips were measured ***(Map 7)***. In this valley the Szinpetri Limestone gradually changes to the uppermost F member of the Szin Marl the lithology of which looks very similar but it is less biturbated and has higher siliciclatic content. Their shallowly (~25-30°) SSE-ward dipping formation boundary is probably located somewhere between *Szn-061* and *Szn-062* points.

In the junction of the Bükk and Szövetény Valleys at *Szn-055* the outcropped relatively thick bedded light grey limestones with red ooids and clasts are interpreted as the E marker member of the Szin Marl ***(Map 7)***. The measured dips in this E member is different from that of the F member: it dips moderately (35°) towards ESE. The Szin Marl continues at *Szn-074—076* where the mapped red and lilac colored mice-rich sandstones found in detritus are the remains of the D member. On the other side of the Szövetény Valley at the same topographical high as the *Szn-055* oppositely dipping Szinpetri Limestone was found at *Szn-054 and Szn-073*, indicating a structural boundary running practically in the middle of the valley ***(Fig.43)***. Based on the measured dip data the Szinpetri Limestone and the Szin Marl dip symmetrically away from this displacement surface and the steeper dips at this surface quickly flatten within a narrow zone. In the northern part of the Szövetény Valley once again in-situ outcrops of the Szinpetri Limestone were found at *Szn-077* with moderate (~40°) dips towards.

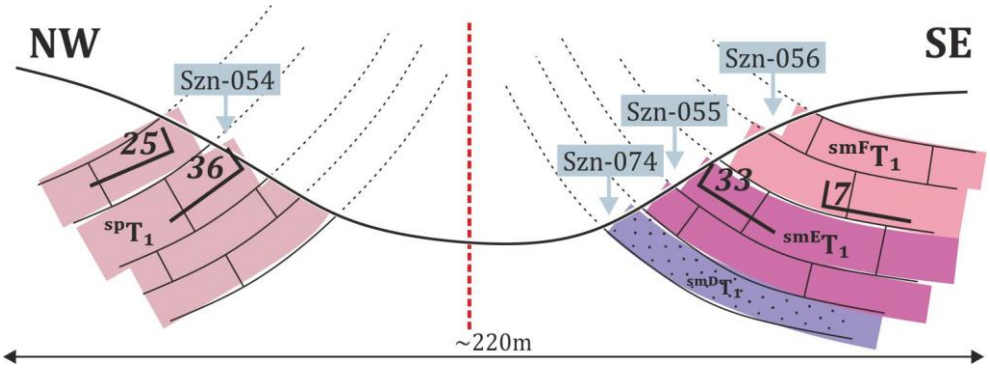

Fig.43. Schematic cross-section running in the area around the junction of the Bükk and Szövetény Valleys. The sectons presents the simmetrically dipping Szinpetri Limestone *(Szn-054, Szn-073)* and Szin Marl *(Szn-055—056)* on the two sides of the NE-SW trending valley.

Meanwhile in the southern parts of the Szövetény Valley red and lilac colored mica-rich sandstones and thin bedded limestones and marls were discovered at *Szn-023—026* and *Szn-065—070* ***(Map 8)***. These formations were interpreted as the Bódvaszilas Sandstone and the lower A-B members of the Szin Marl. Going from S towards N in the valley the outcrops start with the B member of Szin Marl and the section gets older and older until the Bódvaszilas Sandstone at *Szn-023 and Szn-065*. After these points the repetition of the succession was observed: at *Szn-066* the A and B members of the Szin Marl returned. The repetition was accompanied by the gradual change in the measured dip directions as well: while at *Szn-024—025* the measured shallow (20-30°) dips were S-ward directed, by *Szn-023 and Szn-065* the Bódvaszilas Sandstone turned towards SE, and finally with the reappearance of the Szin Marl the dips turned towards ENE-NE. The repeated succession together with the observed change in the dip direction suggest a gentle to open antiformal structure. This anticline is discordantly surrounded on every side by the Szinpetri Limestone *(Szn-021—022, Szn-*

062—063), except for on the northeastern part where the E member of the Szin Marl was found *(Szn-070)*. Furthermore it cannot be excluded that it is not the B member of the Szin Marl that is outcropped in the southernmost in-situ outcrop of the Szövetény Valley at *Szn-026* but it is already the Szinpetri Limestone as the observed lithology here is very similar to that of the Szinpetri Limestone. In addition to that the measured dips were much steeper (~60°) here than in the other outcrops here.

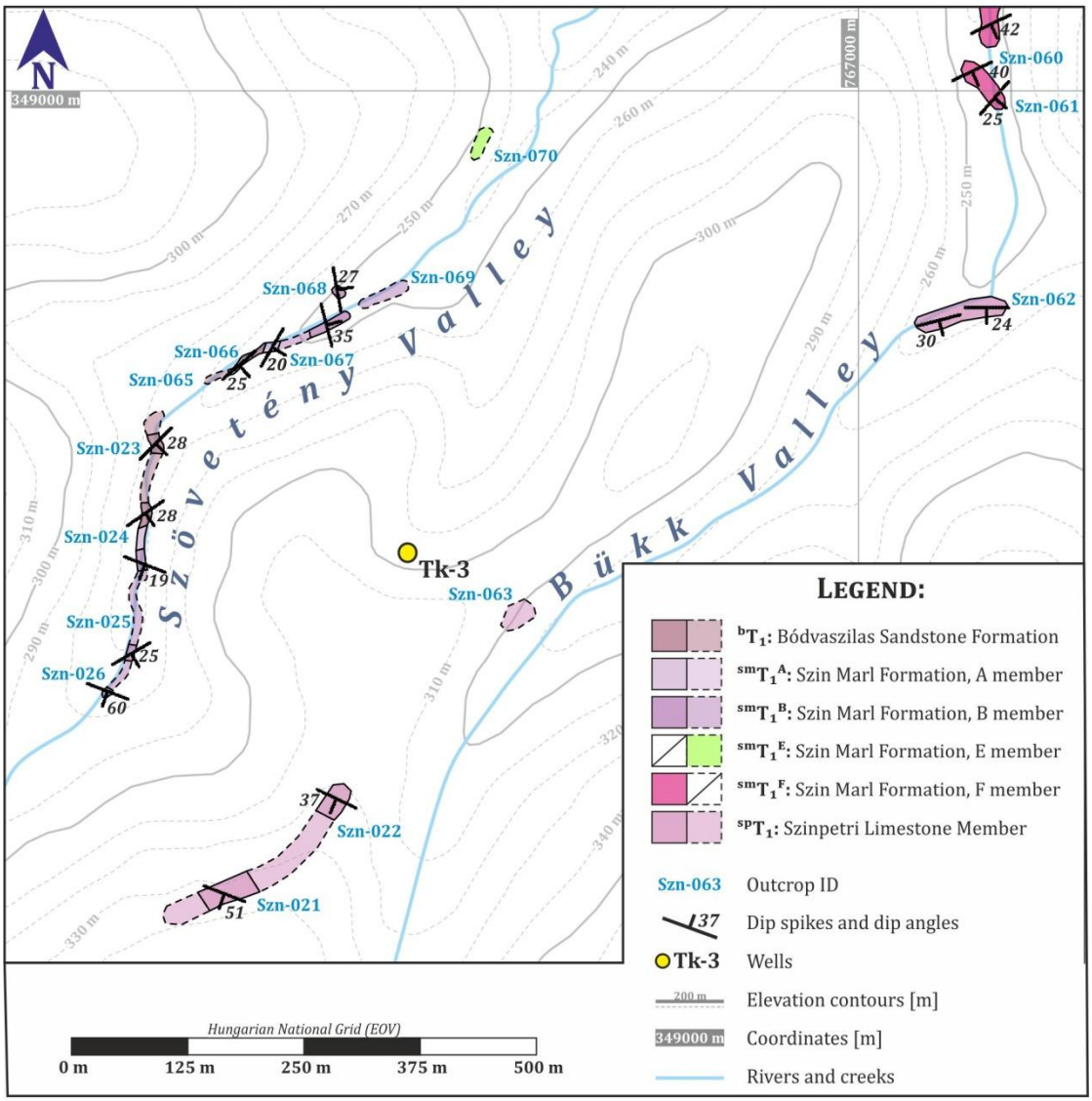

Map 8. Observation map of the southern part of the Szövetény Valley and the area around the Tk-3 well. The Bódvaszilas Sandstone and the Szin Marl is folded into a gentle to open antiformal structure which is discordantly surrounded by the Szinpetri Limestone.

IV.8. The road to Tornakápolna

The hilly area between the Szövetény and Kecskekút Valleys is covered by the Szinpeti Limestone ***(Map 9)***. Along the road from Szinpetri to Tornakápolna outcrops of the Szinpetri Limestone show alternating dips *(Szn-016—018, Szn-028)*. The general dip angle is between 15-35° and the measured dip strike directions change between approximately N-S and NW-SE. Considering this the Szinpetri Limestone is probably folded into NE-SW and E-W trending map-scale gentle to open folds.

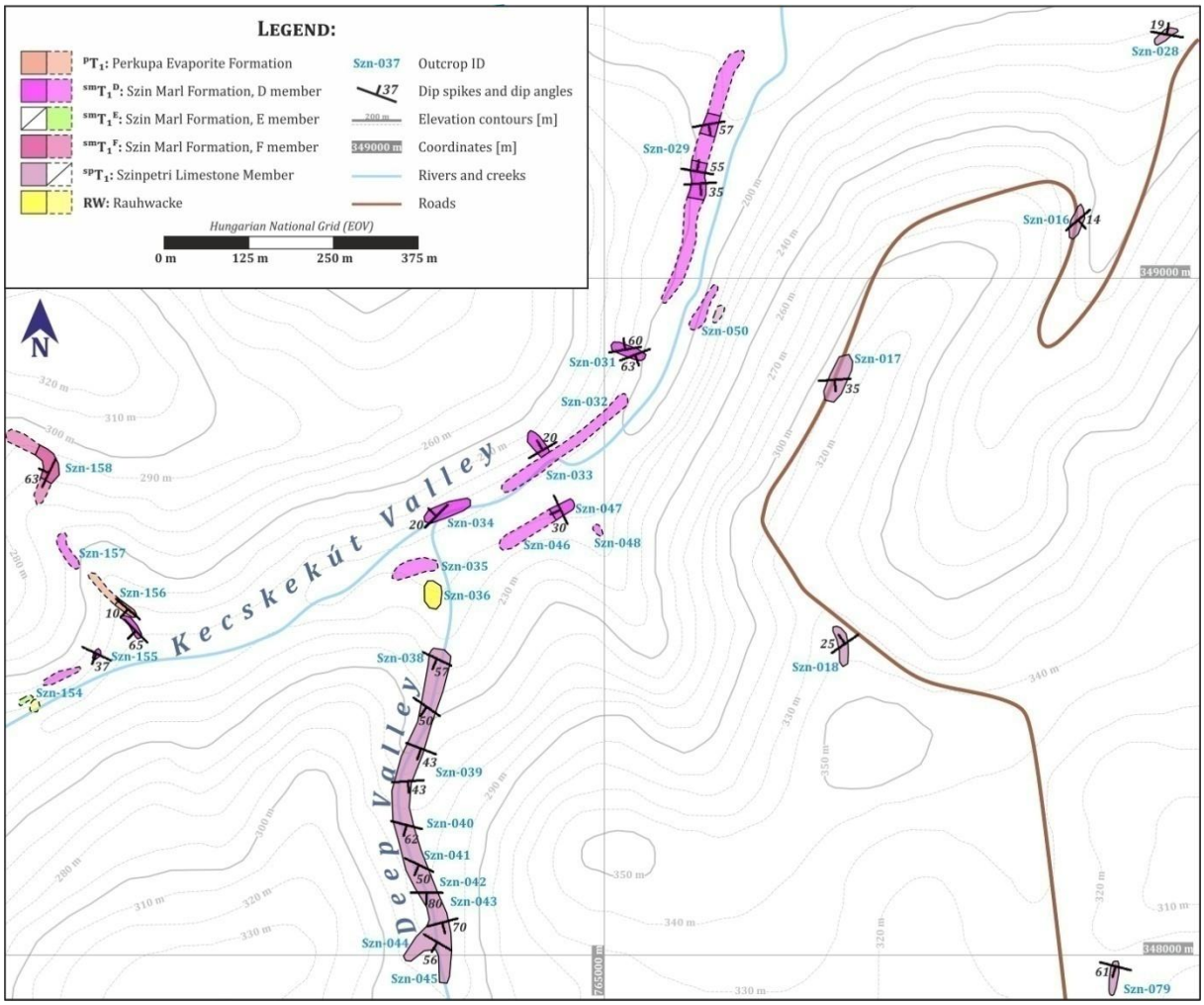

Map 9. Observation map of the road to Tornakápolna and the Kecskekút Valley.

Important outcrops along the road to Tornakápolna:

Szn-016: $^{sp}T_1$

A small but very well outcropped section was found in the Szinpetri Limestone at *Szn-016* where small-scale normal faults are the dominant structural features ***(Fig.44)***. Most normal fault has discrete fault planes, although some seem to have its fault plane sealed. In another part of the outcrop thickening of the beds within a small graben structure was observed ***(Fig.44/b)***. In their present-day position the NNE-SSW trending faults have moderate (~45°) dip angles while the NE-SW and ENE-WSW trending faults are much steeper (~70-80°). In spite of the differences in the measured strike directions and dip angles the normal fault kinematic is proved by the visible offset direction and the normal drag folds observed along the faults. Moreover, the symmetry axis of the oppositely dipping normal faults is approximately perpendicular to the bedding. The positive tilt-test suggests that the normal faults formed prior to the main tilting. Based on the back-tilted data NW-SE extension could be estimated.

In the upper part of the outcrop the small-scale normal faults obviously detach in a marl layer which thus forms a major detachment surface that is nearly bedding-parallel ***(Fig.44/a)***. This major detachment decouples the normal fault-related deformation from that of the lower part of the

outcrop. In the lower part the sealed normal faults detach on another moderately dipping detachment surface. This second detachment seems to be sealed by the upper major detachment as well, although their intersection is not very well outcropped.

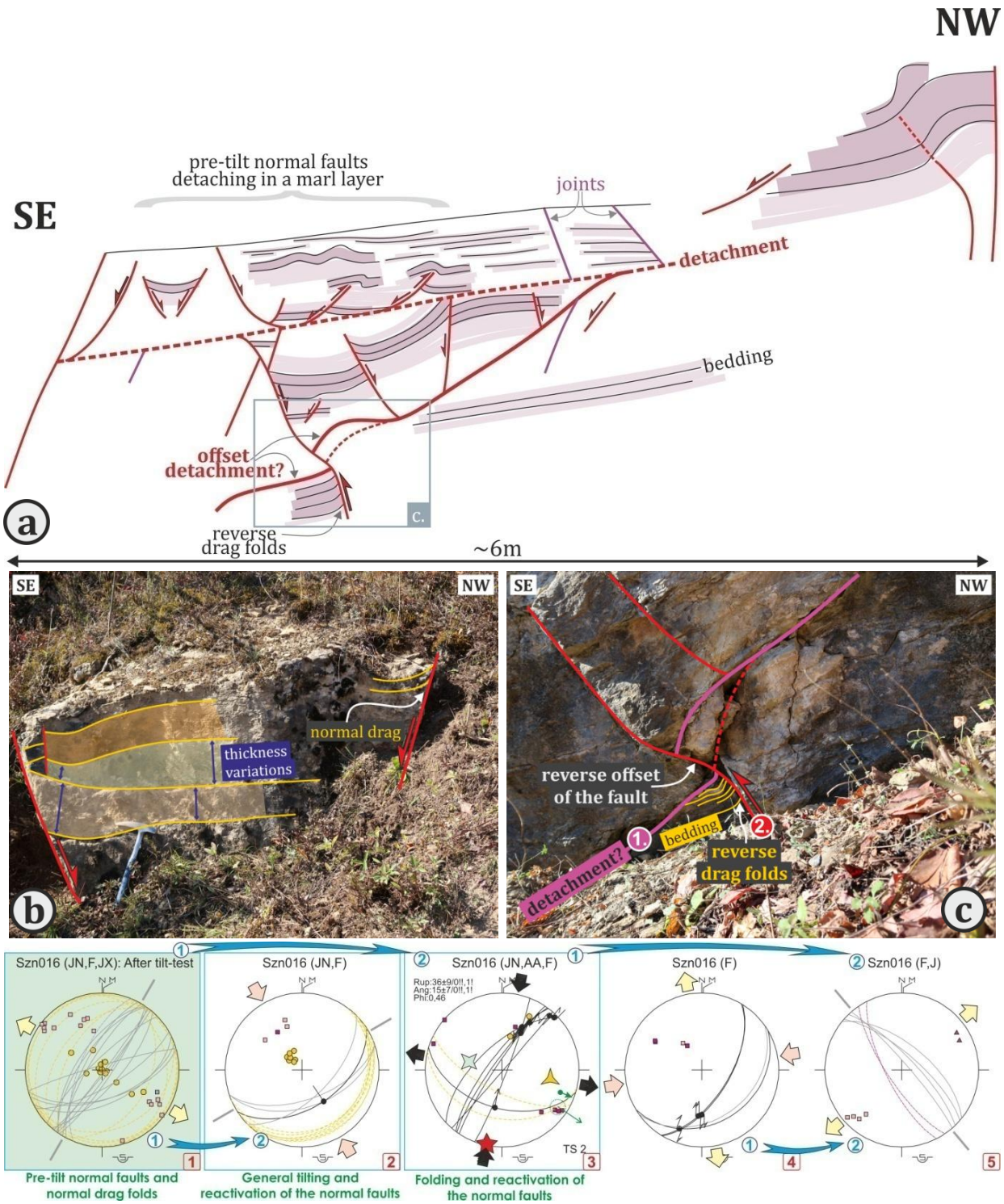

Fig.44. Cross-section and interpreted field photos from *Szn-016*. **A.)** Schematic cross-section of the main part of the outcrop. The normal faults on the top of the outcrop detach in a marl layer which forms a major detachment. Another detachment may be present below. Reverse drag folds along the normal faults indicate compressional reactivation of the pre-existing faults. **B.)** Field photo showing the second detachment which is offset by a high-angle fault with reverse drag folds. **C.)** Field photo of a pre-tilt normal fault conjugate pair along which thickness variations were observed. **Stereoplots** show the separated deformation phases in relative chronological order.

Along some of the normal faults reverse fault-related folds were also observed, indicating compressional deformation (reactivation) along the same faults. One of the high-angle faults cross-cuts the lower detachment and offsets it reversely ***(Fig.44/c)***. The amount of this offset is about 10 cm. Even if it were to be questioned whether the normal fault or the reverse fault movement followed the other (though it is very unlikely that the fractures were originally formed as high-angle reverse faults and then were later reactivated as normal faults), the reverse offset of the lower detachment clearly prove the relative chronological order of the different kinematics: the pre-existing normal faults were reactivated as high-angle reverse faults. This reactivation is caused by approximately NW-SE compression, and the general tilting of the bedding is probably related to this event. Furthermore, fault lineations indicating oblique sinistral strike-slip movement were also found along the high-angle (~70-80°) NNE-SSW trending tilted normal faults. These striations are related to a second (probably post-tilt) reactivation event with N-S σ_1. The folding with E-W trending axis observed in the northwestern part of the outcrop is probably related to this last N-S compression ***(Fig.44/a)***. Every previously introduced normal fault and detachment, as well as the fold are cut by two other groups of faults and joints which suggest the presence of at least two other post-tilt deformation phase: an E-W compression and perpendicular extension, and an uncertain NE-SW extension.

Szn-017: $^{sp}T_1$

Similarly, the normal fault that cross-cut the Szinpetri Limestone beds at *Szn-017* are interpreted as pre-tilt structures as their stereoplot becomes symmetric after tilt correction ***(Fig.45/a)***. The difference between these faults and the faults at *Szn-016* is that 1) they are shallower (40-50°), 2) there is no indication for thickness variation, and 3) their stereoplot suggests NE-SW extension that is completely perpendicular to the estimated stress-field at *Szn-016* ***(Fig.45)***. The compressional reactivation of the pre-tilt normal faults is evident at *Szn-017* as well: fault lineations measured on the shallowly dipping NW-SE trending normal faults are related to N-S compression. ***Fig.45/b*** shows a WNW-ESE trending tight fold the formation of which is controlled by the presence of a pre-existing normal fault. Further discrete E-W trending sinistral strike-slip faults and NNE-SSW trending oblique dextral thrust faults post-date the tilting event.

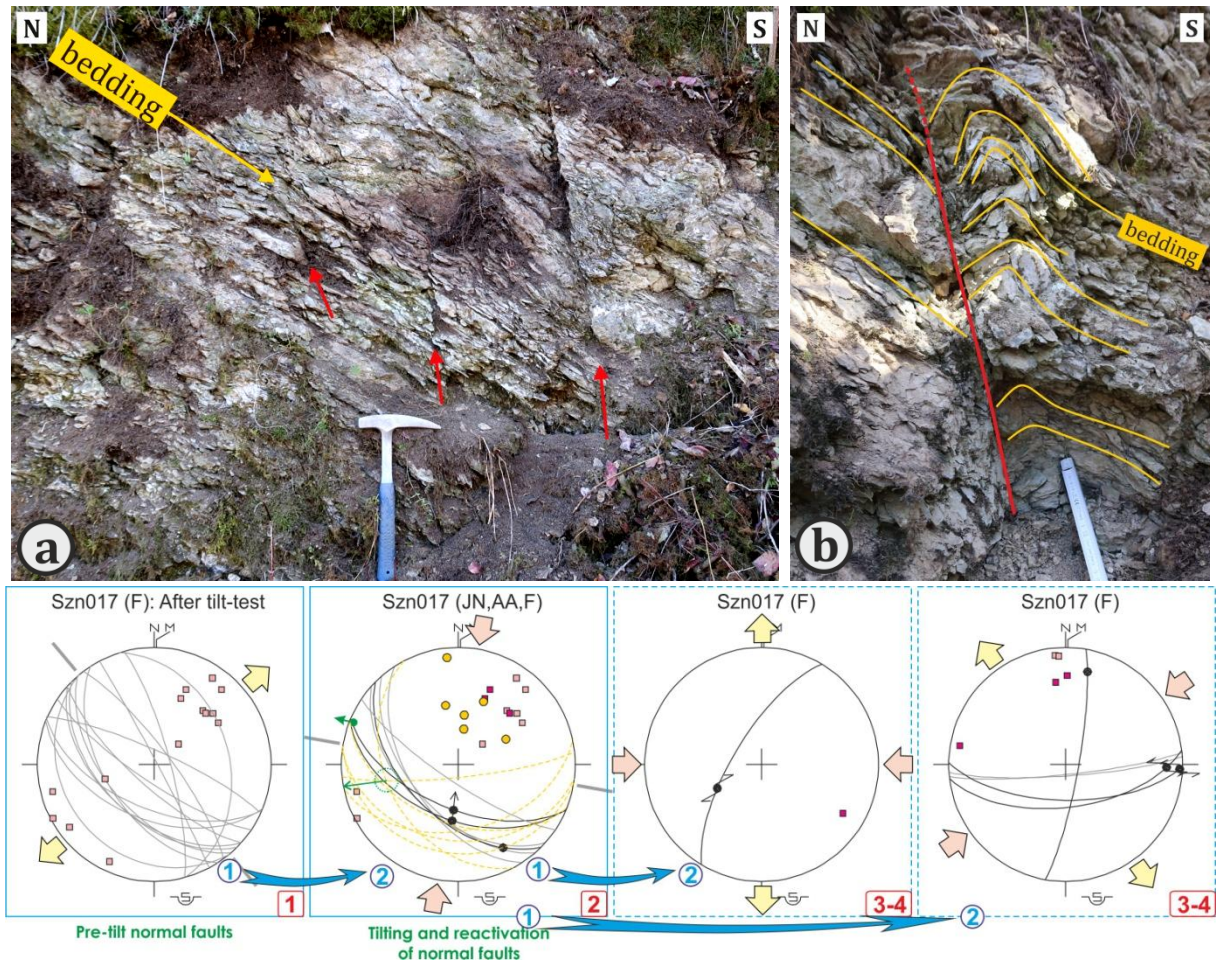

Fig.45. Field photos of pre-tilt normal faults and a fold found at *Szn-017*. **A.)** Tilted normal faults in the thin bedded Szinpetri Limestone. **B.)** Tight fold controlled by a pre-existing normal fault. **Stereoplots** show the measured and back-tilted data from *Szn-017* which suggest at least four different deformation events. The second event with N-S σ_1 obliquely reactivated the pre-tilt normal faults.

Szn-018: $^{sp}T_1$

Normal faults continue to be the dominant features at *Szn-018* as well where NW-ward and N-ward dipping high-angle normal faults and 2-3 cm thick calcite veins cross-cut the Szinpetri Limestone ***(Fig.46)***. The difficulty in this outcrop was that it was a badly outcropped section on the sole of the road so everything was observed from map view. The strike of the bedding was always parallel to the strike of the normal faults. The measured dip angles alternate between very shallow (~10°) and very steep (~75°) angles. The shallower (15-35°) dips seemed to be the general dips, whereas the steeper dips almost always appeared right next to the faults and veins. Moreover, the dip direction was always the same as that of the brittle structures. All this indicates monocline fold geometry and that there is a structural relationship between the faults and the tilted bedding.

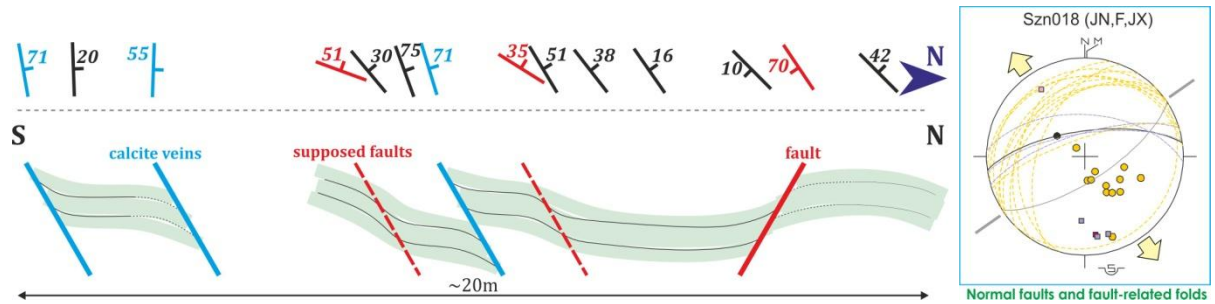

Fig.46. The measured dips and the reconstructed schematic cross-section at *Szn-018*. The strike of the measured dips are always parallel to the normal faults and calcite veins, the dip direction is almost always the same as that of the fractures, and the dips steepen always right at the faults. **Stereoplot** shows that the measured data suggest NW-SE extension.

IV.9. The Kecskekút Valley

The eastern and southern side of the Kecskekút Valley is covered by Szinpetri Limestone. The outcrops E of the valley has already been discussed in the previous chapter *(Chapter IV.8)*. In the canyon-like Mély Valley S of the main Kecskekút Valley a more or less continuous section of the Szinpetri Limestone was found ***(Map 9**, Szn-038—045)*. The measured dips here alternate between moderate and steep (45-70°) S-ward or SSW-ward dips.

On the western side of the Kecskekút Valley the mica-rich red and lilac colored sandstones of the D member of the Szin Marl were mapped *(Szn-029—035, Szn-048—050)* which is thus in contact with the Szinpetri Limestone ***(Map 9)***. At *Szn-045* and *Szn-047—048* the sandstones cross the valley and appear also on the eastern side of the valley, indicating that the valley does not strictly follow the boundary between the D member and the Szinpetri Limestone. Rauhwackes do, however, appear almost all along their boundary, even in in-situ outcrops (e.g. *Szn-037*). The measured dips in the D member change mainly between ~N-ward and ~S-ward moderate to steep (35-65°) dips that indicates approximately E-W trending folding.

In the southwestern part of the valley the E and F members of the Szin Marl also appear after the SSW-ward dipping D member *(Szn-154, Szn-158)*. The D member here steepens towards NE until *Szn-156* where dark gray and green colored shales appear in a NW-SE trending zone. These shales interpreted as part of the Perkupa Evaporite sequence are accompanied by the presence of rauhwackes.

Most important outcrop of the Kecskekút Valley:

Szn-041—043: $^{sp}T_1$

Outcrop-scale folds with similar E-W trending axis were found at *Szn-041—043* ***(Fig.47)***. At *Szn-041* there was a dewatering structure next to the fold whose axis was parallel to that of the fold. The folds are open to tight folds with more or less angular hinge zones, and they show opposite vergencies: while the folds at *Szn-041 and Szn-043* had N-ward vergency, the folds at *Szn-042* showed top-to-S vergency. Furthermore, at *Szn-042* discrete faults and fractures cross-cut the folded strata, thus they post-date the folding (or they happened contemporaneously). These fractures were NNW-SSE trending oblique dextral strike-slip faults and NNE-SSW trending high-

angle (75-87°) fractures without striae that may be the conjugate pairs of the dextral strike-slip faults. These brittle structural elements suggest N-S compression and perpendicular tension.

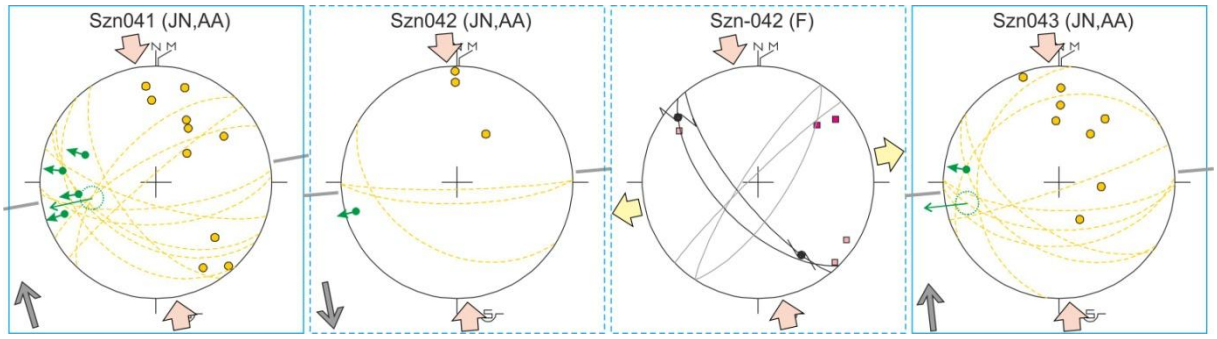

Fig.47. Stereoplots of the measured data at *Szn-041—043*. Both the fold and fault data suggest N-S shortening, the question is whether the formation of the strike-slip faults post-dates the folding or they happened contemporaneously.

Szn-034: $^{sm/D}T_1$

A few meters from the contact zone between the D member of the Szin Marl and the Szinpetri Limestone, a very fractured zone was found within the sandstone layers at *Szn-034* ***(Fig.48)***. Along this fracture zone normal and reverse drag folds indicate multiphase deformation of the discrete structural element. Considering its high-angle, the fault zone must have originally formed as a normal fault and was later reactivated as a(n oblique) reverse fault. Further NNW-SSE trending small-scale faults and fractures discretely cross-cut the tilted bedding at around 60°. This suggests that these fractures formed prior to tilting, during ENE-WSW extension.

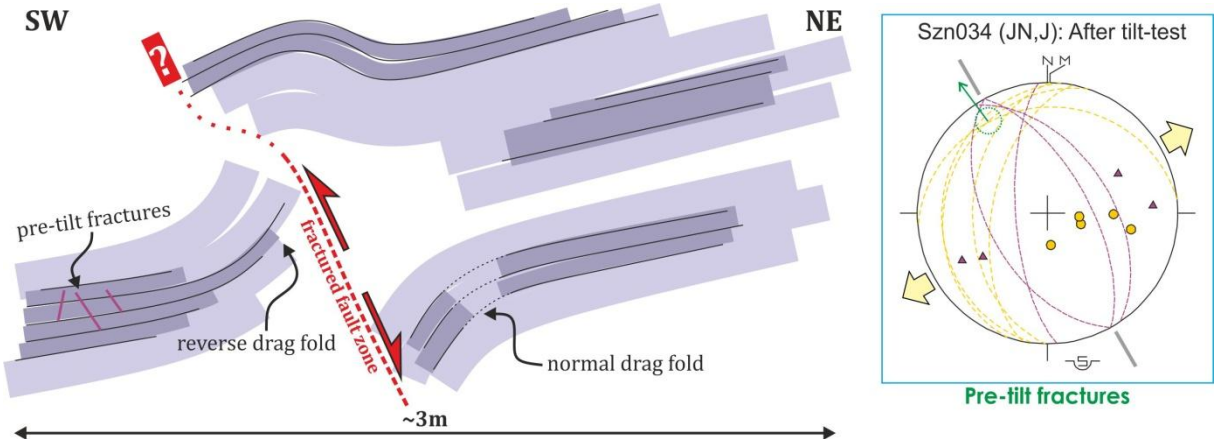

Fig.48. Reactivated normal pre-tilt normal faults in the D member of the Szin Marl at *Szn-034*. **Stereoplot** of the measured data suggests approximately NE-SW extension.

IV.10. The Kecskekút Spring and its surroundings

At the head of the valley S of the Kuriszlán Spring light grey, almost white limestones were found in detritus that suggest the presence of Middle Triassic platform carbonates (*Szn-123*, Steinalm Limestone according to LESS ET AL. 1988). The southern part of this valley outcrops a continuous section of the F member of the Szin Marl between *Szn-124—127* ***(Map 10)***. Based on the shallow to moderate S- and N-ward dips the Szin Marl here forms a very gentle map-scale fold which is slightly asymmetric (S-ward vergency). In the upper part of the western side of the valley the Szin Marl is

overlain first by discordantly W-ward dipping Jósvafő Limestone layers at *Szn-128*, and then by the Gutenstein Limestone at *Szn-122 and Szn-131*.

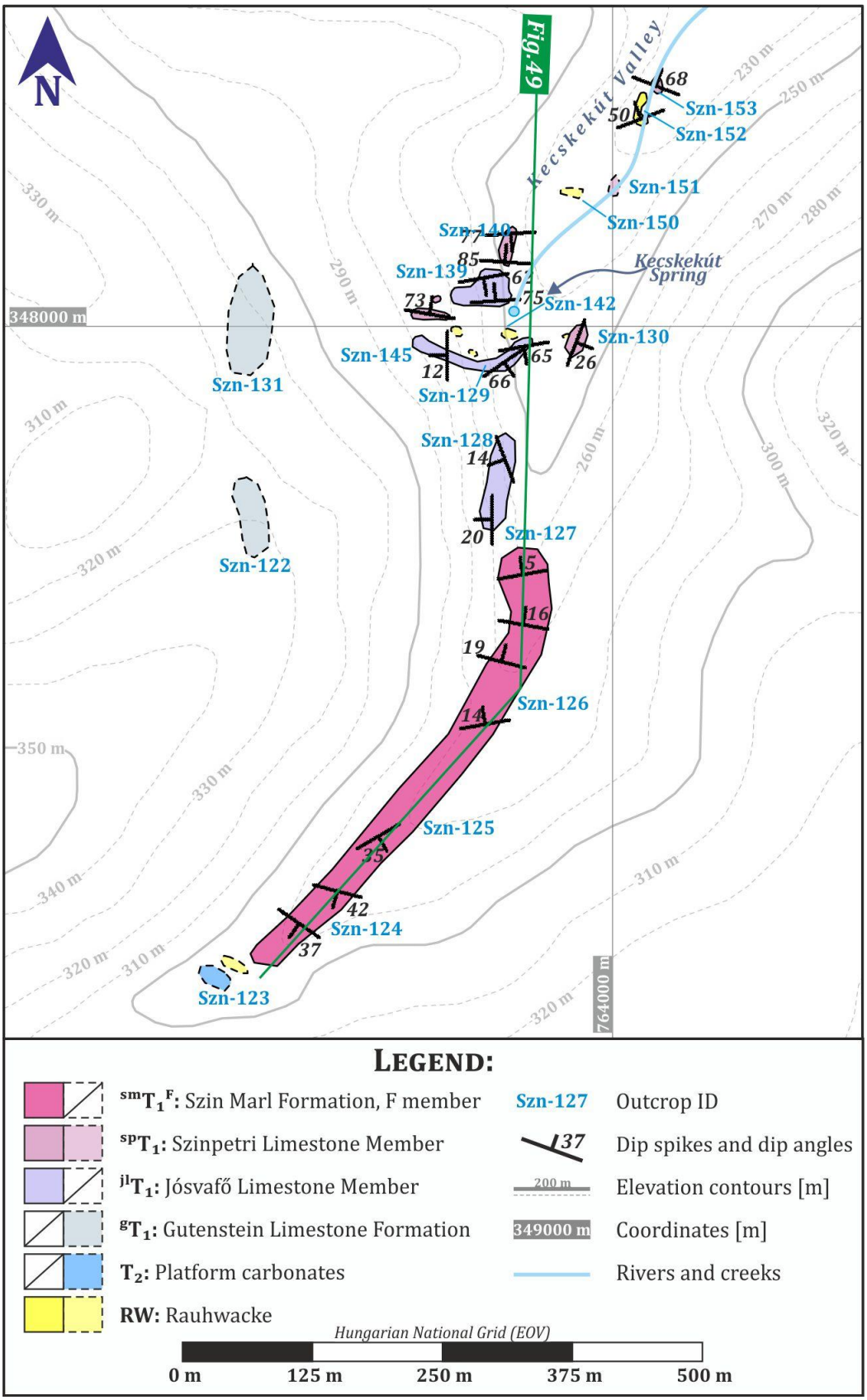

Map 10. Observation map of the area around the Kecskekút Spring. In the upper part of the valley the F member of the Szin Marl forms a very gentle fold. The fold is discordantly overlain first by the Jósvafő Limestone, then by the Gutenstein Limestone. Directly at the Kecskekút Spring steep to sub-vertical dips were measured in the Jósvafő and Szinpetri Limestones.

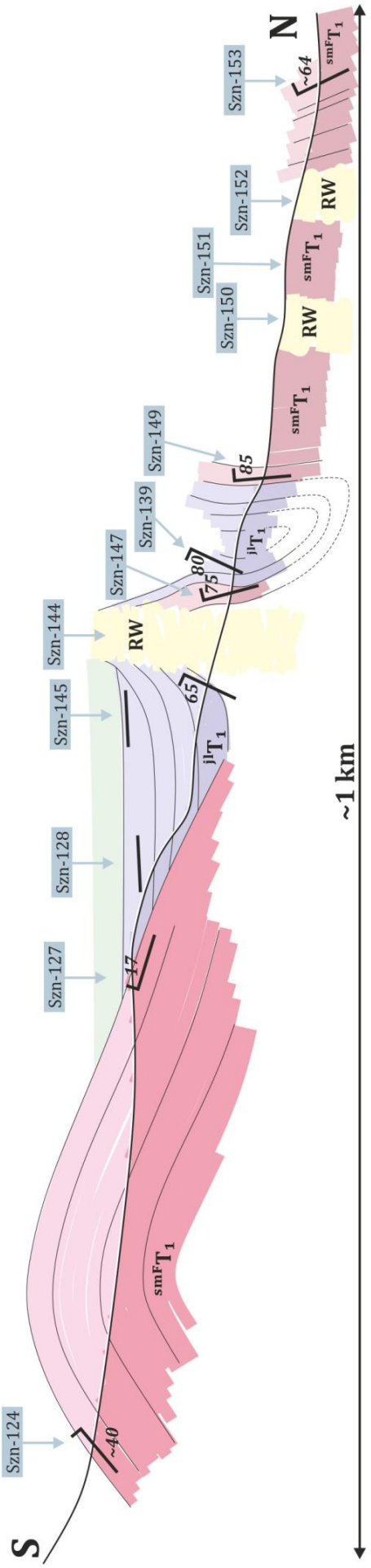

As we go in strike direction from *Szn-128* the dip of the Jósvafő Limestone takes a sharp turn toward S at *Szn-129*. The dip angle also changes from the shallow 20° to steep 65° ***(Map 10)***. Here the Jósvafő Limestone practically forms a narrow comb here the strike of which is parallel to the strike of the bedding. This narrow ridge is bordered in the N by an ~E-W trending rauhwacke zone. After this rauhwacke zone another ~E-W trending limestone ridge follows at *Szn-139* and *Szn-147—148*. Right at the contact of the rauhwacke zone and the limestone ridge the in-situ outcrop of the rauhwackes and partly altered but still foliated limestone layers was found as well *(Szn-147)*. These limestone layers are, however, part of the Szinpetri Limestone Member *(Szn-147—148)* — the Jósvafő Limestone only returns at *Szn-139*. Within this second ridge the measured dip was N-ward directed directly at the rauhwacke zone then the S-ward dips were restored. Further N another outcrop of the Szinpetri Limestone was found at *Szn-140 and Szn-149* which also showed both S-ward and N-ward dipping sub-vertical (~80-85°) dips. More Szinpetri Limestone outcrops were mapped in the northern parts of the valley at *Szn-151 and Szn-153* but these outcrops alternated with several rauhwacke occurrences *(Szn-150, Szn-152)*.

Most important outcrop of the area around the Kecskekút Spring:

Szn-129 and Szn-139: $^{jl}T_1$

In this area the steeply dipping Jósvafő Limestone forms very remarkable outcrops with numerous small-scale folds ***(Fig.50/a-b)***. These folds are detachment folds and contain layers with lateral thickness variations or even onlap surfaces. There are symmetric and asymmetric folds among them as well, and the asymmetric ones show both NNW and SSE vergency. In addition to the folds layer-parallel striations

◀ ***Fig.49.*** Schematic cross-section through the valley S of the Kecskekút Spring. In its southern part the Szin Marl is folded into a gentle map-scale fold. It is discordantly overlain in the W and N by the Jósvafő Limestone. In the direct surrounding of the Spring the steeply dipping Jósvafő Limestone alternates with ~E-W trending narrow zones of rauhwackes and Szinpetri Limestone occurrences.

were measured on the steeply dipping bedding planes. These striations revealed two different movements: one was normal or oblique (dextral) normal movement along with respect to the present-day NNE-ward dip, whereas the other group of lineations consisted of oblique sinistral faults on steeply NNW-ward dipping surfaces ***(Fig.50)***. Based on the superimposed striations the normal movement preceded the sinistral one. Further NW-SE striking oblique dextral strike-slip faults were also observed that cut through the bedding and that might be the conjugate pairs of the sinistral faults.

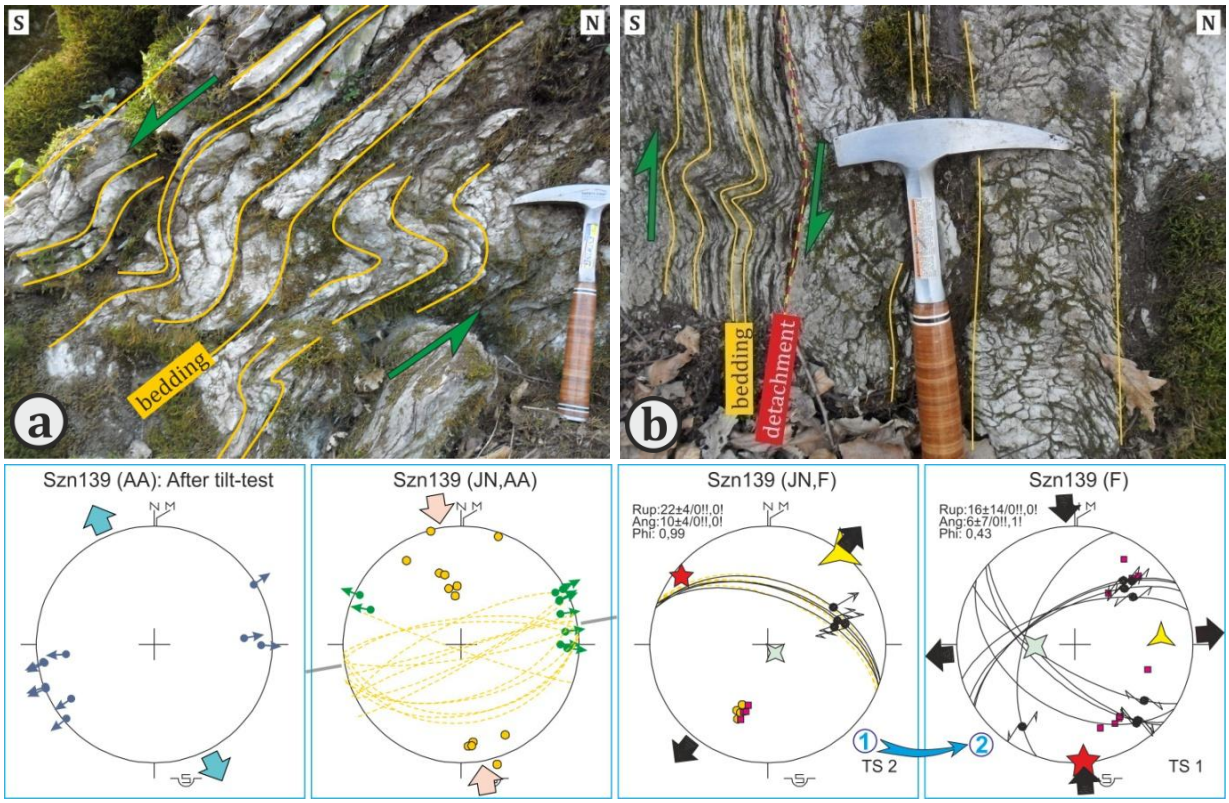

Fig.50. Small-scale detachment folds (slump folds) in the Jósvafő Limestone and the measured data at *Szn-139*. **A and B.)** Interpreted field photos of the detachment folds that show opposite vergency. **Stereoplots** show the back tilted small-scale fold data, the measured dip and fold axis data, and the measured layer-parallel and discrete fault data.

IV.11. Almás Valley and the Jő-3 well

The northern part of the Almás Valley outcrops the Szinpetri and Jósvafő Limestones ***(Map 11)***. With a few local exceptions both limestone dips moderately or steeply (45-75-85°) towards W or NW. There are two adjacent outcrops of the Jósvafő and Szinpetri Limestones at *Szn-133 and Szn-137* where the measured dips permit the possibility that there may be a structural boundary between the two outcrops but not necessarily.

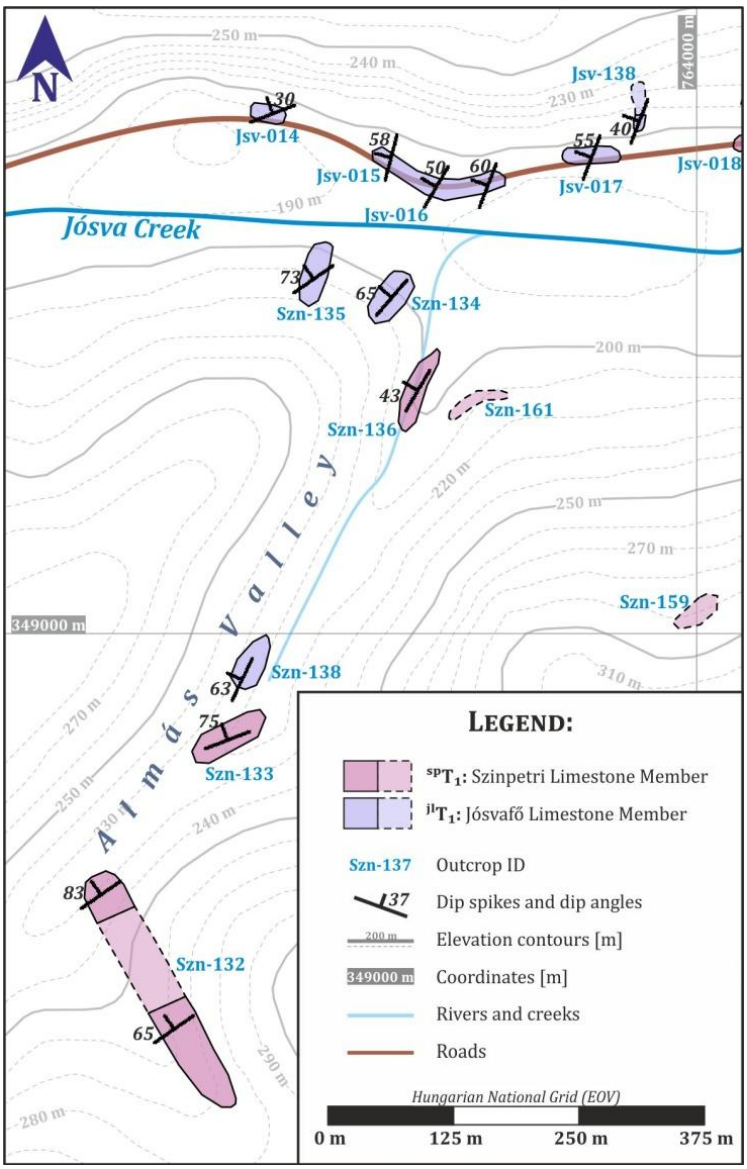

Map 11. Observation map of the northern part of the Almás Valley. The Szinpetri and Jósvafő Limestones dip almost uniquely towards SW. Their boundary is most probably sedimentary but their boundary may be discordant between *Szn-133* and *Szn-138* (not necessarily though).

After the *Szn-132* outcrop with steep and sub-vertical (65-85°) Szinpetri Limestone a sharp change in lithology was observed ***(Map 12)***: first mica-rich red and lilac colored sandstones appeared as part of the D member of the Szin Marl *(Szn-115, Szn-121)*, which was then substituted by the marl and limestone beds of the B member *(Szn-116—118, Szn-120)*. In the southernmost part of the outcrops the measured dips in the B member are shallow to moderate (25-45°) S-ward and SW-ward dips. Towards W the B member is in direct contact with the Szinpetri Limestone, and this relatively narrow Szinpetri Limestone zone is followed by the appearance of the Jósvafő Limestone at *Szn-119*. Here the Jósvafő Limestone dips moderately (~40°) towards S. Interestingly while a lot of breccias and rauhwacke accompany the boundary between the D member and the Szinpetri Limestone, there are no evidences for brecciation or any other kind of mechanical or chemical alteration along the contact zone of the B member and the Szinpetri Limestone.

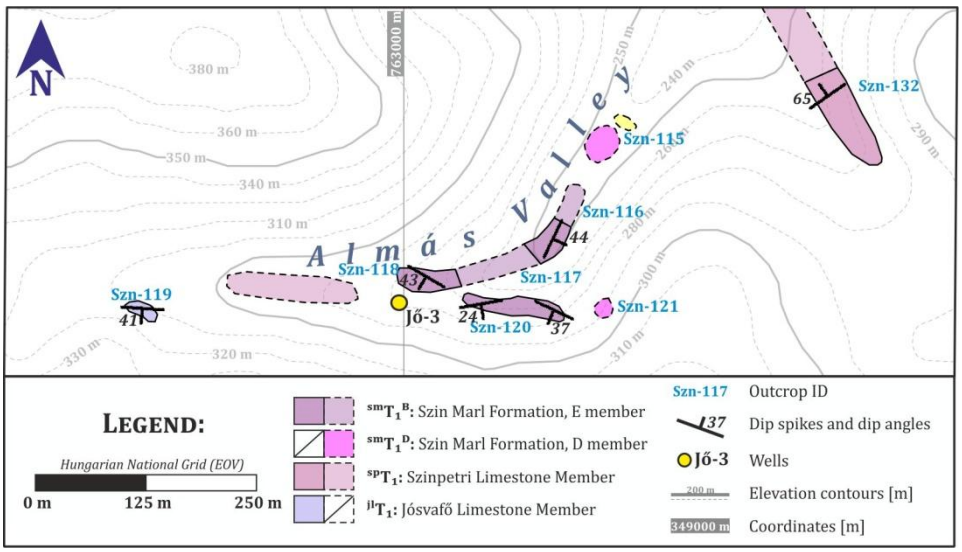

Map 12. Observation map of the area around the Jő-3 well, at the head of the Almás Valley. While breccias and rauhwackes indicate that the contact zone between the Szinpetri Limestone and the D member of the Szin Marl is strongly tectonized, there were no indications for brecciation in the S at the boundary between the B member and the Szinpetri Limestone.

Important outcrops of the Almás Valley:

Szn-134—135: $^{jl}T_1$

Right at the entrance of the Almás Valley two combs of steeply (55-85°) SW-ward dipping Jósvafő Limestone run parallel with each other *(Szn-134 and Szn-135)*. The strike of these combs coincides with the strike of the bedding. The Jósvafő Limestone here is full of with 10-15 cm scale and 1-2 m scale asymmetric folds ***(Fig.51, Fig.52)***. The smaller scale folds are NW-vergent asymmetric folds with rounded hinge zones and open to tight interlimb angles. In ***Fig.52/a*** these folds detach on a lower undeformed bed (detachment folding) and they are also covered by undeformed beds. Furthermore, thickness variations were observed within the deformed strata. The bigger folds are also asymmetric folds with NE-SW trending axes and their geometry differs from that of the smaller folds: the folds with tight interlimb angles and rather angular hinge zones are more frequent, and thickness variation or detachment surfaces were not observed at all. In case of the bigger scale folds the space problem occurring within the fold hinge zone is accommodated by brittle imbrication of the deformed bed slices (fold-accomodation faulting, ***Fig.52/b***). In case of the smaller scale folds the same problem is solved by "plastical" changes in the thickness of the bedding.

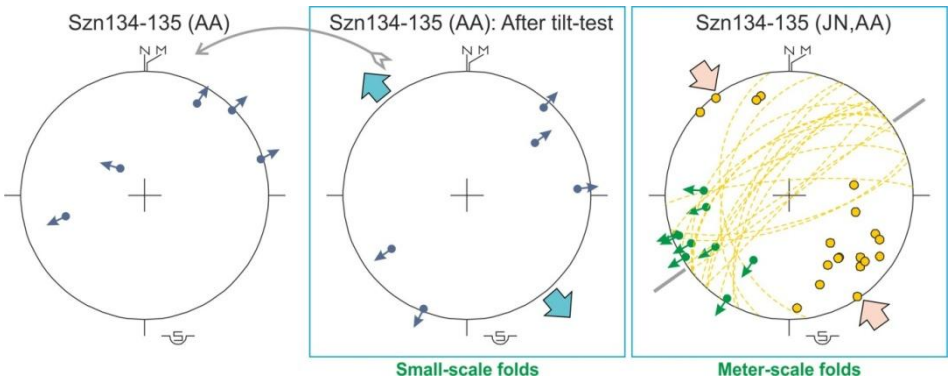

Fig.51. Stereoplots of the two groups of folds in the Jósvafő Limestone at *Szn-134—135.* Both groups had NE-SW trending axes.

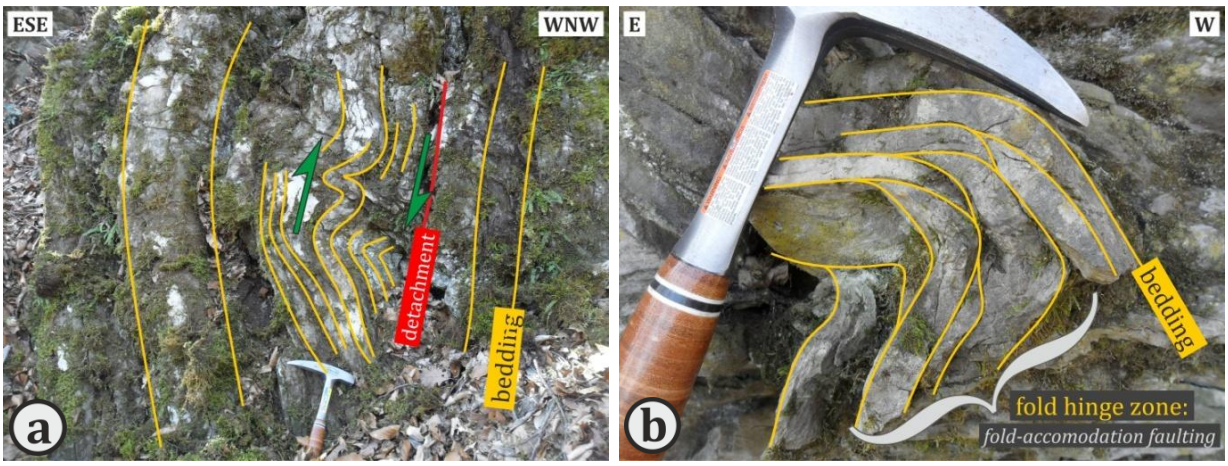

Fig.52. Field photos of the folds at *Szn-134—135*. **A.)** Small-scale asymmetric detachment (slump) folds with lateral changes in bed thicknesses. **B.)** Zoomed-in photo of the hinge zone of a 2 m scale fold. The space problem of the hinge zone is accommodated by brittle imbrications of the bedding (fold-accomodation faulting).

Szn-118: $^{sm/B}T_1$

The SSW-ward dipping B member of the Szin Marl at *Szn-118* is cut through by NNE-SSW/NE-SW shallow (25-35°) and NW-SE striking steep (~85°) normal faults. Their symmetry axes are perpendicular to the bedding and the tilt-test carried out on the measured data gave positive results. Striae indicating oblique normal fault movement and normal drag folds formed along the faults. Thickness changes within the hanging wall strata was observed as well ***(Fig.53/a)***, moreover, almost all of the normal faults were sealed and covered by the subsequent marl beds ***(Fig.53/b)***. The overall geometry of their stereoplot suggests approximately E-W extension ().

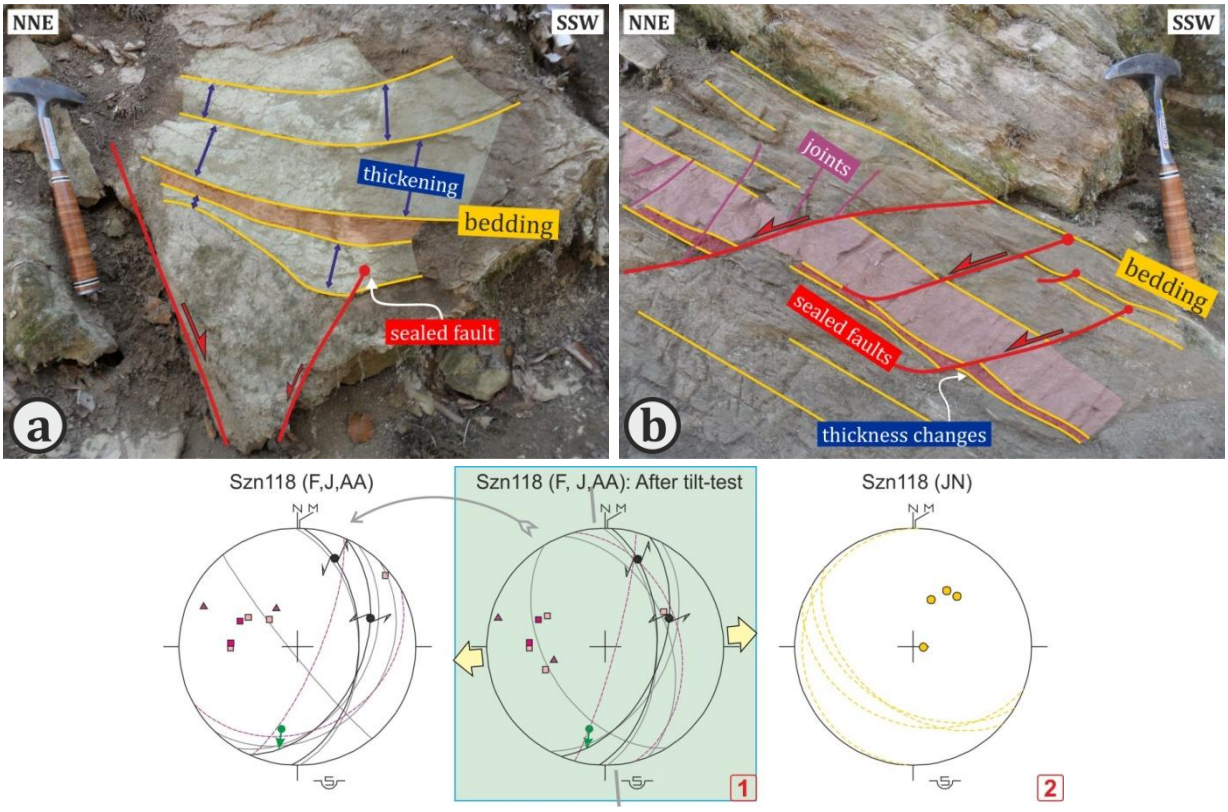

Fig.53. Pre-tilt (syn-sedimentary) normal faults in the B member of the Szin Marl at *Szn-118*. **A.)** Normal fault conjugate pairs. The symmetry axes of the normal faults are perpendicular to the bedding, suggesting the pre-tilt age of deformation. Normal drag folding and thickening of beds in the hanging wall was also observed. **B.)** Sealed normal faults. The **stereoplot** of the back-tilted normal fault data suggests E-W extension.

IV.12. Roadside outcrops between Szinpetri and Jósvafő

Starting from the western end of the village of Szinpetri well outcropped sections were observed in the roadside cuts ***(Map 13)***. These sections start at Szinpetri with the thin bedded, typically nodular and vermicular Szinpetri Limestone that has a general shallow to moderate (15-30°) dip towards the W *(Jsv-027—030)*. A sharp change in lithology was observed between *Jsv-027 and Jsv-026*: the limestone is substituted by relatively thick bedded (10 cm in average but occasionally 40 cm thick) grey and red fine-grained sandstone with high mica content and small snail fossils. At *Jsv-025* the in-situ rocks are still fine-grained sandstones and aleurolits but in the detritus grayish and pinkish limestones with grainstone pattern and red ooids were also discovered. Between the *Jsv-020 and Jsv-024* points thin bedded grey, yellow and occasionally red sandstones, aleurolits, marls and linestones alternate. The limestone and marl beds sometimes are lenticular or vermicular. The above mentioned sequence of lithologies is interpreted as different members of the middle and upper parts of the Szin Marl: the gray and red sandstones and aleurolits at *Jsv-026* are interpreted as the D member while the ooidic grainstone detritus at *Jsv-025* indicate the nearby present of the E member. Finally, the mixed lithologies between *Jsv-020—025* may be correlated with the F member. The moderate (45-30°) WNW-ward dip of the Szinpetri Limestone at *Jsv-027—028* continues at *Jsv-026* in the Szin Marl as well, but then it turns towards N at *Jsv-022—025*. The general WNW-ward dip direction returns again at *Jsv-021* and stays in the Szinpetri Limestone as well. Even though the same dip was measured both in the Szinpetri Limestone at *Jsv-027* and in the Szin Marl at *Jsv-026*, there is clearly a structural boundary between the two outcrops.

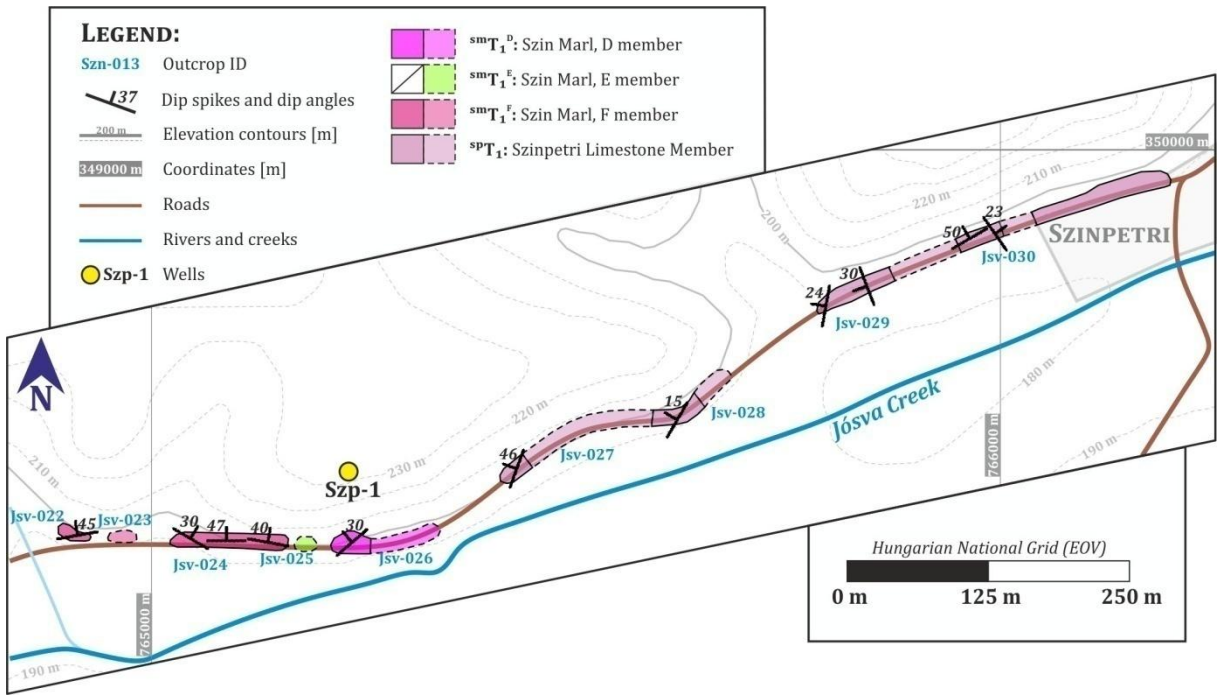

Map 13. Observation map along the eastern part of the road between Szinpetri and Jósvafő. The Szinpetri Limestone is discordantly in contact with the D-E-F members of the Szin Marl between *Jsv-026 and Jsv-027*.

At *Jsv-019* typical thin bedded dark grey and black bioturbated, vermicular limestone with thin marl and shale laminaes indicate the return of the Szinpetri Limestone that gradually evolves from the F member of the Szin Marl ***(Map 14)***. The change from the Szinpetri Limestone to the Jósvafő Limestone happens between *Jsv-018—Jsv-136* and *Jsv-017—Jsv-139* points. While the measured

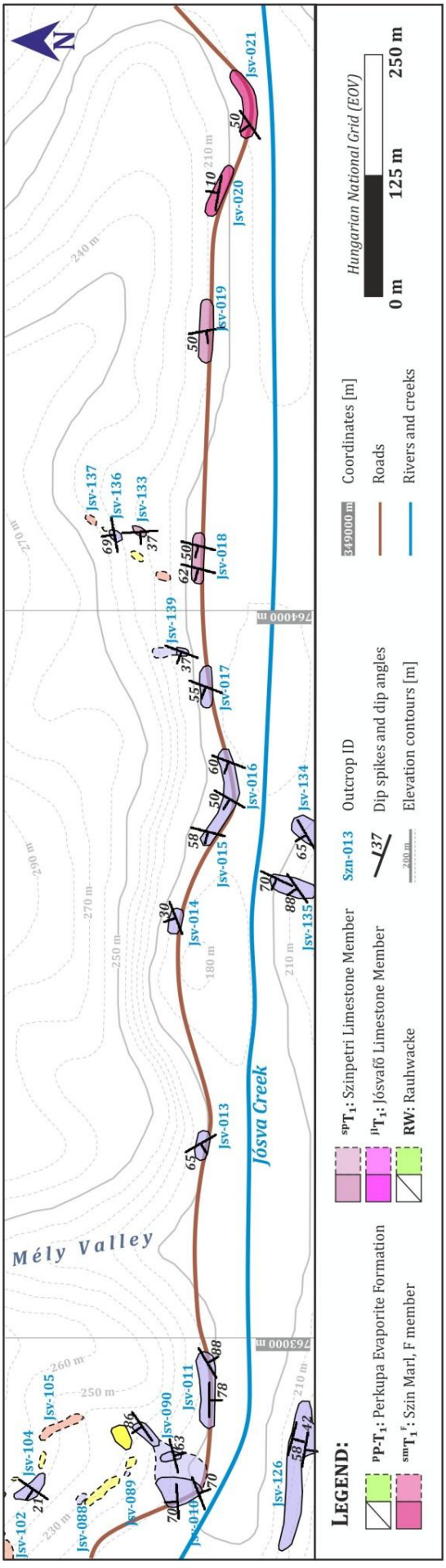

dips are very similar, practically the same in the two limestones, their boundary may not be a continuous sedimentary boundary as rauhwackes as well as grey and green colored shale detritus were found between the limestone outcrops within a NNW-SSE trending zone *(Jsv-133—137)*.

In the Jósvafő Limestone the general W-ward facing dips remains until *Jsv-011* where the limestone beds dip sub-vertically towards S and are folded into asymmetric shear folds (see details below). This S-ward dip still appears in *Jsv-090* and in the southernmost part of the *Jsv-010* point but in its northern parts the measured dips turn towards N and gradually becomes shallower and shallower (85-70-50°). On the other side of the Jósva Valley a remarkable cliff was found where the Jósvafő Limestone dips towards S *(Jsv-126)*. Here the measured dip angles gradually change towards S from 60° to 35-40° ***(Fig.54)***.

◀ ***Map 14.*** Observation map of the western part of the road between Szinpetri and Jósvafő.

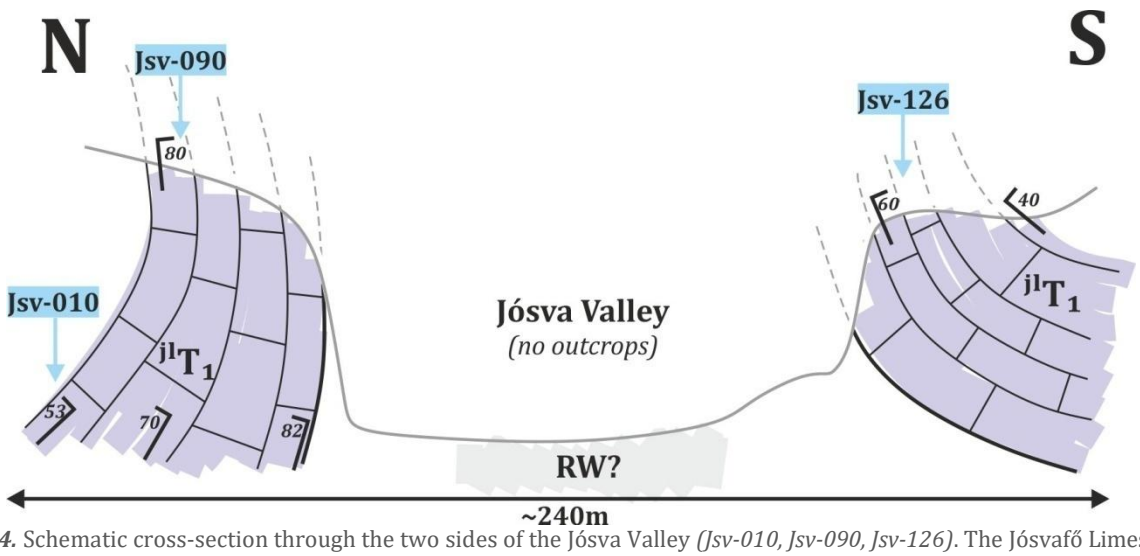

Fig.54. Schematic cross-section through the two sides of the Jósva Valley *(Jsv-010, Jsv-090, Jsv-126)*. The Jósvafő Limestone dips oppositely on the two sides and the dip angles seem to increase toward the axis of the valley. On the northern limb even overturned bedding was observed.

Important outcrops along the road between Szinpetri and Jósvafő:

Jsv-029: $^{sp}T_1$

In the shallowly (20-25°) dipping Szinpetri Limestone beds at the *Jsv-029* outcrop moderately steep and almost vertical (55-80°) brittle structural elements were measured with NNW-SSE strike directions. The kinematics of these faults must have originally been normal based on the normal drag folds found along them ***(Fig.55/b)***. Strike-slip striae found on the fault planes suggest reactivation of the extensional faults which is – based on the measured lineations – connected to a NNW-SSE compressional and perpendicular tensional deformation phase. Even though the symmetry axis of the normal fault Mohr pairs is roughly parallel to the normal vector of the bedding, the faults are nearly symmetrical in their present day position as well so it cannot be fully determined whether they were formed pre-tilt or post-tilt ***(Fig.55/a)***. There are, however, strike-slip lineations which are roughly parallel to the tilted bedding, thus they must have formed as originally subhorizontal lineations, so prior to tilting ***(Fig.55/c)***. Considering that these strike-slip pre-tilt faults and the normal fault Mohr pairs on ***Fig.55/a***, as well as the axis of the measured normal drag folds along the faults indicate ENE-WSW extension, it may be supposed that the normal faults were also formed as pre-tilt structural features and were then later reactivated during a very similar but post-tilt NNW-SSE compressional and perpendicular extensional strike-slip phase.

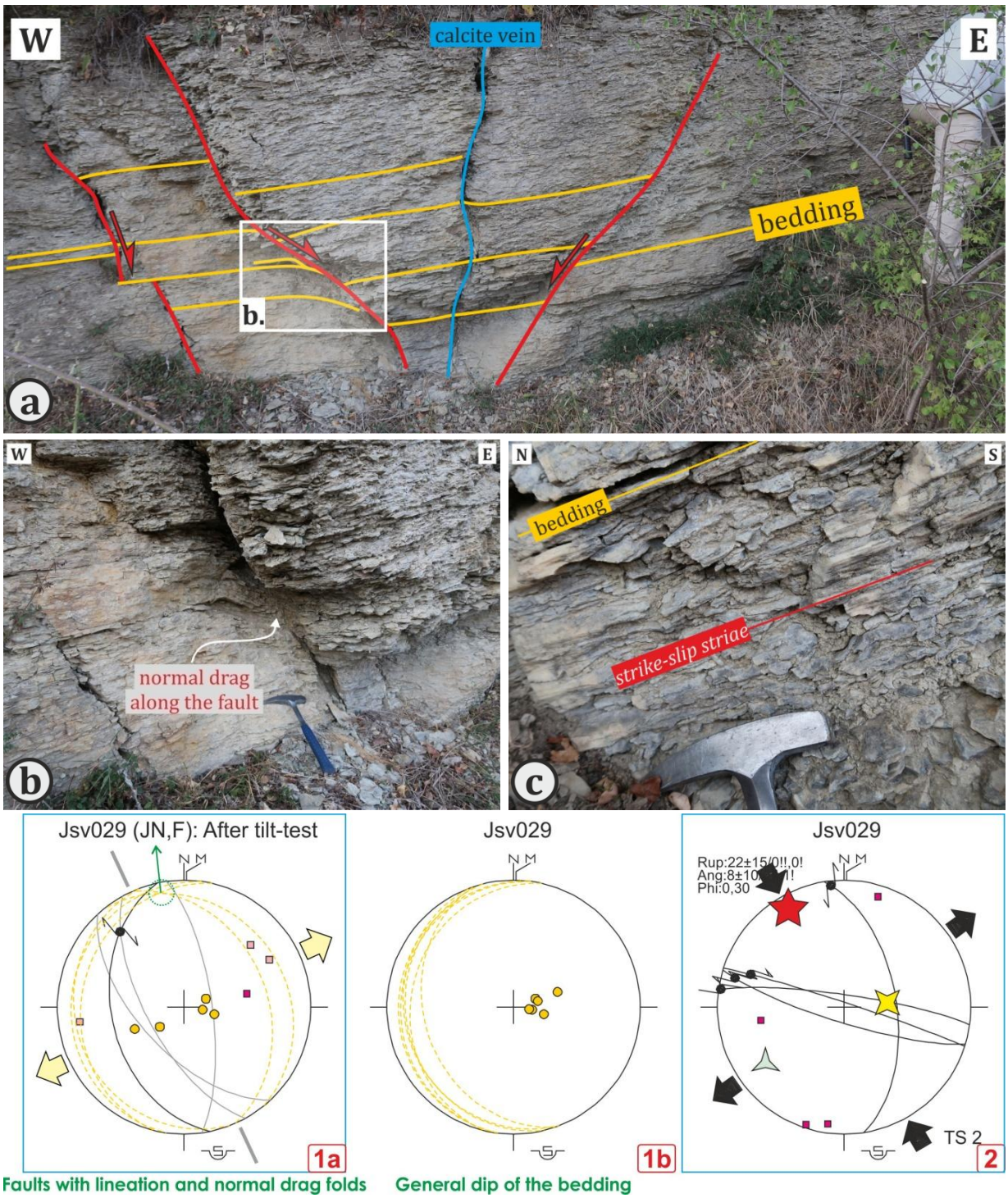

Fig.55. Reactivated normal faults and normal drag folds at *Jsv-029*. **A.)** Symmetric normal fault Mohr pairs whose symmetry axis is parallel to the normal vector of the bedding. This may indicate that the normal faults formed prior to tilting. **B.)** Normal drag folds along the faults, suggesting normal kinematics of the faults which were later reactivated as strike-slip faults. **C.)** Strike-slip striations running roughly parallel to the bedding which indicates pre-tilt age. **Stereoplots** show that a pre-tilt ENE-WSW extensional phase (1) was followed by a post-tilt strike-slip phase (2).

Besides the drag folds, small-scale folds with maximum of a few centimeters size were discovered as well. The folding affected only one or two layers ***(Fig.56)***. Some folds have even overturned wings while others contain onlap surfaces or pinch-outs. The folds are associated by small (maximum of 2 centimeters) thrust faults with minimal offset. These faults are sealed and flatten downward into the bedding ***(Fig.56/a)***. Both the folds and thrust faults show a steady top-to-SW vergency. Furthermore, in the same stratigraphical level small-scale normal faults were observed as well which were covered by the subsequent layers or by normally dragged monocline folds (fault-

related folds, ***Fig.56/b***). Some beds even thicken towards the normal faults. The strike of the normal faults is NW-SE which is parallel to the axis of the small-scale folds.

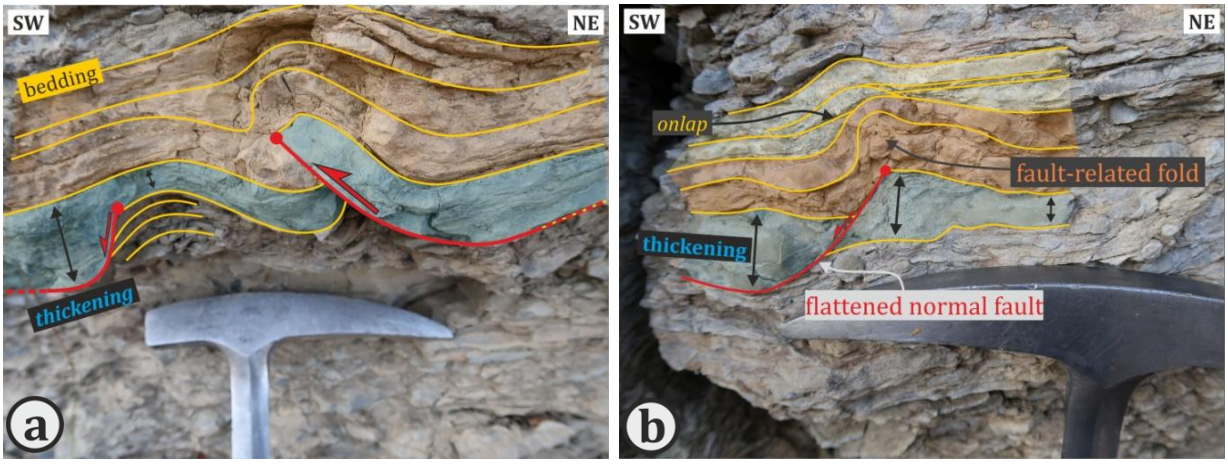

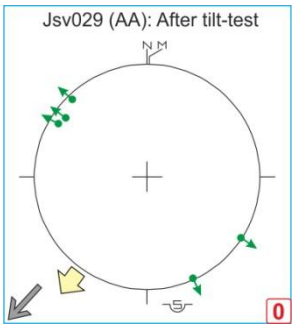

Fig.56. Sedimentary deformation structures at *Jsv-029*. **A.)** Small-scale thrust fault and normal fault observed in the same stratigraphical level. Both faults are sealed and the deformed beds show thickness variations. **B.)** Sealed normal fault and fault-related fold. The fault itself is sealed and flattens into the bedding. Thickness variations and the observed onlap surface indicate syn-sedimentary deformation. **Stereoplot** shows that the main vergency of the sedimentary structures is towards SW.

Jsv-028: $^{sp}T_1$

The outcrop at *Jsv-028* looks pretty much the same as at *Jsv-029*: the dominant features of the section are E-ward dipping moderate to steep (50-80°) discrete NNW-SSE trending faults with normal drag folds along them ***(Fig.57)***. The interesting thing about these drag folds is that their amplitude change along dip – e.g. the drag folds at the fault to the right in ***Fig.57*** have significantly higher amplitude downdip than updip where only a small dragging of the layers indicate the normal direction of the fault movement. Along one of the faults reverse dragging was observed as well, indicating compressional reactivation along some of the faults. There are also asymmetric folds with top-to-SE vergency. The general shallow (15°) dip of the Szinpetri Limestone here makes it hard to decide based on only the fault geometry whether the faults are pre- or post-tilt faults but the observed reverse drag fold along one of the faults may indicate that the formation of the normal faults preceded the compressional deformation accompanied by folding and reactivation of the faults. On the other hand two dip-slip lineations were measured along one of the faults which may suggest (another) post-tilt ENE-WSW extensional phase as well ***(Fig.57)***.

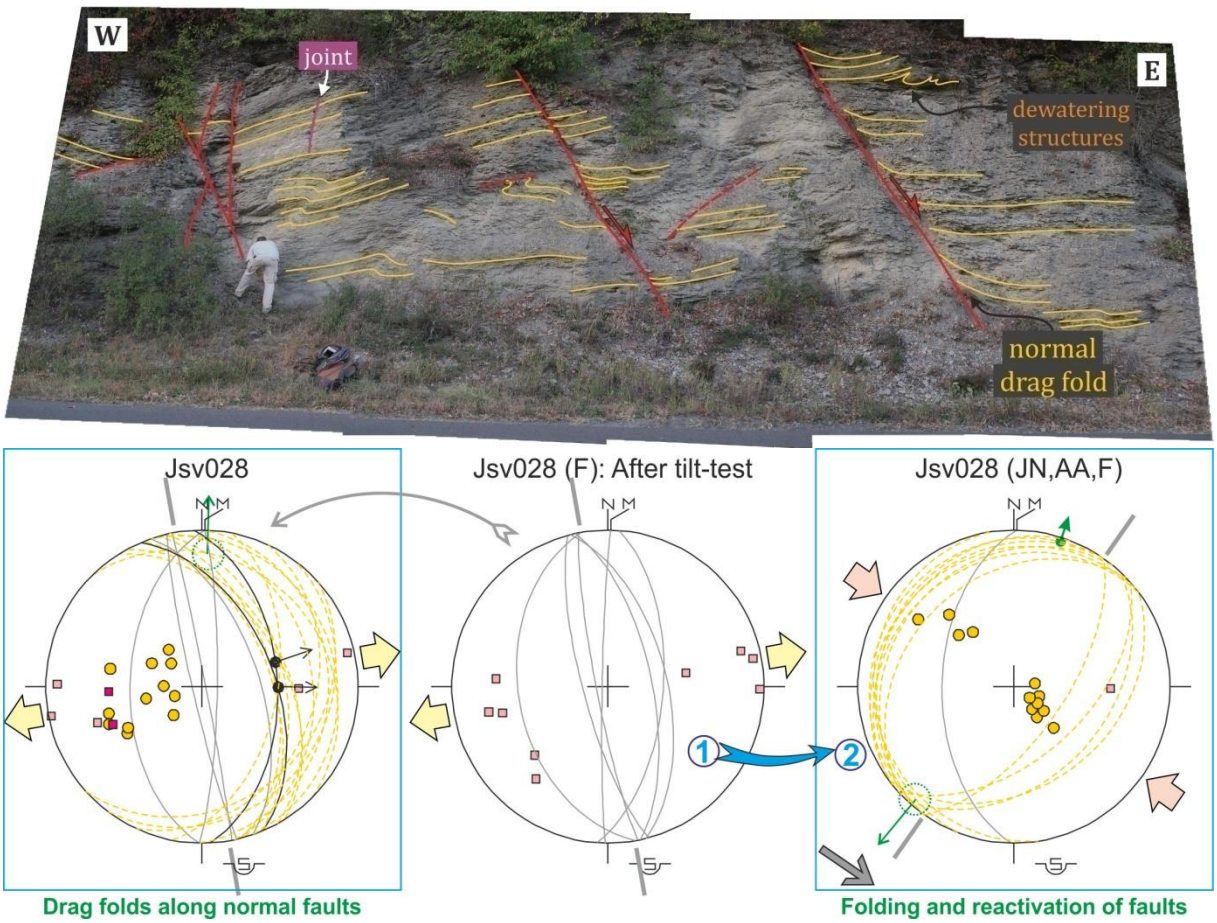

Fig.57. Interpreted cross-section of *Jsv-028* with E-ward dipping discrete faults and SE-vergent folds. The drag folds along the faults indicate normal kinematics while a reverse drag fold indicates compressional reactivation of the same faults. **Stereoplot** shows the measured and back-tilted data.

Jsv-018: spT1

Moderate to steep (45-65°) dips were measured in the Szinpetri Limestone at *Jsv-018*. Here several small-scale folds confined to only a few layers were observed ***(Fig.58/a-b)***. The folding only affected the thin bedded marls and limestones while the thick bedded limestone layers were left undeformed. The axis of these folds is parallel to the strike of the bedding and their axial plane is currently sub-horizontal. The steeply dipping bedding is cut by several shallow to moderately (20-45°) dipping discrete fractures which at first glance appear to be thrust faults but the drag folds along them indicate that the hanging wall moved in downdip direction (normal fault movement). The stereoplots in ***Fig.58*** show that in their present day position the strike of the fractures have wide scattering but after tilt correction, the faults become more or less parallel (the still visible scattering may be due to averaging the measured dips along the section for gaining a single tilting value). This along with the normal drag folds suggest that the discrete fractures must have formed as pre-tilt normal faults. This does not exclude the possibility that the tilted faults were later reactivated as thrust faults though.

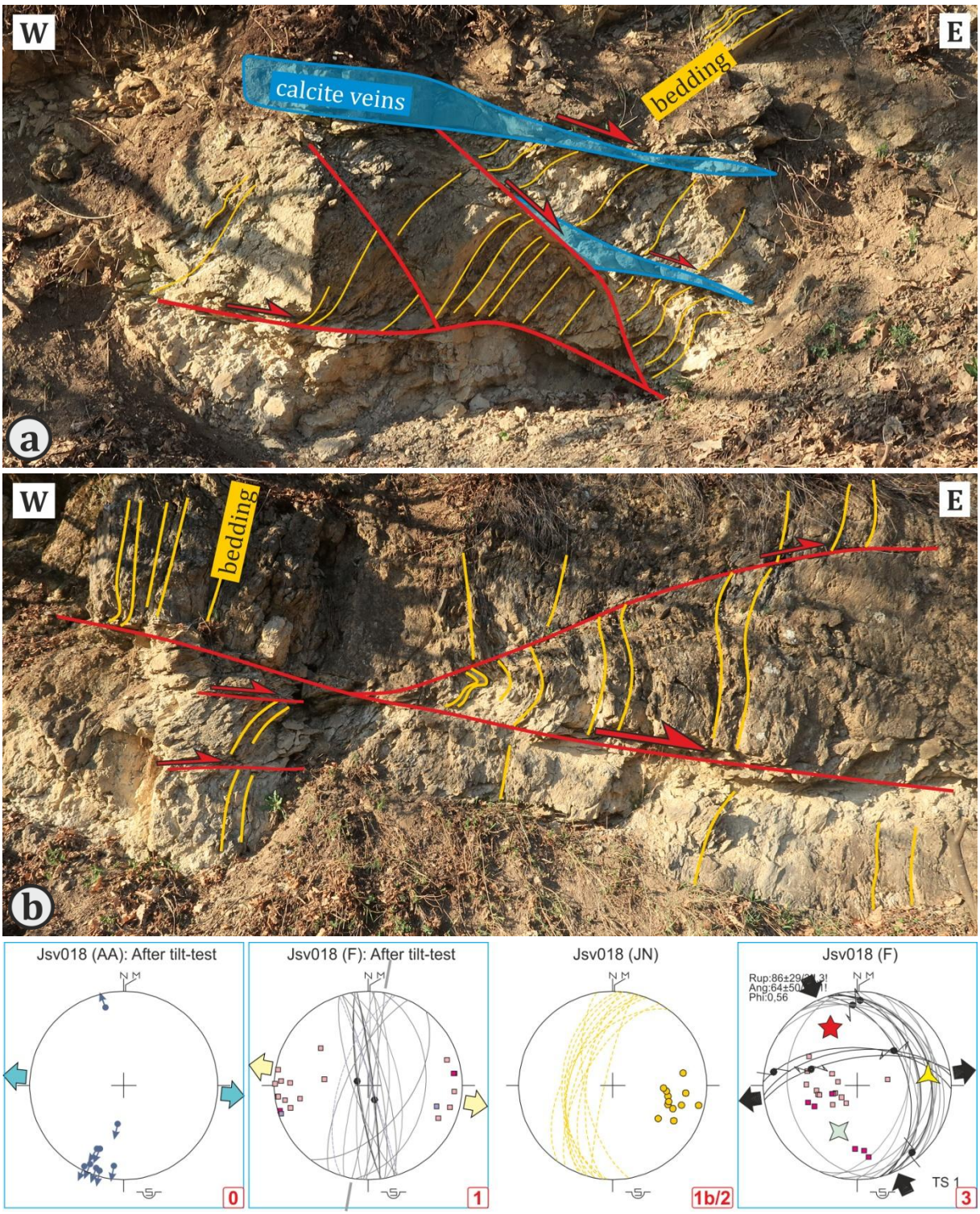

Fig.58. Low-angle shear zones in the Szinpetri Limestone at *Jsv-018*. **A. and B.)** Drag folds and the observed offset directions indicate that the shear zones were originally formed as pre-tilt normal faults. **Stereoplots** of the back-tilted data suggest ~E-W pre-tilt extension. The normal faults were later reactivated as oblique faults that indicate post-tilt NNW-SSE compression and perpendicular extension.

Jsv-017: $^{sp}T_1$

Very similar low-angle faults and calcite veins accompanied by oppositely dipping steep fractures were found in the Szinpetri Limestone at *Jsv-017* **(Fig.59).** The tilt-test of these fractures gave positive results so they were originally formed as pre-tilt NNW-SSE striking normal faults. Further discrete NE-SW trending shallow (20-40°) dip slip thrust faults and approximately E-W trending

dextral oblique thrust faults were found which all together suggest NW-SE compression. Dip-slip striae on NNW-SSE trending moderately steep (~60°) normal faults indicate a post-tilt ENE-WSW extensional phase.

In this outcrop it is evident that not only one but multiple folding event affected the Szinpetri Limestone ***(Fig.59)***. First, small-scale folds confined to only one or two layers are present and they are slightly asymmetric: their vergency is mainly to the SW. In a few cases there are also thin marl layers onlaping on the fold wings. Second, there are also folds which were very difficult to observe as their axis is parallel to the strike of the outcrop. These folds are mainly asymmetric, SSW-vergent folds with 20-40 cm amplitudes and rounded hinge zones. The stereographic projections of the data measured on these folds look chaotic in their present day position and their axess have significant plunge (40-60°). Moreover, several pre-tilt NNW-SSE striking calcite veins cross-cut these folds, indicating that the formation of these folds also preceded the general tilting. After carrying out the tilt correction, the stereoplots of these folds became symmetrical and their axes became sub-horizontal, so the tilt-test gave positive results. The tilt correction was carried out by the general dip value for the outcrop which is 52° towards WNW. This general tilting is probably the result of a third folding event.

Fig.59. Interpreted sections and stereoplots of *Jsv-017*. **A.)** Interpreted field photo of the whole section. The section is dominated by E-ward dipping pre-tilt normal faults and calcite veins. **B.)** Zoomed-in drawing of the most remarkable part of the section where the SW- and S-vergent asymmetric sedimentary (slump) folds are offset by pre-tilt normal fault conjugate pairs. The **stereoplots** show the two groups of slump folds, the back-tilted data of the pre-tilt normal faults and the oblique thrust faults related to NW-SW compression.

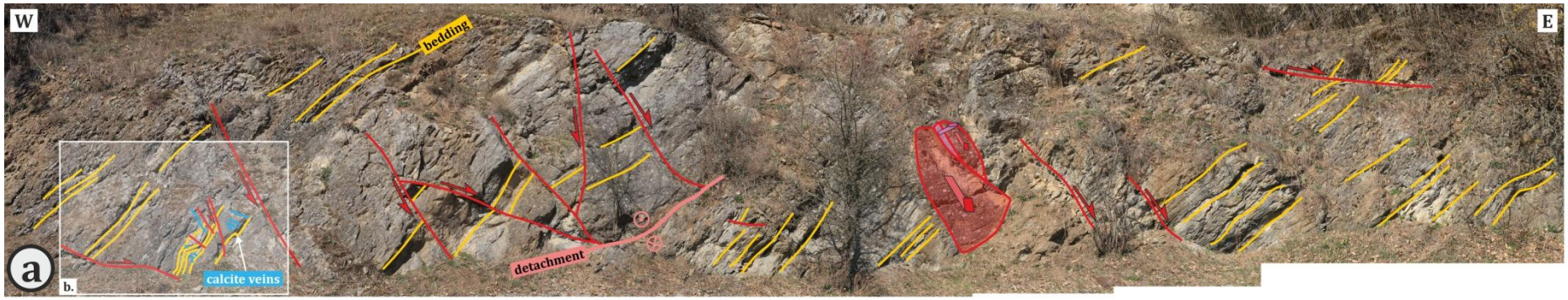
W
E
bedding
detachment
calcite veins
a
b.

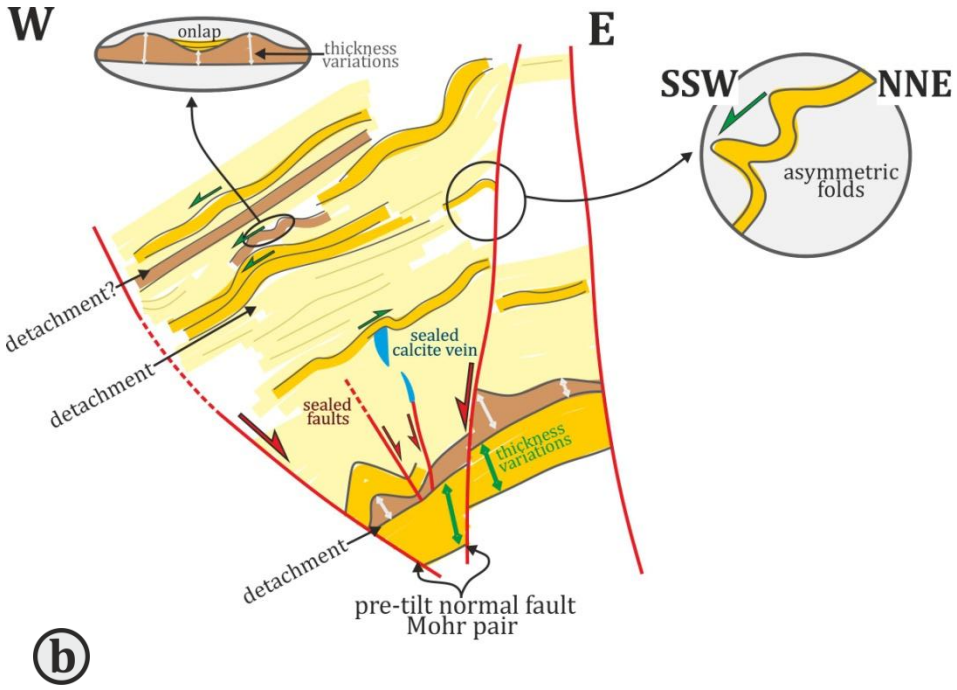
W
E
onlap
thickness variations
SSW
NNE
asymmetric folds
detachment?
detachment
sealed calcite vein
sealed faults
thickness variations
detachment
pre-tilt normal fault
Mohr pair
b

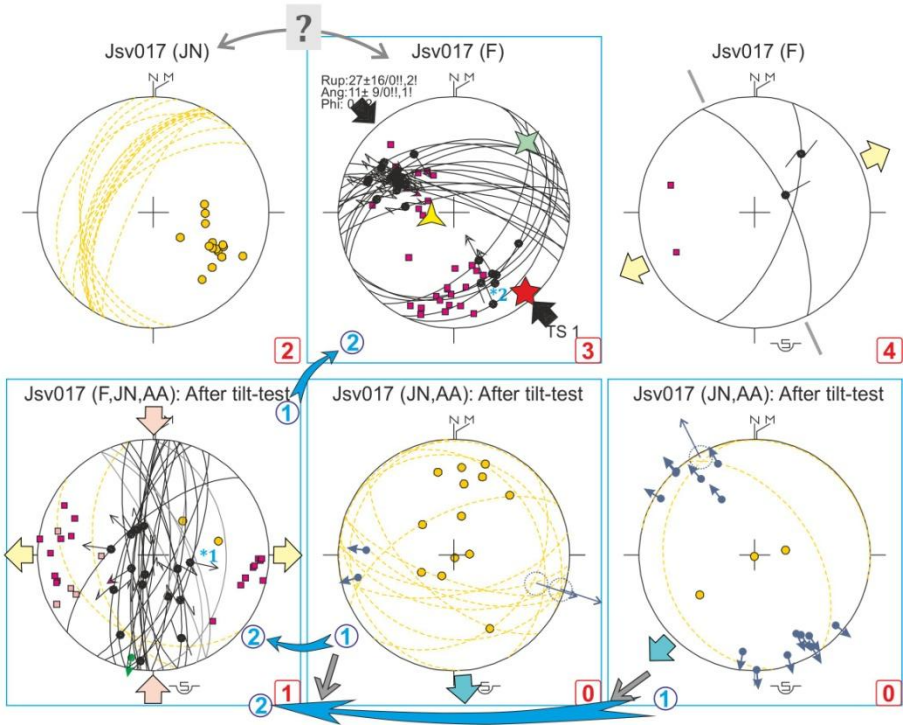
?
Jsv017 (JN)
Jsv017 (F)
Jsv017 (F)
Rup:27±16/0!!,2!
Ang:11± 9/0!!,1!
TS 1
2
3
4
Jsv017 (F,JN,AA): After tilt-test
Jsv017 (JN,AA): After tilt-test
Jsv017 (JN,AA): After tilt-test
1
2
0

Jsv-016: j^lT_1

At *Jsv-016* brittle structural elements dominate the quarry. In most cases the offset along the faults is unknown, it may be only a few cm or may even exceed several meters. On the very discrete fault plane of the biggest steep (~70°) fault three different striae overprinted each other. In ***Fig.60*** the stereographic projection of one of the three striae is positioned on the bedding plane, meaning that the lineation is parallel to the cutaway line of the bedding and the fault. Furthermore, another lineation is oblique relative to the ideal dip-slip direction by the same degree as the dip of the bedding. This geometry indicates that both striae were formed prior to tilting: after tilt correction the former lineation becomes totally horizontal while the latter becomes dip-slip. The relative chronological order of these two fault movements could not be observed unfortunately but based on the fault geometry the dextral strike-slip fault should be the younger one because considering its 70° dip angle the fault plane itself most probably formed as a normal fault, and later the strike-slip movement must have only reactivated an already present fault plane. Finally the presently sub-horizontal strike-slip lineations are interpreted as post-tilt features.

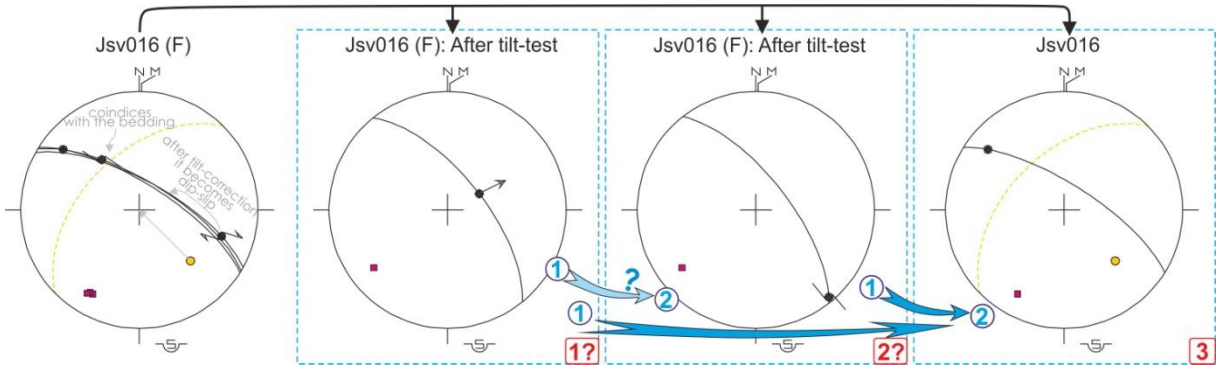

Fig.60. Overprinting lineations of a major fault plane at the quarry of *Jsv-016*. The first stereoplot shows all three of the measured lineations while the other three stereoplots show them in their pre-tilt or post-tilt state, Note how the first two lineations becomes dip-slip and totally horizontal after tilt correction. The relative chronological order of the different fault movements is set based on only the fault geometry.

In another part of the quarry numerous brittle structural elements were found. Within these faults and joints one can discover the following orderliness: even though the present day dip of these fractures is very various, it is between 6-60°, the imaginary symmetry plane of the shallow and moderately steep fractures is perpendicular to the tilted bedding ***(Fig.61/a)***. This means that these fractures were originally formed as Mohr pairs which were then tilted. As after carrying out the tilt correction the faults and joints became NE-SW trending fractures with approximately 60° dip angle they must have been originally normal faults. Calcite precipitation also occurring along the normal faults should have been at least partly syn-kinematic which is proved by calcite dominoes along the tilted faults ***(Fig.61/b)***. Furthermore, small offsets of the calcite veins indicate the frequent presence of bedding parallel joint surfaces related probably to pressure solution ***(Fig.61/c)***. Since these pressure solution surfaces are bedding parallel their presence also proves the early (pre-tilt) age of the calcite veins. Finally, oblique thrust fault striations on the calcite veins indicate compressional reactivation of the former extensional structures ***(Fig.61)***.

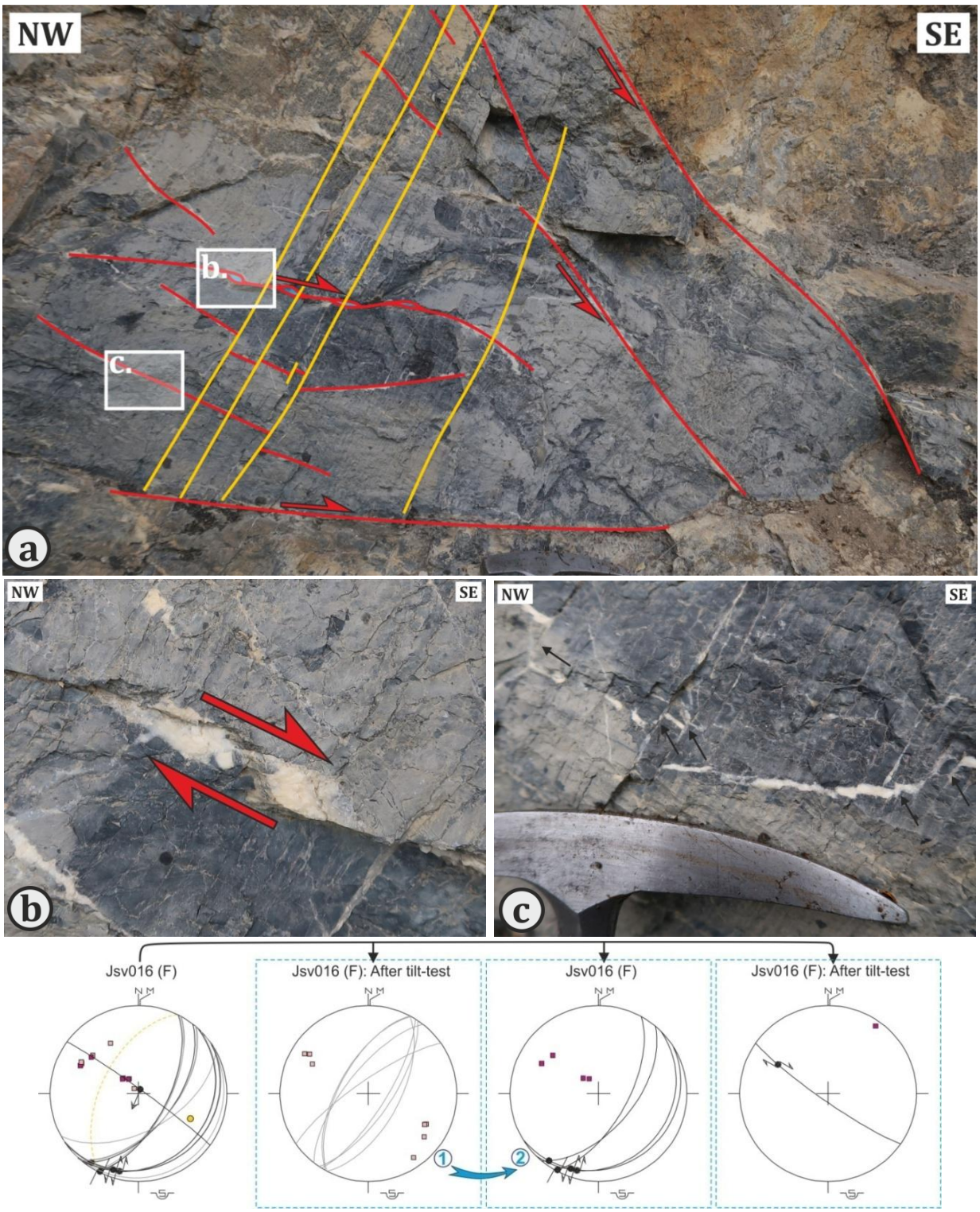

Fig.61. Pre-tilt normal faults and related structural features at *Jsv-016*. **A.)** Interpreted field photo of the pre-tilt fractures cross cutting the tilted bedding planes at 60°. **B.)** Calcite precipitation along a pre-tilt fracture indicating normal kinematics of the fault. **C.)** Small offsets of the calcite veins along pressure solution surfaces. **Stereoplots** show that the fault planes becomes symmetric normal fault Mohr pairs after tilt correction. Measured lineations indicate compressional reactivation of the pre-existing faults.

Beside all this ~E-W trending moderately steep dextral or oblique dextral strike-slip faults were also frequent in the quarry. After the positive tilt-correction these faults became oblique dextral thrust faults ***(Fig.62)***. On the steeply NW-ward dipping bedding planes layer-parallel striations were observed and their kinematics was determined as normal. The present-day dip of the Jósvafő Limestone here is at least partly but maybe completely connected to this normal movement along

the bedding planes. The limestone layers are furthermore full of with small-scale – mostly symmetric – folds. These folds often show lateral thickness variations, have detachment surfaces below them and are sealed by underformed layers from above. Their vergency is either NE or SW.

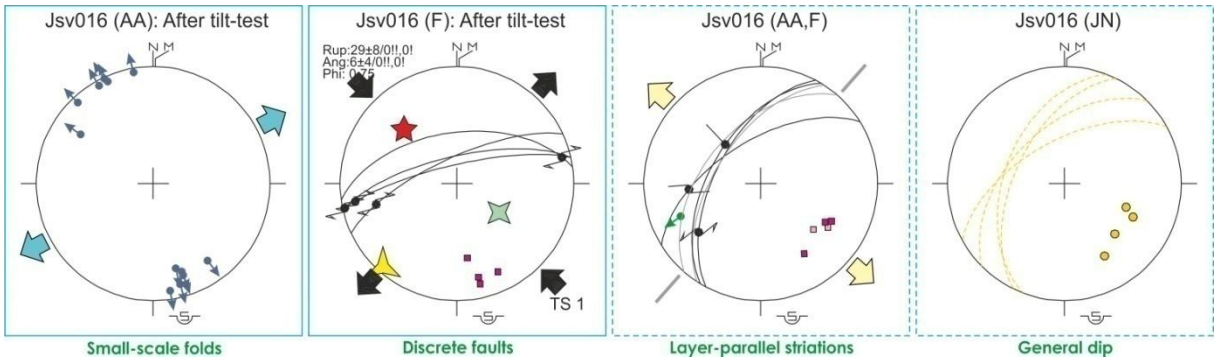

Fig.62. Stereoplots of every other data measured in the quarry at Jsv-016. The symmetric small-scale folds suggest NE-SW vergency. The discrete faults indicate NW-SE compression and perpendicular extension. The "normal" layer-parallel striations may (but not necessarily) be connected to the present-day dip of the Jósvafő Limestone here.

Jsv-011: $^{jl}T_1$

The general W-ward directed dip of the Jósvafő Limestone changes to steep or sub-vertical S-ward dip between the *Jsv-012 and Jsv-011* points. At *Jsv-011* the sub-vertical limestone beds are folded into an asymmetric fold ***(Fig.63/a)***. This fold is a similar fold with rounded hinge zone and ENE-WSW trending axis. Its interlimb angle tightens northward (upward?): while the lower part of the fold is only a gentle fold, its upper part is a tight fold. ***Fig.63/b*** shows another 10 cm scale open fold with rounded hinge zone, NE-SW trending axis and exactly the opposite sense of shear than in ***Fig.63/a***. In this case the folded beds thin in the hinge zone of this second fold and they are covered by the subsequent beds.

Striae found on the bedding planes of the longer fold limbs prove layer parallel slip. The interesting thing was that these layer-parallel striations mark two different movement directions: one group suggests normal movement with respect to the present-day dip of the limestone beds, while the other shows reverse movement ***(Fig.63)***. Further WNW-ESE striking dextral and oblique thrust faults were measured that may have formed contemporaneously with the reverse layer-parallel slip. Beside these, sub-vertical E-W striking sinistral and NE-SW striking dextral strike-slip faults indicate post-tilt NW-SE extension. Based on the superimposed calcite fibers and lineations the E-W striking sinistral faults post-date the reverse layer-parallel movement.

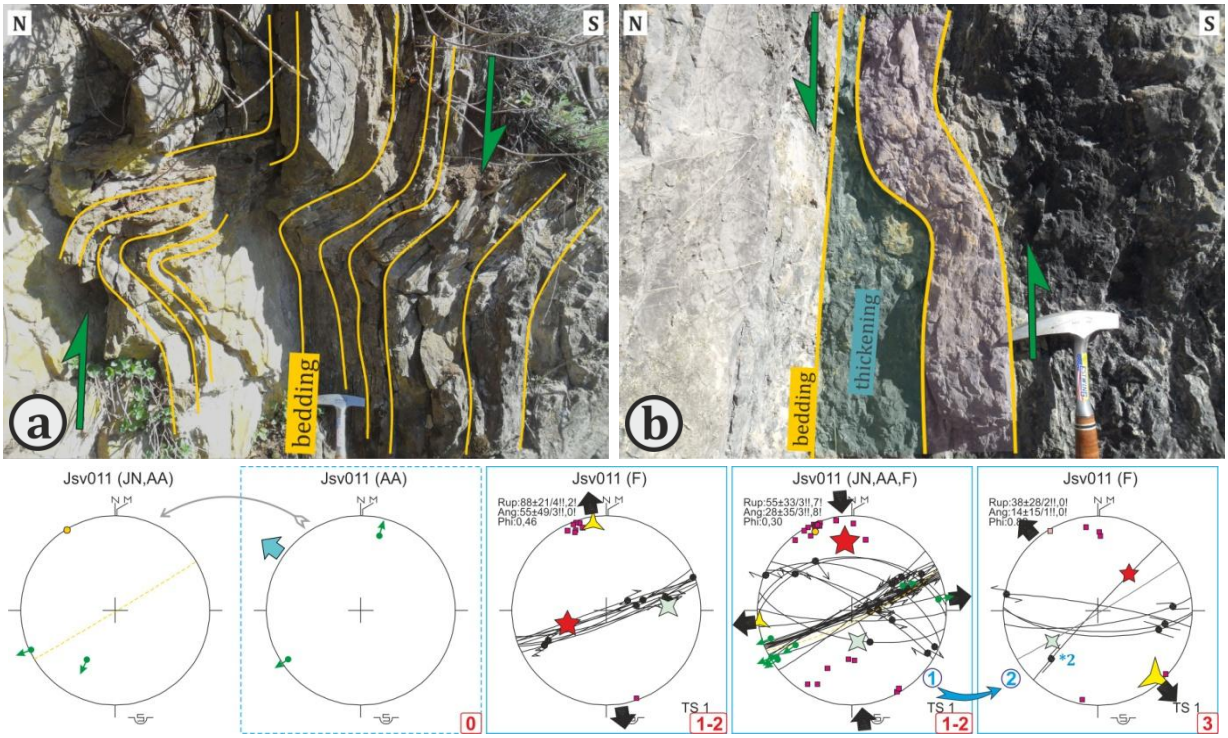

Fig.63. Field photos of folds and stereoplots at *Jsv-011*. **A.)** ENE-WSW trending asymmetric folds with upward tightening interlimb angle. **B.)** NE-SW trending asymmetric fold covered by the subsequent beds. The sense of folding is exactly the opposite than in the previous case. **Stereoplots** show the two groups of layer parallel slip data (1-2), as well as the fold axis (0) and post-tilt strike-slip fault data (3).

Jsv-010: $^{jl}T_1$

The last significant cliff before reaching Jósvafő outcrops the Jósvafő Limestone at *Jsv-010*. The measured N-facing dips generally steepen towards S from 50° up to 80°. At the northern part of the section the N-ward dipping beds turn into very shallow (15°) S-directed dips while forming a fold with rounded hinge zone ***(Fig.64/a)***. This fold is a result of top-to-S shearing and its deformed beds show lateral thickness variations. Further to S another E-W trending open fold was observed ***(Fig.64/a-b)***. Based on the relationship of the shorter and longer limbs its vergency is just the opposite of the previous fold (top-to-N shearing). In the southernmost part of the section intensive folding resulted in Chevron-type folds with tight and angular hinge zone geometry ***(Fig.64/a,c)***. These folds also show top-to-S vergency.

In the middle part of the outcrop folds with still E-W trending axis but different geometry may be observed: the fold wings dip shallowly (30-50°) towards N ***(Fig.64/d)***. They may be simple bends or based on the geometry they may be part of a compressional duplex system, we just cannot see the detachment surfaces and thrust faults well. Moreover, the folds are cut through by brittle discrete faults which consequently post-date or at least are contemporaneous with the folding. It very hard to determine the kinematics in a lot of cases but where it was possible there mainly NW-SE trending dextral oblique thrust faults, approximately N-S trending sinistral strike-slip faults and NNW-SSE trending normal faults were measured ***(Fig.64)***. Based on the superimposed calcite fibers the formation of the sinistral oblique thrust faults were followed by normal fault movement along the NNW-SSE trending faults.

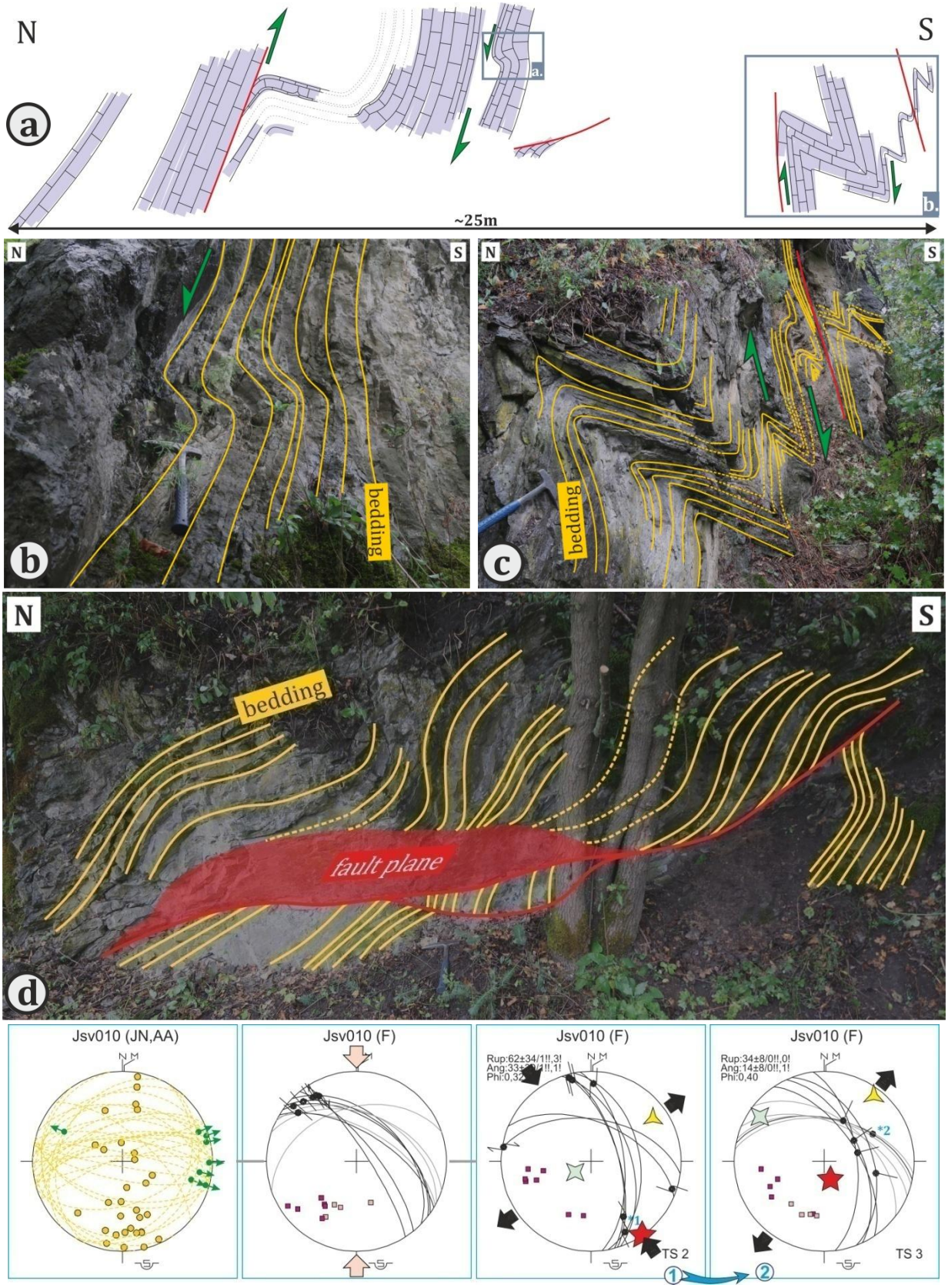

Fig.64. Schematic cross-section, field photos and stereoplots at *Jsv-010*. **A.)** Field cross-section showing all of the observed folds together. **B.)** Small open fold with top-to-N vergency and lateral thickness variations. **C.)** Intensively deformed Chevron-type folds with top-so-S vergency. **D.)** Folds (duplex system?) with overprinting brittle faults. **Stereoplots** of the measured data suggest that the already steeply dipping Jósvafő Limestone was affected by NNW-SSW trending dextral faulting. Further superimposed fault data indicate that a NW-SE compression and perpendicular extension was followed by NE-SW extension with dip-slip normal faults.

IV.13. The Jő-2 well and its surroundings

E of Jósvafő, along the road between Jósvafő and Szinpetri a continuous E-W trending in-situ rauhwacke zone was mapped *(**Map 15**, Jsv-004, Jsv-031, Jsv-052, Jsv-076—077)*. The width of this zone varies between 25 and 50 meters. The rauhwacke is in contact with the Jósvafő Limestone on both sides of the zone which dips steeply or vertically toward N or S ***(Fig.66/a)***. This major E-W trending rauhwacke zone can be followed continuously until *Jsv-086*, then it changes its strike direction to approximately WNW-ESE. Moreover, in the continuation of this zone outcrops of riffle-green and black shales were also found which were interpreted as the remains of siliciclastic intercalations of the Perkupa Evaporite *(Jsv-095, Jsv-102, Jsv-105)*.

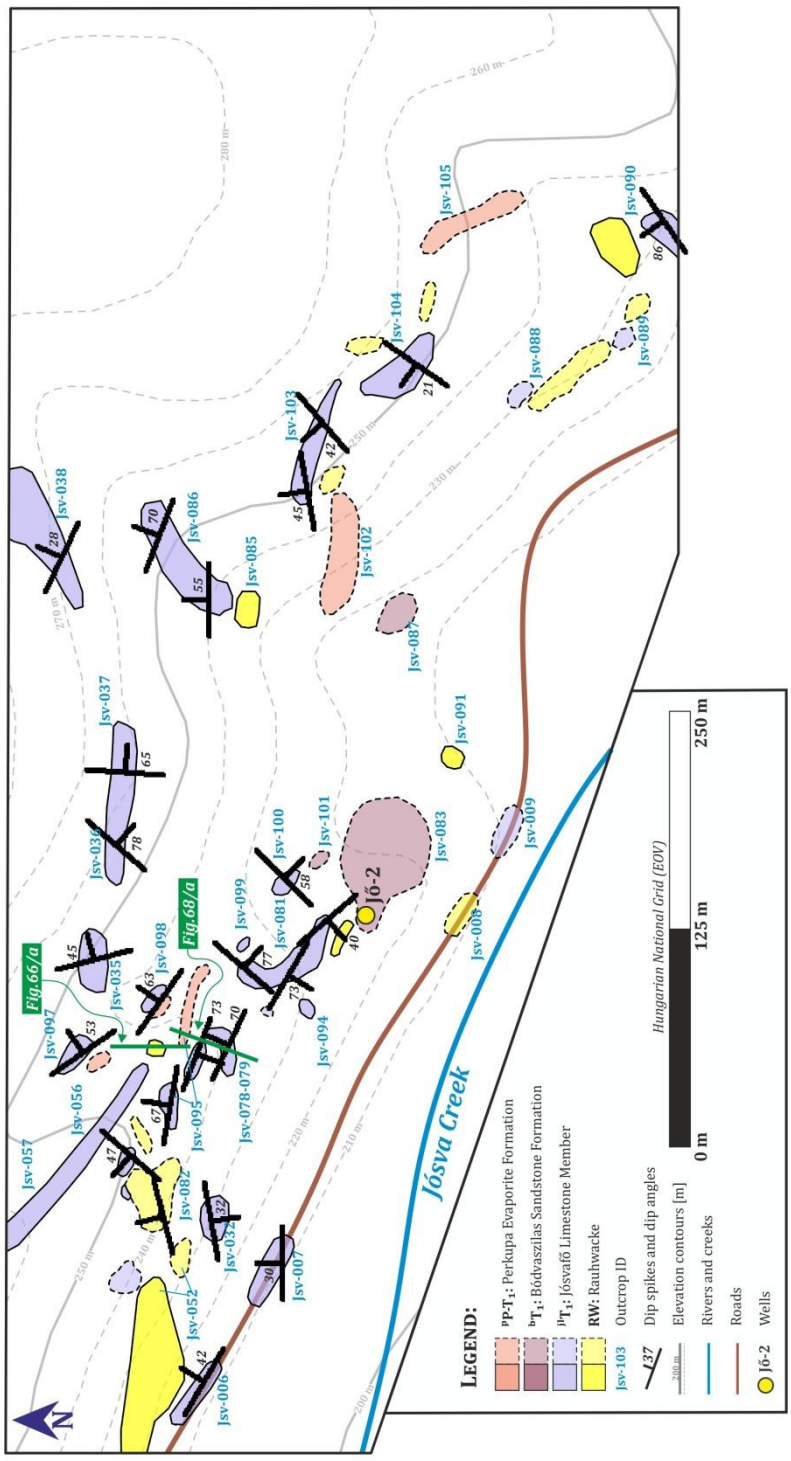

▲ ***Map 15.*** Observation map in the area around the Jő-2 well, E of Jósvafő. Rauhwackes, the Perkupa Evaporite and Bódvaszilas Sandstone occurrences form first an approximately E-W, then a WNW-ESE trending narrow zone within the Jósvafő Limestone.

N of the E-W trending rauhwacke zone various dips were observed in the Jósvafő Limestone at *Jsv-055—058* ***(Map 15)***. In ***Fig.65*** the steeply N-ward or S-ward dipping limestone beds turn into E-ward – also steep – dips, with the E-W striking layers being in the longer limbs. The axis of this fold is near vertical. In the N-ward or S-ward dipping beds further small-scale folds were observed whose axis is parallel to the E-W strike of the bedding. Similarly folded Jósvafő Limestone layers were observed further to the S, at *Jsv-080—082 and Jsv-093—094*.

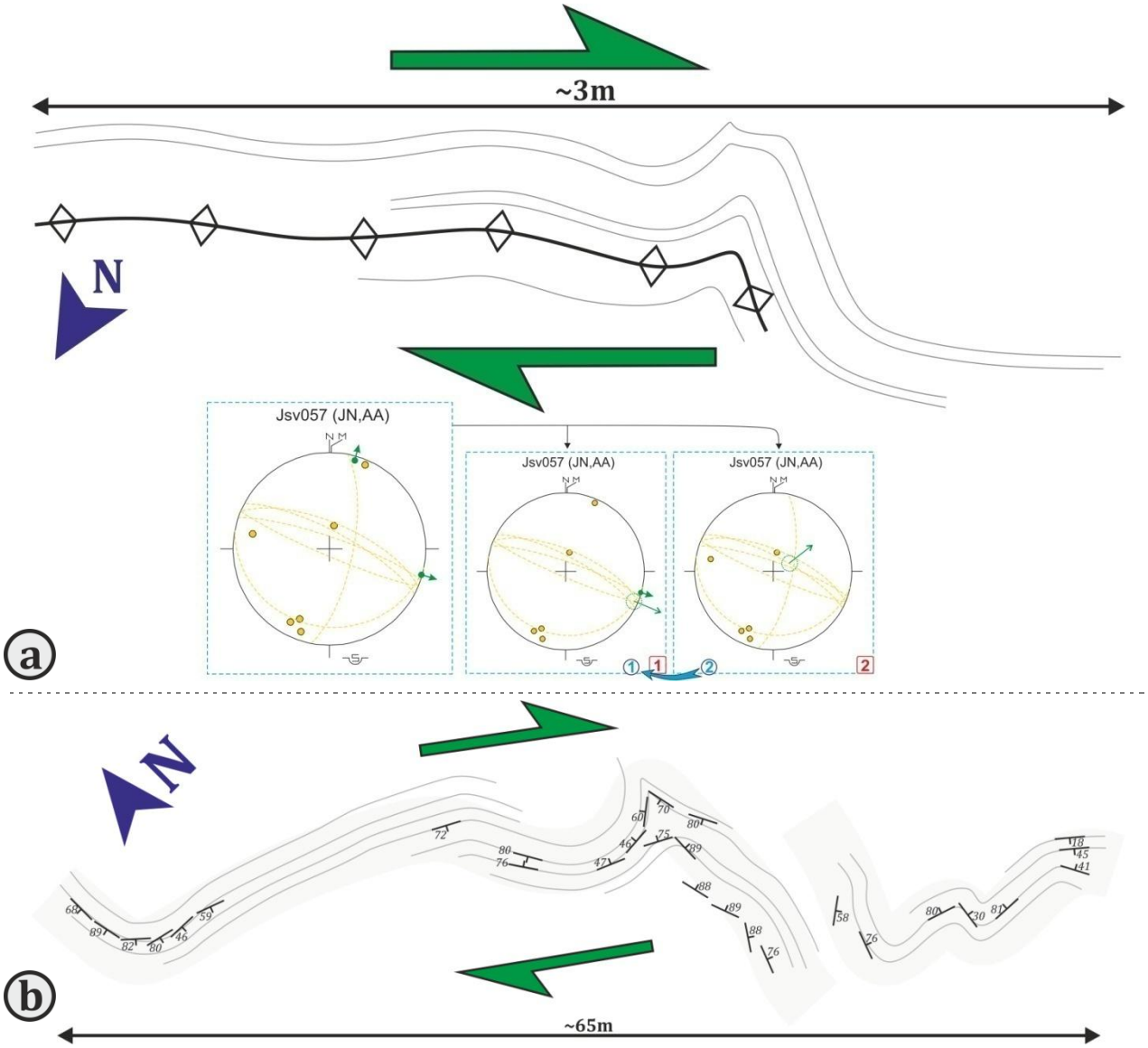

Fig.65. Map view and stereoplots of the folds found in the Jósvafő Limestone. **A.)** Outcrop-scale folds at *Jsv-057*. The longer limb of the fold is made up by E-W striking sub-vertical layers, whereas the shorter limb is formed by ~E-ward dipping steep beds. The axis of the fold is also sub-vertical. The overall fold geometry suggests dextral shear folding of the already steeply dipping Jósvafő Limestone. **B.)** Intensively folded and steeply dipping beds of the Jósvafő Limestone at *Jsv-080—082 and Jsv-093—094*.

S of the rauhwacke the mapped formations look like a Mosaic: isolated occurrences of the Jósvafő Limestone and the Bódvaszilas Sandstone are surrounded party or fully by rauhwacke and/or Perkupa Evaporite ***(Map 15)***.

Important outcrops of the area around the Jő-2 well:

Jsv-053: RW

At *Jsv-053* shale clasts with 4-10 or even 50 cm size are sitting within this rauhwacke zone, orientated by their longer axis. These clasts usually dip moderately (50°) towards S or they are sub-vertical ***(Fig.66/b)***. At *Jsv-095* a large map-scale black shale body was discovered. Besides the shale clasts, calcite veins dissected from the weathered rauhwacke have also steep (60-70°) or sub-vertical dips and are oriented in E-W or NE-SW strike ***(Fig.66/c)***.

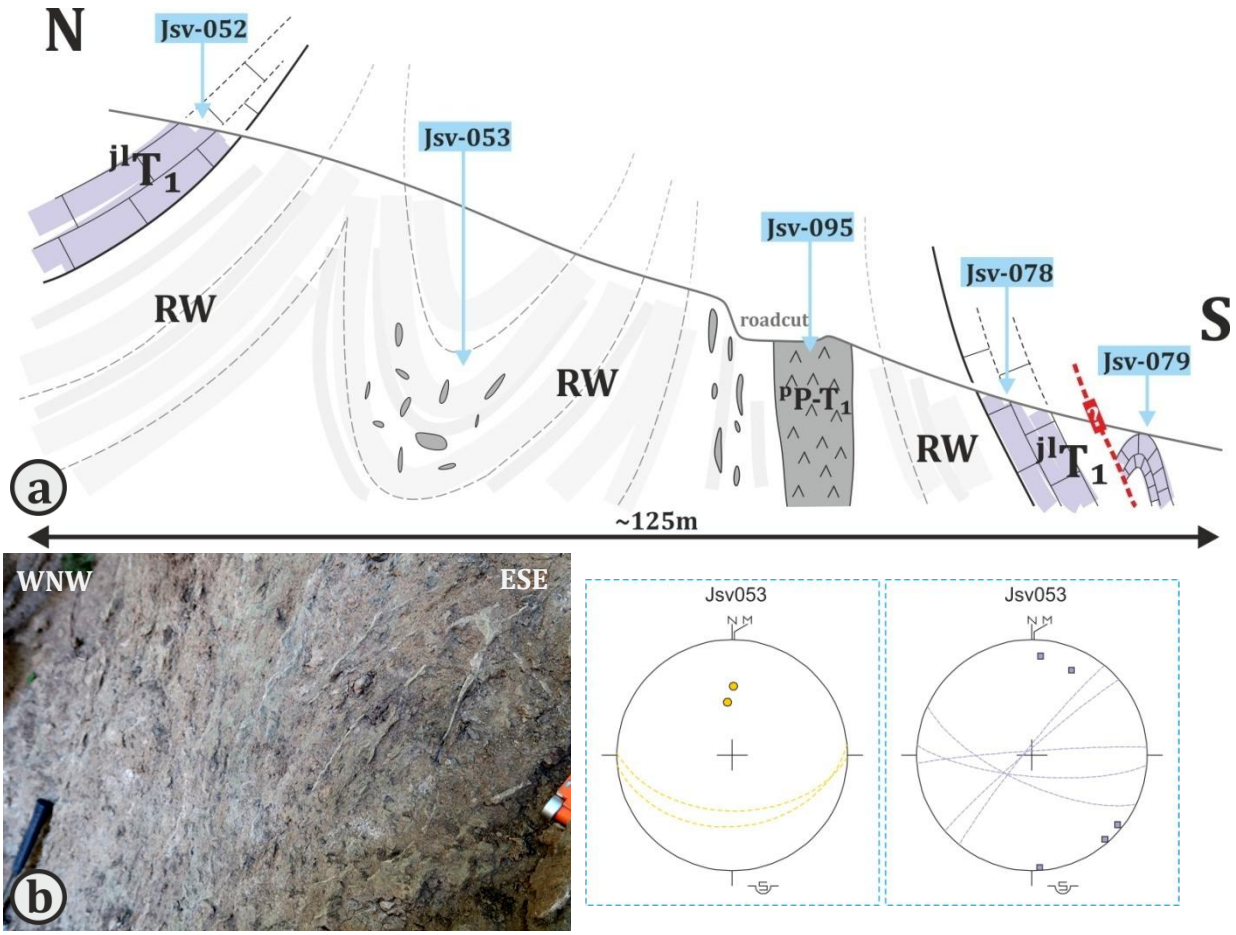

Fig.66. Oriented shale clasts and calcite veins within the E-W trending rauhwacke zone E of Jósvafő. **A.)** Schematic field cross-section through the rauhwacke zone which is bordered by steeply dipping or sub-vertical Jósvafő Limestone on both sides. Its inner structure is reflected by the oriented clasts and rock bodies (~Perkupa Evaporite), the still observable dips in the transitional zone between the limestone and the rauhwacke, as well as by the dissected calcite veins. See the section trajectory in ***Map 15***. **B.)** Field photo and stereoplots of the measured dips clasts and calcite veins.

Jsv-098: ^{p}P-T_1 and $^{jl}T_1$

At *Jsv-098* the Perkupa Evaporite is in direct contact with the Jósvafő Limestone. Within their sub-vertical contact zone the limestone is folded into an E-W trending asymmetric shear fold ***(Fig.67)***.

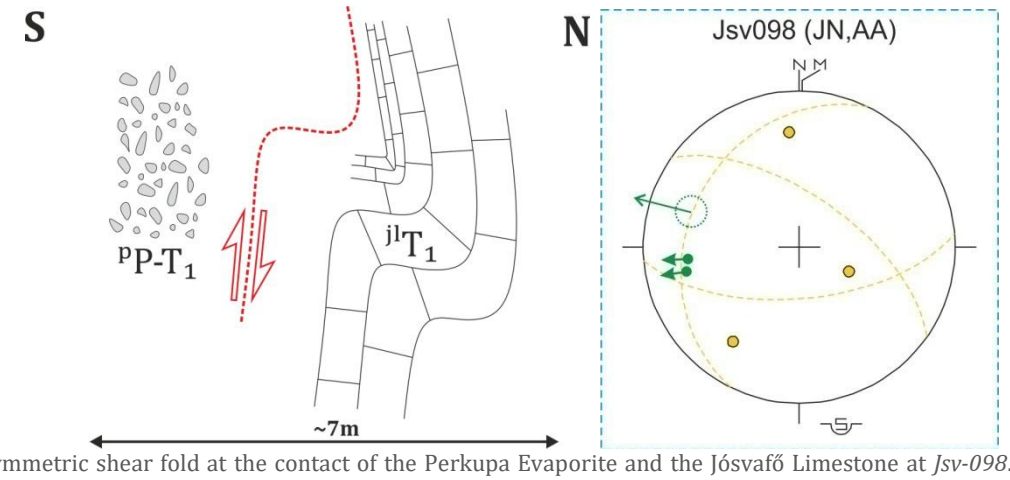

Fig.67. Asymmetric shear fold at the contact of the Perkupa Evaporite and the Jósvafő Limestone at *Jsv-098*. The axis of the fold is E-W.

Jsv-078—079: $^{jl}T_1$

Based on the measured 70-75° steep dips at *Jsv-078—079* the Jósvafő Limestone form a very tight/isoclinal ESE-WNW trending synform ***(Fig.68/a)***. In the N this synform is bordered by black shales of the Perkupa Evaporite while in the S the steeply dipping in-situ limestone outcrops suddenly disappear in spite of the slope being very steep. Moreover, the last few beds of the Jósvafő Limestone are very altered chemically and show strong brecciation. Based on all this, the synform is bordered by structural boundaries both from N and S, and it is probably surrounded by more incompetent rauhwackes and/or black shales. An additional symmetric tight fold with E-W trending axis and rounded hinge zone was observed on the northern limb of the fold ***(Fig.68/b)***. A similar but not so tight synform with E-W trending axis was mapped at *Jsv-007 and Jsv-032* as well which is also surrounded by rauhwackes.

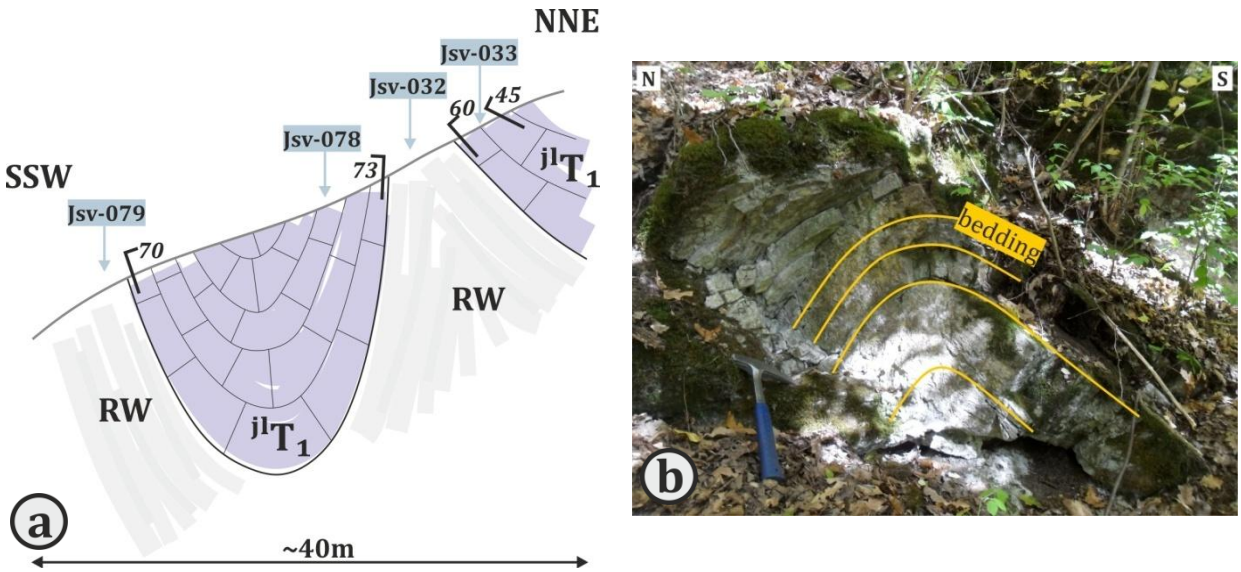

Fig.68. The observed structural elements at *Jsv-078—079*. **A.)** Schematic field cross-section through the Jósvafő Limestone that is surrounded by rauhwackes. The limestone forms a very tight/isoclinal synform. See the section trajectory in ***Map 15***. **B.)** Field photo of the symmetric and rounded E-W trending fold found at *Jsv-079*. See its exact position on ***Fig.66/a***.

IV.14. Outcrops SE from Jósvafő and the Fenyves Slope

The hills bordering the Jósva Valley from S have small outcrops only in the foresters' roadcuts and on the sole of the road itself so only pointwise structural data are available ***(Map 16)***. Except for a few spots with rauhwacke occurrences *(Jsv-123, Jsv-125, Jsv-129)* solely the Jósvafő Limestone was mapped in this area. Walking from the southeastern end of Jósvafő towards the Fenyves Slope, on the lower part of the side of the valley S- and SSW-ward dips were measured with very varying (25-85°) angles *(Jsv-109, Jsv-131—132)*.

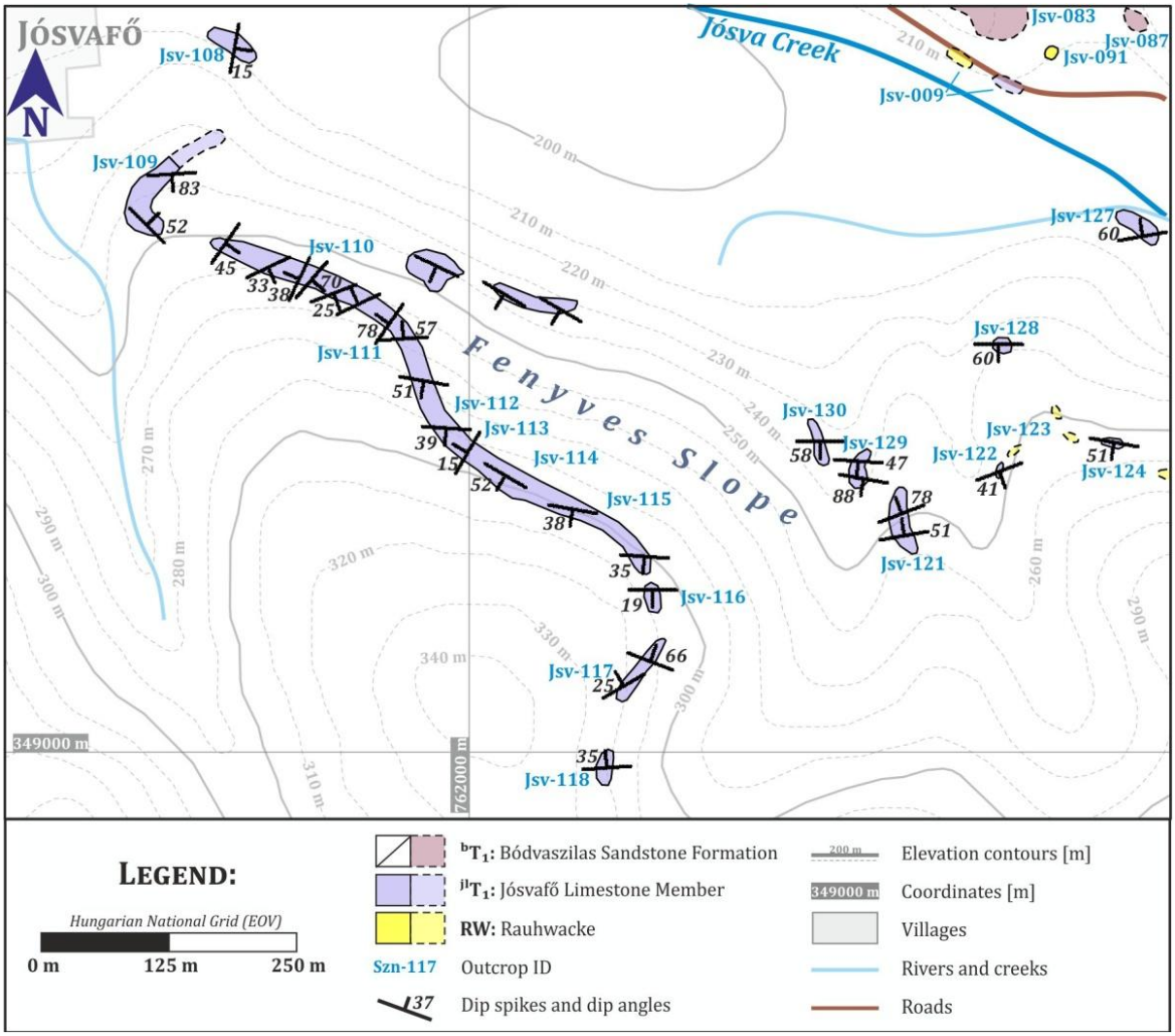

Map 16. Observation map of the area SE of Jósvafő and the Fenyves Slope.

Jsv-110—111: $^{jl}T_1$

On the upper part of the valley side, however, heavily folded beds were observed *(Jsv-110—111)*. The measured shallow to very steep, almost vertical (20-80°) dips point towards E-SE and W-NW. Based on the field data NE-SW trending asymmetric folds may be reconstructed ***(Fig.69)***. Their eastern shorter limbs are even overturned sometimes, indicating a general top-to-SE vergency. Additional small-scale S-folds were observed on the normal limbs of the folds while the overturned limbs had Z-folds.

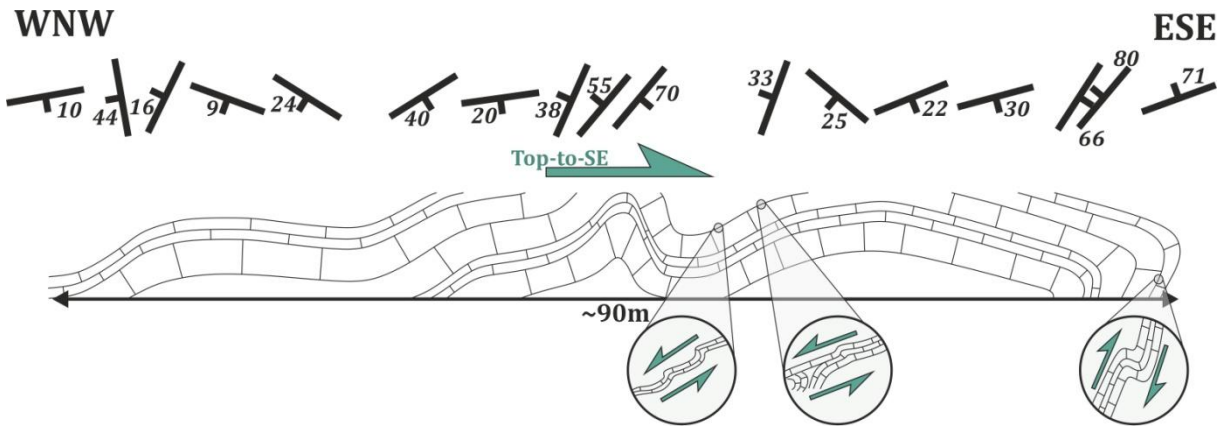

Fig.69. Schematic field cross-section of the observed folds at *Jsv-110—111*. The reconstructed asymmetric geometry indicates top-to-SE vergency. The heightened details show the observed shear indicators (S- and Z-folds).

From the *Jsv-112* locality the same S-ward moderate to steep dips return that were previously observed on the lower part of the side of the Jósva Valley ***(Map 16, Fig.70)***. If the measured dips are normal dips (not overturned) the reconstructed folds are open, slightly asymmetric folds with top-to-S vergency. It cannot be excluded, however, that there are overturned limbs as well but the monotonous lithology does not make it possible to observe on the field. In this case the general vergency would be the opposite, top-to-N.

After the *Jsv-116* point the measured dips turn over: the general S-ward dips change to N-ward ***(Map 16)***. The same turn-over is observed at the *Jsv-121 and Jsv-130* points as well ***(Fig.70)***. While at *Jsv-116—117* the dip angles are shallow (20-35°), the *Jsv-121 and Jsv-130* points have steep, even sub-vertical dips. These steep dips form a very tight to isoclinals map-scale synform that is probably a part of a very complex structure. E from this synform rauhwacke detritus were mapped *(Jsv-123, Jsv-125, Jsv-129)*.

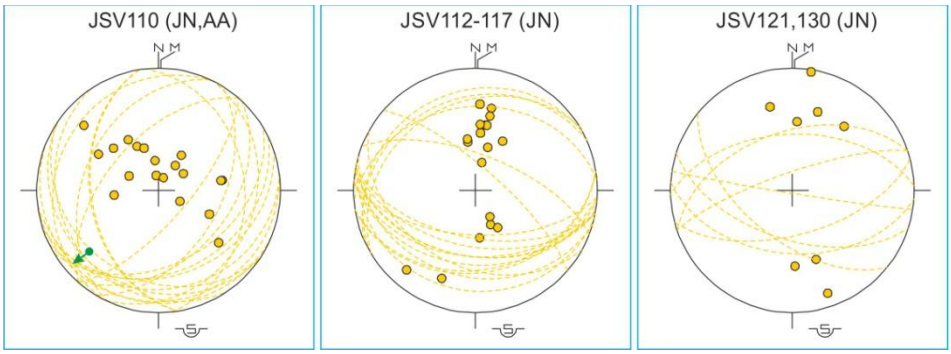

Fig.70. Stereoplots of the measured dips SE from Jósvafő and on the Fenyves Slope *(Jsv-110, Jsv-112, Jsv-117, Jsv-121, Jsv-130).*

IV.15. Along the tourists' road N of Jósvafő

On the top of the hills E of Jósvafő in-situ blocks of Middle Triassic platform carbonates were discovered *(**Map 17**, Jsv-066—068).* These carbonates may be followed until the tourists' road located W of the hills *(Jsv-069).* The southern boundary of the platform carbonate blocks is E-W trending on the top of the hills, then its strike changes to NE-SW.

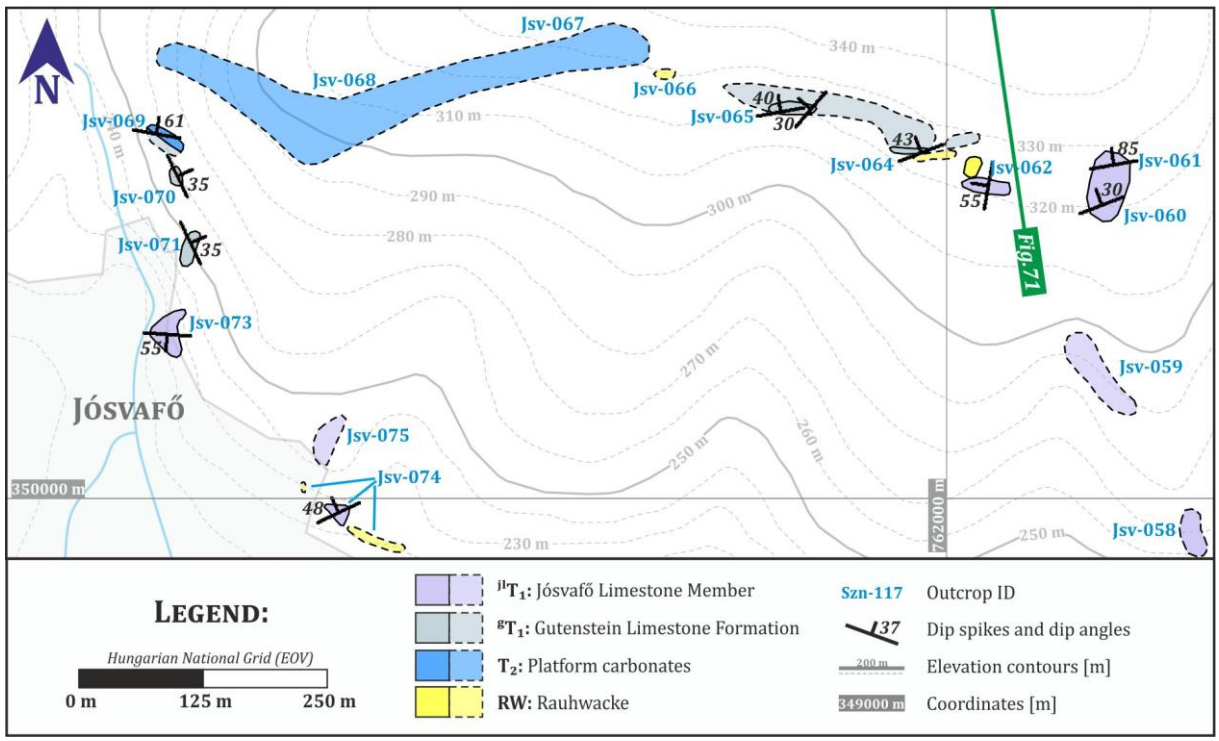

Map 17. Observation map of the area N and NE of Jósvafő. The Middle Triassic platform carbonates are in contact with the Gutenstein Limestone along a moderately NW-ward dipping low-angle fault zone. Both this fault zone and the boundary of the Gutenstein and Jósvafő Limestones are accompanied by the presence of breccias and rauhwackes.

The limestone exposed S of the platform carbonates is a dark grey to black fine-grained limestone whose thin beds are densely pervaded by white calcite veins. This limestone is interpreted as the Gutenstein Limestone. The contact between the Middle Triassic platform carbonates and the Gutenstein Limestone is a moderately (30-40°) NW-ward dipping structural boundary which is directly outcropped at *Jsv-069* (see details below). On the top of the hills the moderately (~40°) dipping Gutenstein Limestone has dominantly W-ward, partly NW-ward dips at *Jsv-062, Jsv-064—065, Jsv-069, Jsv-072 (**Map 17**)*. At several locality rauhwackes and intensively tectonized breccias rocks were discovered along the boundary of the platform carbonates and Gutensetin Limestones ***(Fig.71)***. The same tectonic rocks were found also along the boundary between the Gutensein and Jósvafő Limestones that runs parallel to the main fault zone.

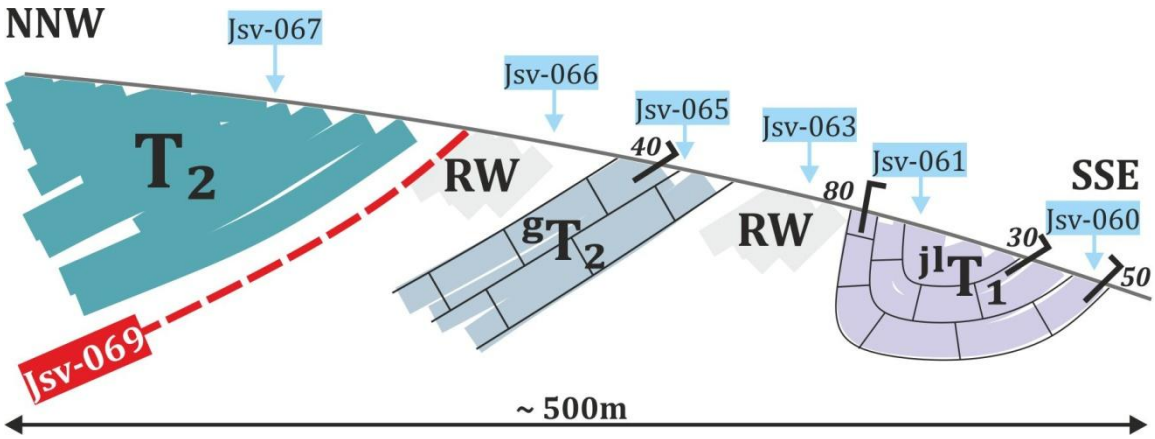

Fig.71. Schematic cross-section through the Middle Triassic platform carbonates and the Lower Triassic formations *(Jsv-060—069)*. See the position of the section in ***Map 17***.

Important outcrops along the tourists' road N of Jósvafő:

Jsv-069: $^{g}T_2$ és T_2

At *Jsv-069* the steeply dipping (~60°) in-situ platform carbonates – Wetterstein Limestone based on LESS ET AL. 1988 – were observed directly above the Gutenstein Limestone. Their structural boundary dips towards NW in 30-40°. Within the Lower Triassic SSW-vergent asymmetric folds with tight interlimb angle and rounded hinge zone were discovered a few meters below the structural contact ***(Fig.73/a)***. The contact zone itself is highly tectonized: a 2 m thick fault breccias/rauhwacke zone is located between the Middle and Lower Triassic formations. This tectonized zone has a gradual transition into the Lower Triassic limestone while its upper boundary toward the Middle Triassic carbonates is a very sharp surface ***(Fig.72)***. On the fault plane several dip-slip and a few obliquely dipping fault lineation were measured but due to the erosion the exact kinematics of the striations could not be determined (they are either thrust faults or low-angle normal faults). Further faults with striae were measured in other parts of the outcrop: moderately (30-45°) dipping thrust faults indicate NNE-SSW compression and NNE-SSW trending high-angle (60-70°) normal faults indicate perpendicular extension ***(Fig.72)***. As the normal faults overprint every other structural element, the WNW-ESE extension must be the youngest deformation phase.

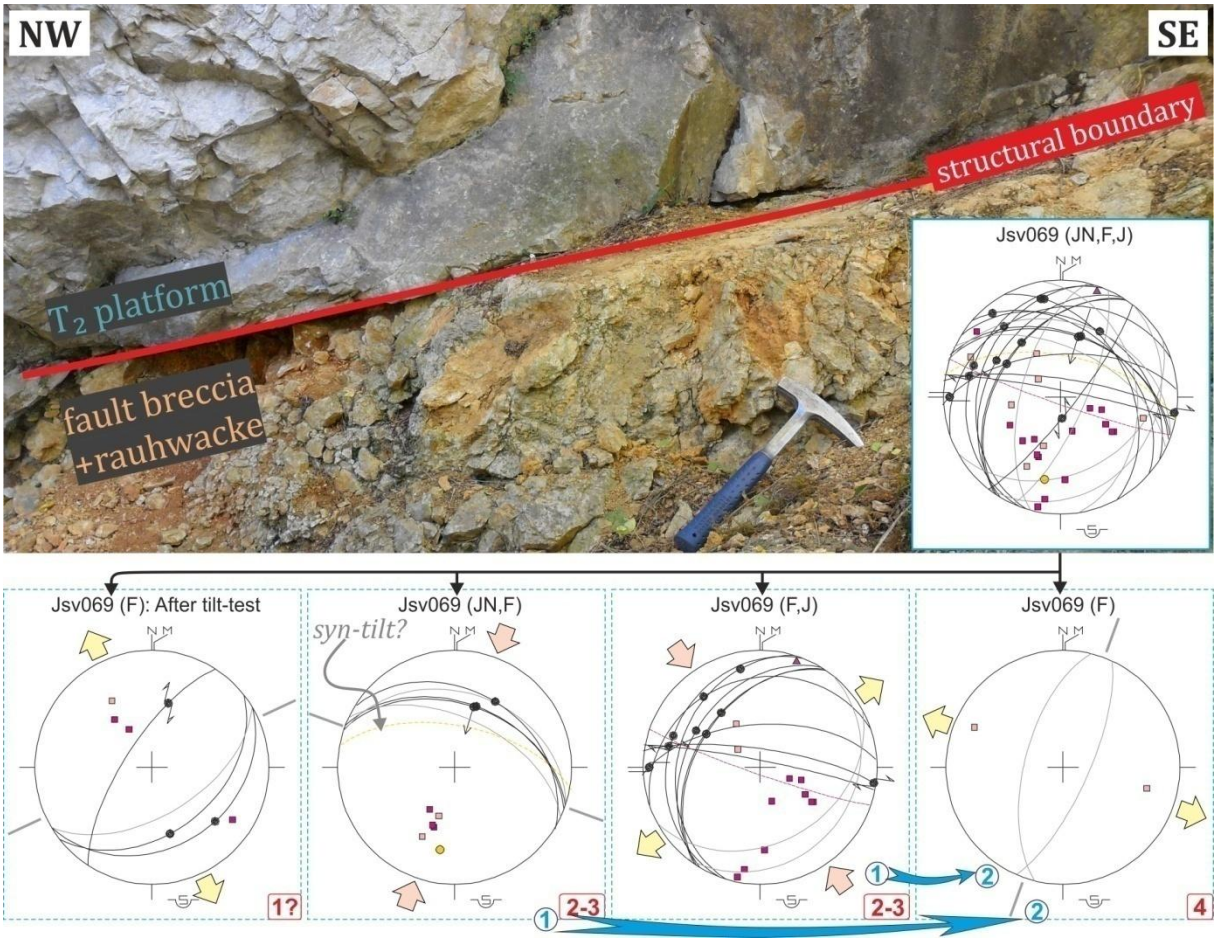

Fig.72. Field photo of the contact zone between the Middle Triassic platform carbonates (hanging wall) and the Lower Triassic limestone (footwall) at *Jsv-069*. **Stereoplots** of the fault data suggest four deformation phase.

Jsv-073: $^{jl}T_1$

On the top of the hills *(Hegytető)* similarly to the Gutenstein Limestone the N-ward or NW-ward dip of the Jósvafő Limestone is moderately steep, rarely sub-vertical. Along the tourists' road it is obvious that the Jósvafő Limestone is intensively folded: the amplitude of the folds exceeds even the 5-6 meters, their axis is E-W trending and their wings dip steeply towards S or moderately towards N *(Jsv-073, **Fig.73/c**)*. The vergency of the folds is very uncertain because of their symmetrical geometry and sub-horizontal axial planes. Furthermore, in the higher parts of the outcrop a shallow shear zone with approximately top-to-N shearing was observed ***(Fig.73/c)***. Because this shear zone gave positive result for the tilt-correction, it may have originally been a pre-tilt NNW-SSE striking normal fault ***(Fig.74)***.

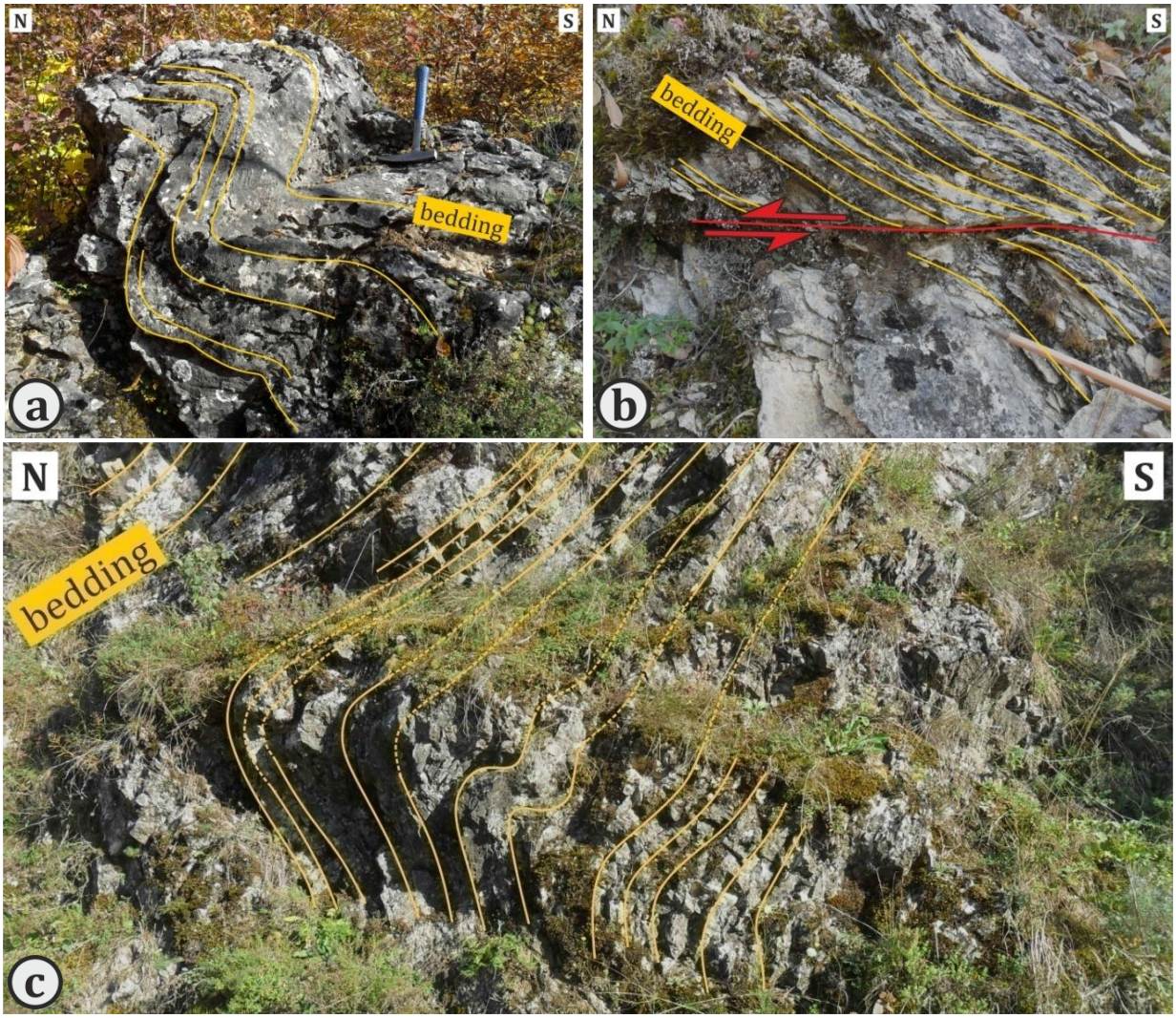

Fig.73. Field photos of the folds and shear zones found at *Jsv-069* and *Jsv-073*. **A.)** SSW-vergent asymmetric folds in the Lower Triassic carbonates a few meters below the main T_1-T_2 contact at *Jsv-069*. **B.)** A low-angle top-to-N shear zone at *Jsv-073*. **C.)** A few meter scale folds with sub-horizontal axial planes at *Jsv-073*.

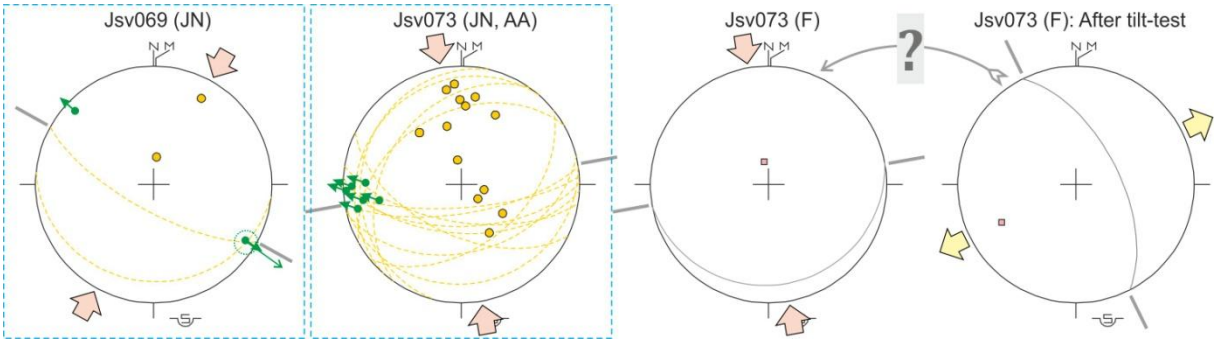

Fig.74. **Stereoplots** showing the measured and estimated fold axis, as well as the top-to-N shear zone or back-tilted normal fault at *Jsv-069* and *Jsv-073*.

IV.16. The Palonták Slope and the Kuriszlán Spring

In the southern part of the Palonták Slope small outcrop spots do occur along the foresters' road while still in the forest but upon reaching the orchards and the meadows in-situ rocks only appear on the sole of the road floor. The measured dips are first mainly towards N, then the general dip direction changes to NW-ward ***(Map 18)***.

On the eastern side of the Kis-galya the change in the vegetation may be correlated to changes in lithology: while in the orchards and on the meadows it was still the Jósvafő Limestone that represented the in-situ rocks, at the border of the following forest a huge block (approximately 10 meters in diameter) built of carbonatic rocks appears and is followed by several smaller but still more than 1 m in size limestone blocks *(**Map 18,** Jsv-042)*. These blocks are interpreted as in-situ blocks of the Middle Triassic platform carbonates. The southern boundary of these carbonate appearances can easily be followed in a NE-SW strike. The size and amount of the blocks gradually decrease towards N until they totally disappear in the saddle S from the Kuriszlán Spring *(Jsv-043—044)*. Here within a NNW-SSE trending narrow zone the color of the previously black and dark brown soil changes to deep red and tiny (maximum of 0,5 cm) red and tawny colored shale clasts appear within the soil. Apparently the same clasts are present on the northern side of the saddle, around the Kuriszlán Spring but with larger (several cm) size *(Jsv-044)*. In addition, rauhwackes were also found in detritus. E of this zone in-situ platform carbonates were mapped *(Jsv-045)* that was only disturbed by another local occurrence of the red soil and red and tawny colored shale clasts at *Jsv-047*.

On the Szőlő-tető a foresters' road run just along the southernmost NE-SW trending boundary of the platform carbonates ***(Map 18)***. This road outcrops tawny or more rarely riffle-green colored shales that dip shallowly (~20°) towards WNW at *Jsv-046*. The occurrence of shales is accompanied by occurrences of rauhwackes as well both of which appear within a narrow zone between the platform carbones and the Jósvafő Limestone *(Jsv-048)*.

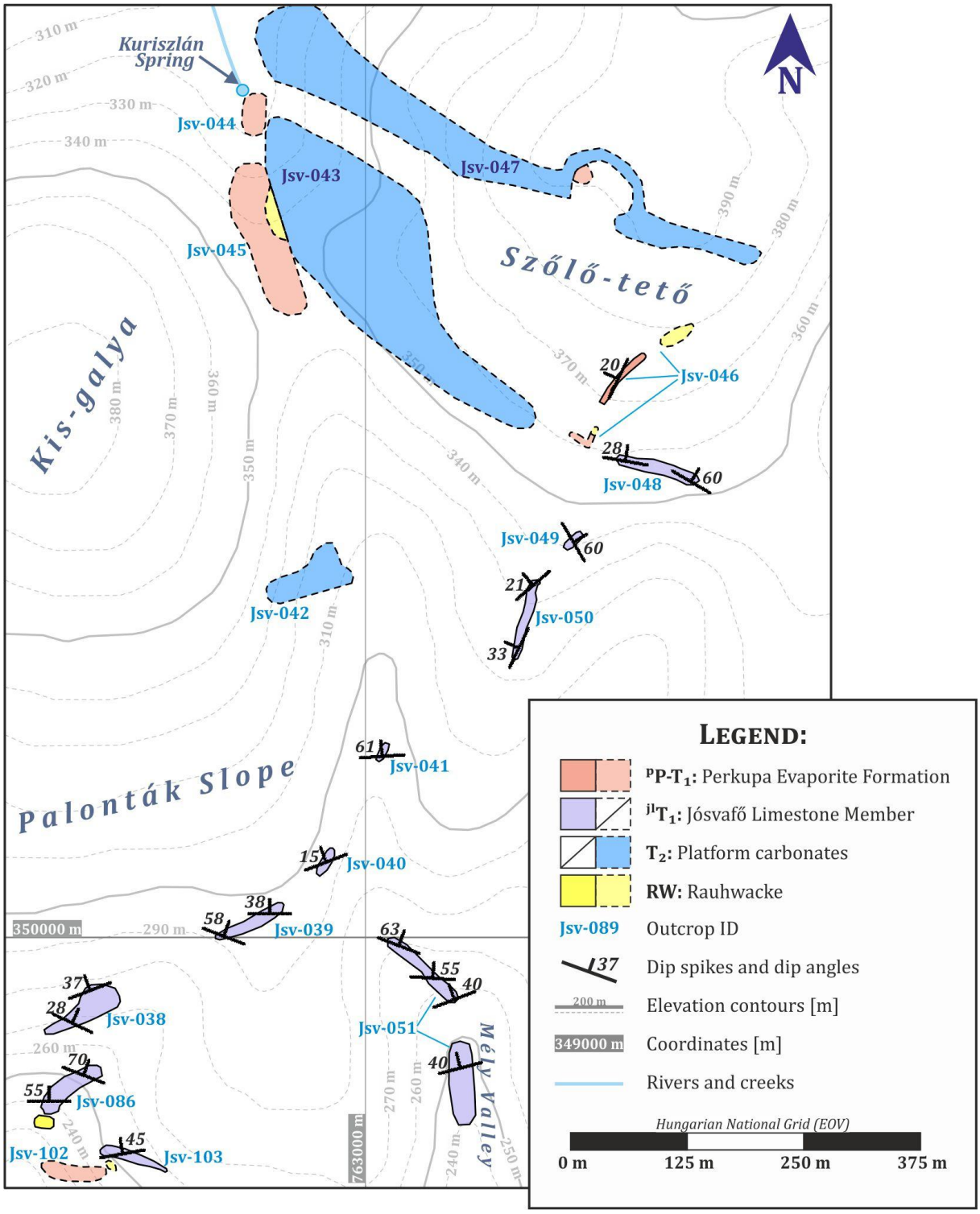

Map 18. Observation map of the Palonták Slope and the area around the Kuriszlán Spring. While the Palonták Slope is covered by the Jósvafő Limestone, the area around the Kuriszlán Spring outcrops the Middle Triassic platform carbonates. There are rauhwacke and Perkupa Evaporite outcrops as well within two narrow zones: one is NNW-SSE trending W of the Kuriszlán Spring, the other is NE-SW trending along the boundary between the Jósvafő Limestone and the Middle Triassic platform carbonates.

IV.17. The road to Szelcepuszta

Szn-001: $^{sp}T_1$

The roadcut of the road from Szin to Szelcepuszta reveals a long section of the thin bedded vermicular Szinpetri Limestone ***(Map 19)***. The general dip is first 15° to NW that is only disturbed by locally steepened layers which form maximum of 10 cm wide monoclonal bends. These small folds are localized along NW-SE trending high-angle faults, suggesting that the observed folds are the result of drag folding related to normal fault movement. Results of tilt-tests indicates that at least some of the normal faults may have originally been pre-tilt faults, the observed dip-slip lineations, however, prove post-tilt (reactivation) fault movement as well ***(Fig.75)***. Dextral strike-slip striae measured on the same NW-SE trending fault planes indicate strike-slip reactivation of the pre-existing fractures during a later deformation phase. After a few meters the NW-ward dipping Szinpetri Limestone becomes steeper and steeper, it reaches 65° dip angles, until finally it turns into near vertical (~80°<) dips. This NE-SW strike of dominates the whole section from here. The exact dip directions constantly change, however. Based on all this the section of the Szelcepuszta Roadcut is folded into asymmetric, often even overturned folds but the fold vergency cannot be determined due to poor outcrop conditions.

Right after the last outcrops of the Szinpetri Limestone a sharp change in flora and morphology was observed: the scrubs and bushes growing on the Szinpetri Limestone are substituted by a dense forest with high trees and scanty underwood while at the beginning there are no outcrops of hard rocks on the flattened morphology ***(Map 19)***. Instead of the expected outcrops of the platform carbonates forecasted on the geological map of LESS ET AL. (1988), only red shale and siltstone clasts were found at the roots of the trees and in washed-out soil sections at *Szn-002*. Hard limestone blocks appear only at *Szn-003*, about 80 m from the edge of the forest where the large carbonatic blocks are in-situ outcrops of the platform carbonates. The field occurrences of these blocks clearly reflect the structural boundary of the Lower and Middle Triassic sequences. This boundary is first NE-SW trending, then it is approximately E-W trending towards W, at the Kis-Koponya Spring, after which the boundary becomes NNW-SSE trending at *Szn-008*, and finally turns back into ENE-WSW strike at *Szn-012*.

Breccias, altered rocks and rauhwackes were mapped along almost the whole length of this structural boundary *(**Map 19,** Szn-007, Szn-011, Szn-013—014)*. Within the in-situ rauhwackes at *Szn-007* larger siliciclastic rock bodies made of thin bedded limestones and thin bedded, foliated yellowish siltstones were found. These isolated bodies are completely surrounded by rauhwackes and dip steeply (55-85°) towards N. At *Szn-013*, directly at the southern boundary of the platform carbonates the soil gains a red color and red shale clasts appear sometimes. These phenomenons continue in a larger area around *Szn-009—010* where the morphology clearly suggests the presence of very “soft”, easily weatherable rocks, and what is more, in-situ red and lilac colored mica-rich sandstone were observed as well. This sandstone is interpreted as the Bódvaszilas Sandstone while the other foliated siliciclastic rock bodies within the rauhwacke zones are either the remains of

siliciclastic intercalations of the Perkupa Evaporite or isolated bodies of the Szin Marl (most probably its B member).

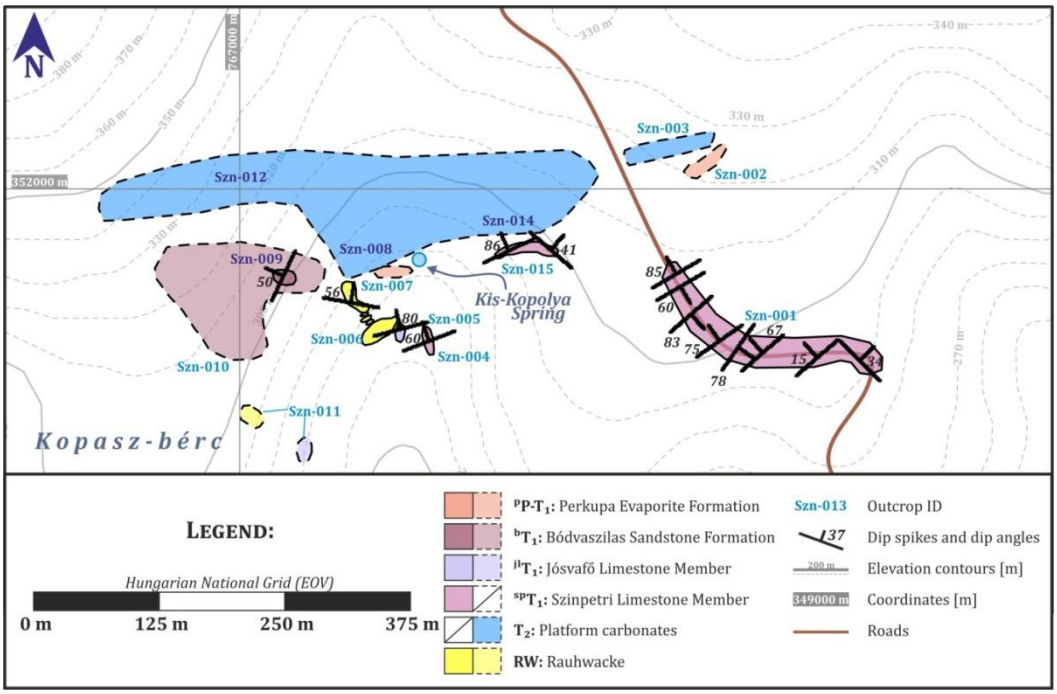

Map 19. Observation map of the mapped area along the road to Szelcepuszta. The contact zone between the Lower and Middle Triassic marks a structural boundary which cuts through the whole area in approximately E-W and ENE-WSW direction. The Bódvaszilas Sandstone and the Perkupa Evaporite also have isolated outcrops along this contact zone.

The thin bedded limestone bodies may have came from a very carbonatic part of the Szinpetri Limestone or from the Jósvafő Limestone. The latter idea is based on the occurrence of thin bedded limestones with flat bedding planes outcropped at *Szn-006* that absolutely lack of the typical characteristics of the vermicular Szinpetri Limestone (and HIPS (2001) also indicated the presence of the Jósvafő Limestone in the area on her map). The supposed Jósvafő Limestone at *Szn-006* dips steeply, almost vertically (70-80°) towards N or NNW ***(Fig.75)***. The last nearby outcrop of the Szinpetri Limestone at *Szn-005* has a similar dip (60° towards NNW). The Szinpetri Limestone at *Szn-015* is clearly folded: while in the western part of the outcrop is dips steeply towards NNW, it gradually turns first towards NNE and NE, then finally it turns back towards N. As the dip measurements in other outcrops suggest that the NNW and NW are the general dip directions in this area which show by the way steep or sub-vertical dip angles, the gradual turns in the dip directions towards NNE and NE are related to the (re)folding of already steeply dipping beds. Based on the position of the shorter and longer fold wings the map-scale asymmetric folds are related to approximately E-W directed dextral shearing.

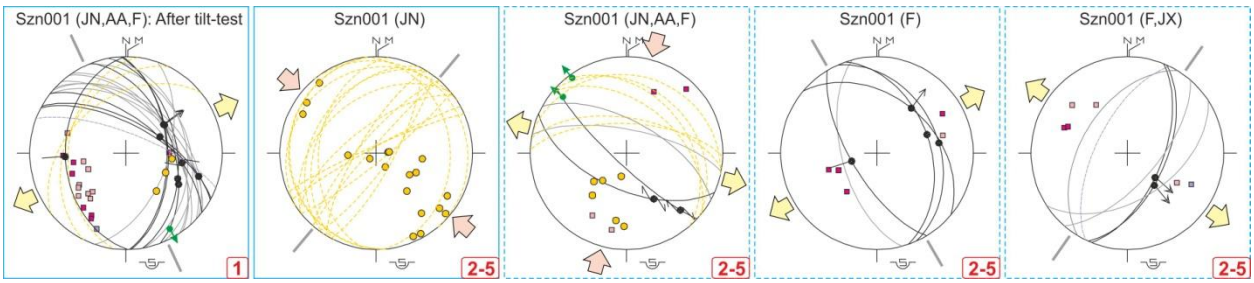

Fig.75. Stereoplots of the separated data measured in the area of the Szelcepuszta Road. The pre-tilt normal faults (1) were inverted and reactivated several times and the Szinpetri Limestone is folded into NE-SW trending folds.

V. DISCUSSIONS

V.1. Structural interpretation of the observed structures

Slump folds

Based on their geometrical features several groups of folds were separated during data evaluation and interpretation. The first group of the observed outcrop-scale folds consists of open to tight, symmetric or asymmetric, both upright and overturned folds with rounded hinge zones ***(Fig.79/a)***. These folds are characteristically detachment folds, meaning that a detachment surface completely decouples the folded beds from the undeformed strata below (e.g. ***Fig.25/a, Fig.30, Fig.31/a, Fig.52/a, Fig.59/b***). The folds usually are also covered by undeformed beds, sometimes the subsequent beds even onlap on the folds' limbs (e.g. ***Fig.30, Fig.31/a, Fig.56/a, Fig.59/b***). Moreover, thickness changes within the deformed strata may occur (e.g. ***Fig.25/a, Fig.56/a, Fig.59/b, Fig.63/b***).

Their geometry suggests that these folds are **sedimentary slump folds which formed in semi-consolidated sediments** prior to the initiation of true lithification (***Fig.79/a***, BRANNEY & KOKELAAR 1994, MALTMAN 1984, LEWIS 1971, PEEL 2014a, STRACHAN & ALSOP 2006). This means that the first deformation affecting the Lower Triassic formations of the Silica Nappe was sedimentary in nature and purely atectonic. Slumping is related to sediment instability on the sloping depositional area. Besides slump folds dewatering structures were observed as well (e.g. in the B member of the Szin Marl in ***Fig.31*** and in the Szinpetri Limestone in ***Fig.10***), reflecting the compaction of water-saturated sediments due to rapid sedimentation and/or episodic events (e.g. earthquakes) (BRAY & KARIG 1985, BYRNE 1994, COSGROVE 2001).

As in theory slumped sediments move roughly in the direction of the maximum slope gradient **measuring slump fold axis makes it possible to estimate the paleoslope direction** (ALSOP & HOLDSWORTH 2002, HANSEN 1971, JONES 1939, STRACHAN & ALSOP 2006, WOODCOCK 1979). These estimations have, however, several drawbacks. First of all, the smaller a slump fold is, the more uncertain it is that the actual slumping direction was parallel to the true slope gradient as the slope is not a totally flat surface, it always have a morphology, and the local deviations may divert folds significantly – especially the small-scale ones. Paleoslope estimations are all statistical calculations thus the final interpretation should be treated just as such. Secondly, early studies on paleoslope estimations considered only the simplest case of slump folding: when the semi-consolidated layers sag and start to slump a cylindrical asymmetric fold forms and its axis will be perpendicular to the slope direction (JONES 1939, STRACHAN & ALSOP 2006). In this model shearing is only permitted in flow direction so there is no shortening parallel to the strike of the slope (***Fig.76/a***, FARREL & EATON 1987, 1988). This model and the related *Mean axis estimation method* of JONES (1939) may be applied to slightly sagged sediments and small-scale slump folds with no major internal deformation. Needless to say nature is full of with complexities so in reality the slump fold

geometry varies in a wide range that extends from simple cylindrical folds to completely non-cylindrical folds (***Fig.76/b***, HANSEN 1971, STRACHAN & ALSOP 2006). The hinge line of the latter group of folds may be so curved that the fold axis becomes parallel to the main slope gradient. These folds with extremely curved hinge limes are called sheath folds (ALSOP & MARCO 2011). Sheath folds evolve from simple cylindrical folds by progressively increasing deformation during slumping and by the appearance of shearing perpendicular to the slope gradient (FARREL & EATON 1987, 1988). For more deformed slump folds the *Separation arc method* of HANSEN (1971) should be applied to estimate the slope direction.

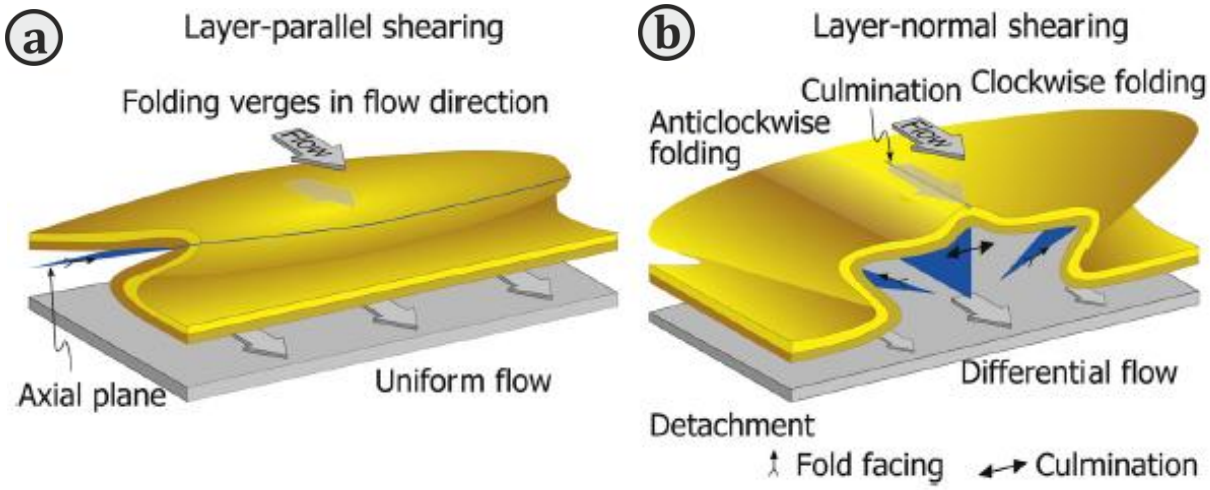

Fig.76. Two end members of the slump folds (ALSOP & MARCO 2011). **A.)** Cylindrical slump fold the axis of which is perpendicular to the main slope gradient. In this case the deformation rate is low and there is no shearing parallel to the strike of the slope, For similarly slightly deformed folds the *Mean axis method* of JONES (1939) should be applied. **B.)** Non-cylindrical slump fold with cured hinge line. The hinge line may be so curved due to the progressive deformation that the fold axis may become parallel to the main slope gradient. For these folds the Separation arc method of HANSEN (1971) should be applied. During the progressive evolution of a slump fold its geometry starts with a simple cylindrical geometry, then its geometry gets more and more complicated until the hinge line becomes so curved that it becomes parallel to the slope gradient.

All this means that the measured slump fold axis may be parallel or perpendicular to the slope direction depending on the degree of deformation and on the fold geometry. Fortunately most of the observed slump folds in the Aggtelek Mts. were slightly deformed cylindrical folds (e.g. ***Fig.52, Fig.56/a, Fig.63/b***). In case of the more deformed slump folds the geometrical factor was kept in mind but as sheath folds were not observed anywhere, the *Mean axis method* was applied on these more complex folds as well (e.g. ***Fig.25/a, Fig.30, Fig.31/a***). The stereoplots in ***Fig.77*** and the map in ***Fig.86*** show the estimated paleoslope directions within the study area. At first glance the estimated directions divert in a wide range, they may even look random, but the explaination behind the slope directions will be revealed in the *Chapter V.4*.

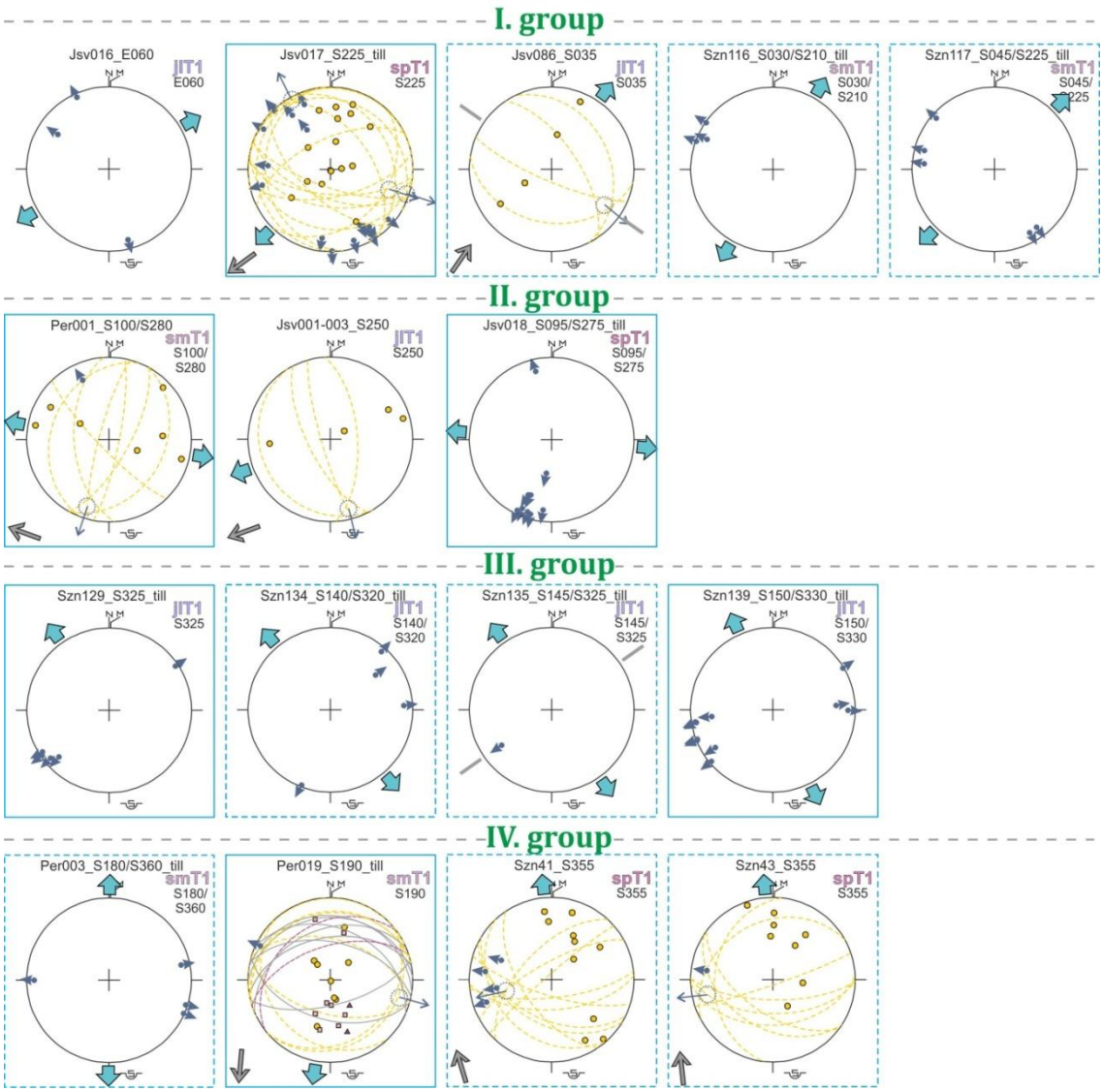

Fig.77. Stereoplot examples for slump folds indicating different vergencies and paleoslope directions.

A special group of the pre-tilt faults have no discrete fault planes, although the displacement can be seen by correlating fragmented beds. Fodor et al. (1992) named fractures like these cosed faults and considered it the result of diagenetic processes that the fault planes have sealed back. Moreover, the displacement zones themselves are sealed by the subsequent beds, indicating that fault movement had already ceased by the time of the sedimentation of the subsequent beds (e.g. ***Fig.30, Fig.34/a, Fig.36, Fig.39, Fig.53, Fig.56/b***). Some normal faults are low-angle normal faults or they flatten into the bedding (e.g. ***Fig.36***, ***Fig.39***, ***Fig.53/b***). Several sections also showed fan-shaped thickening of beds in the hanging wall (growth strata, e.g. ***Fig.30, Fig.34, Fig.39, Fig.44/b, Fig.53, Fig.56/b***) and/or the deformed strata contained onlap surfaces (e.g. ***Fig.34/b, Fig.39, Fig.56/b***). All these features clearly suggest **syn-sedimentary deformation** which means that sedimentation and deformation were cotemporaneous (PRESTHOLM & WALDERHAUG 2000).

Syn-sedimentary extensional deformation was observed throughout the Early Triassic, starting from the Bódvaszilas Sandtone (e.g. *Per-063*), then the Szin Marl (e.g. *Per-011, Per-025, Per-028, Szn-118*) and the Szinpetri Limestone (e.g. *Jsv-030, Szn-016*) and finally in the Jósvafő Limestone (e.g. *Jsv-110—130*). The stereoplots in ***Fig.78*** and the map in ***Fig.86*** show the calculated pre-tilt and syn-

sedimentary extensional directions in the different outcrops. The same map displays the estimated paleoslope directions (see details in the previous sub-chapter). Regarding the whole area – just as in the case of the slump fold vergencies – the syn-sedimentary and pre-tilt extensional directions constitute a seemingly chaotic network, but there is a clear correlation between the sedimentary slumping directions and the extensional directions: the estimated paleoslope gradient vectors are almost always perpendicular to the strike of the local normal faults. Considering that the all-time basement topography should reflect somehow the tectonic faults and structures, a correlation between syn-sedimentary deformation and sedimentary processes like slumping should be expected. It is also possible that some of the normal faults may have formed due to atectonic sagging or slumping. In this sense these faults would only be atectonic slip surfaces. What is surprising either way is that the different fault strike directions and paleoslope directions indicate that **the basement topography was accentuated already during the Early Triassic**. What is even more surprising is that the estimated slump fold vergencies correlate with the measured general dip: **the sedimentary transport direction is approximately parallel to the present-day dip direction**.

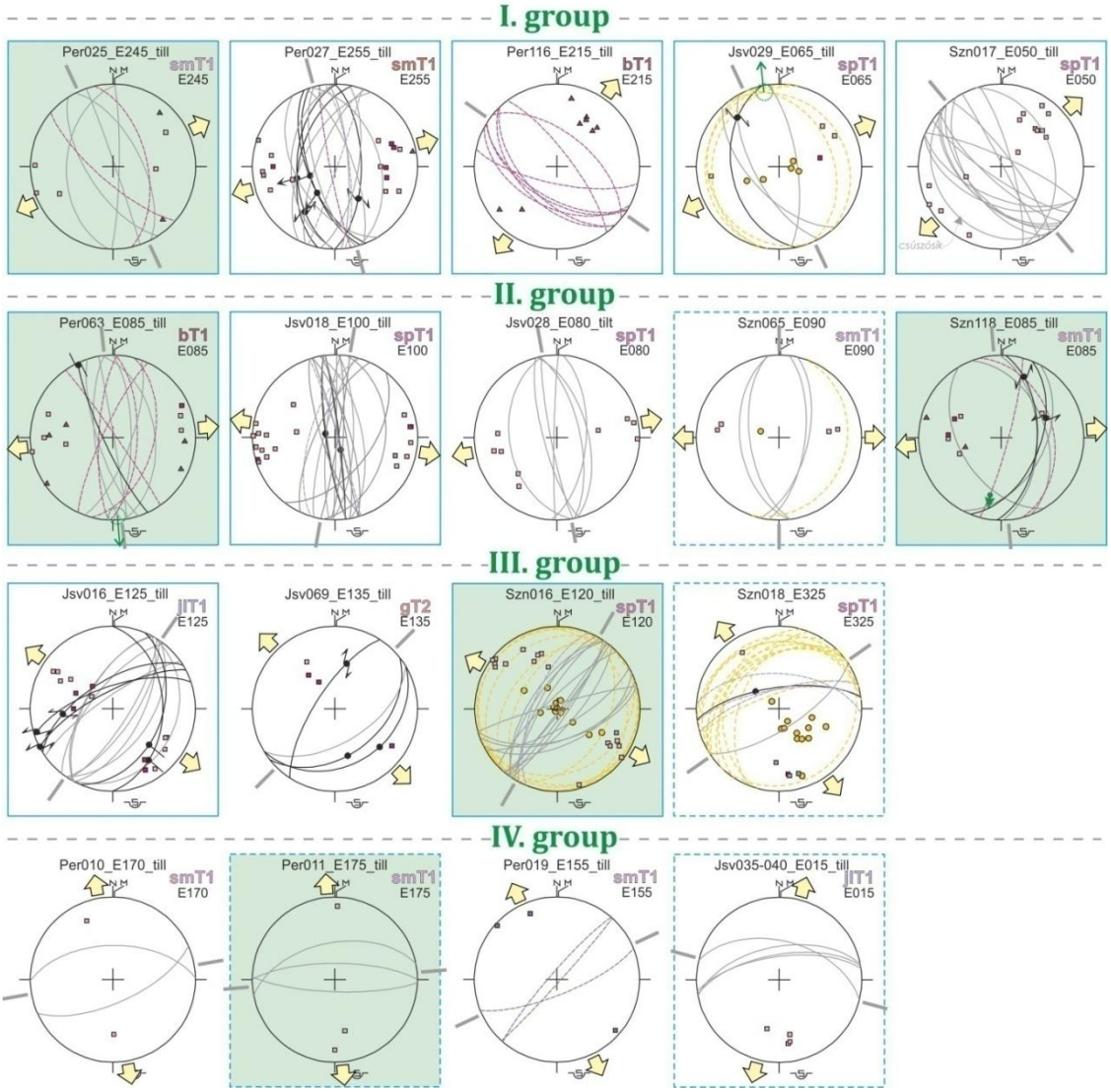

Fig.78. Stereoplot examples for the different groups of pre-tilt and syn-sedimentary normal faults. NW-SE, N-S, NE-SW and E-W trending normal faults were separated, indicating high deviation among the strike directions of the early extensional structures. At least some of these faults may have formed due to atectonic sagging and slumping.

Monoclinal folds

In an unnamed valley W of the Jósvafő-Aggtelek train station the general dip of the Bódvaszilas Sandstone and the lowermost A-B members of the Szin Marl was between 15°-25°(-30°) towards SW *(Per-032—036)*. The measured dips varied, locally steepened until about 55° but the dip direction remained the same, and then the general dip was always restored. The same geometry was observed at *Szn-018*, the difference was that the steepening was always connected to the presence of a high-angle (normal) fault or thick calcite vein (***Fig.46*** - in the previous example no faults were observed).

The measured beds form monoclinal folds that are folds with only one inclined limb (2nd group of folds, FOSSEN 2010, RECHES & JOHNSON 1978). The presence of normal faults and calcite veins suggests that the monoclonal folding is related to these brittle structural elements, namely they are fault-related folds. Fault-related folds may form directly along the faults due to fault movement (drag folding) or above the folds (drape folding, ***Fig.79/b***, JOHNSON & JOHNSON 2001, MILLER & MITRA 2010, SCHLISCHE 1995, STEARNS 1978, WILLSEY ET AL. 2002, WITHJACK & CALLAWAY 2000, WITHJACK ET AL. 1990). Examples for both kind of monoclonal folding were seen in the field in several outcrops (drag folding e.g. in ***Fig.34/b, Fig.36, Fig.37/b, Fig.39, Fig.48***, ***Fig.58***, drape folding e.g. in ***Fig.48, Fig.56/b***). In the case of *Szn-018* and probably at *Per-032—036* as well, **the observed monoclonal folds are either extensional fault-related folds or fault-related folds formed by the reactivation of pre-existing normal faults *(Fig.79/b)*.** As the axis of fault-related folds reflects the strike of the underlying faults, the faults must be NW-SE trending at *Per-032—036* and NE-SW trending at *Szn-018*.

Linear rauhwacke zones and isoclinal map-scale folds

Rauhwackes often appear in linear map-scale zones. Based on the observed textural features within the mapped rauhwackes these zones were affected by strong physical and chemical processes which altered the original host rocks into rauhwackes with scarcely recognizable or completely unrecognizable clasts or original rock fragments (GYENGE 2017, KÖVÉR ET AL. 2018b). The most remarkable rauhwacke zones are located E of Jósvafő along the westernmost part of the so-called Jósvafő-Perkupa Fault Zone (e.g. *Jsv-004, Jsv-031, Jsv-074, Jsv-088—090*) and along the Jósvafő-Bódvaszilas Fault Zone that is the structural contact between the Lower Triassic formations and the Middle Triassic platform carbonates (e.g. *Jsv-046, Jsv-066, Szn-007*). The strike of the rauhwacke zones is E-W trending in most cases, but N-S and NE-SW trending zones were mapped as well.

Rauhwackes are systematically present around the isolated occurrences of much deeper stratigraphical units outcropping within the higher parts of the Lower Triassic or in the Middle Triassic platform carbonates. These isolated occurrences of the Bódvaszilas Sandstone and Szin Marl were found at several localities, e.g. in the surrounding of the Jő-2 well ($^{b}T_1$ – *Jsv-083*), in the southernmost part of the Almás Valley ($^{sm}T_1$ – *Szn-115—121*) and Kecske-kút Valley ($^{sm}T_1$ – *Szn-*

124—127), in the middle of the Szövetény Valley ($^{sm}T_1$ – *Szn-023—026 and Szn-065—069*) and around the mapped part of the Szelcepuszta road ($^{b}T_1$ – *Szn-009—010*).

Besides the Bódvaszilas Sandstone and the Szin Marl, the Perkupa Evaporite occurred in isolated areas. Even though the salt rocks themselves are no longer present in outcrops, the Perkupa Evaporite Formation is still mappable by meeting the following conditions: (1) complete lack of outcrops in places where normal outcrops or cliffs should be expected in case of harder rocks (e.g. *Jsv-079*); (2) sudden changes in the morphology or vegetation (e.g. *Jsv-043—044*); and (3) the presence of the interbedded siliciclastic rock masses of the evaporitic succession (e.g. *Szn-019, Jsv-095*). These siliciclastic rock bodies are interpreted as the remnants of the originally sedimentary parts of the evaporitic succession that include red, yellowish, green, rifle-green or black shales and siltstones ***(Fig.6)***. The problem with mapping the siliciclastic components of the Perkupa Evaporite is that the red, yellowish and even the green fine-grained siliciclastics are not exclusively present in the Perkupa Evaporite succession but they may come from the Bódvaszilas Sandstone or the Szin Marl as well. The riffle-green and especially the black colored shale and siltstone components are, however, not known from any other Lower Triassic formation (LESS ET AL. 2006) so their presence clearly indicate the presence of the Perkupa Formation and the former presence of salt rocks as well. The mapped siliciclatic remains of the Perkupa Evaporite are always accompanied by rauhwackes as well (e.g. at *Jsv-052, Jsv-095, Jsv-102, Szn-019, Szn-156*), what is more, small cm-scale angular clasts identified as the remains of the Perkupa Formation were found embedded in in-situ rauhwackes ***(Fig.66/a)***.

In most cases the map appearance of the rauhwacke zones and the measured/mapped structural contacts between these deeper units and the surrounding late Lower Triassic rocks indicate that they must be **high-angle or near vertical structural boundaries**. Based on the juxtaposed formations the throw of these faults should be at least several hundred meters (e.g. the Bódvaszilas Sandstone and the Jósvafő Limestone it should be at least 400-800 m, probably more based on the thickness calculations of HIPS 1995 and LESS ET AL. 2006). The small clasts and map-scale rock bodies of the Perkupa Evaporite sitting within the rauhwacke zone indicate that the formation of rauhwackes is connected to the (former) presence of evaporites. Moreover, several well-positioned wells drilled in these isolated rock bodies of the Bódvaszilas Sandstone or Szin Marl (*Jő-2, Jő-3, Szi-1, Tk-3*) proved that the Perkupa Evaporite itself is present in shallow depths underneath the surface ***(Fig.24)***.

Rauhwacke zones not necessarily but often were found in the core of tight to isoclinal, mostly upright but sometimes overturned antiforms with steep or sub-vertical limbs and tapering, sharp hinges. Away from the rauhwacke zone the measured dips decreases rapidly and flatten into shallow (15-30°) dips. These folds are also map-scale folds and their axes are parallel to the strike of the rauhwacke zones, e.g. along the Jósvafő-Perkupa Fault Zone ***(Fig.54, Fig.66/a)***. The same fold geometry was observed at several other places but without observable rauhwackes, e.g. on the two sides of the Szövetény Valley ***(Fig.43)***, in the Vég-Gelleház Valleys, N of Perkupa ***(Fig.29)*** and on the Fenyves Slope SE of Jósvafő. This latter antiform is known as the Jósvafő Anticline after SCHRÉTER (1935) and JASKÓ (1935). The majority of these antiforms are E-W trending. While both

limbs of the Jósvafő Anticline are made up by the Jósvafő Limestone, in case of the antiforms in the Szövetény and Vég-Gelleház Valleys showed **structural boundaries** as well, as if the fold limbs were offset approximately along the axial plane. Considering all the above mentioned observations and geometrical features the mapped folds cannot be simple shortening-related folds. The map-scale tight to isoclinals fold geometry itself is unusual but the presence of the Lowermost Triassic formations and the rauhwackes within the core of the antiforms cannot be explained without salt tectonics. The two limbs of the present-day antiforms originally formed as drag folds along the two opposite sides of the salt wall or salt anticline. When later the area underwent compression and the salt rocks were squeezed out, the opposite sides of the diapir got in direct contact along a **secondary salt weld** (***Fig.22***, HUDEC & JACKSON 2007, WAGNER III & JACKSON 2016). The present-day geometry is thus the result of juxtaposed drag folds along the welds which now form tight to isoclinal antiforms. As the two sides of the salt structure not necessarily evolve the same was during salt movement, the secondary welds often but not necessarily show structural discordance (WAGNER III & JACKSON 2016). This explains the observed apparent offset of the antiforms' limbs approximately along the axial plane which is in fact the secondary weld itself (3rd and 4th group of folds, ***Fig.79/c-d***).

All the aforementioned observations can be explained by salt tectonics: evaporites get to near-surface depths by flow and diapir formation (HUDEC & JACKSON 2007, VENDEVILLE & JACKSON 1992, WARREN 2016, ***Fig.17***). Whenever a salt diapir forms the contact between the upward flowing salt and the surrounding host rocks is in fact a normal fault. As the salt flow intensifies the bordering normal fault contact becomes steeper and steeper until it reaches sub-vertical positions. Oppositely to simple tectonic normal faults the offset along a salt diapir may exceed even several 100 meters which would explain the abnormal amount of offset along even smaller structural elements. Based on the linear geometry of the salt structures the diapirs should have originally formed a **fault-related salt anticline or salt wall** (or a salt roller, ***Fig.18***, FOSSEN 2010).

The present-day remains of these salt anticlines or salt walls are the secondary salt welds marked by the rauhwacke zones formed by the contraction of the former salt structures and squeezing of salt rocks during later (Cretaceous) compressional processes. The presence of rauhwackes along the (late) salt diapirs is the result of the strong mechanical fracturing due to the upward movement of salt rocks (GOLDMAN 1925, KYLE & POSEY 1991). In this sense rauhwackes are similar to fault breccias and cataclasites (SIBSON 1977, WOODCOCK & MORT 2008). Furthermore, evaporites act as excellent aquitards (near-impermeable medias) but the surrounding heavily fractured host rock possesses the necessary permeability to induce vertical fluid flow and intensive chemical alterations along the salt diapirs. Several sections proved that the continuous alteration of the "fresh" host rocks into rauhwackes. The alteration process contains the following steps: (1) partly altered rocks (mostly limestones) with still observable sedimentary features like bedding and with multiphase mineral vein network; (2) brecciation and already dissolved components; and (3) completely altered rauhwackes, sometimes even with unrecognizable components (e.g. at *Jsv-007—Jsv-032—Jsv-052* and at *Szn-147*).

Buckling and passive folding

Folds may form in several ways. We have already covered the sedimentary folds formed by slumping shortly after sedimentation ***(Fig.79/a)*** and drag folding along normal faults and salt structures ***(Fig.79/b-d)*** (ALSOP & MARCO 2006, BRANNEY & KOKELAAR 1994, JOHNSON & JOHNSON 2001, HUDEC & JACKSON 2007, MALTMAN 1984, MILLER & MITRA 2010, LEWIS 1971, PEEL 2014a, SCHLISCHE 1995, STEARNS 1978, WAGNER III & JACKSON 2016, WILLSEY ET AL. 2002, WITHJACK & CALLAWAY 2000, WITHJACK ET AL. 1990). The second and third group of folds are formed by bending which is a folding process associated with forces acting across the layers at a high angle (FOSSEN 2010). In this case the observed (normal or reactivated normal) fault-related folds are so-called forced folds, i.e. the deformation is "forced" on the layers by fault movement (COSGROVE & AMEEN 2000a,b, STEARNS 1978, WITHJACK ET AL. 1990). In the same way, the salt diapirs bend the layers of the surrounding host rock during their upward movement (ALSOP ET AL. 2000, NIKOLINAKOU ET AL. 2017, ROWAN ET AL. 2016, SCHULTZ-ELA 2003).

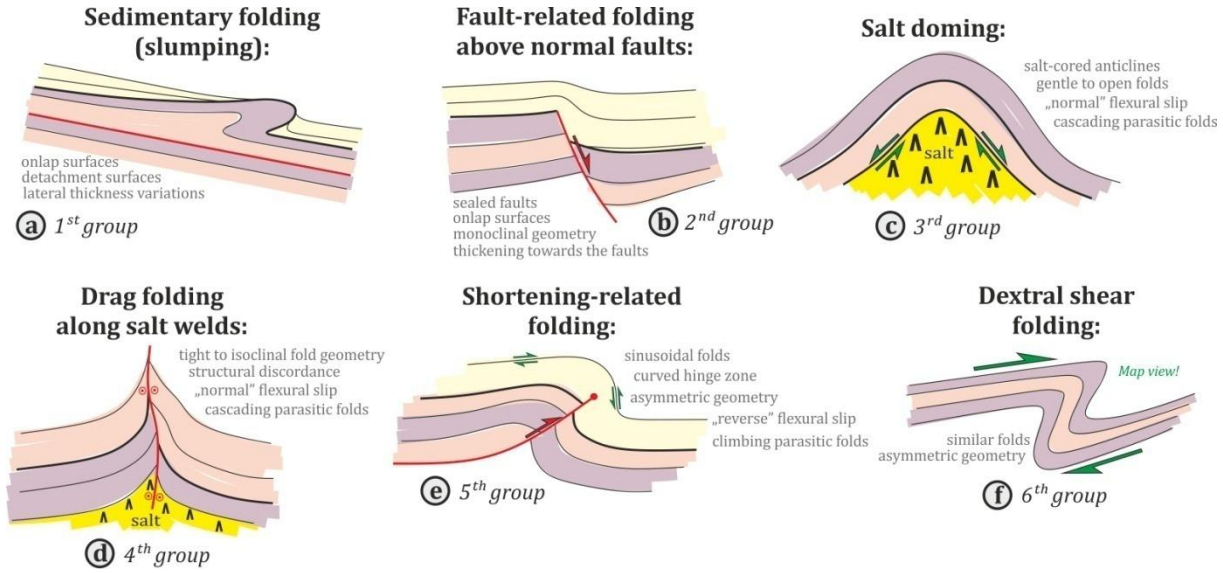

Fig.79. Schematic drawings displaying the characteristic features of the different groups of folds observed in the Aggtelek Mts. **A.)** Sedimentary slump folds (1st group). **B.)** Monoclinal folds formed above pre-tilt normal faults (2nd group). **C.)** Gentle to open folding (doming) above salt diapirs (3rd group). **D.)** Drag folds formed along secondary salt welds (4th group). **E.)** Shortening-related buckle folds (5th group). **F.)** Dextral shear folds (6th group).

When talking about folds, however, most people associate to shortening-related folds formed in compressional tectonic regimes. One of the most common folding process in compressional regimes is active folding or buckling that is initiated by layer parallel shortening and results in rounded and sinusoid folds (COSGROVE & AMEEN 2000B). When the layers mechanically do not affect the folding, passive folding occurs (BILLINGS 1954, FOSSEN 2010, DE SITTER 1956). Passive folding may be the result of – among others – simple shear or transpression and they are usually associated with harmonic and similar folds (DONATH & PARKER 1964). In both cases (buckling and passive folding) asymmetric fold geometries suggest tectonic transport direction or the sense of shear.

In the Aggtelek Mts. two additional groups of folds were separated that may probably be identified as buckle folds and passive folds (5th and 6th groups, ***Fig.79/e-f***). The most remarkable semi-map-scale representatives of the 5th group of folds were found on the Teresztenye Plateau at *Szn-093* ***(Fig.42)*** and on the Fenyves Slope at *Jsv-110—111* ***(Fig.69)***. These folds are sinusoid asymmetric

folds with SE-ward vergency on the Fenyves Slope and N-ward vergency on the Teresztenye Plateau ***(Fig.79/d)***. The necessary competence contrast for buckle folding is probably there in but the deformation is also complicated by salt tectonics in both cases (see explanation later in *Chapter V.2 and V.3*) so even these examples do not represent "pure" buckle folds ***(Fig.80)***.

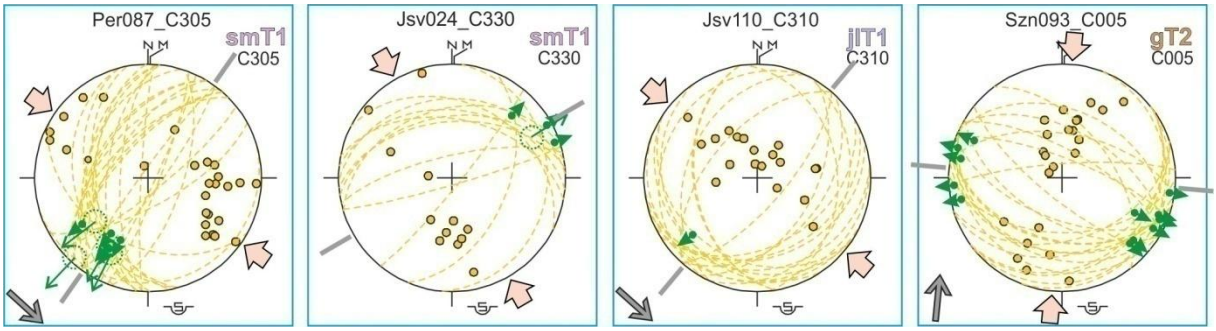

Fig.80. Stereoplot examples for map-scale *(Per-087, Szn-093)* and outcrop-scale *(Jsv-024, Szn-093)* buckle folds. Field evidences indicate that the folding at *Jsv-110* and *Szn-093* affected salt rocks at shallow depths as well.

The 6th group of folds consists of asymmetric map-scale and map-scale folds with steep to sub-vertical limbs and sub-vertical axes. The best examples in this group were found e.g. N of Tornakápolna in the new drainage ditch at *Szn-019—020* ***(Map 6, Fig.40/d)***, E of Jósvafő at *Jsv-057* and at *Jsv-081—082/Jsv-093—094* ***(Fig.65)*** and around the read to Szelcepuszta at *Szn-015* ***(Map 15)***. In all of these cases the N-ward or S-ward dipping layers in the longer limbs turn temporarily toward E or even ESE (shorter limb). The position of the longer and shorter fold limbs suggests dextral shearing ***(Fig.79/d)***. This also means that in the beginning of the dextral shearing the geometry of the layers was already sub-vertical thus the dextral shear overprinted a previous E-W trending fold set. Of course theoretically it cannot be completely excluded that the relative order of the two folding phases is reverse in the sense that the shear folds are only apparently related to dextral shearing, they were originally formed as fault-related drag folds along ~N-S striking normal faults and they were later tilted during a second folding phase. These folds were, however, observed along ~E-W striking fault zones which seems to support the interpretation of dextral shear folds. One of these fault zones is the Jósvafő-Perkupa Fault Zone along which oblique dextral thrust fault striations were measured in several outcrops (e.g. ***Fig.55***, ***Fig.58***, ***Fig.59***). These striations clearly suggest transpressional deformation. Furthermore, in the E-W striking zone N of Tornakápolna small-scale strike-slip duplex structures also indicate dextral shearing ***(Fig.40/b)***. In summary the 6th group of folds are the results of multiphase folding: firstly, there was a N-S directed folding phase which tilted the layers until sub-vertical or even overturned positions, then the steeply dipping layers were re-folded by a second folding phase related to transpression and dextral shearing.

V.2. Salt-related structures vs. shortening-related structures

It has been know for a very long time that the Permian to Lowermost Triassic evaporitic succession forms the base of the Silica Nappe and several study has suggested that the evaporites may be more than just an easily deformable sliding surface in the Aggtelek Mts. (GRILL 1989, GRILL ET AL. 1984, GRILL & SZENTPÉTERY 1988, LESS 2000, LESS ET AL. 2006). The presence of rauhwackes and the

unusual fold geometries clearly demonstrate that the evaporites did indeed have much bigger role in the deformation history of the Aggtelek Mts. than previously thought. The greatest challenge of salt-bearing fold-and-thrust belts, however, is how to separate the "purely" shortening-related structures from salt-related structures (DOOLEY ET AL. 2009, DUFFY ET AL. 2018, GRANADO ET AL. 2018, JAHANI ET AL. 2017, KERGARAVAT ET AL. 2017). Are there even any structure (fault zones or folds) that has no connection to the evaporites at all? In the following section several points are proposed that may serve as distinctive observations for shortening and salt-related folds. All these points are based on the observations made in the eastern part of the Aggtelek Mts.

Evaporites (rauhwackes) or other deep stratigraphical units in the cores of antiforms

Evaporites – or rauhwackes which mark the late presence of evaporites even after they had been squeezed out – **within the cores of antiforms** are the most direct evidence of salt diapirism (HUDEC & JACKSON 2007). Evaporites may drag slices or relatively thick parts of deeper stratigraphical units isolated lenses or narrow linear zones into the core of the antiform or along the fold limbs. The antiformal geometry forms when the layers are bent and dragged during the upward flow of the salt rocks. Depending on the type and shape of the diapir the antiforms may have a linear axis (around salt walls and salt anticlines, ***Fig.18***) or they may show concentric geometry (e.g. around a salt plug or salt stock, ***Fig.18***). As the salt penetrated its sedimentary cover the contact between the evaporites and the surrounding host rocks (e.g. Jósvafő or Szinpetri Limestones) becomes structural – in the simplest case it is a high-angle normal fault. Evidently, during later tectonic phases such contacts can be reactivated as a strike-slip or thrust fault (HUDEC & JACKSON 2006, WARREN 2016). In the mapped area linear rauhwackes- or salt-cored aniforms were mapped e.g. E of Jósvafő ***(Map 15, Fig.66/a, Fig.68/a)*** and on the Fenyves Slope ***(Map 16)***. Both folded area contains lens-like Bódvaszilas Sandstone occurrences (*Jsv-083*, and the observations of LESS ET AL. 1988).

S- and Z-folds along the folds' limbs

S- and Z-folds are practically asymmetric parasitic folds formed by shearing along the limbs of bigger-scale folds (FOSSEN 2010). In a shortening-related tectonic fold the sense of shear folding is always top-to-the direction of the hinge zone, so in ***Fig.81/b*** S-folds evolve on the left limb and Z-folds form on the right limb ("climbing" folds). Just as in the case of layer-parallel slip, **the sense of shear folding also invert during salt-related folding so when a salt dome forms its parasitic folds will vergent away from the hinge zone** (cascading folds, ***Fig.81/a***). BURG ET AL. (2004), DIXON (1987) and WHITNEY ET AL. (2004) observed similar situation in the case of gneiss domes and gravitational cascade folds in collisional orogens – these examples may in fact be used as analogues for salt diapirism (buoyant diapirism).

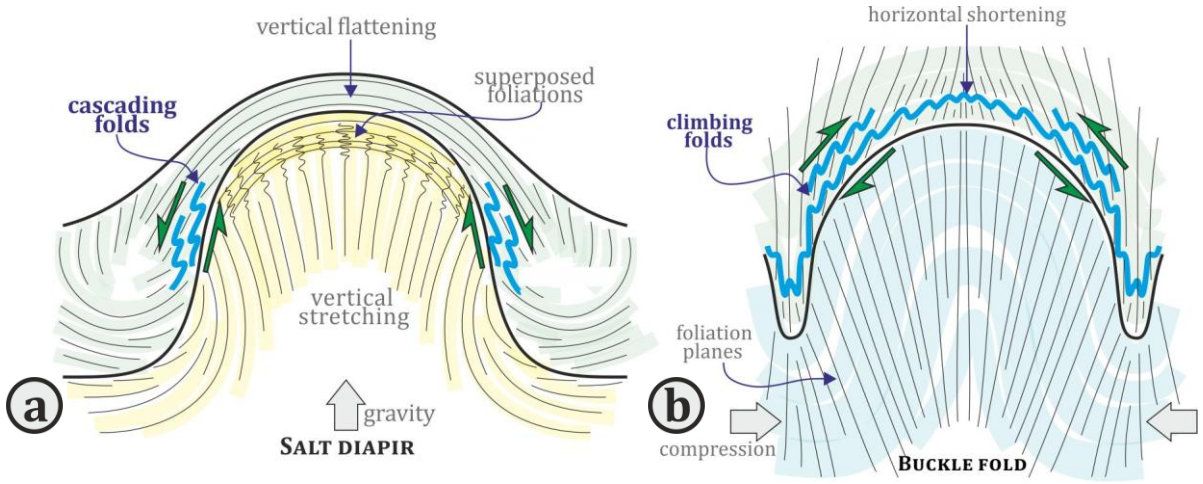

Fig.81. Asymmetric shear folds along salt diapirs and shortening-related buckle folds (modified after DIXON 1987 and BURG ET AL. 2004). **A.)** Cascading folds above a salt dome. The sense of shear is always top-away from the hinge zone of the dome. **B.)** "Climbing" parasitic (second order) folds along the limbs of a buckle fold. These folds have top-to-the hinge zone vergency.

S- and Z-folds were observed in several outcrops. One of the best sections is the folded Gutenstein Limestone at *Szn-093* ***(Fig.42)***. Here the N-vergent outcrop-scale folds have S-folds on the southern limbs and Z-folds on the northern limbs (cascading folds) which indicate that the folding is probably coupled by salt movement as well (see details in *Chapter V.4*). Based on the geometry of these decimeter-scale asymmetric folds at *Szn-093* it cannot be excluded that some of them is slump folds which would further confirm the role of salt tectonics in the folding. The same is true for the folded sections of the D member of the Szin Marl at *Per-087* ***(Fig.27)*** and of the Jósvafő Limestone at *Jsv-110—111* ***(Fig.69)***, both sites show top-to-SE vergency. Further individual outcrop-scale asymmetric folds were observed in the Gutenstein Limestone at *Jsv-069* ***(Fig.73/a)*** and in the Jósvafő Limestone e.g. at *Jsv-010* ***(Fig.64/a,c)*** and *Jsv-011* ***(Fig.63/a)***.

Flexural slip folding

Flexural slip mechanism is one of the most common mechanisms for folding (FOSSEN 2010, SUPPE 1983). Flexural slip folding means that the folding is achieved by layer-parallel slip along bedding planes or along very thin layers, and all deformed layers preserve their original thicknesses (BILLINGS 1954, DONATH & PARKER 1964, DE SITTER 1956, TANNER 1989). A clear evidence for flexural slip folding is the presence of layer-parallel striations on bedding planes. When the layers are shortened and folded these striations show reverse movement, and this reverse layer-parallel slip means displacement with top-to-the hinge zone (the bedding planes practically worked as thrust faults, ***Fig.82/b***).

During salt-related folding flexural slip movement show completely different direction. Let's imagine a salt diapir that is continuously growing vertically and thus bends its sedimentary cover and drags the surrounding host rocks. As in this case the driving force is not layer-parallel but the applied stress is perpendicular to the bedding the sense of movement along the bedding planes will be the opposite. This means that **in a salt-related fold the layer-parallel striations related to flexural slip will show normal sense of movement** (so top-away from the hinge zone direction, ***Fig.82/a***). **The lucky consequence of all this is that salt-related folding may be identified.**

Evidences for reverse and normal flexural slip were found at the same time on the sub-vertically dipping Jósvafő Limestone bedding planes at *Jsv-011* ***(Fig.63)***. They clearly prove the existence of two independent folding processes: one is related to salt diapirism (normal sense of shear) and the other is related to shortening (reverse sense of shear). The "normal" flexural slip striations were measured at *Jsv-016* and at *Szn-139* as well. At *Jsv-016* the salt related folding was NE-SW trending ***(Fig.62)***, whereas at *Szn-139* the layer-parallel striations suggest ENE-WSW trending salt-related folding in the area of the Kecskekút Spring ***(Fig.50)***. These striations on the bedding planes were overprinted by oblique dextral fault movement. Further examples for flexural slip folding were observed in the folded section of the D member of the Szin Marl at *Per-087* but unfortunately the sense of movement could not be determined here ***(Fig.27)***.

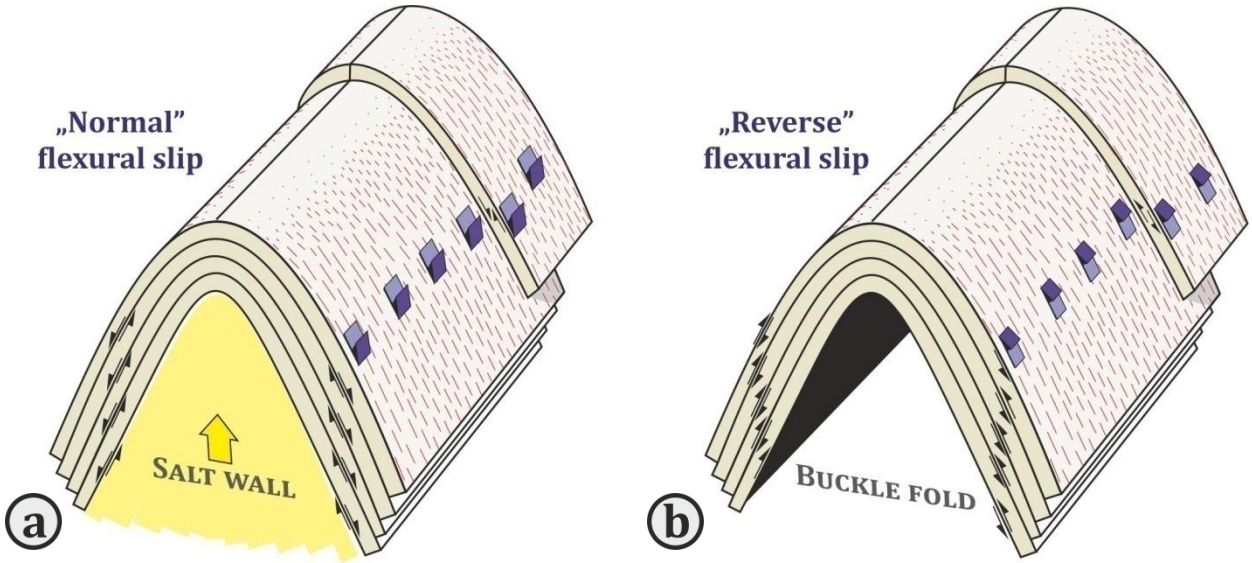

Fig.82. Flexural slip folding along a salt wall and in compressional regime (modified after FOSSEN 2010). **A.)** Layer-parallel striations show that the sense of movement is top-away from the hinge zone ("normal" shearing along the limbs) in salt related anticlines. **B.)** In normal tectonic buckle anticlines the sense of bedding-parallel movement is always to-to-the hinge zone ("reverse" shearing).

Young-on-older contacts

Young-on-older contacts form when younger stratigraphical units of the hanging wall are placed above older stratigraphical units in the footwall. This means that regular normal faults are young-on-older faults, whereas regular thrust faults have older stratigraphical units in their hanging wall then in their footwall (***Fig.83/a***). In fold-and-thrust belts, however, it is possible to form a young-on-older type thrust fault if the (out-of-sequence) thrusting affects already folded strata and a syncline is placed above an anticline (***Fig.83/b***, PAVLIS 2013). Young-on-older thrusts are thus very rare as they require special structural geometry to evolve. Young-on-older thrust contacts can also form due to structural inheritance of pre-existing normal faults as they are frequently cut by younger thrusts which can result in young-on-older contacts or they can be reactivated or inverted as well ***(Fig.83/c)***. Reactivation is easier if the normal fault is a low-angle normal fault and it is the easiest when this low-angle contact is lubricated by easily deformable clay minerals or salt rocks (BONINI ET AL. 2012, DAVIS & LISTER 1988, FOSSEN 2010, HÉJA 2019, HÉJA ET AL. 2018, PACE ET AL. 2014, PÉREZ-GUSSINYÉ & RESTON 2001). Therefore young-on-older thrust contacts are very frequent in inverted salt-bearing basins where the salt diapirs are asymmetric and were reactivated

(Fig.83/d). Differentiating this type of young-on-older thrust contacts from the other types is possible by indentifying early striations with normal fault kinematics besides thrust fault movement along the fault zone and any signs described in the previous sub-chapters suggesting salt deformation (e.g. rauhwacke zones, welding, "normal" flexural slip - ***Fig.82***, "climbing" parasitic folds - ***Fig.81***). Young-on-older contacts are widely present in the Aggtelek Mts, e.g. the remarkable Jósvafő-Bódvaszilas Fault Zone, in the area around Szőlősardó and in the so-called Derenk Zone.

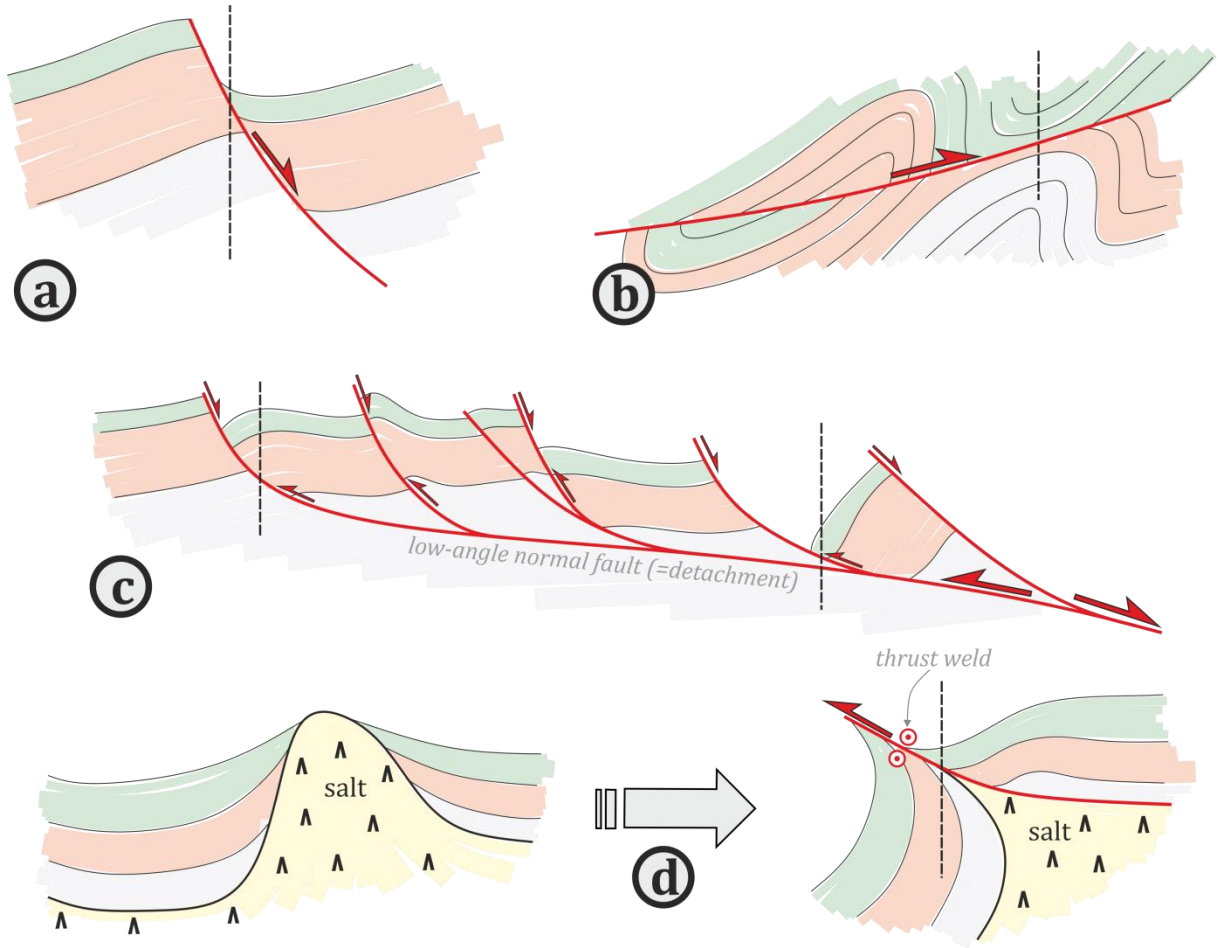

Fig.83. Types of young-on-older contacts. **A.)** Normal faults formed in extensional regimes. **B.)** Young-on-older thrusts faults formed by out-of-sequence thrusting in already deformed fold-and-thrust belts. **C.)** Compressional reactivation of a pre-existing low-angle normal fault. **D.)** Compressional reactivation of a pre-existing salt diapir in an inverted salt-bearing basin. The black dashed lines mark places of young-on-older contacts.

V.3. Kinematics of map-scale structures

The E-W striking Jósvafő-Perkupa Fault Zone

One of the most remarkable structural elements of the eastern part of the Aggtelek Mts. is the E-W trending Jósvafő-Perkupa Fault Zone *(Appendix 4)*. E of Jósvafő its strike slightly changes to WNW-ESE, then W of Jósvafő it is no longer detachable. At its eastern termination the fault zone runs into the Bódva Valley and disappears in the Perkupa Evaporite. In addition to this major fault zone several other E-W trending fault zone were mapped in the area of Varbóc-Perkupa-Szin, all of which run parallel to the Jósvafő-Perkupa Fault Zone. The displacement along these smaller fault zones also accommodated within the Perkupa Evaporite towards E, while in the W the faults are no longer

mappable in the Szinpetri Limestone. LESS (200), LESS ET AL. (1988) and HIPS (2001) interpreted these fault zones as dextral strike-slip faults. The observations regarding the deformation of the Jósvafő-Perkupa Fault Zone may be summarized in the following sections:

1. The Jósvafő-Perkupa Fault Zone is a **sub-vertical** structural element based on its straight trajectory in map view.
2. In the area of Perkupa an apparent dextral offset was observed in map view within the Szin Marl *(Appendix 4)*. This apparent offset may be achieved not only by dextral slip but also by normal faulting. In the latter case the normal fault should dip to N. Outcrop-scale evidences for **E-W striking normal faulting** were observed only locally at *Per-027* where the S-ward dipping normal faults seemingly post-dated both the ~E-W directed folding and tilting event ***(Fig.38)***.
3. Direct evidences for dextral fault movement were found in the Szinpetri and Jósvafő Limestones between *Jsv-017 and Jsv-029* ***(Fig.55, Fig.58, Fig.59)***. These dextral strike-slip faults are mainly **oblique thrust faults** related to NW-SE or NNW-SSE σ_1 and they always post-date the general W-ward tilting event or at least they were active contemporaneously with the folding. Furthermore, S of the fault zone the gradual turn in dip direction from W through NW to N between *Jsv-20 and Jsv-024* points may be interpreted as **dextral shear folds *(Map 13).*** This would also mean that the W-ward tilting preceded the dextral shearing. Similar outcrop-scale dextral shear fold geometry but in outcrop-scale size was observed in the Jósvafő Limestone at *Jsv-057* and at *Jsv-080-082—093-094* ***(Fig.65)***.
4. While in the area of Perkupa the amount of this **apparent dextral offset is approximately 350-450 m in map view**, there is **practically no offset in the western part** of the fault zone as the stratigraphic contact between the Szinpetri and Jósvafő Limestones shows very little or zero offset *(Appendix 4)*. Within the Jósvafő Limestone the continuation of the Jósvafő-Perkupa Fault Zone is marked only by the presence of intensively altered rauhwackes.
5. While in the southern block at least two other significant NE-SW and NNE-SSW trending fault zone merges with the E-W trending Jósvafő-Perkupa Fault Zone, the northern block forms a unified unit in map view with a seemingly continuous sedimentary sequence. Sometimes **the fault zone completely separates fold domains in the two fault blocks:** while in the northern block the dips remain shallow to moderate, in the southern block the measured W-ward dips steepen until 65-85°.
6. While the different members of the Szin Marl show the same thickness on both sides of the Jósvafő-Perkupa Fault Zone, the **thickness of the Szinpetri Limestone change dramatically:** by using the measured general W-ward dips the first basic thickness calculations resulted in about 10 times higher thickness values on the northern than in the southern block (the thickness of the Szinpetri Limestone in the southern block was calculated for between the Almás and Kecskekút Valleys). The outcrop-scale observations proved, however, that neither the southern, nor the northern block is continuous as numerous ~N-S trending pre-tilt normal faults cut through the whole Lower Triassic succession (e.g. ***Fig.34, Fig.36, Fig.37/c, Fig.55/a, Fig.57***). These pre-tilt normal faults

were later tilted, sometimes even until sub-horizontal positions (e.g. ***Fig.58***, ***Fig.59***, ***Fig.61/a***). As the majority of the normal faults dips E-ward while the general tilting is towards W, the true thickness of the Szinpetri Limestone is probably much less on both sides. Nevertheless, the observed difference in the formation thicknesses cannot be solved solely by the effect of normal faulting.

7. Directly at the fault zone the general W-ward dip of the whole Lower Triassic is modified to ~**E-W striking dip**. The measured dip angles also steepen even until sub-vertical or overturned positions (e.g. *Jsv-010—012, Jsv-003 and Jsv-031, Szn-013—104, Per-089*). These steep layers form **tight to isoclinal antiformal structures** (e.g. ***Fig.54***). Within the core of these antiform rauhwackes and/or remnants of the Perkupa Evaporite Formation and/or blocks of deeper stratigraphical units like the Bódvaszilas Sandstone or the lower part of the Szin Marl were found in E-W trending narrow zones. Similar structural geometry but with displacement along the folds' E-W striking axial planes was observed in the Vég Valley as well ***(Fig.29)***.
8. Within the ~E-W striking layers outcrop-scale **asymmetric shear folds with parallel ~E-W trending axes** were observed along the western half of the Jósvafő-Perkupa Fault Zone (e.g. ***Fig.63/a, Fig.64***, **Hiba! A hivatkozási forrás nem található.**, ***Fig.67***). Their axes are usually sub-horizontal or slightly plunging and the sense of movement is either normal or reverse with respect to the present-day dip of the layers. The two opposite shear directions is reflected in the measured layer-parallel striations as well, e.g. at *Jsv-011* where "**normal" and "reverse" flexural slip was found on the same bedding planes** (***Fig.63***, see the explainatory figure in ***Fig.82***).

The presence of rauhwackes, the Perkupa Formation and other deeper Lower Triassic units along the Jósvafő-Perkupa Fault Zone (7) clearly indicates that **its deformation is at least partly related to salt deformation** *(Appendix 4, **Section 1**)*. The *Jő-2* and *Szp-1* wells indeed penetrated the Perkupa Evaporite in shallow depths ***(Fig.24)***. Moreover, cascading parasitic folds also support the model of salt tectonics (e.g. ***Fig.67***). Based on the linear geometry of the rauhwacke zone this salt structure must have originally been an E-W trending salt wall or a salt anticline (***Fig.18***). The exact original geometry of the salt structure is unfortunately unknown as it has been re-deformed during subsequent events. It is probable that the formation of the fault zone preceded the initiation of the salt flow or it was contemporaneous with it. On the other hand, the observed changes in the formation thicknesses on the two sides of the fault zone (6) clearly **date the formation of the salt structure to the Early Triassic**.

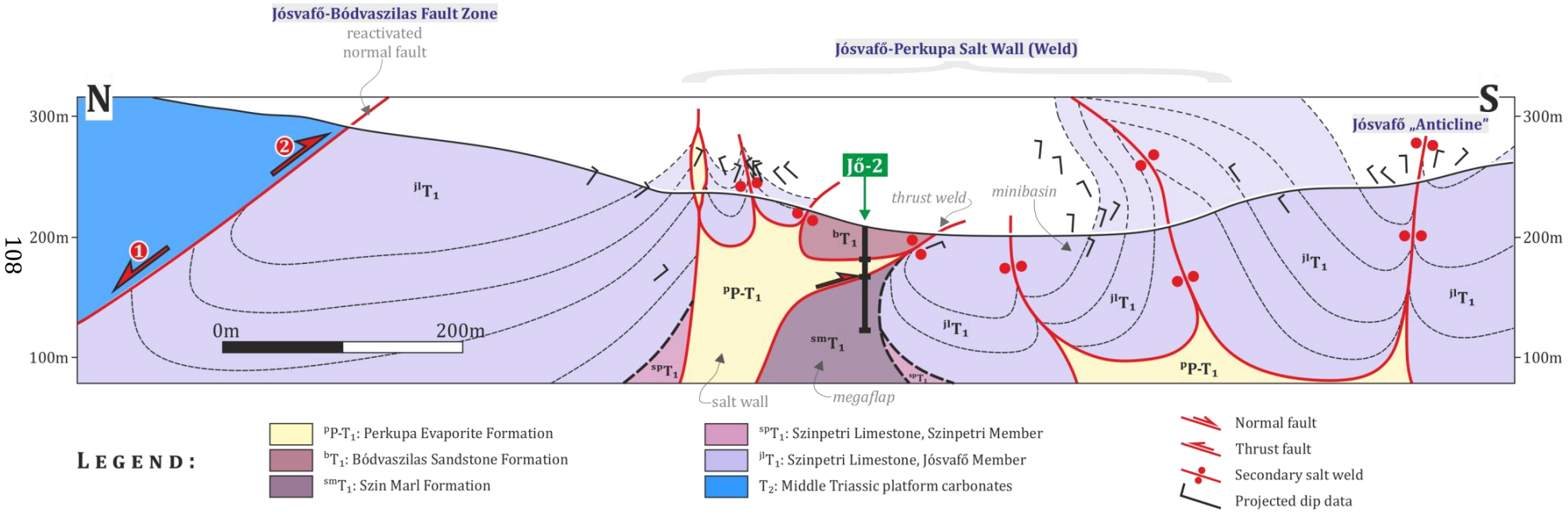
Jósvafő-Bódvaszilas Fault Zone
reactivated
normal fault
Jósvafő-Perkupa Salt Wall (Weld)
N
S
300m
200m
100m
0m
200m
Jő-2
thrust weld
minibasin
Jósvafő „Anticline"
salt wall
megaflap
LEGEND:
$^{p}P\text{-}T_1$: Perkupa Evaporite Formation
$^{b}T_1$: Bódvaszilas Sandstone Formation
$^{sm}T_1$: Szin Marl Formation
$^{sp}T_1$: Szinpetri Limestone, Szinpetri Member
$^{jl}T_1$: Szinpetri Limestone, Jósvafő Member
T_2: Middle Triassic platform carbonates
Normal fault
Thrust fault
Secondary salt weld
Projected dip data

▲ ***Section 1.*** Constructed geological cross-section through the Jósvafő-Perkupa Salt Wall. This ~E-W trending salt wall was squeezed (weld formation) and reactivated as a dextral oblique thrust fault zone during the Cretaceous shortening.

The change in the general dip direction (7) is interpreted as drag folding due to the upward moving salt. As the salt wall/anticline were squeezed and today only rauhwackes and breccias mark the former presence of salt rocks, the oppositely dipping salt drag folds are now in contact with each other along **secondary salt welds** (***Fig.22***, HUDEC & JACKSON 2007, WAGNER III & JACKSON 2016).

The presence of layer-parallel striations reflecting "normal" flexural slip (salt-related folding) and "reverse" flexural slip (shortening-related folding) (8) suggests that the former should have already been on the steeply dipping bedding planes when the second folding phase affected the layers (***Fig.63***). This would mean that the initial tilting was due to Triassic salt tectonics, whereas the Cretaceous deformation only re-worked the bedding planes during flexural slip folding. Two generations of asymmetric shear folds can prove that two separate slip phases along the fault zone: one is related to the buoyant upward flow of the evaporites, whereas the other is shortening-related. The secondary salt weld developed most probably during the second, shortening-related deformation which resulted in the squeezing of diapirs.

The above mentioned observations and reasonings could be summarized in the following: (1) the Jósvafő-Perkupa Fault Zone originally worked as a salt-wall in the Triassic. (2) The salt wall evolved into a secondary weld, (3) and this weld was then reactivated as an oblique dextral fault with reverse slip component *(Jsv-010—030,* ***Fig.55***, ***Fig.58***, ***Fig.59***, ***Fig.63)***. Fault-slip data suggest NW-SE oriented compression to this transpressional deformation ***(Fig.84)***. The dextral shear folds may also be attributed to this phase (3).

This relative chronology would also imply that the N- or S-ward tilting near the fault zone did indeed precede the dextral movement, thus the steep to vertical, or even overturned dips are the result of the salt tectonics. Similarly, the overprinting transpressional phase obliquely reactivated not only the weld itself but the pre-existing ~N-S or ~NW-SE striking pre-tilt normal faults as well (e.g. in ***Fig.58***). Local scatter deviations from the main NW-SE shortening direction may be attributed to pre-existing structures like the already sub-vertical E-W striking layers at *Jsv-011* ***(Fig.63)*** or the pre-tilt normal faults at *Jsv-018* ***(Fig.58)***. This slight scatter may also be observed in the outcrop-scale folds' geometry: again at *Jsv-011* the measured axes were ENE-WSW trending that is parallel to the strike of the bedding.

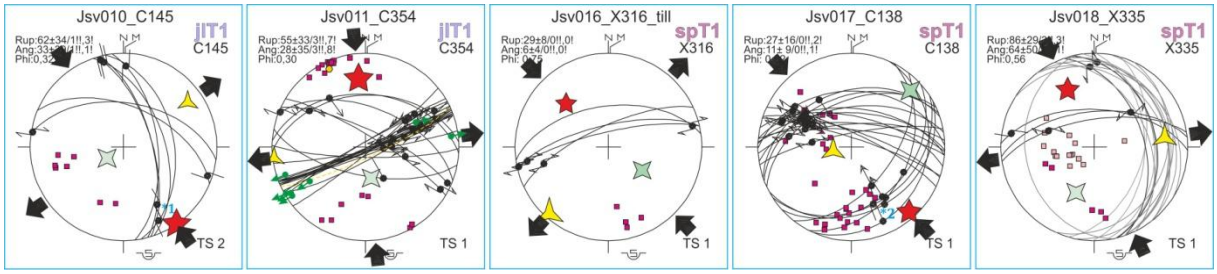

Fig.84. Stereoplots from the outcrops along the Jósvafő-Perkupa Fault Zone indicating approximately NW-SE compression and perpendicular tension. Scatter around from the general NW-SE shortening direction may be attributed to local control of pre-existing structures like already sub-vertical layers *(Jsv-011)* and normal faults *(Jsv-018)*.

Jósvafő "Anticline"

The so-called Jósvafő Anticline was originally defined by SCHRÉTER (1935) and PANTÓ (1935) as an E-W or ESE-WNW trending anticline located SE of Jósvafő *(Appendix 4)*. The same anticline appears on the structural maps of LESS ET AL. (1988) and HIPS (2001) as well. LESS ET AL. (1988) did not finish the anticline at the Kecskekút Valley like HIPS (2001) but bent its axis and continued it as a major slightly bent NE-SW trending anticline running through both the Jósva and Bódva Valleys, until the village of Tornaszentandrás. On the map of HIPS (2001) the Jósvafő Anticline runs through the Almás Valley until the Kecskekút Valley where it is cross-cut by a NNW-SSE trending fault zone. She has already suggested that the Jósvafő Anticline is only an apparent anticline, meaning that its E-W or ESE-WNW trending axis is the result of interference of multiple folding events.

As discussed in *Chapter V.1* the presence of rauhwackes *(Jsv-123, Jsv-129)* and the isoclinal map-scale antiforms with sharp, pointy hinge zones *(Jsv-115—117, Jsv-121—122, Jsv-130)*, the Jósvafő "Anticline" it is in fact a **secondary salt weld** structure running in E-W direction along a precursor salt wall or salt anticline (***Section 1***, HUDEC & JACKSON 2007, WAGNER III & JACKSON 2016). The anticline structure fades out E-ward and only the regional W-ward dips are visible *there (Appendix 4)*. The disappearance of this anticline is possible due to interference of several halokinetic structure.

The Kecskekút Fault Zone, the Almás and Kecskekút Diapirs

The Kecskekút Fault Zone is a NNE-SSW trending fault zone running sub-parallel to the Kecskekút Valley. It divides the Szinpetri Limestone on the eastern side from the continuous succession of the D-E-F members of the Szin Marl and the overlying Szinpetri and Jósvafő Limestones on the western side. The Kecskekút Fault Zone was previously interpreted as a W-ward dipping thrust fault by HIPS (2001), LESS (2000) and LESS ET AL. (2006). In the southern part of the valley they curved the fault zone into an ~E-W trending dextral strike-slip fault which surrounds the lens-like block of the Szin Marl (B-C-D members) at the head of the Almás Valley. The appearance of the Szin Marl here was attributed to the presence of a push-up structure (HIPS 2001, LESS 2000, LESS ET AL. 2006). My observations in this area and the related interpretations are summarized in the following points:

Kecskekút Fault Zone

1. The measured dips in the continuous succession of the Szin Marl (D-E-F), the Szinpetri and Jósvafő Limestones steepen from 25-35° to 65-70-85° towards W-NW, forming a **map-scale anticline** *(Appendix 4)*. Even though the eastern limb of this anticline is missing, the geometry would suggest W-NW vergency. This is in contradiction with the Kecskekút Fault Zone being a W-ward dipping thrust fault. Layer-parallel striations indicating **"normal" flexural slip folding** at *Jsv-016* suggest that the anticline is salt-related ***(Fig.62)***. The (former) presence of evaporites in shallow depths is evidenced by the in-situ rauhwackes found along the southern segment of the fault zone. The kinematics of the NNE-SSW striking

fault zone is questionable: it could be a normal fault with strong relation to salt deformation or a thrust fault. It is also not evident which block is the hanging wall.

Almás Diapir

2. The rauhwacke zone continues as the southern segment of the Kecskekút Fault Zone turns into an E-W and WNW-ESE striking zone. The B-(C-)D members of the Szin Marl outcropping at the head of the Almás Valley appear in an ellipsoidal lens within the Szinpetri and Jósvafő Limestones. The Szin Marl may have a **dome structure** as the measured dips in the southern part of the lens dip outward *(Appendix 4)*. This dome structure is interpreted folding on top of a **concentric salt diapir** (Almás Diapir). The subsurface presence of the Perkupa Evaporite was confirmed by the *Jő-3* well ***(Fig.24)***. Along the contact zone between the northeastern part of the diapir and the WNW-ESE striking fault zone rauhwackes were found, whereas the southern part of the diapir was completely lack of rauhwackes or any king of breccias. Consequently, nevertheless the hiatus in the southern part between the B member of the Szin Marl and the Szinpetri Limestone, their boundary is interpreted as a discordance, not a structural boundary. Even so, the dip direction of the Szinpetri and the overlying Jósvafő Limestones is very similar to the Szin Marl. SW from this diapir both limestones are very thin with respect to their other localities which also suggests that in this area the accommodation space may have been limited, probably due to being on the top of a salt diapir. On the other hand, the rauhwackes in the northern part suggest that the diapir is presently bordered by a fault zone along which some of the salt rock could have escaped. Based on the displaced formation boundaries on its two sides, this fault zone worked as a **dextral strike-slip fault zone**. According to both LESS ET AL. (1988) and HIPS (2001) in the westward continuation of the ~E-W striking fault zone the displacement decreases to zero by the boundary of the Jósvafő and the overlying Gutenstein Limestones, indicating that the fault zone was covered (syn-sedimentary deformation) or we see the fault tip W of the diapir.

Kuriszlán Diapir

3. S of the *Jő-3* well another E-W striking sub-vertical fault zone runs. The apparent dextral displacement along it is 1400m at the minimum (based on LESS ET AL. 1988). In the area of the Kuriszlán Spring the segments of this fault zone coincide with several E-W striking secondary welds *(Appendix 4)*. Between the welds and rauhwacke zones the Szinpetri and Jósvafő Limestones are folded into tight to isoclinal synclines with very steep (60-85°) limbs ***(Fig.49)***. Further S the contact between the uppermost Lower Triassic limestones and the F member of the Szin Marl is interpreted as a sedimentary discordance: they probably **onlap on the Szin Marl** which forms a **very gentle anticline or dome**. This dome and the **secondary welds** are both the result of primary diapirism (Kuriszlán Diapir). S of this diapir there is yet another E-W striking fault zone with dextral offset.

The Varbóc Syncline and the bordering structures

W of Perkupa and in the surroundings of Varbóc the measured dips in the D-E-F members of the Szin Marl and the Szinpetri Limestone forms a map-scale open syncline: the eastern limb dip W-ward or SW-ward while the northwestern limb dip to S or SE *(Appendix 4)*. All authors interpreted thy syncline to continue across the Teresztenye Plateau with slightly curved axis (LESS ET AL. 1988, HIPS 2001). The following observations and interpretations were made regarding the Varbóc Syncline – five segments of the syncline boundaries and one internal structure (Teresztenye Plateau) will be presented.

1. From the E the syncline is bordered by the largest known outcrop of the Perkupa Evaporite (Bódva Valley).
2. Along the southeastern limb near Szőlősardó, the tectonic situation is complicated: HORVÁTH ET AL. (2012) demonstrated Jurassic to Cretaceous nappes and windows where Lower Triassic formations appear. The original structural geometry thus cannot be determined. The observations of HIPS (2001) included the area of the Henc Valley E of Szőlősardó where she has observed lens-like isolated outcrops of the different members of the Szin Marl, as well as curved structural boundaries between the Szin Marl—Szinpetri Limestone and the Middle Triassic carbonates. On her map this structural boundary was interpreted as a young-on-older thrust. **The lens-like geometries, the curved structural boundaries and the young-on-older contacts are typical features of salt-related deformation.** This means that **the Varbóc Syncline is probably bordered by salt structures from S as well.**
3. The northern boundary of the syncline is the Jósvafő-Perkupa Fault Zone which is presently a secondary salt weld (see details in the previous sub-chapter). Thus the northern S-ward dipping limb of the Varbóc Syncline is the result of **drag folding along the E-W trending salt structure**.

Tornakápolna Diapir and Szövetény Fault Zone

4. Near Tornakápolna the northwestern limb of the syncline is bounded by the NE-SW trending Szövetény Fault Zone running almost parallel to the Szövetény Valley. Along this fault zone the Perkupa Evaporite is certainly positioned in shallow depths as proved by the *Tk-3* well ***(Fig.24)***. The geometry of the Bódvaszilas Sandstone and the lowermost parts of the Szin Marl covering the Perkupa Evaporite at *Tk-3* indicates a more or less **concentric salt diapir** *(Appendix 4, **Section 2**)*. Let's call this salt structure **Tornakápolna Diapir**. There is angular discordance between the doming Bódvaszilas Sandstone — Szin Marl beds and the surrounding Szinpetri Limestone but their contact is probably sedimentary as there are no signs of salt welding or brecciation. On the northern side of the diapir the E member of the Szin Marl also onlap on the doming beds B member. This dates the diapirism to at least to deposition time of the E member *(Szn-070)*.
5. The exact deformation history of the Szövetény Fault Zone is questionable ***(Appendix 4)***. Unfortunately the fault zone itself has no direct outcrops but it is evident that there are salt structures along it. On the top of the Tornakápolna Diapir the measured dips in the

Bódvaszilas Sandstone becomes parallel to the fault zone itself, suggesting that at least the present-day geometry of the diapir is in connection with the fault zone. Along its northern segment the opposite dips in the two fault blocks suggest salt welding ***(Fig.43)***. In its southern segment the Gutenstein Limestone is in direct contact with the Szinpetri Limestone along the fault zone – the Jósvafő Limestone is either completely missing or it is present but it cannot be separated from the very similar Gutenstein Limestone.

In summary the evolution of the Szövetény Fault Zone was probably strongly influenced by the presence of salt structures. It is not even necessary that the fault zone itself had existed in the Triassic (or it may had existed but did not necessarily reach the surface) but when the fault zone finally formed, the salt structures localized the deformation. It also caused secondary welds to form in the northern part.

Teresztenye Minibasin

6. The Teresztenye Plateau located in the southwestern part of the syncline is covered by the Gutenstein Limestone. It is almost completely surrounded by the Szinpetri Limestone and their boundary is curved *(Appendix 4).* This curved boundary is interpreted to be an original (Triassic) geometry that is related to salt deformation. This is also supported by the remains of the Perkupa Formation and rauhwackes *(Szn-019—020, Szn-086,* ***Map 6****)*. Moreover, the observed cascading parasitic folds in the N-vergent folds at *Szn-093* also imply that the folding is related to salt deformation. The relative small fold amplitudes indicate that **the salt must be in very shallow depths below the Gutenstein Limestone**.

   The whole Teresztenye Plateau may be a completely salt-floored and salt-bordered minibasin. For this basin to be a Triassic salt-floored basin its subsidence should have started syn-sedimentary with the deposition of the Gutenstein Formation. This also implies that prior to the initiation of the subsidence there was a relative significant salt diapir that must have reached the surface or near-surface depths. Subsidence above a salt diapir results from diapiric collapse that is most probably caused by outflow of the salt rocks from this diapir to another one ***(Fig.86/a)***. The minibasins formed by the collapse of a salt structure are called salt-withdrawal basins (LEHNER 1969, JACKSON & TALBOT 1991, PEEL 2014b, ROWAN & VENDEVILLE 2006, TRUSHEIM 1960, VENDEVILLE & JACKSON 1991).

   The Teresztenye Minibasin must have been affected by post-Triassic deformation. It is possible that the Teresztenye Minibasin was thrust over the surrounding Szinpetri Limestone ***(Section 2)***. Firstly, the presence of salt rocks favors its reactivation as a thrust fault once the area gets in a compressional stress field. In the northern part of the minibasin this thrusting would have N-ward vergency. Secondly, the folded section of the Gutenstein Limestone at *Szn-093* also showed N-ward vergency ***(Fig.42)***, indicating that the Teresztenye Minibasin was indeed thrust over the Szinpetri Limestone. Their boundary is thus currently a thrust weld (WARREN 2016).

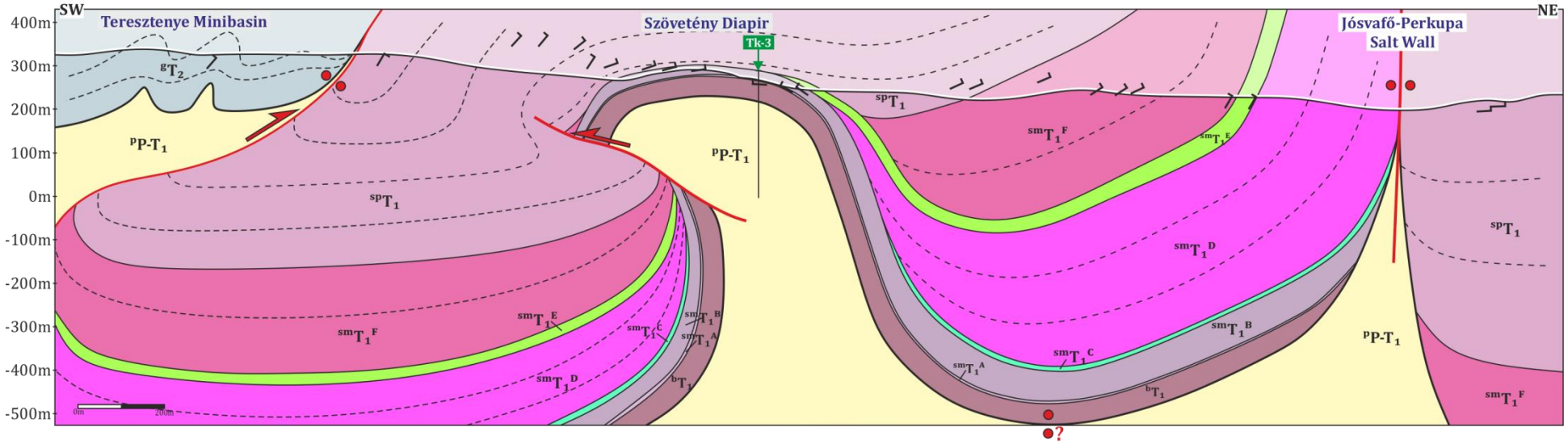

LEGEND:

- $^{p}P\text{-}T_1$: Perkupa Evaporite Formation
- $^{b}T_1$: Bódvaszilas Sandstone Formation
- $^{sm}T_1{}^{A}$: Szin Marl Formation, A member
- $^{sm}T_1{}^{B}$: Szin Marl Formation, B member
- $^{sm}T_1{}^{C}$: Szin Marl Formation, C member
- $^{sm}T_1{}^{D}$: Szin Marl Formation, D member
- $^{sm}T_1{}^{E}$: Szin Marl Formation, E member
- $^{sm}T_1{}^{F}$: Szin Marl Formation, F member
- $^{sp}T_1$: Szinpetri Limestone, Szinpetri Member
- $^{g}T_2$: Gutenstein Limestone Formation
- Thrust fault
- Primary salt weld
- Secondary salt weld
- Projected dip data

▲ ***Section 2.*** Constructed geological cross-section through the Jósvafő-Perkupa Fault Zone, the Tornakápolna Diapir and the Teresznye Minibasin.

Varbóc Syncline

7. All the above mentioned observations indicate that the Varbóc Syncline is a very broad and very gentle syncline which is surrounded by salt structures on all sides. These are the typical features of minibasins *(**Fig.86**, Appendix 4, **Section 2**)*. Its boundaries were clearly reactivated and the salt structures were re-deformed during the Cretaceous shortening.

Jósvafő-Bódvaszilas Fault Zone

Beside the Jósvafő-Perkupa Fault Zone the other remarkable structural element of the eastern part of the Aggtelek Mts. is the approximately WSW-ENE or SW-NE striking major fault zone between Jósvafő, Szögliget and Bódvaszilas, called Jósvafő-Bódvaszilas Fault Zone after HIPS (2001) *(Appendix 4)*. Along this fault zone the Lower Triassic sequence is in contact with the Middle Triassic platform carbonates. Their contact was previously interpreted as a young-on-older thrust in almost every previous structural work (HIPS 2001, LESS 2000, LESS ET AL. 1988, 2006). During my thesis work three segments of this fault zone was mapped to understand its geometry in details. Based on the observations the following can be stated:

1. NE of Jósvafő the Jósvafő-Bódvaszilas Fault Zone is WNW-ESE striking which is also reflected by the measured dips at *Jsv-060—065 (**Map 17**)*. Breccias and rauhwackes are present along almost the whole mapped segment of the fault zone *(Jsv-066)*, indicating that **evaporites may have been present along the contact zone**. Moreover, there is a thin slice of Gutenstein Limestone between the Middle Triassic platform and the Jósvafő Limestone. Its boundary towards the Jósvafő Limestone has been previously interpreted as a sedimentary boundary but there are also breccias and rauhwackes between them ***(Fig.71)***. These deformed rocks suggest that **there is another structural boundary running parallel to the main fault zone between the Gutenstein and Jósvafő Limestones**.
2. NW of Jósvafő the *Jő-1* well penetrated first Middle Triassic platform carbonates, then it reached the Jósvafő Limestone at 118 meters (the Gutenstein Limestone is missing, ***Fig.24***). By using the map of HIPS (2001) the fault's trajectory was projected to the position of the drilled contact zone in the *Jő-1* well ***(Section 3)***. This permitted to calculate **the dip angle of the E-W trending segment of the fault zone here which is at least 60°, probably more**.
3. The contact zone between the Middle Triassic platform carbonates and the Gutenstein Limestone is directly outcropped at *Jsv-069* where the fault zone dip moderately (~35-45°) towards NW. The majority of the measured striations on the fault plane itself were dip slip lineations with unidentifiable sense of movement (supposedly thrust faults) but there were a few oblique striations as well which proved to be **pre-tilt normal fault lineations**

(Fig.72). These pre-tilt normal faults were originally NE-SW striking low-angle normal faults.

4. N of the Palonták Slope and in the area of the Kuriszlán Spring the Jósvafő-Bódvaszilas Fault Zone is NE-SW striking and it separates the Jósvafő Limestone and the Middle Triassic platform carbonates ***(Map 18)***. In-situ outcrops of the Perkupa Evaporite and the high amount of rauhwackes were found along the fault zone, indicating that the salt rocks clearly has important role in the deformation *(Jsv-046)*. Evaporites were furthermore found in a narrow but definite NNE-SSW trending zone at *Jsv-043—045*. This zone probably widens towards S and disappears at the Jósvafő-Bódvaszilas Fault Zone *(Appendix 4).*
5. In the area of the Szelcepuszta Road rauhwackes, remains of the Perkupa Evaporite and the ma-scale isolated lens of the Bódvaszilas Sandstone along the fault zone are clear evidences for salt deformation ***(Map 19)***. HIPS (2001) observed further lens-like occurrences of other deeper stratigraphical units (i.e. the different members of the Szin Marl) along other parts of the fault zone.
6. Again in the area of the Szelcepuszta Road **dextral shear folds with sub-vertical fold axes** were observed along the ~E-W trending segments of the fault zone, suggesting dextral strike-slip movement ***(Map 19)***. This dextral shear post-dates the ~E-W trending fold set in the Szinpetri Limestone.
7. **The Jósvafő-Bódvaszilas Fault Zone seems to be offset by several NNW-SSE trending fault** (e.g. N and NE of Jósvafő, in the area of the Szelcepuszta Road, *Appendix 4*). This deformation seems to be related to dextral strike-slip shearing that post-dates the formation of the whole fault zone.

Jósvafő-Bódvaszilas Fault Zone

Contrary to the previous interpretations (GRILL 1989, GRILL ET AL. 1984, HIPS 2001, LESS 2000, LESS ET AL. 1988), based on the high-angle or even sub-vertical dip of the zone (2nd point) it can be almost completely excluded that the fault zone initially formed as a thrust fault as thrust contacts are usually very low-angle faults, they only steepen until 40° at their ramp segments, everywhere else they run almost horizontally (BUTLER 1982, COOPER & TRAYNER 1986, ELLIOTT 1977). In addition to that – as described in *Chapter V.2* – it requires a special structural situation to form the young-on-older contacts in the previously interpreted way, that is folding of the whole Lower to Middle Triassic sequence into large-scale gentle folds and then putting the younger platform carbonates on the top of older formations ***(Fig.83/b)***.

Considering the presence of rauhwackes and the lenses of deeper stratigraphical units (1st, 4th and 5th points), as well as the geometry of the beds along the Jósvafő-Bódvaszilas Fault Zone (6th point), the deformation of this zone is probably linked to salt deformation. This is also in agreement with the high-angle or sub-vertical dip of the fault zone. The present-day offset along the Jósvafő-Bódvaszilas Fault Zone is at least 1000-1200m as inferred from the *Szi-2* well ***(Fig.24)***. The majority of this offset is attributed to the Triassic salt deformation. When the area was compressed and the salt rocks were squeezed out, the former salt wall/anticline evolved first into a secondary weld, then it was further reactivated as a high-angle thrust weld ***(Section 3, Fig.83/d).*** Practically

this thrust weld is the young-on-older contact that we see today. The continuous thrusting may have modified the original geometry of the salt deformation zone and even new thrust faults may have formed cutting through the footwall of the major young-on-older thrust (e.g. 1st point).

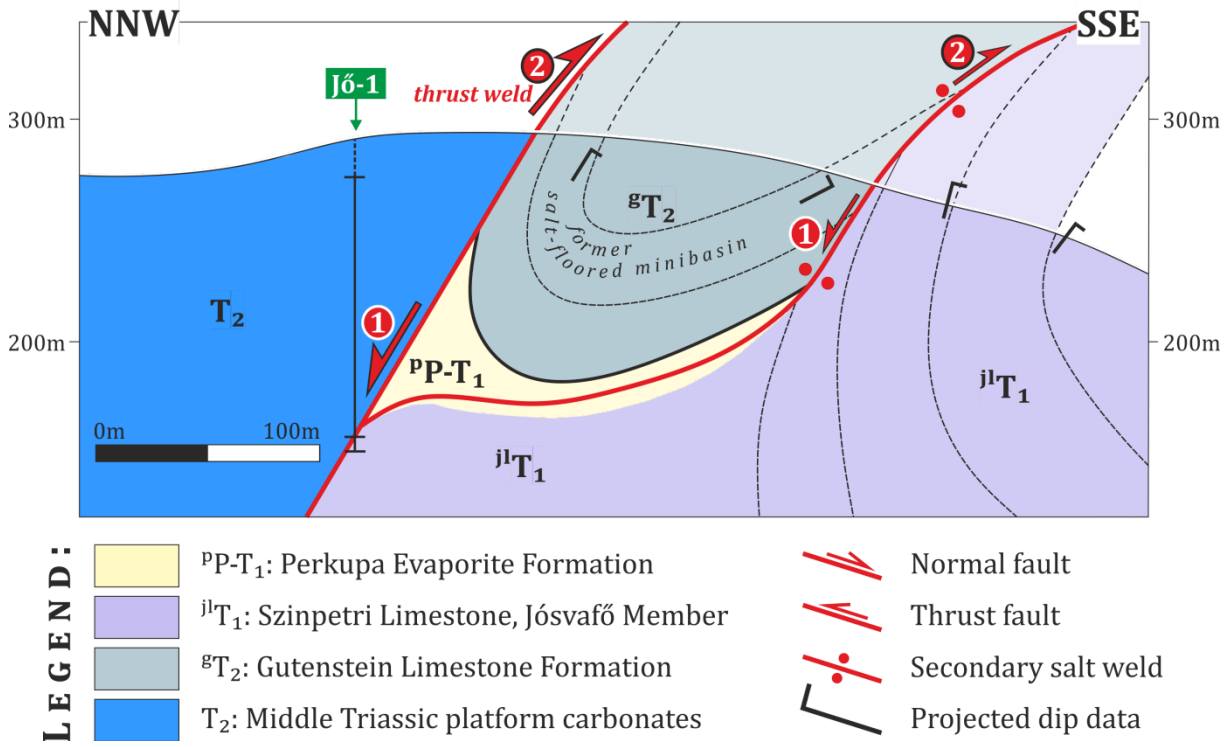

Section 3. Constructed geological cross-section through the Jósvafő-Bódvaszilas Fault Zone that bounds the Lower Triassic ramp formations in the footwall with the Middle Triassic platform carbonates in the hanging wall. Field evidences indicate that this fault zone was originally a high-angle normal fault and it was also related to a Triassic salt wall which was later compressed (welding) and the squeezed contact zone was reactivated as a thrust fault, resulting in the present-day young-on-older contact.

V.4. Reconstructed structural evolution of the Silica Nappe

Based on the structural interpretation of the individual map-scale structural elements *(Appendix 4)* and the results of the fault-slip analysis *(Appendix 3)* I separated the following deformation phases:

D_0 phase: syn-sedimentary deformation. This phase includes every structural element that formed quazi contemporaneously with the sedimentation but certainly prior to the consolidation, including outcrop-scale slump folds and early, syn-sedimentary normal faults.

D_1 phase: Triassic salt tectonics (and extension). During this phase map-scale salt walls and diapirs was controlling the deformation. The most remarkable salt walls are the E-W striking Jósvafő-Perkupa Salt Wall, and the salt walls N of the Almás and Kecskekút Diapirs, the ~ENE-WSW striking Jósvafő-Bódvaszilas Salt Wall, the NNW-SSE striking Bódva Diapir, and the NE-SW striking salt walls below the Szövetény and Kecskekút Fault Zones. Between the salt structures minibasins like the Varbóc and Teresztenye Minibasins evolved. The Lower Triassic formations were dragged along the salt structures or they form anticlines and domes (first tilting). Pre-tilt (mainly NW-SE striking) normal faults and monoclonal fault-related folds also formed during this phase.

D_2 phase: Cretaceous shortening. This phase was separated into two sub-phases: D_{2a} event presented NW-SE oriented shortening, whereas D_{2b} showed N-S shortening. Both sub-phases were transpressional. The active map-scale elements during this phase were the E-W striking dextral strike-slip fault zones that reactivated the secondary salt welds, and E-W and NE-SW striking young-on-older thrust faults. The best examples for young-on-older contacts are the Jósvafő-Bódvaszilas Fault Zone and the northern boundary of the Teresztenye Minibasin. There are also three NNW-SSE striking dextral strike-slip fault zones that displaces the Jósvafő-Bódvaszilas Fault Zone, thus they are probably related to the D_{2b} phase. The observed outcrop-scale elements were mainly SE-vergent asymmetric folds (second tilting) and reactivated normal faults.

D_3 phase: post-tilt deformation phase with ENE-WSW striking dextral and WNW-ESE striking sinistral strike-slip and oblique thrust faults, and resumably with E-W striking normal faults. No map-scale structural elements were observed.

D_4 phase: the first post-tilt extensional phase. Dominantly (N)NW-(S)SE striking normal faults evolved. This phase may have also reactivated the parallel striking inherited high-angle structures but no significant map-scale deformation occurred.

D_5 phase: the second post-tilt extensional phase. NE-SW striking normal faults were accompanied by N-S striking dextral and E-W striking sinistral strike-slip faults. Relevant map-scale structures did not forme.

The aforementioned deformation phases along will be discussed in details in the following sub-chapters. The summary of the the deformation history of the main map-scale structural elements will also be presented.

D_0-D_1: Triassic syn-sedimentary salt tectonics

As we have already seen there are many indications for syn-sedimentary or very early deformation features like syn-sedimentary faults, slump folds, pre-tilt normal faults and monoclinal fault-related folds formed along or above normal faults (see *Chapter V.1*). These structural elements affected all members of the Lower Triassic succession, starting from the Bódvaszilas Sandstone and continuing up until the Gutenstein Limestone. **Extreme thickness variations** observed within the Lower Triassic formations also clearly suggest syn-sedimentary deformation that intensified contemporaneously with the formation of the Szinpetri and Jósvafő Limestones. Formation thicknesses drastically change across observed major structural elements that are related to salt structures (e.g. Jósvafő-Perkupa Fault Zone, Almás Diapir). Postulated **onlap surfaces** between the dragged deeper stratigraphical units and the overlying upper Lower Triassic formations also suggest that significant salt deformation should have been already in progress by the time of the deposition of the Szinpetri and Jósvafő Limestones. Consequently, the earliest onset for the significant salt tectonics corresponds to the age of the uppermost E and F members of the Szin Marl that is Spathian (Olenekian) but primary salt movement may have started already in the Smithian

(Induan to Early Olenekian, HIPS 1995, 1996a). By this time the thickness of the sedimentary load above the evaporitic sequence should have been 650-800m. Even though a dominant number of the world's diapirs had 1000m or more sedimentary cover above them when the diapirism started, several case studies and modeling proved that 350m (or even less) thick loading is enough for the diapirism to initiate (JACKSON & VENDEVILLE 1994).

At this time of the Early Triassic the Silica Unit was located on the passive margin of the Neotethys Ocean. Whether it was on the northern or on the southern margin, it is still an unanswered question (see details in *Chapter II.4*). According to FINGER ET AL. (2003), MILLER & THÖNI (1997), SCHUSTER ET AL. (2001) and SCHUSTER & STÜWE (2008) the continental rifting in the Neotethyan realm was Permian to Earliest Triassic, whereas the final continental break-up and initiation of the oceanic spreading happened only in the Late Anisian times (GAWLICK ET AL. 2012, GAWLICK & MISSONI 2015, KOZUR 1991, SUDAR ET AL. 2013). It is believed that during the Early Triassic a relative "calm" tectonic phase ruled in the proximal part of the passive marginal areas and very shallowly dipping carbonate ramps evolved with first siliciclastic, then carbonatic shallow water sedimentation (HIPS 1995, 1998). This structural "calmness" probably correlates with the shift of the locus of extension from the proximal areas to the more distal parts of the rifting basin (necking zone, distal and outer domains, PERON-PINVIDIC ET AL. 2013).

Contrary to a tectonically quite early Triassic, findings of this thesis show continuous extensional deformation and salt diapirism accompanied by **dissected seafloor morphology** throughout the whole Early Triassic sedimentation. This last statement comes from the very diverse paleoslope directions estimated from the slump fold geometries and from the various pre-tilt and syn-sedimentary normal fault strike directions ***(Fig.86)***. All the while, the sedimentary facies of the Lower Triassic formations indicates mostly undisturbed shallow water sedimentation without any signs for significant dissection of morphology (HIPS 1995, 1998). This apparent contradiction can be solved if the sedimentation was fast enough to keep up with the differential vertical deformation. This way the sedimentary facies will reflect a near-even sediment surface (ramp environment) while the subsurface structural geometry keeps changing and the deformation (even modest surface tilts) keeps causing sedimentary slumping. This explanation is mostly supported by the interpreted onlap surfaces surrounding the salt diapirs (Almás and Tornakápolna Diapirs, ***Section 2***).

▼ ***Fig.85.*** Triassic strcutural map of the eastern part of the Aggtelek Mts as indicated by salt diapirs and salt walls, sedimentary slump structures, pre-tilt and syn-sedimentary normal faults.

Triassic salt structures of the E-Aggtelek Mts.

By Éva Oravecz

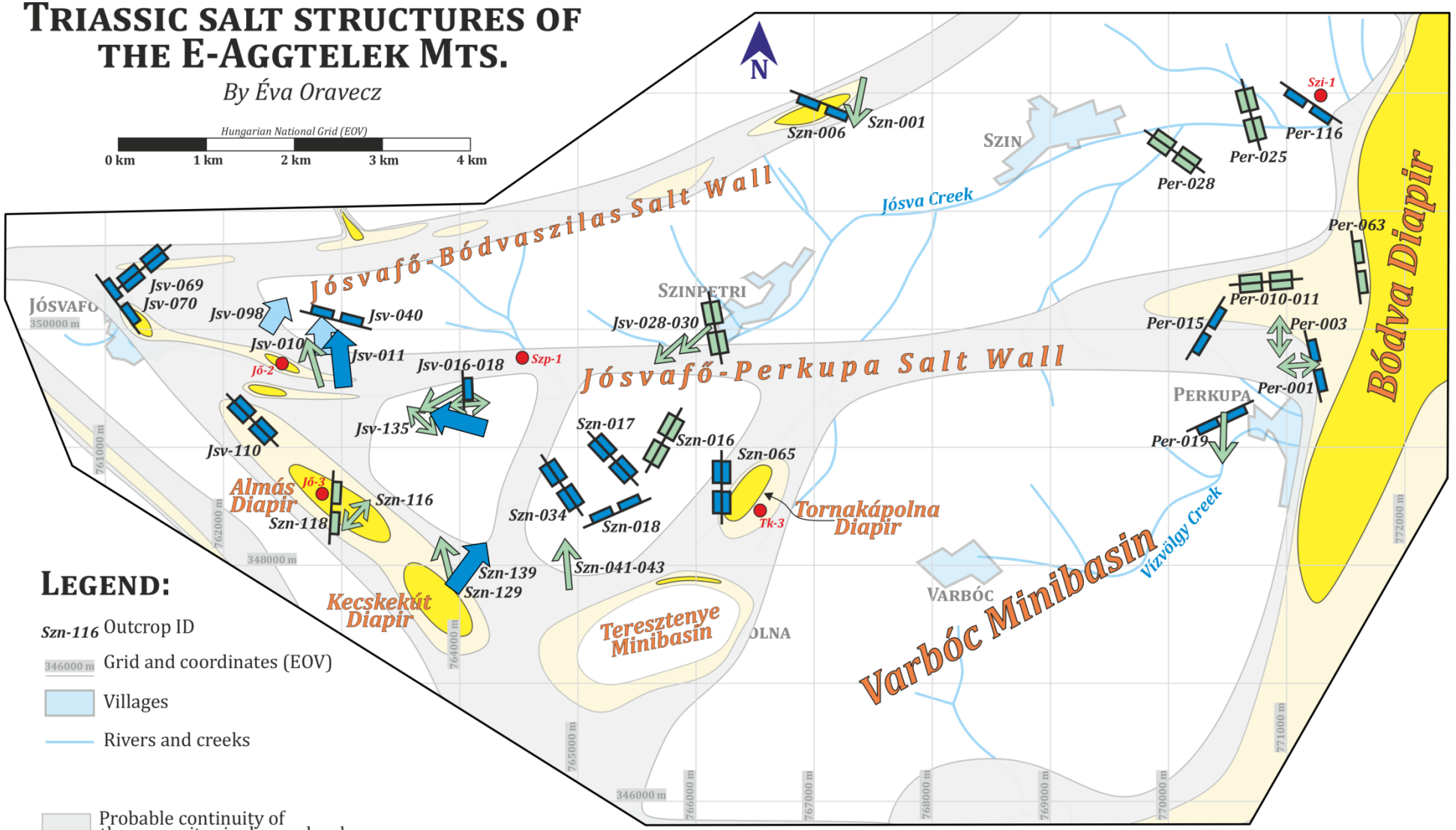

Legend:

- *Szn-116* Outcrop ID
- 346000 m Grid and coordinates (EOV)
- Villages
- Rivers and creeks
- Probable continuity of the evaporites in deeper levels
- Evaporites in shallow depths and rauhwackes
- Clear evidences for salt diapirs and/or Perkupa Formation on the surface
- Well that penetrated evaporites in shallow depths

Syn-sedimentary deformation:

- Slump fold vergency (~paleoslope)
- Syn-sedimentary normal faults

Post-sedimentary (pre-tilt) deformation:

- Pre-tilt normal faults
- „Normal" flexural slip
- Vergency of cascading folds

As for what is the reason behind the relatively slow dissection of the seafloor when tectonically the Early Triassic should be very "calm", it is interpreted to be related to salt tectonics: syn-sedimentary salt diapirism may create the same second-order extensional structures as in a syn-sedimentary rifting basin while it results in drag folding and complex basin geometries at the same time. This model is supported without doubt by ***Fig.86*** which shows that there is a **clear correlation between the interpreted map-scale salt structures, the early (syn-sedimentary and pre-tilt) normal faults and the sedimentary slump folds**: the strike of the salt domes and salt walls are parallel to the strike of the normal faults and the estimated local paleoslopes dip outward radially or at right angles from the salt structure. The same **correlation exists between the observed "normal" flexural slip striations and the vergency of cascading folds**. In a few cases two opposite slumping directions were observed in the same outcrop – this can also be explained by having two different salt structures in both directions that grew contemporaneously and gained height in turns (e.g. *Jsv-018, Jsv-030, Szn-134—135, Szn-139*). While these connections between the structures and the sedimentary features also support the idea of syn-sedimentary salt tectonics, they also explain why we see at least three different extensional directions in the Early Triassic. These normal faults are thus not necessarily related to regional extension but they may be only secondary salt-related structures: faults and fractures evolve above salt diapirs as the salt flow upward and its sedimentary cover is stretched (ALSOP ET AL. 2018, MAIONE & PICKFORD 2001, ROUBY ET AL. 2002). These normal faults may even rotate with the progressive grow of the diapir and they may reach sub-horizontal or even overturned geometries (CHIMNEY & KLUTH 2002, ECOSA ET AL. 2018, VARELA & MOHRIAK 2013, ***Fig.86***). Probably this is the case with the present-day low-angle to sub-horizontal normal faults along the roadcut between Szinpetri and Jósvafő (***Fig.58***, ***Fig.59***, ***Fig.61***).

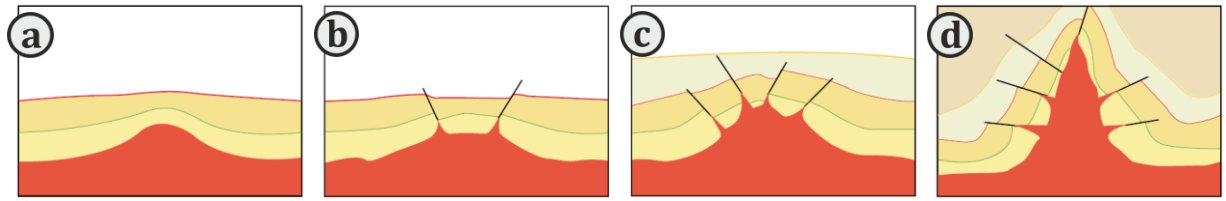

Fig.86. Progressive rotation of normal faults formed above a salt diapir (WARREN 2016 after VARELA & MOHRIAK 2013). Their rotation may continue until the normal faults become sub-horizontal or they may even overturn. **A.)** Initiation of the salt diapir. The sedimentary cover is bent but not fractured. **B.)** The first normal faults appear on the top of the diapir. **C.)** More and more fractures evolve as the sedimentary cover is stretched above the growing diapir. **D.)** With the progressive growth of the diapir the normal faults start to rotate. The rotation may continue until the faults reach sub-horizontal or even overturned position.

It is still possible, however, that the Early Triassic structural geometry may be attributed to both active salt tectonics and regional extension – everything depends on the timing of salt deposition and salt tectonics with respect to the temporal and spatial rift evolution in the broader surroundings of the Silica Unit. Considering the rift evolution model of PÉRON-PINVIDIC ET AL. (2013) and the related salt deformation model of ROWAN (2014) it can be excluded that the Perkupa Evaporite deposited as a pre-rift salt sequence. Its deposition most probably happened during the end of the stretching or at the beginning of thinning phases because the exhumation phase should be closer in time to the final continental break-up that is Late Anisian (GAWLICK ET AL. 2012, GAWLICK & MISSONI 2015, KOZUR 1991, SUDAR ET AL. 2013). As evaporites almost always work as detachment

levels (JAMMES ET AL. 2010) – already in extensional settings – it probably decoupled the major stretching going down in the Paleozoic basement from the deformation in the Mesozoic cover above. This way only a small amount of Early Triassic extension would affect the present-day Silica Nappe. Furthermore, if the Perkupa Evaporite was thick enough and it formed a more or less continuous "sheet" below the whole Mesozoic cover then the Silica Unit could have begun to slide in downslope direction already during the Early Triassic (extensional allochton).

Concerning the overall structural geometry in the Early Triassic, there are salt walls and salt diapirs. The most remarkable salt walls are along the present-day Jósvafő-Perkupa and Jósvafő-Bódvaszilas Fault Zones and in the Bódva Valley (Bódva Diapir). Further salt walls were mapped in the area of the Kuriszlán Spring which are tracable ~700 m in E-W direction; and around the Kuriszlán Spring. The most spectacular diapirs are the Almás Diapir with its concentric structure, the Tornakápolna and Kuriszlán Diapirs. The presence of rauhwacke zones and the observed syn-sedimentary and pre-tilt structures indicate that there are at least two other salt walls below the Kecskekút and Szövetény Fault Zones.

The longest Jósvafő-Perkupa Salt Wall evidently has a more comlex evolution. While the Bódva Diapir is a NNE-SSW trending huge salt diapir that is at least 1600 m vertically *(Szi-1 well)*, it has an E-W trending lateral bulge below the eastern segment of the **Jósvafő-Perkupa Salt Wall**. While there was another E-W trending salt wall below its westernmost segment, there is no evidence that these two smaller salt walls were fully connected in the middle part of the Jósvafő-Perkupa Fault Zone. As the geometry of diapirs keep changing continuously in time, obviously the two salt walls may have "propagated" towards each other until finally, they were connected. However, it is possible that the two salt walls remained two separate salt bodies. In this case the salt wall below the present-day Szövetény Fault Zone (Teresztenye Minibasin — Tornakápolna Diapir) may have not terminated at the Jósvafő-Perkupa Fault Zone but continued northward (unfortunately due to very poor outcrop conditions it is impossible to tell from mapping).

Moreover, the map-scale geometry of the Jósvafő-Perkupa Salt Wall in the area around the *Jő-2* well is similar to a pull-apart basin based on which **the area directly E of Jósvafő is marked by frequent combination of E-W and NW-SE trending salt structures**. The Almás-Diapir also appears at the step-over structure of an E-W striking fault zone which indicates that the parallel trending salt walls may be related to strike-slip or oblique fault zones (see examples for strike-slip salt tectonics in ALSOP ET AL. 2018, CANÉROT ET AL. 2005, SMIT ET AL. 2008). Beside salt walls, the diapirs often appear in rows or in the elongation of other known salt walls/rauhwacke zones, suggesting that the seemingly individual diapirs are also connected to linear salt structures in deeper depths ***(Fig.86)***. Based on their linear geometry I suggest that **these elements probably formed above basement faults** (***Fig.87,*** BODEGO ET AL. 2018, CANÉROT ET AL. 2005, ROWAN 2014, TARI ET AL. 2014, 2016, TARI & JABOUR 2013, VENDEVILLE AT AL. 1995). As the majority of the pre-tilt normal faults dip E-ward or NE-ward and as the syn-sedimentary normal faults formed prior to the onset of the major salt tectonics are also (N)NW-(S)SE striking, these basement faults were also most probably N-S/NW-SE striking, whereas the E-W striking salt walls like the Jósvafő-Perkupa Salt Wall may have formed above transfer zones.

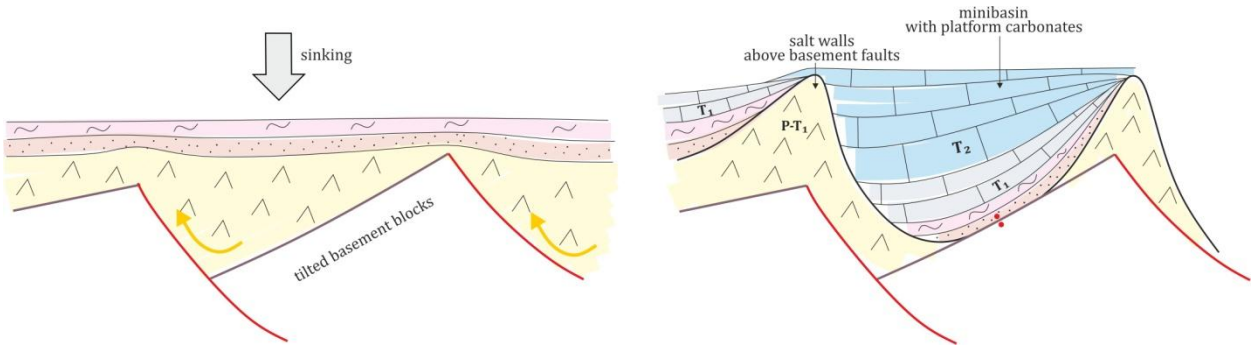

Fig.87. Schematic model of how salt walls form above basement structures. In case of the Silica Unit the normal faults in the basement may be NW-SE striking while E-W striking salt walls also formed above transfer zones. The figure in the right also shows how the thick Middle Triassic platform carbonates could have formed in minibasins sinking rapidly between basement faults-related salt walls.

During diapirism the cover formations of the Perkupa Evaporite were dragged and folded during the upward flow of the salt rocks, therefore they formed **salt flaps and salt walls/anticlines**. After the initiation of salt diapirism the syn-salt sedimentation continued in minibasins. The best example for minibasins in the Aggtelek Mts. is the **Varbóc Minibasin**. If forms a very broad but gentle syncline that is more or less concentric (the general dip is always towards the basin) but certainly not cylindrical ***(Fig.86**, Appendix 4)*. As the up-building of the Bódva Diapir required a lot of evaporite refill withdrawn from under the surrounding areas, it is possible that the Perkupa Evaporite is tectonically pinched out at the bottom of the Varbóc Syncline, thus forms a primary salt weld.

The **Teresztenye Plateau** may be another, a special kind of minibasin: contrary to the normal type minibasins, salt-withdrawal basins do not form by active diapiric piercement of the sedimentary cover but by collapse of a relatively board salt diapir or salt wall which permits the top of the structure to subside and be filled with syn-collapse sediments. This suggests a dynamic connection between the individual salt structures and also indicates that the original overall thickness of the Perkupa Evaporite should be rather thick. The Gutenstein Limestone was present in a narrow zone along the Jósvafő-Bódvaszilas Fault Zone and in a narrow NW-SE trending zone SW and S of Jósvafő. The former zone is clearly related to a salt wall, and supposedly the latter one also formed along a salt structure based on the geological map of PÉRÓ ET AL. (2015). The formation of the Gutenstein Limestone therefore is connected to elevated areas above salt structures.

Another remarkable minibasin could be the hanging wall of the **Jósvafő-Bódvaszilas Fault Zone**. While this fault zone and the related salt walls form the southern and southeastern boundaries of this minibasin, the Middle Triassic platform carbonates are bordered by the so-called Derenk Zone in the N. Even though the study area of this master thesis did not extend to the Derenk Zone, its map geometry displayed on the geological map of LESS ET AL. (1988) shows almost every typical features and characteristics of a salt deformation zone (i.e. curved structural boundaries, isolated lense-like bodies, remains of the Perkupa Evaporite Formation and other deeper stratigraphical units, young-on-older contacts). Furthermore, the Middle Triassic platform carbonates have significant thickness – the *Szn-2* well located not far away from the fault zone reached 1000 m depth but still did not drilled out of the platform carbonates. Even though the carbonate production could obviously keep up with the subsidence of this basin, the total amount of subsidence was very

significant within a relatively short time. Only a few structural scenarios could explain this rate and amount of basin subsidence and the most evident scenario is that the subsidence is related to the salt deformation. If the Middle Triassic platform carbonates did indeed form in a salt-bearing basin the initiation of the salt diapirism at the border of the basin together with the initiation of rapid carbonate production started a vicious circle with every step being a positive feedback in the system. As the diapirs begun to grow, the evaporites slowly flowed in the direction of the salt structures from the neighbouring areas that later formed the basement of a syn-salt minibasin. As the evaporites were flowing out, the newly formed basin was subsiding and the carbonate sedimentation kept pace with its subsidence ***(Fig.87)***. The continuous carbonate production meant increasing sediment loading on the evaporite basement which caused even more salt withdrawal, which then caused even more subsidence in the basin. A cycle like this could continue until no evaporite has remained under the minibasin so a primary salt weld has formed. If this is truly the case with the Middle Triassic platform carbonates in the minibasin between the Jósvafő-Bódvaszilas Fault Zone and the Derenk Zone then the syn-sedimentary salt deformation must have continued until the Middle Triassic. This is also evidenced by the smaller salt structures within the Middle Triassic carbonates in the area of the Kuriszlán Spring *(Appendix 4,* ***Map 18****).*

D_2: Cretaceous shortening

As the Aggtelek Mts. is a part of a fold-and-thrust belt one would rightly expect both map-scale and outcrop-scale shortening-related structures like ramp anticlines, fault-propagation folds and imbricates to dominate the area. Contrary to that, a significant part of the mapped area was dominated by extensional structures and the only indications for shortening were reverse or oblique strike-slip striations on the reactivated normal faults and reverse drag folds overprinting normal drag folds (see details in *Chapter V.1).* The explanation behind this probably lies in the understanding the pre-existing Triassic structural geometry. Numerous recent studies focused on understanding the role of these pre-existing structures in the evolution of the different fold-and-thrust belts around the world (e.g. in the Northern Calcareous Alps: GRANADO ET AL. 2018; in the French Alps: GRAHAM ET AL. 2012; in the High Atlas: MARTÍN-MARTÍN ET AL. 2017, MORAGAS ET AL. 2018, SAURA ET AL. 2014; in the Pyrenees: LÓPEZ-MIR ET AL. 2015; in the Zagros: CALLOT ET AL. 2007, FERNANDEZ & KAUS 2014, HASSANPOUR ET AL. 2018; in Central Anatolia: KERGARAVAT ET AL. 2017; in the Gulf of Mexico and in the Fliners Range in Australia: ROWAN & VENDEVILLE 2006; modeling: DUFFY ET AL. 2018). All of these studies concluded that the geometry of the salt-bearing fold-and-thrusts radically depends on the geometry and locality of the precursor salt diapirs and related structures: salt structures will localize the deformation and the salt rocks themselves will also remobilize during subsequent shortening, whereas the pre-orogenic normal faults will be inverted and reactivated.

In the Aggtelek Mts. the Cretaceous deformation reactivated the dominant Triassic salt structures and brittle features in the deformed sedimentary cover. Consequently, as a first the pre-existing salt diapirs and salt walls were squeezed and **secondary salt welds formed** ***(Section 1, Section 2, Section 3)***. The welding process was probably coupled with further salt-related drag folding which

either **highlighted the previous Triassic salt drag folds and flaps or created new folds** where the salt structures were previously sealed and the salt only pierced its cover when squeezed. This contraction deformation concentrated to previous halokinetic structures that resulted in the tight to isoclinal antiformal folds (e.g. Jósvafő-Perkupa Fault Zone – ***Section 1***). The geometry of these folds depends on the geometry of the pre-existing salt structures, i.e. the axes of the fold sets follow the strike of the former salt walls/anticlines.

When some of the salt rocks have already been squeezed out but the shortening still continues, the lubricated welds evolved into thrust welds (WARREN 2016), e.g. in the northern part of the Teresztenye Minibasin, along the Jósvafő-Bódvaszilas Salt Wall ***(Section 3)***, and probably along Szövetény and Kecskekút Fault Zones. As in case of the latter the minibasin filled with a thick Middle Triassic platform carbonate became the hanging wall of the thrust weld. Due to former top-to-N salt-related slip, this thrust weld got to be a young-on-older contact. Based on this, the other **young-on-older contacts** observed in the geological maps of the Aggtelek Mts. (S of Szőlősardó and in the Derenk Zone) are also the results of two deformation phases: (1) Triassic salt-controlled sedimentation basin evolution, and (2) Cretaceous thrusting connected to precursor halokinetic structures.

This continuous shortening may have re-deformed the original shape of the salt structures, i.e. the minibasins may have been compressed from one side. Furthermore, where the salt rocks got stuck beneath the surface (covered diapir) brittle thrusting may still favor their locations (probably in case of the Kecskekút Fault Zone or Szövetény Fault Zone). As the salt structures took up most of the deformation, the minibasins behaved as quasi-rigid blocks. This explains why there is **no significant internal shortening-related deformation within the minibasins**. For example W of Szinpetri the sole signs of shortening in the Szinpetri Limestone were the reversely or obliquely reactivated tilted normal faults (e.g. ***Fig.58, Fig.59***). In the Szin Marl at *Per-027* evidently even the folds were controlled by the geometry and location of the Triassic pre-tilt normal faults ***(Fig.37/a)***. In the majority of the thick Szinpetri Limestone N of the Jósvafő-Perkupa Salt Wall and in the Varbóc Syncline no important deformation (folding or thrusting) occurred, only minor gentle folds appears *(Appendix 4).*

Considerable amount of shortening affected the Lower Triassic successions only where the Perkupa Evaporite is suspected to be present in very shallow depths underneath the surface, e.g. on the Fenyves Slope ***(Fig.69)***, in the valley of the Vízvölgy Creek ***(Fig.27)*** and below the Teresztenye Minibasin ***(Fig.42)***. In all of these sections the Lower Triassic formations were folded into open to tight asymmetric folds with mostly rounded hinge zones. During folding the evaporites constituted an easily deformable detachment media, so the these asymmetric folds either formed as detachment folds or the related thrust faults probably detach in the evaporite.

In summary the pre-existing normal faults and salt structures had major role during shortening and they practically controlled the nature and geometry of the Cretaceous deformation. This is well expressed in the evolution of the two most important structural elements of the eastern part of the Aggtelek Mts: both the evolution of the Jósvafő-Bódvaszilas Fault Zone and

Jósvafő-Perkupa Fault Zone can be traced back to the Triassic deformation. The exact evolution of the latter one, however, remains unclear at certain points. It is evident that the eastern and western segments of the **Jósvafő-Perkupa Fault Zone** are now salt welds but we have no information on its middle part (see detailed discussion in the previous sub-chapter). Regarding its role in the Cretaceous deformation, one option is that the segments still have not merge completely and only the individual segments were reactivated (in the middle segment of the zone there is no clear displacement in the Szinpetri Limestone). On the other hand, it is possible that two segments did indeed merge either already during the Triassic as a continuous salt wall or later, during shortening.

JAHANI ET AL. (2017) and HASSANPOUR ET AL. (2018) showed that if the salt diapirs appear in a row and the shortening direction is sub-parallel with or oblique to their line, a **tear-fault system** could evolve through the diapirs ***(Fig.88)***. This could be the case with the Jósvafő-Perkupa Fault Zone as well. As a rule, all other E-W striking weld and fault zone could form part of this tear-fault system while between the tear faults, Cretaceous thrusts and folds may evolved at right angles to the shortening direction.

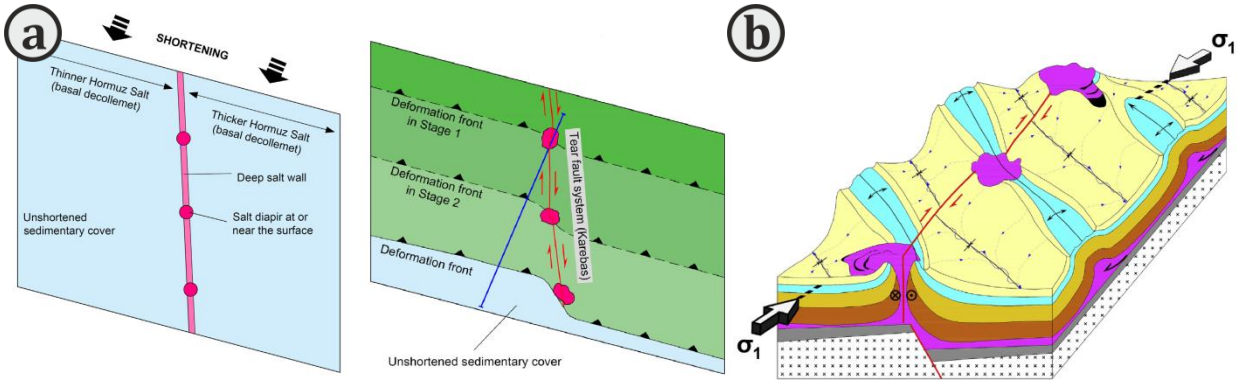

Fig.88. Pre-existing salt diapirs reactivated by tear-faulting. **A.)** Map view of the diapirs located in a row and their reactivation by tear-faulting due to oblique shortening (HASSANPOUR ET AL. 2018). **B.)** Block diagram of the diapirs, the tear-fault and the associated thrust faults and folds (JAHANI ET AL. 2017).

In agreement with the tear-fault model, the Cretaceous deformation was **transpressional** as the measured striations were dominantly oblique thrust faults and strike-slip faults. Results of the fold axis estimations and fault-slip analysis suggest that two shortening-related phases may exist: one with a WNW-ESE or NW-SE directed σ_1 and another with NNW-SSE or N-S σ_1. However, their direction overlap so they cannot be unequivocally separated into two individual phases *($D_{2a\text{-}b}$ phases, **Fig.89**)*. Moreover, the rotation of the shortening direction may be due to temporal or spatial stress field variations. Even so, their relative chronological order is very uncertain, there were only one outcrop where the overprinting chronology of the different striae generations was estimated *(Szn-016)*: there the NW-SE oriented shortening was older than the N-S directed. Furthermore, the Jósvafő-Bódvaszilas Fault Zone is displaced at three places by NNW-SSE striking dextral strike-slip fault which also suggest that the NW-SE oriented shortening preceded the N-S shortening. The inferred vergency of the clearly shortening-related structures is S-SE. Local opposite vergency may be due to structural inheritance (e.g. northern segment of the Teresztenye Plateau).

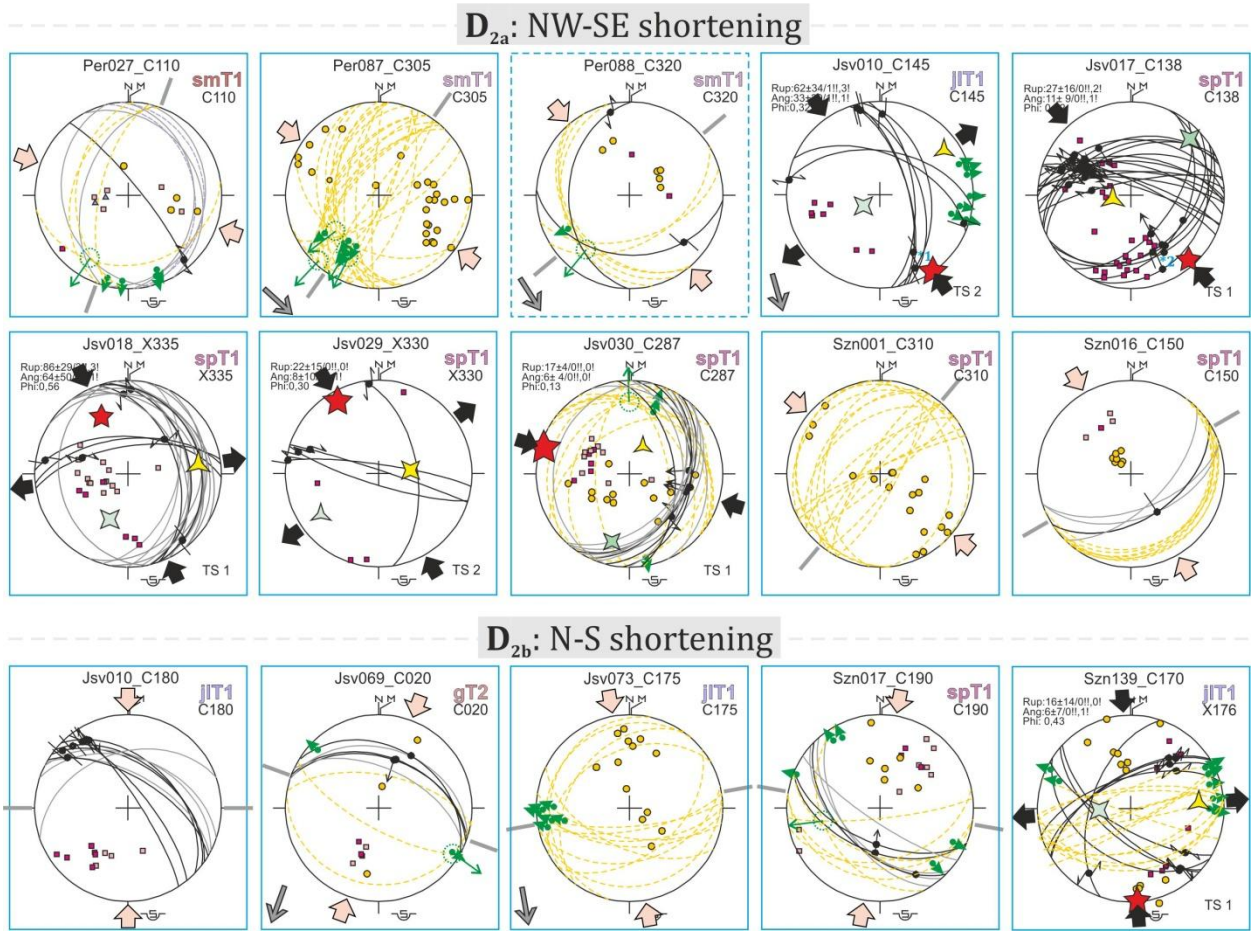

Fig.89. Stereoplot examples for the Cretaceous shortening-related structures. D2a and D2b may be two separate phases but they could not be separated completely. The vergeny is S-SE.

$D_{3\text{-}5}$: Younger post-tilt deformational phases

As the result of fault-slip analysis three further fault groups could be separated. These faults clearly formed only after the main tilting events *(Appendix 3)*. Unfortunately only a few structural elements were observed and measured from these last three groups so their profound understanding was not possible.

The oldest deformation phase (D_3 phase) of these post-tilt phases is probably the ~E-W compression and ~N-S extension during which ENE-WSW striking dextral and WNW-ESE striking sinistral strike-slip faults were active. PETRIK ET AL. (2016) observed similar stress field in the middle Eggenburgian to early Ottnangian formations near the southern part of the Darnó Deformation Zone. The relative chronological order of the other two extensional deformation phases was determined according to the already established phases of the extensional evolution of the Pannonian Basin (FODOR 2010, PETRIK ET AL. 2016) but in theory the NW-SE striking normal faults in the D_4 phase could have also formed contemporaneously with the main Cretaceous tilting (NW-SE compression and perpendicular extension) or it could be a late event in the D_2 phase.

VI. CONCLUSIONS

The aim of my thesis work was to study the effects of salt deformation in the Silica Nappe, Aggtelek Mts. in order to understand the kinematics and structural geometry of the major map-scale structures and to estimate the timing of salt movements. The following methods were applied:

1. Detailed structural mapping in the eastern part of the Aggtelek Mts., between Perkupa, Szin, Szinpetri, Jósvafő and Tornakápolna villages. The observations were summarized in nineteen detailed observation maps.
2. Field data were evaluated by fold axis estimations and fault-slip analysis.
3. Cross-section construction through the most important structural elements.
4. A new geological map focusing on the pre-Cenozoic formations was constructed from existing data and new observations.

According to the results significant salt deformation occurred during the Triassic. The following conclusions were drawn regarding the Triassic salt deformation:

1. Not only simple diapirs but complex salt walls formed as well.
2. Slump folds, syn-sedimentary and pre-tilt normal faulting, and extreme thickness changes observed within the Lower Triassic sequences prove that the salt tectonics must have initiated as soon as in the Early Triassic. The onset of intensive salt movement can probably be dated to the Spathian (Olenekian).
3. The Early Middle Triassic sedimentation occurred in minibasins, the evolution of which was controlled by the continuously growing salt structures (e.g. Varbóc and Teresztenye Minibasins, Middle Triassic platform carbonates NW of the Jósvafő-Bódvaszilas Fault Zone).
4. Salt movements were coupled with doming and drag folding along the salt structures which resulted in significant map-scale folding. The exact extent of this tilting cannot always be determined but locally, directly next to the salt bodies even sub-vertical dips may have been reached. This means that most folds observed presently in the Silica Nappe are not related to the Cretaceous deformation but were formed much earlier in the Triassic.

The kinematics and geometry of the subsequent Cretaceous deformation was strongly influenced by the pre-existing salt structures and normal faults.

1. Firstly, secondary salt welds formed by the squeezing of diapirs and salt walls, then the welds and tilted normal faults were reactivated as oblique thrust faults.
2. During the main NW-SE oriented shortening the E-W trending salt structures evolved into tear fault zones (Jósvafő-Perkupa Fault Zone).
3. Young-on-older thrust contacts evolved along the minibasin borders by the inversion of former salt-related structures (Jósvafő-Bódvaszilas Fault Zone, Teresztenye Minibasin).

4. The main tectonic transport direction was between S and SE but due to structural inheritance local deviations do occur. This is in agreement with previous concepts (GRILL 1989, GRILL ET AL. 1984, LESS 2000).

The evidences clearly demonstrate that unraveling the still debated deformation history of the problematic Silica Unit is only possible by first separating the salt-related structures from the purely shortening-related structures. This master thesis means the first steps in understanding the Triassic pre-orogenic structural geometry and its role during the Cretaceous deformation.

ABSTRACTS

Complex deformation history of the Silica Nappe, Aggtelek Mts:
Inherited Triassic salt structures and their role during Alpine deformation

The Permian to Lowermost Triassic Perkupa Evaporite form the base of the enigmatic Silica Nappe which is the uppermost tectonic unit of the Aggtelek Mts. This evaporitic sequence played the role of the main detachment level of the Silica Nape during the Cretaceous shortening. Several previous studies suggested that there may be salt diapirs rooting in this evaporitic detachment level but their role in the evolution of the Silica Nappe have not been studied in details.

Results of this master thesis revealed that not only simple salt diapirs but also map-scale salt walls are present in the Aggtelek Mts. Slump folds, syn-sedimentary and pre-tilt normal faulting, and extreme thickness changes observed within the Lower Triassic sequences indicate that these salt structures originally formed syn-sedimentary with the Early Triassic sedimentation when extensive salt deformation occurred. The onset of intensive salt movement can be probably dated to the Spathian (Olenekian). From this time the sedimentation occurred in minibasins, the evolution of which was controlled by the continuously growing salt structures. Salt movements were coupled with doming and drag folding along the salt structures which resulted in significant map-scale folding. The exact extent of this tilting is unknown but locally, directly next to the salt bodies even sub-vertical dips may have been reached. This means that not all folds observed presently in the Silica Nappe are related to the Cretaceous deformation but were formed much earlier in the Triassic.

The kinematics and geometry of the Cretaceous deformation was strongly influenced by the pre-existing salt structures and normal faults. Firstly, secondary salt welds formed by the squeezing of diapirs and salt walls, then the welds and tilted normal faults were reactivated as oblique thrust faults. During the main NW-SE oriented shortening the E-W trending salt structures evolved into tear faults zones (Jósvafő-Perkupa Fault Zone), whereas young-on-older thrust contacts evolved along the minibasin borders by the inversion of former salt structures (Jósvafő-Bódvaszilas Fault Zone). The main tectonic transport direction was to the S-SE but due to structural inheritance local deviations do occur. Consequently, the key for understanding the still debated deformation history and nappe transport direction of the Silica Nappe if to first understand the Triassic pre-orogen deformation geometry and its role in the Cretaceous shortening.

Átöröklött triász sószerkezetek és azok szerepe az aggteleki Szilicei-takaró alpi deformációja során

Az enigmatikus Szilicei-takaró az Aggteleki-hegység legfelső helyzetű takarója, amely fő lenyesési szintjét a permi—korat-triász korú Perkupa Evaporit Formáció alkotta a kréta deformáció során. Több korábbi tanulmányban is felvetették, hogy az Aggteleki-hegységben jelen lehetnek a Perkupai Evaporitban gyökerező sódiapírok is, de ezek deformációtörténeti jelentőségét mindeddig nem vizsgálták részleteiben.

Jelen diplomamunka eredményei azt mutatják, hogy nemcsak egyszerű sódiapírokról, hanem komplex szerkezetű térképi léptékű sófalakról is beszélhetünk. A megfigyelt csuszamlási redők, szin-szediment és pre-tilt normálvetők, valamint az alsó-triász képződményekben megfigyelt extrém vastagságbeli különbségek alapján ezek a sószerkezetek szin-szediment jelleggel már a kora-triász során is működtek. Az intenzív sómozgás legkorábbi időpontja az olenyoki emeletre tehető. Ettől kezdve az üledékképződés sómedencékben *(minibasin)* folyt, amelyek fejlődését a folyamatosan növekvő sószerkezetek geometriája határozta meg. A sómozgás együtt járt a rétegek felboltozódásával és elvonszolódásával a sószerkezetek mentén, ami térképi léptékű redőződéshez is vezetett. A triász redőződés pontos mértéke kérdéses, de a sószerkezetek közvetlen környezetében akár a függőleges vagy átbuktatott helyzetig is billentődhettek a rétegek. Ez azt jelenti, hogy a Szilicei-takaróban nem minden redő a kréta deformációhoz kapcsolódik – sőt talán a legtöbb nem –, hanem sokkal idősebbek annál.

A már eleve jelenlévő sószerkezetek és normálvetők erősen befolyásolták a kréta deformáció jellegét és geometriáját. A só kipréselődésével első lépésben másodlagos sókicsípődési felületek (weld) képződtek, amelyek aztán ferde rátolódásokként reaktiválódtak. A fő ÉNy-DK-i rövidülés során a közel K-Ny-i csapású sószerkezetek kényszervetőkké *(tear fault)* alakultak (Jósvafő-Perkupa Vetőzóna), míg a sómedencék határainak reaktivációjával fiatal idősön *(young-on-older)* típusú rátolódások jöttek létre (Jósvafő-Bódvaszilas Vetőzóna). A rövidüléses eredetű szerkezeti elemek vergenciája elsősorban D-DK-I, de az átöröklött szerkezeti elemek következtében lokális eltérések több helyen is adódnak a vergenciát és a rövidülés irányát illetően.

Összességében az eredmények jól mutatják, hogy a Szilicei-takaró máig vitatott szerkezetfejlődésének és takarószállítási irányának megértéséhez mindenképpen a triász pre-orogén szerkezeti geometria megértésén keresztül vezet az út.

ACKNOWLEDGEMENTS

I would like to say “Thank You” for my supervisors, **Gábor Héja** and **László Fodor** for their numerous ideas, guidance but mainly for giving me enough credit in advance. I would also like to express my sincerest gratitude for my mother **Éva Oraveczné** and my not-so-little brother **József Oravecz** who have spent many exhausting field days with me in both very hot and very cold weather. I am also grateful for the consultations I had with **Szilvia Kövér** and **Kinga Hips** who know my study area very well, and for **Ádám Csicsek** who shared his extensive publication list on salt tectonics with me.

This research was supported by the **ÚNKP-2018-2 New National Excellence Program** of the Hungarian Ministry of Human Capacities and by the research found **NKFIH OTKA 113013**. The field work was partly supported by the **SzalMOLgozat Program** of the MOL Hungary. My thesis work is related to the regional tectonic research project of the **MTA-ELTE Geological, Geophysical and Space Sciences Research Group**.

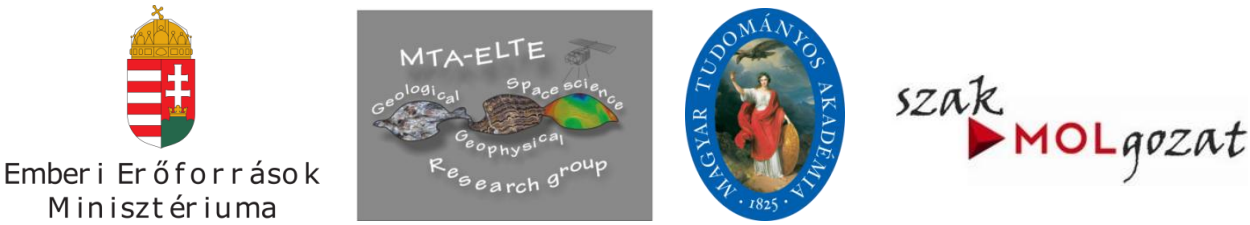

REFERENCES

Alsop, G.I., Brown, J.P., Davison, I., Gibling, M.R., 2000: The geometry of drag zones adjacent to salt diapirs — *Journal of the Geological Society* 157, 1019-1029.

Alsop, G.I., Holdsworth, R.E., 2002: The geometry and kinematics of flow perturbation folds —*Tectonophysics* 350, 99-125.

Alsop, G.I., Marco, S., 2011: Soft-sediment deformation within seismogenic slumps of the Dead Sea Basin — *Journal of Structural Geology* 33, 433-457.

Alsop, G.I., Weinberger, R., Marco, S., Levi, T., 2018: Fault and fracture patterns around a strike-slip influenced salt wall — *Journal of Structural Geology* 106, 103-124.

Andrusov, D., 1956: Stand der Durchforschung des Slowakischen Mesozoikums — *Geologicky Sbornik* 7/1-2, 68-73 (in German).

Angelier, J., 1984: Tectonic analysis of fault slip data sets — *Journal of Geophysical Research* 89/B7, 5835-5848.

Árkai, P., Faryad, S.W., Vidal, O., Balogh, K., 2003: Very low-grade metamorphism of sedimentary rocks of the Meliata unit, Western Carpathians, Slovakia: implications of phyllosilicate characteristics — *International Journal of Earth Sciences* 92/1, 68-85.

Árkai, P., Kovács, S., 1986: Diagenesis and regional metamorphism of the Mesozoic of Aggtelek-Rudabánya Mountains (Northeast Hungary) — *Acta Geologica Hungarica* 29/3-4, 349-373.

Árva-Sós, E., Balogh, K., Ravasz-Baranyai, L., Ravasz, Cs., 1987: K-Ar dates of Mesozoic igneous rocks in some areas of Hungary — Annual Report of the Hungarian Geological Institute of 1985, Budapest, pp. 295-307.

Balla, Z., 1988: The origin of the structural pattern of Hungary — *Bulletin of the Hungarian Geological Society* 118, 195-206 (in Hungarian with English abstract).

Billings, M.P., 1954: Structural geology — Prentice-Hall, New York, pp. 514.

Bodego, A., Iriarte, E., López-Horgue, M.A., Álvarez, I., 2018: Rift-margin extensional forced folds and salt tectonics in the eastern Basque-Cantabrian rift basin (western Pyrenees) — *Marine and Petroleum Geology* 91, 667-682.

Bonini, M., Sani, F., Antonielli, B., 2012: Basin inversion and contractional reactivation of inherited normal faults: a review based on previous and new experimental models — *Tectonophysics* 522–523, 55–88.

Branney, M.J., Kokelaar, P., 1994: Volcanotectonic faulting, soft-state deformation, and rheomorphism of tuffs during development of a piecemeal caldera, English Lake District — *Geological Society of America Bulletin* 106, 507-530.

Brun, J-P., Fort, X., 2011: Salt tectonics at passive margins: Geology versus models — *Marine and Petroleum* Geology 28, 1123-1145.

Burg, J-P., Kaus, B.J.P., Podladchikov, Y.Y., 2004: Dome structures in collision orogens: Mechanical investigation of the gravity/compression interplay — *Geological Society of America Special Paper* 380, 47-68.

Bray, C.J., Karig, D.E., 1985: Porosity of sediments in accretionary prisms and some implications for dewatering processes — *Journal of Geophysical Research: Solid Earth* 90/B1, 768-778.

Butler, R.W.H., 1982: The terminology of structures in thrust belts — *Journal of Structural Geology* 4/3, 239-245.

Byrne, T., 1994: Sediment deformation, dewatering and diagenesis: illustrations from selected mélange zones — In: *Maltman, A. (eds.):* The Geological Deformation of Sediments – Springer, Dordecht, pp. 239-260.

Callot, J.P., Jahani, S., Letouzey, J., 2007: The Role of Pre-Existing Diapirs in Fold and Thrust Belt Development — In: *Lacombe, O., Roure, F., Lavé, J., Vergés, J. (eds.):* Thrust Belts and Foreland Basins – Springer, Berlin, Heidelberg, pp. 309-325.

Callot, J-P., Salel, J-F., Letouzey, J., Daniel, J-M., Ringenbach, J-C., 2016: Tree-dimensional evolution of salt-controlled minibasins: Interactions, folding, and megaflap development — *AAPG Bulletin* 100/9, 1419-1442.

Canérot, J., Hudec, M.R., Rockenbauch, K., 2005: Mesozoic diapirism in the Pyrenean orogen: Slat tectonics on a transform plate boundary — *AAPG Bulletin* 89/2, 211-229.

Chimney, P., Kluth, C., 2002: Evidence for low-angle, subhorizontal hanging faults in rotated fault blocks, Cabinda, offshore Angola — *The Leading Edge* 21/11, 1084-1090.

Cooper, M.A., Trayner, P.M., 1986: Thrust-surface geometry: implications for thrust-belt evolution and section-balancing techniques — *Journal of Structural Geology* 8/3-4, 305-312.

Cosgrove, J.W., 2001: Hyraulic fracturing during the formation and deformation of a basin: A factor in the dewatering of low-permeability sediments — *AAPG Bulletin* 85/4, 737-748.

Cosgrove, J.W., Ameen, M.S., 2000a: Forced folds and fractures: An introduction — *Geological Society, Special Publications* 169, 1-7.

Cosgrove, J.W., Ameen, M.S., 2000b: A comparison of the geometry, spatial organization and fracture patterns associated with forced folds and buckle folds — *Geological Society, Special Publications* 169, 7-21.

Csontos, L., Nagymarosy, A., Horváth, F., Kovács, M., 1992: Tertiary evolution of the Intra-Carpathian area: a model – *Tectonophysics* 208, 221-241.

Csontos, L., Vörös, A., 2004: Mesozoic plate tectonic reconstruction of the Carpathian region — *Paleogography, Paleoclimatology, Paleoecology* 210, 1-56.

Dallmeyer, R.D., Neubauer, F., Fritz, H., 2008: The Meliata sututre in the Carpathians: regional significance and implications for the evolution of high-pressure wedges within collisional orogens — *The Geological Society of London, Special Publications* 298/1, 101-115.

Davis, G.A., Lister, G.S., 1988: Detachment faulting in continental extension; Perspectives from the Southwestern U.S. Cordillera — *Geological Society of America, Special Paper* 218.

Deák-Kövér Sz., 2012: Structure, metamorphism, geochronology and deformation history of Mesozoic formations in the central Rudabánya Hills — PhD dissertation, Eötvös Loránd University, Budapest.

Dixon, J.M., 1987: Mantled gneiss domes — In: *Sexfert, C.K. (eds.):* The encyclopedia of structural geology and plate tectonics – Van Nostrand Reinhold Company, Inc., New York, pp. 398-412.

Donath, F.A., Parker, R.B., 1964: Folds and Folding — *Geological Society of America Bulletin* 75, 45-62.

Dooley, T.P., Jackson, M.P-A., Hudec, M.R., 2006: Inflation and deflation of deeply buried salt stocks during lateral shortening — *Journal of Structural Geology* 31, 582-600.

Dosztály, L., Józsa, S., 1992: Geochronological evaluation of Mesozoic formations of Darnó Hill and Recsk on the basis of radiolarias and K-Ar data — *Acta Geologica Hungarica* 35, 371-394.

Duffy, O.B., Dooley, T.P., Hudec, M.R., Jackson, M.P.A., Fernandez, N., Jackson, C.A-L., Soto, J.I., 2018: Structural evolution of salt-influenced fold-and-thrust belts: A synthesis and new insights from basins containing isolated salt diapirs — *Journal of Structural Geology* 114, 206-221.

Ecosa, F.O., Roca, E., Ferrer, O., 2018: Testing thin-skinned inversion of a prerift salt-bearing passive margin (Eastern Prebetic Zone, SE Iberia) — *Journal of Structural Geology* 109, 55-73.

Elliott, D., 1977: Some aspects of the geometry and mechanics of thrust belts — Canadian Society of Petroleum Geology, 8th Annual Seminar Publication Notes, Continuing Education Department, University of Calgary.

Farrel, S.G.,Eaton, S., 1987: Foliations developed during slump deformation of Miocene marine sediments, Cyprus — *Journal of Structural Geology* 10, 567-576.

Farrel, S.G., Eaton, S., 1988: Foliations developed during slump deformation of Miocene marine sediments, Cyprus — *Journal of Structural Geology* 10, 567-576.

Faryad, S.W., Henjes-Kunst, F., 1997: Petrological and K-Ar and 40Ar-39Ar age constraints for the tectonothermal evolution of the high-pressure Meliata unit, Western Carpathians (Slovakia) — *Tectonophysics* 280, 141-156.

Fernandez, N., Kaus, B.J.P., 2014: Influence of pre-existing salt diapirs on 3D folding patterns — *Tectonophysics* 637, 354-369.

Finger, F., Broska, I., Haunschmid, B., Hrasko, L., Kohút, M., Krenn, E., Petrík, I., Riegler, G., Uher, P., 2003: Electron-microbprobe dating of monazites from Western Carpathian basement granitoids: plutonic evidence for an important Permian rifting event subsequent to Variscan crustal anatexis — *International Journal of Earth Sciences* 92, 86-98.

Fodor, L., 2010: Mesozoic-Cenozoic stress-fields and fracture systems in the north-western part of the Pannonian Basin – methodology and structural interpretation — Academical Doctorate Dissertation, Hungarian Academy of Sciences (in Hungarian).

Fodor, L., Radócz, Gy., Sztanó, O., Koroknai, B., Csontos, L., Harangi, Sz., 2005: Post-Conference Excursion: Tectonics, Sedimentation and Magmatism along the Darnó Zone — *Geolines* 19, 141-161.

Frotzheim, N., Plašienka, D., Schuster, R., 2008: Alpine tectonics of the Alps and Western Carpathians — *In: McCann, T. (eds):* The Geology of Central Europe, Volume 2: Mesozoic and Cenozois – The Geological Society, London.

Gawlick, H-J., Frisch, W., Vecsei, A., Steiger, T., Böhm, F., 1999: The change from rifting to thrusting in the Northern Calcareous Alps as recorded in Jurassic sediments — *Geologische Rundschau* 87, 644-657.

Gawlick, H-J., Goričan, Š., Missoni, S., Lein, R., 2012 : Late Anisian platform drowning and radiolarite deposition as a consequence of the opening of the Neotethys ocean (High Karst nappe, Montenegro) — *Bulletin de la Société géologique de France* 183/4, 349-358.

Gawlick, H-J., Missoni, S., 2015: Middle Triassic radiolarite pebbles in the Middle Jurassic Hallstatt Mélange of the Eastern Alps: Implications for Triassic-Jurassic geodynamic and paleogeographic reconstructions of the western Tethyan realm — *Facies* 65, 3, 13.

Giles, K.A., Lawton, T.F., 2002: Halokinetic sequence stratigraphy adjacent to the El Papalote diapir, northeastern Mexico — *AAPG Bulletin* 86/5, 823-840.

Goldman, M.I., 1925: Petrography of Salt Dome Cap Rock — *AAPG Bulletin* 9/1, 42-78.

Graham, R., Jackson, M., Pilcher, R., Kilsdonk, B., 2012: Allochtonous salt in the sub-Alpine fold-thrust belt of Haute Provence, France — In: *Alsop, G.I., Archer, S.G., Hartley, A.J., Grant, N.T., Hodkinson, R. (eds.):* Salt Tectonics, Sediments and Prospectivity – Geological Society of London, Special Publications 363, pp. 595-615.

Granado, P., Roca, E., Strauss, P., Pelz, K., Munoz, J.A., 2018: Structural styles in fold-and-thrust belts involving early salt structures: The Northern Calcareous Alps (Austria) — *Geology* 47/1, 51-54.

Grill J., 1989: Structural evolution of the Aggtelek-Rudabánya Mountains, NE Hungary — Annual Report of the Hungarian Geological Institute of 1986, 69-103 (in Hungarian with English abstract).

Grill, J., Kovács, S., Less, Gy., Réti, Zs., Róth, L., Szentpétery, I., 1984: Geological constitution and history of evolution of the Aggtelek-Rudabánya Range — *Geological Research* 27/4, 49-56 (in Hungarian with English abstract).

Grill, J., Szentpétery, I., 1988: Prospecting for gypsum-anhydrite deposits in the Aggtelek Karst and the Rudabánya Mountains, N Hungary — Annual Report of the Hungarian Geological Institute of 1986, pp. 441-450 (in Hungarian with English abstract).

Gyenge, Cs., 2017: Petrographical analysis of nappe base breccias from the Aggtelek-Rudabánya Mts. — MSc Thesis, Eötvös Loránd University, Budapest (in Hungarian).

Haas, J., Budai, T., Csontos, L., Fodor, L., Konrád, Gy., Koroknai, B., 2014: Geology of the pre-Cenozoic basement of Hungary: Explanatory notes for „Pre-Cenozoic geological map of Hungary" (1:500 000) — Geological and Geophysical Institute of Hungary, Budapest, 31-40.

Haas, J., Kovács, S., Krystyn, L., Lein, R., 1995: Significance of Late Permian-Triassic facies zones in terrane reconstruction in the Alpine-North Pannonian domain — *Tectonophysics* 242, 19-40.

Haas, J., Mioč, P., Pamič, J., Tomljenovič, B., Árkai, P., Bérczi-Makk, A., Koroknai, B., Kovács, S., Rálisch-Felgenhauer, E., 2000: Complex structural pattern of the Alpine-Dinaridic-Pannonian triple junction — *International Journal of Earth Sciences* 89, 377-389.

Hansen, E., 1971: Strain Facies — Springer-Verlag, Berlin, pp. 207.

Hassanpour, J., Jahani, S., Ghassemi, M.R., Alavi, S.A., Zeinali, F., 2018 : Evolution of the Karebas Fault System and adjacent folds, central Zagros fold-and-thrust belt, Iran : Role of pre-existing halokinesis (salt strcutures and minibasins) and detachment levels — *Journal of Asian Earth Sciences* 164, 125-142.

Hearon, T.E., Rowan, M.G., Giles, K.A., Hart, W.H., 2014: Halokinetic deformation adjacent to the deep-water Auger diapir, Garden Banks 470, northern Gulf of Mexico: Testing the applicability of an outcrop-based model using subsurface data — *Interpretation* 2, SM57-SM76.

Héja, G., 2019: Mesozoic deformations of the southwestern Transdanubian Range: the role of Triassic-Jurassic inherited normal faults in the development of Cretaceous folding and thrusting — PhD dissertation, Eötvös Loránd University of Sciences, Budapest.

Héja, G., Kövér, Sz., Csillag, G., Németh, A., Fodor, L., 2018: Evidences for pre-orogenic passive-margin extension in a Cretaceous fold-and-thrust belt on the basis of combined seismic and field data (western Transdanubian Range, Hungary) — *International Journal of Earth Sciences* 107/8, 2955-2973.

Hips, K., 1995: Sedimentology and stratigraphy of the Lower Triassic formations in the Aggtelek-Rudabánya Mts. — PhD Thesis, MTA Geological Research Group, Eötvös Loránd University, Budapest.

Hips, K., 1996a: Stratigraphical and facies evaluation of the Lower Triassic formations in the Aggtelek–Rudabánya Mountains, Northeastern Hungary — *Acta Geologica Hungarica* 39/4, 369–411.

Hips, K., 1996b: The biostratigraphic significance of the Cyclogyra–Rectocornuspira association (Foraminifera, Lower Triassic): Data from the Aggtelek Mountains (Northeastern Hungary) — *Neues Jahrbuch für Geologie und Paläontologie Monatshefte* 7, 439–451.

Hips, K., 1998: Lower Triassic storm-dominated ramp sequence in northern Hungary: an example of evolution from homoclinal trough distally steepened ramp to Middle Triassic flat-topped platform — In: *Wright, V.P., Burchette, T.P. (eds.):* Carbonate Ramps – *Geological Society of London, Special Publications* 149, pp. 315-338.

Hips K., 2001: The structural setting of Lower Triassic formations in the Aggtelek-Rudabánya Mountains (Northeastern Hungary) as revealed by geological mapping — *Geologica Carpathica* 52/5, 287-299.

Hók, J., Kováč, P., Rakús, M., 1995: Structural investigations of the inner Carpathians – Results and interpretation — *Mineralia Slovaca* 27/4, 231-235.

Horváth, F., 1993: Towards a mechanical model for the formation of the Pannonian basin — *Tectonophysics* 225, 333-358.

Horváth, B., Fodor, L., Kövér, Sz., 2012: Complex structural evolution and thrust systems in the Henc Valley near Szőlősardó (Aggtelek-Rudabánya Hills) — *Bulletin of the Hungarian Geological Society* 142/4, 321-338 (in Hungarian with English abstract).

Horváth, P., 1997: High-pressure metamorphism and p-T path of the metabasic rock sin the borehole Komjáti-11, Bódva Valley area, NE Hungary — *Acta Mineralogica-Petrographica* XXXVIII, 151-163.

Horváth, P., Árkai, P., 1998: Comparison of the Alpine metamorhic evolution of the Bódva Valley, Darnó Hill and Szarvaskő Ophiolite Complexes in NE Hungary — Abstract Volume, Carpathian-Balkan Geological Association, XVI. Congress, Vienna, pp. 45.

Hudec, M.R., Jackson, J-A., 2006: Advance of allochthonous salt sheets in passive margins and orogens — *AAPG Bulletin* 90, 1535-1564.

Hudec, M.R., Jackson, J-A., 2007: Terra infirma: understanding salt tectonics — *Earth-Science Reviews* 82, 1-28.

Hudec, M.R., Jackson, M.P.A., Schultz-Ela, D.D., 2009: The paradox of minibasin subsidence into salt: Clues to the evolution of crustal basins — *GSA Bulletin* 121/1-2, 201-221.

Ilavská, Z., 1965: Kotázke veku meliatskej série — *Spr. Geol. Výsk.,*31-32 (in Slovakian).

Jackson, C.A-L., Rodriguez, C.R., Rotevatn, A., Bell, R.E., 2014: Geological and geophysical expression of a primary salt weld: An example from the Santos Basin, Brazil — *Interpretation* 2/4, 77-89.

Jackson, M.P-A., Cramez, C., 1989: Seismic recognition of salt welds in salt tectonic regimes — Conference presentation at GCSSEPM Foundation, 10th Annual Bob F. Perkins Research Conference, pp. 66-71.

Jackson, M.P-A., Vendeville, B.C., 1994: Regional extension as a trigger for diapirism — *Geological Society of America Bulletin* 106, 57-73.

Jackson, M.P-A., Talbot, C.J., 1994: A glossary of salt tectonics — *Geological Circular* 91/4, 44.

Jahani, S., Hassanpour, J., Mohammadi-Firouz, S., Letouzey, J., de Lamotte, D.F., Alavi, S.A., Soleimany, B., 2017: Salt tectonics and tear faulting in the central part of the Zagros Fold-Thrust Belt, Iran — *Marine and Petroleum Geology* 86, 426-446.

Jammes, S., Manatschal, G., Lavier, L., 2010: Interaction between prerift salt and detachment faulting in hyperextended rift systems: the example of the Parentis and Mauléon basins (Bay of Biscay and western Pyrenees) — *AAPG Bulletin* 94, 957-975.

Jaskó, S., 1935: Geological observations in the upper part of the Jósva Valley — *Bulletin of the Hungarian Geological Society* 65, 291-300 (in Hungarian with German abstract).

Jeřábek, P., Lexa, O., Schulmann, K., Plašienka, D., 2012: Inverse ductile thinning via lower crustal flow and fold-induced doming in the West Carpathian Eo-Alpine collisional wedge — *Tectonics* 31/5, 5002-5028.

Johnson, K.M., Joshnson, A.M., 2001: Mechanical analysis of the geometry of forced-folds — *Journal of Structural Geology* 24, 401-410.

Jones, O.T., 1939: The geology of the Clowyn Bay district: study of submarine slumping during the Salopian period — *Quarterly Journal of Geological Society* 95, 335-382.

Kázmér, M., Kovács, S., 1985: Permian-Paleogene paleogeography along the eastern part of the Insubric-Periadriatic lineament system: Evidence for continental escape of the Bakony-Drauzug unit — *Acta Geologica Hungarica* 28, 71-84.

Kergaravat, C., Ribes, C., Callot, J-P., Ringenbach, J-C., 2017: Tectono-stratigraphic evolution of salt-controlled minibasins in a fold and thrust belt, the Oligo-Miocene central Silvas Basin — *Journal of Structural Geology* 102, 75-97.

Korikovsky, S.P., Putiš, M., Plašienka, D., 1997: Cretaceous low-grade metamorphism of the Veporic and North-Gemeric Zones: a result of collisional tectonics in the central Western Carpathians — In: *Grecula, P., Hovorka, D., Putiš, M., (eds.):* Geological evolution of the Western Carpathians – -Mineralia Slovaca, Monograph, Bratislava, pp. 107-130.

Kovács, S., 1984: North Hungarian Triassic facies types: a review — *Acta Geologica Hungarica* 27/3-4, 251-264.

Kovács S., 1989: Geology of North Hungary, Paleozoic and Mesozoic terraines —XXIst European Micropalaeontological Colloquium, Guidebook, Hungarian Geological Society, Hungary, Budapest, 1989, pp. 15–37.

Kovács, S., Less, Gy., Piros, O., Réti, Zs., Róth, L., 1989: Triassic formations of the Aggtelek-Rudabánya Mountains (Northeastern Hungary) — *Acta Geologica Hungarica* 32, 1-2, 31-63.

Kövér, Sz., Fodor, L., Judik, K., Németh, T., Balogh, K., Kovács, S., 2009: Deformation history and nappe stacking in Rudabánya Hills (Inner Western Carpathians) unravelled by structural geological, metamorphic petrological and geochronological studies of Jurassic sediments — *Geodinamica Acta* 22/1-3, 3-29.

Kövér, Sz., Fodor, L., Kovács, Z., Klötzli, U., Haas, J., Zajzon, N., Szabó, Cs., 2018a: Late Triassic aciditic volcanic clasts in different Neotethyan sedimentary mélanges: paleogeographic and geodynamic implications — *International Journal of Earth Sciences* 107, 2975-2998.

Kövér, Sz., Pomella, H., Fodor, L., Győri, O., 2018b: Magnetic fabric of basal carbonatic cataclasite: First attempts to reveal direction of thin-skinned nappe-stacking by AMS analysis —Environmental, Structural and Stratigraphical Evolution of the Western Carpathians, Abstract Volume, pp. 48.

Kozur, H., 1991: The evolution of the Meliata-Hallstatt Ocean and its significance for the early evolution of the Eastern Alps and Western Carpathians — *Paleogeography, Paleoclimatology,* Paleoecology 87, 109-135.

Kozur, H., Mock, R., 1973/a: Die Bedeutung der Trias-Conodonten fiir die Stratigraphie und Tektonik der Trias in den Westkarpaten — *Geologisch Paläontologische Mitteilungen Innsbruck* 3/2, l-14 (in German).

Kozur, H., Mock, R., 1973/b: Zum Alter und zur tektonischen Stellung der Meliata-Serie des Slowakischen Karstes — *Geologica Carpathica* 24/2, 365-374 (in German).

Králiková, S., Vojtko, R., Andriessen, P., Kováč, M., Fügenschuh, B., Hók, J., Minár, J., 2014: Late Cretaceous-Cenozoic thermal evolution of the northern part of the Central Western Carpathians (Slovakia): revealed by zircon and apatite fission track thermochronology — *Tectonophysics* 615-616, 142-153.

Krauter, E., 1971: Zur Gense rauhwackiger Breccien der alpinen Trias. Beispielen us der Schweiz und Österreich – *Geologische und Paleontologische Mitterlungen des Universität Innsbruck* 1, 1-112 (in German).

Kyle, J.R., Posey, H.H., 1991: Halokinesis, Cap Rock Development and Salt Dome Mineral Resources — In: *Melvin, J.L. (eds.):* Evaporites, Petroleum and Mineral Resources – *Developments in Sedimentology* 50, pp. 413-474.

Lehner, P., 1969: Salt tectonics and Pleistocene stratigraphy on continental slope of northern Gulf of Mexico — *AAPG Bulletin* 53/12, 2431-2479.

Leitner, C., Spötl, C., 2017: Multistage Development of Extremely Deformed Evaporites — In: *Soto, J.I., Flinch, J., Tari, G. (eds):* Permo-Triassic Salt Provinces of Europe, North Africa and the Atlantic Margins: Tectonics and Hydrocarbon Potential – Elsevir Publication.

Less, Gy., 2000: Polyphase evolution of the structure of the Aggtelek-Rudabánya Mountains (NE Hungary), the southernmost element of the Inner Western Carpathians – a review — *Slovak Geiological Magazine* 6, 2-3, 260-268.

Less, Gy., Grill, J., Szentpétery, I., Róth, L., Gyuricza Gy., 1988: Geological map of the Aggtelek-Rudabánya Mts. (1:25 000) — Hungarian Geological Institute, Budapest.

Less, Gy., Kovács, S., Szentpétery, I., Grill, J., Róth, L., Gyuricza, Gy., Sásdi, L., Piros, O., Réti, Zs., Elsholz, L., Árkai, P., Nagy, E., Borka, Zs., Harnos, J., Zelenka, T., 2006: Geology of the Aggtelek-Rudabánya Mts. –

Explainatory book for the geological map of the Aggtelek-Rudabánya Mts. — Hungarian Geological Institute, Budapest.

Lewis, K.B., 1971: Slumping on a continental slope inclined at 1°-4°— *Sedimentology* 16, 97-110.

Lewis, S., Holness, M., 1996: Equilibrium halite-H2O dihedral angles: High rock-salt permeability in the shallow crust? — *Geology* 24/5, 431-434.

Lexa, O., Schulmann, K., Jezek, J., 2003: Cretaceous collision and indentation in the West Carpathians: View based on structural analysis and numerical modeling — *Tectonics* 22/6, 1066-1071.

López-Mir, B., Munoz, J.A., García-Senz J., 2015: Extensional salt tectonics in the partially inverted Cotiella post-rift basin (south-central Pyrenees): structure and evolution — *International Journal of Earth Sciences 104*, 419-434.

Maione, S.J., Pickford, S., 2001: Discovery of ring faults associated with salt withdrawal basins, Early Cretaceous age, in the East Texas Basin — *The Leading Edge* 20/8, 818-829.

Maltman, A., 1984: On the term „soft-sediment deformation" — *Journal of Structural Geology* 6/5, 589-592.

Martín-Martín, J.D., Vergés, J., Saura, E., Moragas, M., Messager, G., Baqués, V., Razin, P., Grélaud, C., Malaval, M., Joussiaume, R., 2017: Diapiric growth within an Early Jurassif rift basin: the Tazoult salt wall (central Hight Atlas, Morocco) — *Tectonics* 32, 2-32.

Marton, L.Gy., Tari, G., Lehmann, C.T., 2000: Evolution of the Angolan Passive Margin, West Africa, with Emphasis on Post-Salt Structural Styles — In: *Mohriak, W., Taiwani, M. (eds):* Atlantic Rifts and Continental Margins – American Geophysical Union, Geophysical Monograph Series 115, pp. 129-149.

Mello, J., Elečko, M., Pristaš, J., Reichwalder, P., Snopko, L., Vass, D., Vozárová, A., 1996: Geologická mapa Slovenského Krasu, 1:25 000 — Geologická služba Slovenskey republiky, Bratislava.

Mello, J., Gaál, L., Mock, R., Planderová, E., 1983: Nové stratigrafické poznatky a meliatskej skupine — *Geologické Práce* 79, ppp. 55-81 (in Slovakian).

Miller, J.F., Mitra, S., 2011: Deformation and secondary faulting associated with basement-involved compressional and extensional structures — *AAPG Bulletin* 95, 4, 675-689.

Miller, C., Thöni, M., 1997: Eo-alpine eclogitisation of Permian MORB-type gabbros in the Koralpe (Eastern Alps, Austria): new geochronological, geochemical and petrological data — *Chemical Geology* 137/3-4, 283-310.

Milovsky, R., Plasienka, D., Sotak, J., 1999: Rauhwackes - A key to understanding of the superficial thrusting mechanisms: Case study from the Muran Nappe — *Geologica Carpathica* 50, 157-158.

Moragas, M., Vergés, J., Saura, E., Martín-Martín, J-D., Messager, G., Merino-Tomé, Ó., Suárez-Ruiz, I., Razin, P., Grélaud, C., Malaval, M., Joussiaume, R., Hunt, D.W., 2018: Jurassic rifting to post-rift subsidence analysis in the Central High Atlas and its relation to salt diapirism — *Basin Research* 30/1, 336-362.

Nikolinakou, M.A., Heidari, M., Hudec, M.R., Flemings, P.B., 2017: Initiation and growth of salt diapirs in tectonically stable settings: Upbuilding and megaflaps — *AAPG Bulletin* 101/6, 887-905.

Oszczypko, N., 2006: Late Jurassic-Miocene evolution of the Outer Carpathian fold-and-thrust belt and its foredeep basin (Western Carpathians, Poland) — *Geological Quarterly* 50/1, 169-194.

Ožvoldová, L., 1998: Middle Jurassic radiolarian assemblages from radiolarites of the Silica Nappe (Slovak Karst, Western Carpathians) — *Geologica Carpathica* 49/4, 289-296.

Pace, P., Di Domenica, A., Calamita, F., 2014: Summit low-angle faults in the Central Apennines of Italy: younger-on-older thrusts or rotated normal faults? Constraints for defining the tectonic style of thrust belts — *Tectonics* 33/5, 756–785.

Pavlis, T.L., 2013: Kinematic model for out-of-sequence thrusting: Motion of two ramp-flat faults and the production of upper plate duplex systems — *Journal of Structural Geology* 51, 132-143.

Peel, F.J., 2014a: The engines of gravity-driven movement in passive margins: Quantifying the relative contribution of spreading vs. gravity sliding mechanisms — *Tectonophysics* 633, 126-142.

Peel, F.J., 2014b: How do salt withdrawal minibasins form? Insights from forward modelling, and implications for hydrocarbon migration — *Tectonophysics* 630/3, 222-235.

Pérez-Gussinyé, M., Reston, T.J., 2001: Rheological evolution during extension at nonvolcanic rifted margins: Onset of serpentinization and development of detachments leading to continental breakup — *Journal of Geophysical Research* 106/B3, 3961-3975.

Péró, Cs., Velledits, F., Kovács, S., Blau, J., 2015: The Middle Triassic post-drowning sequence in the Aggtelek Hills (Silica Nappe) and its Tethyan context – first description of the Raming Formation from Hungary — *Newsletters on Stratigraphy* 48/1, 1-22.

Peron-Pinvidic, G., Manatschal, G., Osmundsen, P.T., 2013: Structural comparison of archetypal Atlantic rifted margins: A review of observations and concepts — *Marine and Petroleum Geology* 43, 21-47.

Petrik, A., Beke, B., Fodor, L., Lukács, R., 2016: Cenozoic evolution of the southwestern Bükk Mts. and the southern part of the Darnó Deformation Belt (NE Hungary) — *Geologica Carpathica* 67/1, 83-104.

Plašienka, D., 2003: Development of basement-involved fold and thrust structures exemplified by the Tatric-Fatric-Veporic nappe system of the Western Carpathians (Slovakia) — *Geodinamica Acta* 16/1, 21-38.

Plašienka, D., 2018: Continuity and Episodicity in the Early Alpine Tectonic Evolution of the Western Carpathians: How Large-Scale Processes Are Expressed by the Orogenic Architecture and Rock Record Data — *Tectonics* 37, 1-51.

Plašienka, D., Broska, I., Kissová, D., Dunkl, I., 2007: Zircon fission-track dating of granites from the Vepor-Gemer Belt (Western Carpathians): constraints for the Early Alpine exhumation history — *Journal of Geosciences* 52, 113-123.

Plašienka, D., Grecula, P., Putiš, M., Kováč, M., Hovorka, D., 1997: Evolution and structure of the Western Carpathians: an overview — Mineralia Slovaca – Monograph, Bratislava, pp. 1-24i.

Plašienka, D., Janák, M., Lupták, B., Milovský, R., Frey, M., 1999: Kinematics and Metamorphism of a Cretaceous Core Complex: the Veporic Unit of the Western Carpathians — *Physics and Chemistry of the Earth* 24/8, 651-658.

Reches, Z., Johnson, A.M., 1978: Development of monoclines: Part II. Theoretical analysis of monoclines — In: *Matthews, V. (eds.):* Laramide Folding Associated with Basement Block Faulting in the Western United States - The Geological Society of America, Boulder, Colorado, pp. 273-312.

Prestholm, E., Walderhaug, O., 2000: Synsedimentary Faulting in a Mesozoic Deltaic Sequence, Svalbard, Arctic Norway—Fault Geometries, Faulting Mechanisms, and Sealing Properties — *AAPG Bulletin* 84/4, 505-522.

Rowan, M.G., 2014: Passive-margin salt basins: hyperextension, evaporite deposition, and salt tectonics — *Basin Research* 26, 154-182.

Rowan, M.G., Giles, K.A., Hearon IV, T.E., Fiduk, J.C., 2016: Megaflaps adjacent to salt diapirs — *AAPG Bulletin* 100/11, 1723-1747.

Rowan, M.G., Lawton, T.F., Giles, K.A., Ratliff, R.A., 2003: Near-salt deformation in La Popa basin, Mexico, and the northern gulf of Mexico: A general model for passive diapirism — *AAPG Bulletin* 87/5, 733-756.

Rowan, M.G., Peel, F.J., Vendeville, B.C., Gaullier, V., 2012: Salt tectonics at passive margins: Geology versus models — *Marine and Petroleum Geology* 37, 184-194.

Rowan, M.G., Vendeville, B.C., 2006: Foldbelts with early salt withdrawal and diapirism: Physical model and examples from the northern Gulf of Mexico and the Flinders Ranger, Australia — *Marine and Petroleum Geology* 23, 871-891.

Rouby, D., Raillard, S., Guillocheau, F., Bouroullec, R., Nalpas, T., 2002: Kinematics of a growth fault/raft system on the West African margin using 3-D restoration — *Journal of Structural Geology* 24, 793-796.

Roure, F., Roca, E., Sassi, W., 1993: The Neogene evolution of the outer Carpathian flysch units (Poland, Ukraine and Romania): kinematics of a foreland/fold-and-thrust beltsystem — *Sedimentary Geology* 86/1-2, 177-201.

Royden, L.H., Horváth, F., Burchfiel, B.C., 1982: Transform faulting, extension, and subduction in the Carpathian Pannonian region — *Geological Society of America Bulletin* 93, 717-725.

Saura, E., Verges, J., Martín-Martín, J.D., Messager, G., Moragas, M., Razin, P., Grelaud, C., Joussiaume, R., Malaval, M., Homke, S., Hunt, D.W., 2014: Syn- to post-rift diapirism and minibasins of the Central High Atlas (Morocco): the changing face of a mountain belt — *Journal of Geological Society* 171, 97-105.

Schaad, W., 1995: The origin of rauhwackes (cornieules) by the karstification of gypsum — *Eclogae Geologicae Helvetiae* 88/1, 59-90.

Schlische, R.W., 1995: Geometry and Origin of Fault-Related Folds in Extensional Settings — *AAPG Bulletin* 79/11, 1661-1678.

Schmid, S.M., Bernoulli, D., Fügenschuh, B., Matenco, L., Schefer, S., Schuster, R., Tischler, M., Ustaszewski, K., 2008: The Alpine-Carpathian-Dinaridic orogenic system: correlation and evolution of tectonic units — *Swiss Journal of Geosciences* 101, 139-183.

Schmid, S.M., Fügenschuh, B., Kissling, E., Schuster, R., 2004: Tectonic map and overall architecture of the Alpine orogen — *Eclogae geologicae Helvetiae* 97, 93–117.

Schréter, Z., 1935: Geological observations around Aggtelek — Annual Report of the Hungarian Geological Institute of 1925-28, pp. 145-153 (in Hungarian with German abstract).

Schultz-Ela, D.D., 2003: Origin of drag folds bordering salt diapirs — *AAPG Bulletin* 87/5, 757-780.

Schuster, R., Scharbert, S., Abart, R., Frank, W., 2001: Permo-Triassic extension and related HT/LP metamorphism in the Austroalpine-Southalpine realm — *Mitteilungen der Gesellschaft der Geologie- und Bergbaustudenten in Österreich* 45, 111-141.

Schuster, R., Stüwe, K., 2008: Permian metamorphic event in the Alps — *Geology* 36/8, 603-606.

Sibson, R.H., 1977: Fault rocks and fault mechanisms — *Journal of the Geological Society* 133, 191-213.

de Sitter, L.U., 1956: Structural geology — McGraw-Hill, New York, pp. 552.

Smit, J., Brun, J-P., Fort, X., Cloething, S., Ben-Avraham, Z., 2008: Salt tectonics in pull-apart basins with application to the Dead Sea Basin — *Tectonophysics* 449, 1-16.

Spötl, C., 1989: The Alpine Haselgebirge Formation, Northern Calcareous Alps (Austria): Permo-Scythian evaporites in an alpine thrust system — *Sedimentary Geology* 65/1-2, 113-125.

Stearns, D.W., 1978: Faulting and forced folding in the Rocky Mountains foreland — *Geological Society of America Memoirs* 151, 1-38.

Strachan, L.J., Alsop, G.I., 2006: Slump folds as estimators of paleoslope: a case study from the Fisherstreet Slump of Country Clare, Ireland — *Basin Research* 18, 451-470.

Stüwe, K., Schuster, R., 2010: Initiation of subduction in the Alps: Continent or ocean? — *Geology* 38, 175-178.

Sudar, M.N., Gawlick, H-J., Lein, R., Missoni, S., Kovács, S., Jovanović, D., 2013: Depositional environment, age and facies of the Middle Triassic Bulog and Rid formations in the Inner Dinarides (Zlatibor Mountain, SW Serbia): evidence for the Anisian break-up of the Neotethys Ocean — *Neues Jahrbuch für Geologie und Paläontologie Abhandlungen* 269/3, 291-320.

Suppe, J., 1983: Geometry and kinematics of fault-bend folding — *American Journal of Science* 283, 684-721.

Sýkora, M., Ožvoldová, L., 1996: Lithoclasts of Middle Jurassic radiolarites in debris flow sediments from Silica Nappe (locality Bleskový prámeň, Slovak Karst, Western Carpathians — *Mineralia Slovaca* 28/1, 21-25.

Szentpétery, I., 1997: Borehole Rudabánya-690 — *Bulletin of the Hungarian Geological Society* 127/1-2, 179-198 (in Hungarian with English abstract).

Tanner, P.W.G., 1989: The flexural-slip mechanism — *Journal of Structural Geology* 11/6, 635-655.

Tari, G., 1994: Alpine Tectonics of the Pannonian Basin — PhD Dissertation, Rice University, Houston.

Tari, G., Dellmour, R., Rodgers, E., Asmar, C., Hagedorn, P., 2016: Styles of salt tectonics in the Sab'atayn basin, onshore Yemen — *Arab Journal of Geosciences* 9, 570-592.

Tari, G., Dellmour, R., Rodgers, E., Sultan, S., Al Atabi, A., Daud, F., Salman, A., 2014: Seismic expression of salt tectonics in the Sab'atayn Basin, onshore Yemen – *Interpretation* 2/4, 91-100.

Tari, G., Dövényi, P., Dunkl, I., Horváth, F., Lenkey, L., Stefanescu, M., Szafián, P., Tóth, T., 1999: Lithospheric structure of the Pannonian basin derived from seismic, gravity and geothermal data — In: *Durand, B., Jolivet, L., Horváth, F., Séranne, M (eds.):* The Mediterranean Basins: Tertiary Extension within the Alpine Orogen – Geological Society of London, Special Publications 156, 215-250.

Tari, G., Jabour, H., 2013: Salt tectonics along the Atlantic margin of Morocco — *Geological Society of London, Special Publications* 369, 337-353.

Tollmann, A., 1977: Geologie von Österreich — Deuticke, Wien (in German).

Trusheum, F., 1960: Mechanism of salt migration in northern Germany — *AAPG Bulletin* 44/9, 1519-1540.

Urai, J., Spiers, C.J., Peach, C.J., Franssen, R.C.M.W., Liezenberg, J.L., 1987: Deformation mechanisms operating in naturally deformed halite rocks as deduced from microstructural investigations — *Geologie en Mijnbouw* 66, 165.176.

Varela, C.L., Mohriak, W.U., 2013: Halokinetic rotating faults, salt intrusions and seismic pitfalls in the petroleum exploration of divergent margins — *AAPG Bulletin* 97, 1421-1446.

Velledits, F., Péró, Cs., Blau, J., Senowbari-Daryan, B., Kovács, S., Piros, O., Pocsai, T., Szügyi-Simon, H., Dumitrică, P., Pálfy, J., 2011: The oldest Triassic platform margin reef from the Alpine-Carpathian region (Aggtelek, NE Hungary): platform evolution, reefal biota and biostratigraphic framework — *Rivista Italiana di Paleontoligia e Stratigrafia* 117/2, 221-268.

Vendeville, B.C., Ge, H., Jackson, M.P.A., 1995: Scale models of salt tectonics during basement-involved extension — *Petroleum Geoscience* 1, 179-183.

Vendeville, B.C., Jackson, M.P.A., 1991: The fall of diapirs during thin-skinned extension — *Marine and Petroleum Geology* 9, 354-371.

Vendeville, B.C., Jackson, M.P.A., 1992: The rise of diapirs during thin-skinned extension — *Marine and Petroleum Geology* 9, 331-353.

Wagner III, B.H., Jackson, M.P.A., 2011: Viscous flow during salt welding — *Tectonophysics* 510, 309-326.

Warren, J.K., 2016: Evaporites: A Geological Compendium — Springer International Publishing Switzerland, pp. 491.

Whitney, D.L., Teyssier, C., Vanderhaeghe, O., 2004: Gneiss domes and crustal flow — *Geological Society of America Special Paper* 380, 15-33.

Willsey, S.P., Umhoefer, P., Hilley, G.E., 2002: Early evolution of an extensional monocline by a progragation normal fault: 3D analysis from combined field study and numerical modeling — *Journal of Structural Geology* 24/4, 651-669.

Withjack, M.O., Callaway, S., 2000: Active Normal Faulting Beneath a Salt Layer: An Experimental Study of Deformation Patterns in the Cover Sequence — *AAPG Bulletin* 84/5, 627-651.

Withjack, M.O., Olson, J., Peterson, E., 1990: Experimental Models of Extensional Forced Folds — *AAPG Bulletin* 74/7, 1038-1054.

Woodcock, N.H., 1979: The use of slump structures as paleoslope orientation estimators — *Sedimentology* 26, 83-99.

Woodcock, N.H., Mort, K., 2008: Classification of fault breccias and related fault rocks — *Geological Magazine* 145/3, 435-440.

Worrall, D.M., Snelson, S., 1989: Evolution of the northern Gulf of Mexico, with emphasis on Cenozoic growth faulting and the role of salt — In: *Bally, A., Palmer, A. (eds):* The geology of North America: An overview – Geological Society of America, Boulder, Colorado, pp. 97-138.

Zelenka, T., Kaló, J., Németh, N., 2005: The structure of the gypsum-anhydrite dome at Alsótelekes — *Bulletin of the Hungarian Geological Society* 135/4, 493-511 (in Hungarian with English abstract).

DECLARATION

NYILATKOZAT

Név: Oravecz Éva
ELTE TTK, szak: Geológus MSc
Neptun azonosító: D6412M

Diplomamunka címe:

Complex deformation history of the Silica Nappe, Aggtelek Mts: Inherited Triassic salt structures and their role during the Alpine deformation

A diplomamunka szerzőjeként fegyelmi felelősségem tudatában kijelentem, hogy a dolgozatom önálló munkám eredménye, saját szellemi terméken, abban a hivatkozások és idézések standard szabályait következetesen alkalmaztam, mások által írt részeket a megfelelő idézés nélkül nem használtam fel.

Budapest, 2019. május 20.

a hallgató aláírása

APPENDICES

Appendix 1:

Coordinates of the observation points (coordinates given in EOV = Hungarian National Grid).

Point	X	Y	Point	X	Y	Point	X	Y
Jsv-001	761907.232	349864.85	**Jsv-049**	763222.615	350424.433	**Jsv-098**	762428.446	349851.374
Jsv-002	761938.264	349858.77	**Jsv-050**	763179.455	350377.755	**Jsv-099**	762462.877	349803.653
Jsv-003	761961.294	349857.21	**Jsv-051**	763035.036	349991.691	**Jsv-100**	762501.248	349781.483
Jsv-004	762103.309	349871.54	**Jsv-052**	762270.698	349877.899	**Jsv-101**	762511.558	349760.993
Jsv-005	762197.268	349839.32	**Jsv-053**	762347.773	349858.261	**Jsv-102**	762660.539	349748.098
Jsv-006	762218.54	349821.71	**Jsv-054**	762371.133	349851.15	**Jsv-103**	762722.866	349768.113
Jsv-007	762280.398	349782.08	**Jsv-055**	762391.63	349862.005	**Jsv-104**	762780.292	349717.059
Jsv-008	762480.814	349676.18	**Jsv-056**	762338.71	349894.572	**Jsv-105**	762862.861	349696.533
Jsv-009	762529.187	349656.99	**Jsv-057**	762298.343	349931.945	**Jsv-106**	762801.741	349523.691
Jsv-010	762768.945	349521.49	**Jsv-058**	762247.435	349948.533	**Jsv-107**	762800.298	349586.293
Jsv-011	762898.055	349477.4	**Jsv-059**	762175.449	350098.539	**Jsv-108**	761769.738	349696.987
Jsv-012	762961.471	349479.64	**Jsv-060**	762155.793	350295.949	**Jsv-109**	761750	349597.043
Jsv-013	763266.764	349484.61	**Jsv-061**	762162.63	350332.348	**Jsv-110**	761761.003	349498.471
Jsv-014	763576.966	349518.29	**Jsv-062**	762052.658	350313.639	**Jsv-111**	761911.014	349432.624
Jsv-015	763695.201	349474.67	**Jsv-063**	762003.538	350348.842	**Jsv-112**	761947.734	349381.162
Jsv-016	763740.228	349445.41	**Jsv-064**	761973.747	350348.264	**Jsv-113**	761977.218	349317.657
Jsv-017	763878.856	349474.39	**Jsv-065**	761862.785	350392.171	**Jsv-114**	761994.811	349287.628
Jsv-018	764057.13	349488.14	**Jsv-066**	761714.645	350427.574	**Jsv-115**	762016.401	349276.588
Jsv-019	764371.579	349475.22	**Jsv-067**	761533.675	350432.2	**Jsv-116**	762179.63	349158.943
Jsv-020	764560.401	349468.06	**Jsv-068**	761352.266	350340.708	**Jsv-117**	762183.707	349101.286
Jsv-021	764667.237	349417.89	**Jsv-069**	761203.483	350367.324	**Jsv-118**	762129.764	348987.995
Jsv-022	764912.153	349547.01	**Jsv-070**	761224.858	350324.906	**Jsv-119**	762244.881	348842.053
Jsv-023	764965.593	349548.74	**Jsv-071**	761130.662	350235.545	**Jsv-120**	762300.97	348856.268
Jsv-024	765045.652	349543.44	**Jsv-071**	761241.415	350256.142	**Jsv-121**	762425.857	349212.45
Jsv-025	765106.964	349539.87	**Jsv-072**	761233.129	350240.965	**Jsv-122**	762519.089	349275.226
Jsv-026	765235.605	349538.88	**Jsv-073**	761200.262	350169.581	**Jsv-123**	762588.503	349307.614
Jsv-027	765434.395	349628.84	**Jsv-074**	761393.842	349990.646	**Jsv-124**	762631.331	349303.665
Jsv-028	765619.236	349683.01	**Jsv-075**	761371.239	350069.861	**Jsv-125**	762682.201	349270.393
Jsv-029	765794.224	349816.81	**Jsv-076**	761401.567	349965.876	**Jsv-126**	762845.79	349343.445
Jsv-030	765968.279	349892.83	**Jsv-077**	761712.055	349926.37	**Jsv-127**	762667.029	349502.375
Jsv-031	762008.848	349868.7	**Jsv-078**	762405.232	349828.118	**Jsv-128**	762526.466	349401.631
Jsv-032	762255.372	349852.13	**Jsv-079**	762398.744	349815.644	**Jsv-129**	762575.87	349329.617
Jsv-033	762363.901	349846.56	**Jsv-080**	762449.472	349804.616	**Jsv-130**	762380.588	349284.88
Jsv-034	762402.349	349854.65	**Jsv-081**	762445.658	349783.962	**Jsv-131**	762089.017	349433.848
Jsv-035	762448.82	349895.16	**Jsv-082**	762470.903	349748.41	**Jsv-132**	761967.566	349476.103
Jsv-036	762508.841	349877.75	**Jsv-084**	762570.929	349777.055	**Jsv-133**	764049.731	349533.27
Jsv-037	762572.341	349867.86	**Jsv-085**	762598.657	349777.373	**Jsv-134**	764076.324	349564.943
Jsv-038	762662.291	349901.09	**Jsv-086**	762652.365	349807.009	**Jsv-136**	764107.569	349567.006
Jsv-039	762847.287	350001.82	**Jsv-087**	762651.076	349713.761	**Jsv-137**	764103.781	349601.529
Jsv-040	762953.11	350074.08	**Jsv-088**	762778.108	349643.262	**Jsv-138**	763943.119	349546.186
Jsv-041	763015.91	350194.45	**Jsv-089**	762815.034	349585.357	**Jsv-139**	763942.809	349510.662
Jsv-042	762966.284	350391.38	**Jsv-090**	762833.126	349533.759	**Per-001**	771080.993	349672.597
Jsv-043	762892.493	350731.57	**Jsv-091**	762567.827	349681.881	**Per-002**	770960.137	349859.854
Jsv-044	762883.588	350877.02	**Jsv-092**	762474.399	349736.018	**Per-003**	770919.836	349880.704
Jsv-045	762895.105	350783.35	**Jsv-093**	762451.152	349798.085	**Per-004**	770909.663	349949.799
Jsv-046	763225.144	350536.95	**Jsv-094**	762428.2	349768.938	**Per-005**	770887.462	350028.209
Jsv-047	763388.708	350729.72	**Jsv-095**	762408.738	349837.976	**Per-006**	770864.098	350073.888
Jsv-048	763278.148	350511.4	**Jsv-097**	762400.679	349896.571	**Per-007**	770853.949	350124.182

Point	X	Y	Point	X	Y	Point	X	Y
Per-008	770796.354	350218.874	**Per-062**	771691.084	350499.964	**Per-115**	770215.239	350323.79
Per-009	770831.934	350314.066	**Per-063**	771620.945	350511.949	**Per-116**	771179.621	351921.095
Per-010	770804.096	350322.607	**Per-064**	771515.354	350557.009	**Per-117**	771086.256	351983.885
Per-011	770789.14	350401.28	**Per-065**	771487.681	350550.642	**Per-118**	771036.749	352007.211
Per-012	770772.354	350443.648	**Per-066**	771388.519	350472.799	**Per-119**	770858.922	351979.681
Per-013	770291.111	350487.568	**Per-067**	771498.498	351063.278	**Per-120**	771002.455	351879.558
Per-014	770265.423	350367.998	**Per-068**	771423.027	351199.195	**Szn-001**	767547.668	351848.851
Per-015	770318.529	349980.405	**Per-069**	771403.474	351186.658	**Szn-002**	767402.01	352016.655
Per-016	770316.399	349908.607	**Per-070**	771407.392	351190.189	**Szn-003**	767409.395	352042.503
Per-017	770414.303	349717.854	**Per-071**	771343.66	351013.746	**Szn-004**	767179.207	351854.829
Per-018	770867.062	349373.203	**Per-072**	771123.589	350809.328	**Szn-005**	767163.204	351867.409
Per-019	770468.75	349042.941	**Per-073**	771032.871	350748.466	**Szn-006**	767135.419	351881.307
Per-020	770679.164	349349.365	**Per-074**	770909.677	350843.563	**Szn-007**	767125.783	351878.887
Per-021	770816.504	349261.789	**Per-075**	771100.612	350734.199	**Szn-008**	767093.13	351921.389
Per-022	770879.549	349168.659	**Per-076**	771253.349	350715.152	**Szn-009**	767064.918	351916.257
Per-023	770408.24	348986.168	**Per-077**	771446.775	350727.112	**Szn-010**	767006.979	351863.909
Per-024	770420.624	349048.613	**Per-078**	771402.517	350785.143	**Szn-011**	767008.436	351799.304
Per-025	770694.859	351813.496	**Per-079**	771390.935	350875.345	**Szn-012**	766915.792	351978.539
Per-026	770579.362	351799.737	**Per-080**	770444.271	348968.118	**Szn-013**	767130.457	351929.154
Per-027	770528.697	351811.251	**Per-081**	770384.284	348701.434	**Szn-014**	767191.861	351934.516
Per-028	770046.356	351507.849	**Per-082**	770632.969	349216.573	**Szn-015**	767234.127	351946.609
Per-029	770132.517	351446.339	**Per-083**	770598.677	349200.95	**Szn-016**	765699.75	349086.481
Per-030	770157.529	351431.174	**Per-084**	770573.153	349186.957	**Szn-017**	765340.166	348850.355
Per-031	771422.839	351320.786	**Per-085**	770526.015	349166.617	**Szn-018**	765355.271	348460.299
Per-032	771305.069	351266.916	**Per-086**	770501.226	349149.302	**Szn-019**	765897.122	347944.949
Per-032	771254.568	351129.354	**Per-087**	770327.516	348756.098	**Szn-020**	766103.245	347933.621
Per-033	771213.879	351063.309	**Per-088**	770405.103	348916.574	**Szn-021**	766317.55	348137.167
Per-034	771169.072	350996.066	**Per-089**	771183.015	349604.315	**Szn-022**	766438.073	348239.601
Per-035	771153.986	350964.377	**Per-090**	771145.705	349641.134	**Szn-023**	766247.446	348617.669
Per-036	771124.881	350902.915	**Per-091**	771131.878	349623.268	**Szn-024**	766231.869	348490.981
Per-037	771082.167	350929.832	**Per-092**	770916.221	349926.24	**Szn-025**	766216.918	348395.678
Per-038	771006.547	351193.352	**Per-093**	770912.813	349972.448	**Szn-026**	766191.7	348354.789
Per-039	771045.818	351426.016	**Per-094**	770891.991	349988.477	**Szn-027**	765694.71	347907.633
Per-040	771114.294	351443.359	**Per-095**	770864.107	350069.883	**Szn-028**	765830.953	349360.546
Per-041	769903.854	351362.716	**Per-096**	770836.482	350174.323	**Szn-029**	765177.625	349304.664
Per-042	769932.407	351301.566	**Per-097**	770794.496	350183.903	**Szn-030**	765062.952	348912.023
Per-043	770028.107	351240.141	**Per-098**	770827.647	350306.857	**Szn-031**	765045.252	348887.086
Per-044	770061.825	351222.375	**Per-099**	770760.714	350445.074	**Szn-032**	764970.934	348766.909
Per-046	770143.574	351191.923	**Per-100**	770754.158	350482.761	**Szn-033**	764908.388	348746.532
Per-048	770187.911	351150.682	**Per-101**	770730.106	350565.027	**Szn-033**	764903.565	348750.997
Per-049	770116.427	351074.993	**Per-102**	770397.988	348831.989	**Szn-034**	764778.179	348661.736
Per-050	770096.681	350971.901	**Per-103**	770174.591	348817.093	**Szn-035**	764707.398	348564.216
Per-051	769988.987	351140.652	**Per-104**	770320.661	348658.949	**Szn-036**	764745.327	348572.645
Per-052	770054.684	350843.539	**Per-105**	770281.057	348649.559	**Szn-037**	764753.368	348540.21
Per-053	770038.824	350855.892	**Per-106**	770243.618	348632.093	**Szn-037**	764750.506	348442.147
Per-054	769946.182	350876.551	**Per-107**	770130.827	348588.254	**Szn-038**	764756.004	348437.25
Per-055	769772.269	350865.269	**Per-108**	770953.686	349107.689	**Szn-039**	764728.885	348305.221
Per-056	769682.516	350903.57	**Per-109**	770886.01	349354.91	**Szn-040**	764703.275	348208.932
Per-057	769591.523	350984.009	**Per-110**	770745.375	349440.969	**Szn-040**	764701.999	348206.126
Per-058	769501.88	351120.881	**Per-111**	770550.131	349585.075	**Szn-041**	764720.557	348150.761
Per-059	769444.226	351216.363	**Per-112**	770432.776	349683.196	**Szn-042**	764737.26	348091.91
Per-060	769428.976	351242.302	**Per-113**	770345.178	349865.597	**Szn-043**	764749.036	348091.254
Per-061	769842.219	351329.064	**Per-114**	770253.535	350210.67	**Szn-044**	764759.859	348048.154

Point	X	Y	Point	X	Y	Point	X	Y
Szn-045	764764.089	348026.141	**Szn-098**	767556.298	349588.497	**Szn-152**	764028.985	348199.934
Szn-046	764853.425	348608.832	**Szn-099**	767643.495	349777.72	**Szn-153**	764039.311	348224.055
Szn-047	764935.495	348657.93	**Szn-100**	768080.772	349624.661	**Szn-154**	764139.197	348373.201
Szn-048	764992.485	348624.278	**Szn-101**	768476.938	349515.402	**Szn-155**	764249.396	348445.684
Szn-049	765128.359	348933.46	**Szn-102**	768623.901	349454.338	**Szn-156**	764310.859	348468.703
Szn-050	765166.199	348953.682	**Szn-103**	768706.703	349380.613	**Szn-157**	764220.765	348576.831
Szn-051	766702.661	349989.373	**Szn-104**	768970.315	349434.758	**Szn-158**	764179.25	348712.508
Szn-052	766867.885	349857.547	**Szn-105**	768901.598	349650.609	**Szn-159**	763996.733	349017.72
Szn-053	766988.523	349747.407	**Szn-106**	769228.084	349589.028	**Szn-161**	763779.667	349230.37
Szn-054	767052.971	349629.122	**Szn-107**	769320.768	349391.586			
Szn-055	767072.541	349389.562	**Szn-108**	769868.774	349620.522			
Szn-056	767113.133	349328.198	**Szn-109**	770105.294	349514.518			
Szn-057	767132.179	349198.649	**Szn-110**	770085.451	349294.727			
Szn-058	767131.215	349100.177	**Szn-111**	770183.027	349244.358			
Szn-059	767142.774	349062.699	**Szn-112**	770132.495	348984.123			
Szn-060	767118.378	349021.822	**Szn-113**	770239.389	348935.041			
Szn-061	767145.661	348993.229	**Szn-114**	770389.746	348979.108			
Szn-062	767137.669	348767.016	**Szn-115**	763218.575	348561.236			
Szn-063	766631.964	348434.516	**Szn-116**	763182.796	348442.84			
Szn-064	766514.181	348787.458	**Szn-117**	763160.361	348447.629			
Szn-065	766300.631	348687.71	**Szn-118**	763036.852	348396.934			
Szn-066	766364.555	348727.598	**Szn-119**	762703.82	348366.181			
Szn-067	766415.092	348741.631	**Szn-120**	763086.773	348371.1			
Szn-068	766438.517	348786.935	**Szn-121**	763222.39	348362.63			
Szn-069	766475.715	348772.777	**Szn-122**	763656.57	347823.83			
Szn-070	766603.974	348912.639	**Szn-123**	763621.258	347373.046			
Szn-071	766520.7	349374.185	**Szn-124**	763663.868	347396.02			
Szn-072	766778.461	349338.003	**Szn-125**	763781.901	347507.805			
Szn-073	766992.649	349426.546	**Szn-126**	763877.182	347617.586			
Szn-074	767118.759	349466.701	**Szn-127**	763900.113	347760.541			
Szn-075	767225.636	349561.646	**Szn-128**	763896.202	347872.708			
Szn-076	767361.747	349604.456	**Szn-129**	763896.653	347962.491			
Szn-077	767332.344	349854.163	**Szn-130**	763960.807	347980.664			
Szn-078	766659.186	349439.053	**Szn-131**	763655.423	347995.122			
Szn-079	765754.74	347983.813	**Szn-132**	763515.869	348565.396			
Szn-080	766176.12	347933.527	**Szn-133**	763512.456	348893.721			
Szn-081	766239.354	347912.549	**Szn-134**	763691.015	349341.539			
Szn-082	766505.529	347759.271	**Szn-135**	763617.549	349353.778			
Szn-083	766336.462	347193.305	**Szn-136**	763723.404	349259.188			
Szn-084	766066.395	347181.872	**Szn-137**	763546.736	348954.305			
Szn-085	765925.706	347157.469	**Szn-138**	763542.057	348904.314			
Szn-086	766017.494	347056.075	**Szn-139**	763814.583	348012.603			
Szn-087	765855.417	346839.572	**Szn-140**	763897.031	348078.525			
Szn-088	765824.507	346975.226	**Szn-142**	763902.126	347992.634			
Szn-089	765517.128	347034.601	**Szn-143**	763895.548	347966.029			
Szn-090	765317.148	347144.524	**Szn-144**	763866.553	347973.245			
Szn-091	765255.845	347239.194	**Szn-145**	763836.165	347972.313			
Szn-092	765098.695	347194.125	**Szn-146**	763813.818	347983.776			
Szn-093	765506.108	347641.883	**Szn-147**	763813.934	347996.682			
Szn-094	766117.664	347537.798	**Szn-148**	763831.77	348011.384			
Szn-095	767259.37	349357.082	**Szn-149**	763895.876	348062.038			
Szn-096	767434.848	349333.723	**Szn-150**	763964.501	348127.355			
Szn-097	767429.701	349379.563	**Szn-151**	764002.433	348132.108			

Appendix 2:

Legend for the stereoplots (modified after FODOR 2010).